

University of Kentucky

UKnowledge

Theses and Dissertations--Neuroscience

Neuroscience


2022

EVALUATING THE MICROBIOME TO BOOST RECOVERY FROM STROKE: THE EMBRS STUDY

Tyler Hammond

University of Kentucky, hammond.tyler@yahoo.com

Author ORCID Identifier:

 <https://orcid.org/0000-0002-6141-9150>

Digital Object Identifier: <https://doi.org/10.13023/etd.2022.301>

[Right click to open a feedback form in a new tab to let us know how this document benefits you.](#)

Recommended Citation

Hammond, Tyler, "EVALUATING THE MICROBIOME TO BOOST RECOVERY FROM STROKE: THE EMBRS STUDY" (2022). *Theses and Dissertations--Neuroscience*. 28.

https://uknowledge.uky.edu/neurobio_etds/28

This Doctoral Dissertation is brought to you for free and open access by the Neuroscience at UKnowledge. It has been accepted for inclusion in Theses and Dissertations--Neuroscience by an authorized administrator of UKnowledge. For more information, please contact UKnowledge@lsv.uky.edu.

STUDENT AGREEMENT:

I represent that my thesis or dissertation and abstract are my original work. Proper attribution has been given to all outside sources. I understand that I am solely responsible for obtaining any needed copyright permissions. I have obtained needed written permission statement(s) from the owner(s) of each third-party copyrighted matter to be included in my work, allowing electronic distribution (if such use is not permitted by the fair use doctrine) which will be submitted to UKnowledge as Additional File.

I hereby grant to The University of Kentucky and its agents the irrevocable, non-exclusive, and royalty-free license to archive and make accessible my work in whole or in part in all forms of media, now or hereafter known. I agree that the document mentioned above may be made available immediately for worldwide access unless an embargo applies.

I retain all other ownership rights to the copyright of my work. I also retain the right to use in future works (such as articles or books) all or part of my work. I understand that I am free to register the copyright to my work.

REVIEW, APPROVAL AND ACCEPTANCE

The document mentioned above has been reviewed and accepted by the student's advisor, on behalf of the advisory committee, and by the Director of Graduate Studies (DGS), on behalf of the program; we verify that this is the final, approved version of the student's thesis including all changes required by the advisory committee. The undersigned agree to abide by the statements above.

Tyler Hammond, Student

Ai-Ling Lin, PhD, Major Professor

Warren Alilain, PhD, Director of Graduate Studies

EVALUATING THE MICROBIOME TO BOOST RECOVERY FROM STROKE: THE
EMBRs STUDY

DISSERTATION

A dissertation submitted in partial fulfillment of the
requirements for the degree of Doctor of Philosophy in the
College of Medicine
at the University of Kentucky

By

Tyler Christian Hammond

Lexington, Kentucky

Co- Directors: Dr. Ai-Ling Lin, Professor of Pharmacology and Nutritional Science

and Dr. Joe Edward Springer, Professor of Neuroscience

Lexington, Kentucky

2022

Copyright © Tyler Christian Hammond 2022
<https://orcid.org/0000-0002-6141-9150>

ABSTRACT OF DISSERTATION

EVALUATING THE MICROBIOME TO BOOST RECOVERY FROM STROKE: THE EMBRS STUDY

Accumulating evidence suggests that gut microbes modulate brain plasticity via the bidirectional gut-brain axis and may play a role in stroke rehabilitation. A severely imbalanced microbial community has been shown to occur following stroke, causing a systemic flood of neuro- and immunomodulatory substances due to increased gut permeability and decreased gut motility. Here we measure post-stroke increased gut dysbiosis and how it correlates with gut permeability and subsequent cognitive impairment.

We recruited 12 participants with acute stroke, 12 healthy control participants, and 18 participants who had risk factors for stroke, but had not had a stroke. We measured the gut microbiome with whole shotgun sequencing on stool samples. We measured cognitive and emotional health with MRI imaging and the NIH toolbox. We normalized all variables and used linear regression methods to identify gut microbial levels associations with cognitive and emotional assessments.

Beta diversity analysis revealed that the bacteria populations of the stroke group were statistically dissimilar from the risk factors and healthy control groups. Relative abundance analysis revealed notable decreases in butyrate-producing microbial taxa. The stroke group had higher levels of the leaky gut marker alpha-1-antitrypsin than the control groups, and *roseburia* species were negatively correlated with alpha-1-antitrypsin. Several Actinobacteria species were associated with cerebral blood flow and white matter integrity in areas of the brain responsible for language, learning, and memory. Stroke participants scored lower on the picture vocabulary and list sorting tests than those in the control groups. Stroke participants who had higher levels of *roseburia* performed better on the picture vocabulary task.

We found that microbial communities are disrupted in a stroke population. Many of the disrupted bacteria have previously been reported to have correlates to health and disease. This preparatory study will lay the foundation for the development of therapeutics targeting the gut following stroke.

KEYWORDS: Stroke, Microbiome, Imaging, Functional Recovery

Tyler Christian Hammond

(Name of Student)

03/24/2022

Date

EVALUATING THE MICROBIOME TO BOOST RECOVERY FROM STROKE: THE
EMBRs STUDY

By
Tyler Christian Hammond

Ai-Ling Lin, PhD

Co-Director of Dissertation

Joe Edward Springer, PhD

Co-Director of Dissertation

Warren J. Alilain, PhD

Director of Graduate Studies

03/24/2022

Date

ACKNOWLEDGMENTS

The following dissertation, while an individual work, benefited from the insights and direction of several people. First, my Dissertation Chair, Ai-Ling Lin, PhD, exemplifies the high quality scholarship to which I aspire. In addition, Lumy Sawaki, MD, PhD, provided timely and instructive comments and evaluation at every stage of the dissertation process, allowing me to complete this project on schedule. Next, I wish to thank the complete Dissertation Committee, and outside reader, respectively: Ai-Ling Lin, PhD, Lumy Sawaki, MD, PhD, Arnold Stromberg, PhD, Joe Springer, PhD, Keith Pennypacker, PhD, and John McCarthy, PhD. Each individual provided insights that guided and challenged my thinking, substantially improving the finished product.

In addition to the technical and instrumental assistance above, I received equally important assistance from family and friends. My wife, Katrina, provided on-going support throughout the dissertation process, as well as technical assistance critical for completing the project in a timely manner. My son, Thaddeus, provided much needed diversions and a continual inspiration. My parents, Darin and Gaylynn Hammond, provided resources and inspiration to make my journey here possible. All my other family and friends were the greatest cheerleaders possible. Finally, I wish to thank the respondents of my study (who remain anonymous for confidentiality purposes).

TABLE OF CONTENTS

ACKNOWLEDGMENTS	iii
LIST OF TABLES.....	viii
LIST OF FIGURES	ix
CHAPTER 1. BACKGROUND	1
1.1 Stroke	1
1.1.1 Available Stroke Treatments.....	2
1.1.2 Rehabilitation following stroke.....	2
1.1.3 Neuroplasticity	3
1.1.4 Markers of Stroke Severity	3
1.2 Gut Microbiome.....	4
1.2.1 Gut-Brain Axis.....	7
1.2.2 Stroke and the Gut Microbiome.....	9
1.3 Scope of Dissertation	10
CHAPTER 2. MATERIALS AND METHODS.....	12
2.1 Participants.....	12
2.1.1 Recruitment workflow for participants with acute stroke.....	13
2.1.2 Recruitment workflow for control participants with no stroke.....	14
2.2 Study Design.....	15
2.2.1 Stool Sample Collection.....	17
2.2.2 Metagenomic Sequencing	18
2.2.3 Metagenomic Bioinformatic Analysis	18
2.2.4 Intestinal Inflammation and Permeability Analysis.....	19
2.2.5 Diet Analysis.....	19
2.2.6 APOE Genotyping	19
2.2.7 Imaging Analysis	20
2.2.7.1 Arterial Spin Labeling.....	20
2.2.7.2 Structural Imaging.....	20
2.2.7.3 Diffusion Tensor Imaging	20
2.2.7.4 Fluid-attenuated inversion recovery (FLAIR) imaging.....	21
2.2.7.5 Magnetic Resonance Spectroscopy	21
2.3 Functional Analysis.....	22
2.4 NIH Toolbox	22
2.5 Statistical Analysis.....	22
CHAPTER 3. THE GUT MICROBIOME IS ALTERED IN THE CONTEXT OF STROKE AND IS CORRELATED WITH IMPAIRED FUNCTION.....	27
3.1 Introduction.....	27
3.2 Results.....	29

3.2.1	Participant Characteristics.....	29
3.2.2	Stroke microbiome with more pro-inflammatory and fewer butyrate producing taxa 30	
3.2.3	Stroke dysbiosis is associated with leaky gut markers.....	31
3.2.4	Some bacteria are associated with diet.....	32
3.2.5	Microbiota are associated with markers of stroke recovery.....	32
3.2.5.1	Functional Testing.....	32
3.2.5.1	Cognitive Testing.....	32
3.2.5.1	Emotional Testing.....	33
3.2.5.1	Sensation Testing.....	34
3.3	Discussion.....	34
CHAPTER 4. GUT MICROBIOME IS ASSOCIATED WITH BRAIN IMAGING IN COMMUNITY DWELLING OLDER ADULTS		58
4.1	Introduction.....	58
4.2	Results.....	59
4.2.1	Participant Characteristics.....	59
4.2.2	Microbiome Measurements.....	60
4.2.2.1	Gut microbiome is associated with sex, ApoE Genotype, Obesity, Diabetes, Hypertension.....	60
4.2.2.1	Gut microbiome is associated with calcium intake and vegetables intake.....	61
4.2.3	Imaging Measurements.....	61
4.2.3.1	Gut microbiome is associated with Structural Imaging.....	62
4.2.3.2	Gut microbiome is associated with Brain Metabolites.....	62
4.2.3.3	Equol producers are associated with Cerebral Blood Flow.....	62
4.2.3.4	Equol producers are associated with White Matter Integrity.....	63
4.3	Discussion.....	64
CHAPTER 5. GENERAL DISCUSSION.....		90
CHAPTER 6. [SUPPLEMENT] β -AMYLOID AND TAU DRIVE EARLY ALZHEIMER'S DISEASE DECLINE WHILE HYPOMETABOLISM DRIVES LATE DECLINE		95
6.1	Summary.....	95
6.2	Introduction.....	95
6.3	Results.....	98
6.3.1	Participant characterizations and data selection.....	98
6.3.2	Relative importance of AD biomarkers in early and late AD.....	99
6.3.3	Accuracy of the top 8 features vs all 16 features.....	100
6.3.4	Correlation of AD biomarkers with cognitive performance.....	102
6.3.5	Biomarker quantification for predicting LMCI and AD.....	103
6.4	Discussion.....	103
6.5	Methods.....	111
6.5.1	Data pre-processing.....	111
6.5.2	Machine learning analysis.....	112
6.5.3	Statistics and Reproducibility.....	115
6.5.4	Pearson correlation analysis of cognitive performance.....	116

6.5.5	Calculation of biomarker values	116
6.5.6	Data Availability	117
CHAPTER 7. [SUPPLEMENT] HUMAN GRAY AND WHITE MATTER METABOLOMICS TO DIFFERENTIATE APOE AND STAGE DEPENDENT CHANGES IN ALZHEIMER'S DISEASE 134		
7.2	Introduction	135
7.3	Methods.....	137
7.3.1	Participant Characteristics.....	137
7.3.2	Metabolon Platform	138
7.3.2.1	Ultra-high performance Liquid Chromatography-Tandem Mass Spectroscopy 138	
7.3.2.2	Bioinformatics	139
7.3.2.3	LIMS	140
7.3.2.4	Data Extraction and Compound Identification.....	140
7.3.2.5	Metabolite Quantification and Data Normalization	141
7.3.3	Statistical and Analytical Methods.....	142
7.3.3.1	Statistical Calculations	142
7.3.3.1	Machine Learning Classification.....	142
7.4	Results	143
7.4.1	Metabolomics differences in gray and white-enriched matters.....	143
7.4.2	Machine learning to classify AD from normal with Gray and white-enriched matter metabolomics	144
7.4.3	Gray and white-enriched matter metabolomics between early and late stage in <i>APOE</i> ϵ 4.....	145
7.4.4	Gray and white-enriched matter metabolomics between early and late stage in <i>APOE</i> ϵ 3.....	147
7.4.5	Gray and white-enriched matter metabolomics between <i>APOE</i> ϵ 3 and <i>APOE</i> ϵ 4 at early and late stage	148
7.5	Discussion	149
CHAPTER 8. [SUPPLEMENT] GUT MICROBIAL DYSBIOSIS IS CORRELATED WITH STROKE SEVERITY MARKERS IN AGED RATS FOLLOWING STROKE..... 164		
8.1	Summary	164
8.2	Introduction	165
8.3	Results.....	167
8.3.1	The aged rat gut microbiome is disrupted following stroke.....	167
8.3.2	The top 13 disrupted bacterial species following stroke	168
8.3.3	Bacterial community disruptions following stroke are correlated with stroke severity markers 169	
8.3.4	Bacterial community disruptions following stroke are correlated with rises in inflammatory markers	170
8.4	Discussion	170
8.5	Methods.....	175
8.5.1	Ethics approval and animals.....	175
8.5.2	Middle cerebral artery occlusion.....	176

8.5.3	Post-surgical fluid management and pain control	178
8.5.4	Microbiome Sequencing	179
8.5.5	Magnetic resonance imaging.....	180
8.5.6	Biochemical analysis.....	181
8.5.7	Statistical analysis	182
BIBLIOGRAPHY		193
VITA		220

LIST OF TABLES

Table 2.1 Inclusion and Exclusion Criteria used to evaluate eligibility for acute stroke patients	24
Table 2.2 Inclusion and Exclusion Criteria used to evaluate eligibility for no stroke patients with A) risk factors for stroke and B) no risk factors for stroke	25
Table 2.3 Timeline of study visits and procedures	26
Table 3.1 Participant Characteristics	41
Table 3.2 Microbial Taxa Associated with fecal Alpha-1-Antitrypsin	42
Table 3.3 Diet Correlates with Microbial Taxa in Stroke Participants	43
Table 3.4 Microbial Taxa correlated with Markers of Stroke Recovery	44
Table 4.1 Participant Characteristics	73
Table 4.2 Microbial Taxa associated with Demographic Features	74
Table 4.3 Diet correlates with microbial taxa	75
Table 4.4 Microbial taxa associated with imaging features	76
Table 4.5 Microbial taxa associated with brain metabolites	77
Table 4.6 Microbial Taxa associated with Cerebral Blood Flow	78
Table 4.7 Microbial taxa associated with white matter integrity	79
Table 6.1 Demographic and cognitive data for the cross-sectional study population	118
Table 6.2 Biomarkers used in the feature analysis	120
Table 6.3 Ranking of each biomarker feature importance to prediction of diagnosis classification from the random forest analysis	122
Table 6.4 Accuracy of all 16 features and of the top 8 features in predicting diagnosis for each participant group comparison	124
Table 6.5 Average values of the top 8 biomarker features for each diagnosis group that can be used to predict cognitive status	125
Table 7.1 Participant Characteristics	156
Table 7.2 Number of samples belonging to APOE genotypes and Braak Stages	157
Table 7.3 Top ranked biochemicals in (A) predicting gray vs white matter all belong to the lipid superclass, (B) in predicting AD vs Normal brain tissue in Gray and (C) White Matter	158
Table 7.4 Gray and white matter metabolomics between early and late stage in APOE4	159
Table 7.5 Gray and white matter metabolomics between early and late stage in APOE3	160
Table 7.6 Gray and white matter metabolomics between APOE3 and APOE4 at early and late stages	161
Table 8.1 Top 13 bacterial species changes following stroke as detected by random forest	183
Table 8.2 Linear Regression models predicting infarct, edema, and CBF by top 13 species	184
Table 8.3 Correlation of bacterial species with infarct and edema	185
Table 8.4 Association of Inflammatory Markers and Bacterial Species	186

LIST OF FIGURES

Figure 3.1 Alpha Diversity amongst the participants groups did not differ on Wilcoxon rank sum test	45
Figure 3.2 Beta Diversity amongst the groups	46
Figure 3.3 Relative Abundance of most prevalent phyla	47
Figure 3.4 Significant Associations of Microbial Taxa with Stroke and At Risk Groups as compared to the healthy control group	49
Figure 3.5 Leaky Gut Markers were compared amongst the participant groups using Kruskal-Wallis Test.	50
Figure 3.6 Microbial Taxa Associated with fecal Alpha-1-Antitrypsin.	51
Figure 3.7 Diet composition amongst the groups.	53
Figure 3.8 Microbial Taxa Associated with diet in stroke participants.	54
Figure 3.9 Markers of stroke function at baseline and follow up for acute stroke, at risk, and healthy participants.	56
Figure 3.10 Microbial Taxa associations with Markers of Stroke recovery.	57
Figure 4.1 Microbial taxa associated with demographic features.	82
Figure 4.2 Microbial Taxa Associations with Dietary Calcium intake.	83
Figure 4.3 Microbial Taxa Associations with Structural Imaging Features.	84
Figure 4.4 Notable Microbial Taxa Associations with Brain Metabolites in the white matter of the corpus callosum.	85
Figure 4.5 Species from the <i>eggerthellaceae</i> family are negatively associated with cerebral blood flow (CBF) in language, memory, and limbic brain areas.	86
Figure 4.6 Notable Microbial Taxa Associations with cerebral blood flow (CBF) in limbic and memory regions.	87
Figure 4.7 Species from the <i>eggerthellaceae</i> family are positively correlated with white matter integrity (WMI) in language, memory, and limbic brain circuits.	88
Figure 4.8 Notable Microbial Taxa Associations with cerebral blood flow (CBF) in limbic and memory regions.	89
Figure 6.1 Receiver operating characteristic (ROC) curves depicting the accuracy of all 16 biomarker features (top) vs. the top 8 biomarker features (bottom).	127
Figure 6.2 Correlation of top eight AD biomarkers with composite memory scores.	128
Figure 6.3 Correlation of top eight AD biomarkers with executive functioning scores.	130
Figure 6.4 Relative importance of biomarkers predicting AD clinical diagnosis.	132
Figure 6.5 Flow chart of the random forest method used.	133
Figure 7.1 Schematic representation of study design.	162
Figure 7.2 Schematic representation of overall results.	163
Figure 8.1 Imaging features following stroke	187
Figure 8.2 Motor function skills before and after stroke	188
Figure 8.3 Diversity changes following stroke.	189
Figure 8.4 Phyla changes as a result of stroke.	190
Figure 8.5 Summary figure depicting changes in gut microbial communities in response to stroke	191

CHAPTER 1. BACKGROUND

1.1 Stroke

Every year, more than 795,000 people suffer a stroke in the United States.¹ Stroke is characterized as a neurological deficit caused by an acute focal injury of the central nervous system vasculature, including cerebral infarction, intracerebral hemorrhage, and subarachnoid hemorrhage.² The major blood supply to the brain comes from the anterior, middle, and posterior cerebral arteries.³ Cerebral infarction is most commonly caused by a blockage to the blood supply of the brain in the form of a thrombus or an embolus.⁴ A thrombus is a blood clot consisting of fibrin, platelets, and red blood cells that forms within the artery that it is occluding.⁵ An embolus is a blood clot that travels from another region such as the heart or the carotid artery that lodges in the vasculature of the brain.⁶ When the blood supply to the brain is blocked, the downstream tissue is injured by lack of oxygen and necrosis ensues.⁷ Cell apoptosis, excitotoxicity, and the inflammatory response cause further damage and result in a loss of function.⁸

Thrombus and embolus formation are a natural product of atherosclerosis.⁹ The major risk factors for atherosclerosis include hyperlipidemia, hypertension, cigarette smoking, and diabetes.¹⁰ Most of these risk factors are more likely in an aging population, and stroke is much more prevalent in individuals over 55. According to the Centers for Disease Control and Prevention, the chance of having a stroke about doubles every 10 years after age 55. There are also several genetic factors that make stroke more likely, including the $\epsilon 4$ variant of the apolipoprotein E, a cholesterol carrying protein in the body also associated with a higher incidence of Alzheimer's disease.¹¹

1.1.1 Available Stroke Treatments

The discovery and implementation of tissue plasminogen activator (tPA) therapy and endovascular procedures have greatly reduced stroke mortality.¹² The first line treatment for acute ischemic stroke is tPA; however, it must be given within 4.5 hours of the onset of stroke.¹³ If the stroke is treated within 24 hours of the onset of stroke, mechanical thrombectomy can be used to partially or fully remove the offending clot.¹⁴ These treatments are helpful for minimizing the injury caused by the stroke; however, many patients do not have access to these treatments and are left with disabilities. It is estimated that 26% of survivors of stroke are impaired in activities of daily living and 50% have reduced mobility.¹⁵ Efforts have been made to investigate therapies that will halt the downstream ischemic cascade at the level of various biochemical, metabolic and molecular processes in the infarct border zone using neuroprotective agents, but have all failed in clinical trials.¹⁶

1.1.2 Rehabilitation following stroke

Survivors of stroke are often left with severe impairments. There is a period of about 3 months following stroke that many survivors will see some spontaneous recovery.¹⁷ The molecular changes underlying this spontaneous recovery include structural changes in axons, dendrites, and synapses; increase activation and migration of endogenous neural stems; and changes in extracellular matrix, glia, and angiogenesis.¹⁸ Therapies following stroke are commonly used to supplement this spontaneous recovery.¹⁹ Rehabilitation therapies such as physical therapy, occupational therapy, and speech therapy are designed to induce neuroplasticity in these survivors to promote functional recovery²⁰. Stroke survivors spend three weeks on average in an acute rehabilitation facility followed by

months of outpatient rehab and follow up. Unfortunately, approximately 40% of stroke survivors still remain with moderate to severe impairments that markedly reduce quality of life and require special care²¹.

1.1.3 Neuroplasticity

Rehabilitation strategies following stroke attempt to take advantage of the principles of neuroplasticity to bring about recovery.²² Neuroplasticity encompasses the functional and structural alterations in the brain enabling adaptation to the environment, learning, memory, as well as rehabilitation after brain injury.²³ Basic principles of neuroplasticity include synaptogenesis, neurogenesis, clearance of toxic amyloid beta and tau protein aggregates, and neuroprotection.²⁴ There have been many compounds produced that have been reported to induce long-lasting neuroplasticity including natural products (bilobalides²⁵ and curcumin²⁶) and novel vaccine AADvac1²⁷. Activity-dependent neuroplasticity is also inducible by regimens of exercises and therapies. Mechanical stimulation of brain regions can induce neuroplasticity through therapeutic hypothermia²⁸ or deep brain stimulation.²⁹

1.1.4 Markers of Stroke Severity

Several markers have been developed to monitor stroke severity. Several recovery assessments have been created to monitor functional recovery over the course of rehabilitation. Among these is the Self-Care Assessment created by the American Occupational Therapy Association.³⁰ The Self-Care Assessment determines how independently an individual can perform the follow tasks related to daily living (eating,

oral hygiene, toilet hygiene, shower/bathe self, upper body dressing, lower body dressing, and putting on/taking off footwear).

In addition to functional assessments, other tools such as magnetic resonance imaging can detect neurological recovery following stroke. T1 and T2 structural imaging is commonly used to calculate lesion size and location following stroke,³¹ but advanced imaging modalities such as diffusion tensor imaging,³² magnetic resonance spectroscopy,³³ and arterial spin labelling³⁴ can be used to detect white matter integrity, brain metabolites, and cerebral blood flow, respectively.

Finally, the NIH toolbox has been developed to assess cognitive, emotional, and sensation function in individuals using validated questionnaires.³⁵ It has been validated for use in stroke participants,³⁶ and is an effective way of monitoring additional modalities of recovery.

1.2 Gut Microbiome

The gut microbiome consists of more than a trillion microbes that dwell in the human gut.³⁷ While these microbes include bacteria, archaea, viruses, fungi, and protozoa, the bacterial component of the gut microbiome has been the best studied.³⁸ The major bacterial phyla that dwell in this community are Firmicutes and Bacteroidetes, with Actinobacteria, Proteobacteria, and Verrucomicrobia also making sizable contributions.³⁹ Within these phyla, there are approximately 300-500 bacterial species that live in a delicate balance.⁴⁰ These bacteria perform many metabolic tasks that are symbiotic to the host organism, including breaking down nutrients and producing important vitamins.³⁹ Dysbiosis occurs whenever the delicate balance of microbial communities is disrupted and is seen in the context of antibiotic therapy, inflammatory bowel diseases, diabetes, and obesity.⁴¹

The gut microbiome plays many roles in disease. For example, antibiotic therapy can lead to a dysbiotic state that allows *Clostridium difficile* infection to thrive.⁴² Genome wide association studies have linked inflammatory bowel disease with loci that implicate an aberrant immune response to the intestinal microbiota.⁴³ Acute gastroenteritis following exposure to pathogens can precipitate the development of irritable bowel syndrome, and studies have demonstrated changes in the gut microbiome in irritable bowel syndrome patients.⁴⁴ Bacteria causing weight gain are thought to induce the expression of genes related to lipid and carbohydrate metabolism thereby leading to greater energy harvest from the diet.⁴⁵ Experiments using gut microbiota transplants to germ-free animal models have shown that fatty liver disease development is determined by gut bacteria.⁴⁶

Attempts to modulate the gut microbiome typically come in the following mechanisms: fecal microbiota transplant, antibiotic administration, probiotic administration, dietary modifications, and exercise. Fecal microbiota transplantation is the transfer of stool from a healthy donor into the colon of a patient whose disease is a result of an altered microbiome, with the goal of restoring the normal microbiota and ameliorating the disease.⁴⁷ Fecal microbiota transplant is already an effective and approved therapy for *Clostridium difficile* infection.⁴⁸ Antibiotics have the ability to vastly alter the composition of the microbiome, with different antibiotics affecting the microbiome in different ways.⁴⁹ Probiotics are live organisms that have demonstrated beneficial effect on human health.⁵⁰ Diet modification has an effect on the microbiome since different bacterial species rely on various preferred fuel sources for survival.⁵¹ Prebiotic interventions are comprised of specific fuel sources that beneficial microbiota prefer; in general, these

prebiotic interventions contain some type of dietary fiber.⁵² Finally, aerobic exercise has a positive impact on the microbiome, shifting it towards a more beneficial balance.⁵³

The composition of the microbiome varies across the lifespan. The infant microbiome is thought to initially be colonized by the mother's vaginal bacteria or her skin bacteria, depending on whether the infant was delivered vaginally or by cesarean section.⁵⁴ Whether an infant is breastfed or formula-fed continues to modulate the early microbiome.⁵⁵ During adulthood, the microbiome remains relatively stable, like a dynamic fingerprint whose ridges sharpen or smooth in response to their environment. The microbiome has been shown to remain relatively stable between age 55 and 85, but it tends to look different in younger or older groups⁵⁵.

The microbiome is typically studied and measured by sequencing the bacteria recovered from fresh stool samples. The gut microbiome varies across the length of the gastrointestinal tract, looking a little different in the stomach, duodenum and jejunum, ileum, and large intestine.⁵⁶ Additionally, discrete bacterial communities form in the different layers of the gastrointestinal tract such as the gut lumen, colonic mucus layers, and colonic crypts.⁵⁷ The fecal microbiome is the best studied partly because of its ease of access and partly because a large diversity of microorganisms are known to inhabit the colon and to be transferred to the fecal material. The microbiome has frequently been sequenced using the highly conserved 16S ribosomal RNA gene.⁵⁸ This technique allows genus-level resolution of the microbiota to be detected. Whole genome shotgun sequencing is a newer technique that allows for species-level resolution measurements of the microbiome.

Once the bacteria have been sequenced, there are various metrics used for comparing the microbiome from one sample to another. The most popular metric is called alpha diversity, which measures the richness and evenness of a given microbial community. Richness measures how many different taxa are present while evenness measures how evenly the quantities of one species compare to the quantities of another.⁵⁹ Another metric considers beta diversity, which measures the degree of dissimilarity between one community and another.⁶⁰ Finally, relative abundance is used to measure the taxa as a proportion of the community from one sample to another.⁶¹

1.2.1 Gut-Brain Axis

The microbiome has been shown to affect and be affected by the brain via the bidirectional gut-brain axis⁶². The gut houses the largest collection of neurons outside of the central nervous system, the enteric nervous system. These neurons communicate with the brain via the vagus nerve superhighway. The brain can send autonomic inputs to the gut, modulating gut permeability and gut motility⁶³ and thereby disrupting the microbial ecosystem.

Members of the gut microbiota have been established as potent modulators of intestinal, systemic, and central nervous system immune cell function.⁶⁴ The microbes interact with the gut associated lymphoid tissue and the Peyer's Patches which activate cytokines and immune cells which travel systemically through the circulation and impact central nervous system function.⁶⁵ Immune cells in the blood circulation and gut lymphatic tissues that have been shaped by immune components including gut microbiota and metabolites can infiltrate the brain and, once there, influence neuronal function either directly or by modulating the properties of brain-resident immune cells.⁶⁶

Accumulating evidence suggests that gut microbes are modulators of brain plasticity via the gut-brain axis.⁶⁷ The microbiome is an important modulator of tryptophan metabolism, which is the precursor of the neurotransmitter serotonin.⁶⁸ About 95% of the serotonin in the body is found in the gut, with the other 5% in the brain.⁶⁹ In addition to tryptophan, other microbial metabolites are important in gut-brain signaling. The most important of these appears to be the short chain fatty acids, which are produced during the fermentation of partially and nondigestible polysaccharides. In the brain, the short chain fatty acids act as histone deacetylase inhibitors regulating gene expression and G-protein coupled receptors regulating metabolism and inflammation.⁷⁰ SCFA supplementation can induce cortex connectivity, spine and synapse density, and induce microglial cells to contribute to structural and functional remodeling of the brain via recruitment of T cells.⁷¹

Many changes in the brain associated with the gut microbiome and gut disorders have been documented with imaging. Ulcerative colitis has been associated with a significantly reduced blood oxygen level-dependent signal in the amygdala, thalamic regions, and cerebellar regions.⁷² Irritable bowel syndrome has been associated with long-term white matter integrity changes in the brain, especially in regions associated with integration of sensory information and corticothalamic modulation,⁷³ and lower volumes in the bilateral superior frontal gyrus, insula, amygdala, hippocampus, and middle orbital frontal gyrus.⁷⁴ Probiotic administration for 4 weeks has been associated with changes in brain activation patterns in response to emotional decision-making tasks.^{75,76} Short chain fatty acids (SCFAs) are known to influence blood brain barrier permeability⁷⁷ and alter cerebral blood flow⁷⁸. Finally, the gut microbiome is known to influence the transcriptional

activity of genes involved in neuronal myelination, thereby altering white matter integrity.⁷⁹

Other changes in the brain associated with the gut microbiome and gut disorders have been documented with functional, cognitive, emotional, and sensation testing. Increased proteobacteria and bacteroidetes and decreased firmicutes have been associated with poorer early functional outcomes following stroke⁸⁰ as measured by the modified Rankin Scale (mRS). Increased *Ruminococcaceae* and *Lachnospiraceae* families have been associated with good cognition.^{81,82} Microbiota-modulated metabolites such as cholecystokinin have the ability to impact emotion in the brain.⁸³ The abundance of streptococcus species have been associated with feeling more pain.⁸⁴

1.2.2 Stroke and the Gut Microbiome

Animal studies have shown that stroke causes severe gut dysbiosis⁸⁵. Stress signals project from the brain following stroke via the autonomic nervous system (ANS) and the hypothalamic pituitary adrenal (HPA) axis which lead to immunomodulation and increased gut permeability and decreased gut motility⁸⁶⁻⁸⁸. The microbial communities are subsequently disrupted and can cause issues in the context of stroke rehabilitation. The gut microbiome can produce neuro- and immunomodulatory substances such as short chain fatty acids, tryptophan and indole metabolites, neurotoxins, neurotransmitters, lipopolysaccharide (LPS), and peptidoglycan that can act locally on enteric neurons and immune populations to modulate distant functions in the CNS⁸⁹. In the context of stroke, gut dysbiosis leads to increased TH1 cells, TH17 cells, $\gamma\delta$ -T cells, and monocytes in gut-associated immune tissues that migrate to the peri-infarct region of the brain and increase infarct size^{90,91}. Fecal microbiota transplant can reverse stroke-induced dysbiosis in mice

and its negative effects on stroke recovery^{92,93}. Fecal transplant with sodium butyrate can also attenuate ischemic stroke injury.^{71,94-96} Age,⁹⁷ diet,⁹⁸⁻¹⁰⁰ and exercise¹⁰¹ modify the severity of dysbiosis following stroke.

Very few human studies have been performed to date to examine the gut-brain axis following stroke in a human population. Human studies thus far have suggested that gut dysbiosis occurs shortly following stroke at a single time point and that this dysbiosis is associated with increased alpha diversity,¹⁰² blood Apolipoprotein E,¹⁰³ IL-6,¹⁰⁴ phenylacetylglutamine,^{105,106} blood Trimethylamine-N-Oxide,¹⁰⁷⁻¹¹¹, and risk of pneumonia¹¹² and depression¹¹³ and decreased HDL¹¹⁴ and butyrate¹¹⁵, plus poor functional outcome^{80,116,117}, and 180-day mortality¹¹⁸. The severity of the dysbiosis can be modified by features such as enteral nutrition¹¹⁹ and Vitamin B12 deficiency.¹²⁰ However, no human studies have yet been performed to analyze changes in the microbiome over the first three-month course of stroke rehabilitation when recovery is known to be the greatest, and no human studies have analyzed whether these longitudinal changes correlate with increased gut permeability and subsequent recovery as measured by neuroimaging and functional testing.

1.3 Scope of Dissertation

Novel multimodal rehabilitation approaches are needed to promote plasticity and sensorimotor function to help these survivors by combining current rehabilitation therapies with other treatments designed to foster neuroplasticity. A baseline understanding of how the microbiome is associated with markers of brain health in acute stroke and in community dwelling older adults is foundational to this end. We plan to follow two Specific Aims:

Specific Aim 1. Analyze dysbiosis in the gut microbiome during first three weeks of stroke rehabilitation and associations with functional ability.

From stool samples, we will measure 1) changes in the gut microbiome using metagenomic sequencing and functional analysis of bacterial DNA and 2) intestinal inflammation and permeability markers in human subjects during the first three months of rehabilitation following ischemic stroke compared to control subjects who demonstrate risk factors for, but have not had, a stroke, and healthy controls. We will consider past medical history, medication history, diet, racial/ethnic background, and APOE genotype in our analysis. We will determine the associations between microbiota composition and markers of stroke recovery detectable by functional assessments in the Self Care Assessment and the NIH toolbox (cognitive, emotional, and sensation assessments).

Specific Aim 2. Identify the associations between dysbiosis and downstream neuroimaging markers in community dwelling older adults

We will identify the associations between microbiota composition and markers of brain health detectable by MRI imaging including structural imaging, hyperintensities, cerebral blood flow, and white matter integrity.

CHAPTER 2. MATERIALS AND METHODS

2.1 Participants

We recruited 42 Individuals aged 55-85 for this study. Participants were recruited according to the incidence of stroke statistics taking into consideration the population distribution of Kentucky. According to the Heart Disease and Stroke Statistics-2017 Update: A Report from the American Heart Association,¹²¹ stroke has a higher incidence in females than it does in males (54:46 ratio). Additionally, Blacks and Hispanics may be more likely to have a stroke than non-Hispanic whites. The Kentucky population distribution (Source: US Census 2017 5-Year American Community Survey) is 85.08% White Non-Hispanic and 7.88% Black or African American Non-Hispanic.

We recruited 12 patients in acute stroke rehabilitation care after first time ischemic stroke at Cardinal Hill Rehabilitation Hospital. A complete list of inclusion/exclusion criteria are in **Table 2.1**. Participants were required to not have an acute disease of chronic, clinically significant (unresolved, requiring on-going medical management or medication) pulmonary, gastrointestinal, dermatologic, hepatic or renal functional abnormality. Participants were required to not have had cancer or a positive test for HIV, HBV, or HCV. Participants were required to not be immunosuppressed or have had major surgery of the GI tract in the past five years. We obtained past data, including radiographic studies and medical history. These data were used solely for research purposes. Other variables including age, gender, marital status, education level, Body Mass Index, Apolipoprotein E status, history of conventional vascular risk factors (hypertension, diabetes mellitus, atrial fibrillation, hyperlipoproteinemia, and smoking habit), pre-stroke therapy, and acute

treatment (i.e., oral anticoagulants, antiplatelet agents, tPA, IV thrombolysis and/or mechanical thrombectomy, and/or antibiotics) were recorded for our analyses.

We recruited 30 patients from the University of Kentucky (UK) Internal Medicine clinic to serve as controls. 18 of these participants had not had a stroke but did have 1 or more common cardiovascular risk factors for stroke. 12 of these participants had not had a stroke or common cardiovascular risk factors for stroke. Participants followed the same inclusion/exclusion criteria listed above but must not have had a stroke.

2.1.1 Recruitment workflow for participants with acute stroke

Participants from the University of Kentucky (UK) stroke unit were informed of the study by the case management team at Cardinal Hill Rehabilitation Hospital upon admission. If patient or family gave permission, the case management team alerted study personnel to evaluate eligibility. If the patient was eligible, the study personnel approached the patient and/or family to explain the study and ask for consent. If the patient and/or family consented, the applicant collected demographic information, dietary assessment, NIH toolbox assessments, Self-Care Assessment, and oral swab. To retain the participants, study personnel placed a purple laminated banner in the patient room alerting hospital staff about the research study and alerted the attending physician, case manager, lab manager, Cardinal Hill Clinical Research Director, and department chair for Physical Medicine and Rehabilitation (PM&R) at Cardinal Hill. Study personnel again collected functional recovery assessments at hospital discharge and scheduled a follow-up visit at the UK Magnetic Resonance Imaging and Spectroscopy Center (MRISC) at the participants' preferred date and time. An appointment reminder with map and parking instructions was given to participants to decrease the chance of a forgotten appointment. Participants were

reminded by their preferred method of communication about the follow-up visit. Participants returned for a three-month follow-up visit for functional testing assessment, imaging, and mail-in kit for final stool sample. When the kit was received in the mail, participants received \$50 reimbursement to cover time and travel expenses. Due to the COVID-19 pandemic, many follow up appointments had to take place via Zoom.

2.1.2 Recruitment workflow for control participants with no stroke

Study personnel worked with the Center for Clinical and Translational Research at the University of Kentucky to advertise the study to the community. Brochures were placed in high traffic areas around campus. Study personnel also set up a profile with ResearchMatch that connects interested participants with research studies. When participants submitted interest in the research study, study personnel evaluated them for eligibility. If potential participants were eligible for the study (see **Table 2.2**), they were scheduled for a visit at UK MRISC for consent at the participants' preferred date and time. An appointment card with map and parking instructions was given to participants to decrease the chance of a forgotten appointment. If the participant consented, study personnel administered the functional recovery testing and imaging protocol, collected an oral swab sample, and provided the participant with a mail-in stool collection kit. The participant scheduled a follow-up visit at UK MRISC. Participants were reminded by their preferred method of communication about the follow-up visit. When the kit was received in the mail, participants received \$25 reimbursement to cover time and travel expenses. Due to the COVID-19 pandemic, many study visits were held via Zoom.

2.2 Study Design

Participants were followed over the course of three months as we collected the following information:

- Past medical history, medication history, diet, and racial/ethnic background at admission using questionnaire and Electronic Health Record
- APOE genotype at admission using oral swab
- Cognitive and motor function at baseline, discharge, and 3-month follow-up using NIH toolbox and Self-Care Assessment
- Gut microbiome and permeability markers at admission, discharge, and 3-month follow-up using stool samples
- MRI imaging at 3-month follow-up

The timeline of study visits and procedures is detailed in **Table 2.3**. This is a minimal risk, category 1 protocol that only includes donating stool and oral swab samples and assessing structural and functional outcomes using imaging and standardized cognitive, motor, sensory, and emotional measures that are validated against gold standard instruments. Any measures with a fall risk were eliminated. The only additional risk involved in this research is breach of confidentiality, although all precautions were made to only collect and database de-identified data from the participants. The following was collected from participants:

- **Medical History:** We obtained past medical history from the electronic health record and questionnaire. These data were used solely for research purposes. Each individual received a verbal and written explanation of the purposes, procedures, and potential hazards of the study, and written consent was obtained. Variables

including age, gender, racial/ethnic background, marital status, education level, Body Mass Index, history of conventional vascular risk factors (hypertension, diabetes mellitus, atrial fibrillation, hyperlipoproteinemia, and smoking habit), pre-stroke therapy, and acute treatment (i.e., oral anticoagulants, antiplatelet agents, tPA, IV thrombolysis and/or mechanical thrombectomy, and/or antibiotics) were recorded and used as covariates for our analyses.

- Food Frequency: The Dietary Screener Questionnaires (DSQ) in the NHANES 2009-10: DSQ was used to measure dietary intake over the last month.
- Oral Swab Sample: Oral Swab was used to determine APOE genotype.
- NIH Toolbox: Cognitive, Motor, Emotional, and Sensation measures from the NIH toolbox were performed upon admission and at 3 months follow-up following discharge. These tests are standard in the field and take approximately 30 minutes to perform.
- Self-Care CARE Items: Section GG Self-Care Items are routinely used in the clinical care of inpatient stroke rehab patients to measure functional recovery. We recorded all CARE scores from hospital stay for analysis.
- Stool Samples: Stool samples were collected at admission, discharge, and 3-month follow-up. Samples will be collected, genotyped, and analyzed using methods obtained from the International Human Microbiome Standards consortium to determine gut microbial biodiversity.
- Imaging: A follow-up brain scan using MRI was obtained at outpatient follow-up visit 3 months following discharge for research purposes.

Each individual received a verbal and written explanation of the purposes, procedures, and potential hazards of the study, and written consent was obtained. Study personnel consented subjects using the University of California, San Diego Brief Assessment of Capacity to Consent (UBACC) to ensure capacity. Subjects lacking capacity were allowed to enroll and participate in the study if a legal representative authorized it. Signed consent was obtained before definite enrollment of the subject in this study. Subjects were free to withdraw from the study at any time. This research had minimal risk.

Given the broad heterogeneity of the gut microbiome composition among individuals, the prospect of performing a true case-control study is not likely. However, the study design presented here provides average conglomerates of the gut microbiome in two control groups: 1) older adults who have risk factors for stroke but have never had a stroke and 2) healthy older adults. These conglomerates were important comparators to gain a general idea of which microbial communities are disturbed following stroke and how they change over time. All analyses were performed in a quasi-experimental difference-in-differences fashion¹²² in which the difference of the outcome measures in the stroke rehab group was compared to the difference of the outcome measures in the control groups. The repeated-measures design allows each participant to be compared to his or her own baseline, which was especially useful to reduce variability in the data since randomization was not possible in our setting¹²³.

2.2.1 Stool Sample Collection

Stool samples were collected in Zymo DNA stabilization solution with sarstedt feces tubes from feces catcher placed on toilet seat.

2.2.2 Metagenomic Sequencing

Genomic DNA was extracted from 0.25 grams of stool using ZymoBIOMICS™ DNA Mini Kit and shipped to the Genomics and Microbiome core facility at Rush University for DNA quantification using fluorometer Qubit 3.0. Libraries were constructed and the PCR products purified using 1.0X speed beads and eluted in 15 uL of nuclease-free water and quantified by PicoGreen fluorometric assay (100X final dilution). The libraries were pooled and loaded onto a high sensitivity chip run on the Caliper LabChipGX (Perkin Elmer, Waltham, MA) for size estimation and sequenced using Illumina NextSeq/HiSeq platform.

2.2.3 Metagenomic Bioinformatic Analysis

Unassembled sequencing reads were analyzed by the Core for Research Informatics at the University of Illinois Chicago for microbiome analysis. Alpha diversity, beta diversity, and relative abundance counts were calculated. For alpha diversity, raw counts were rarefied to 2000k and the Shannon diversity index was calculated using the vegan R package. For beta diversity, the Bray-Curtis dissimilarity index was used and a Principal Component Analysis (PCA) plot was generated to visualize the diversity. We used MetaPhlAn (Metagenomic Phylogenetic Analysis) to profile the composition of microbial communities using unique clade-specific marker genes identified from ~17,000 reference genomes (~13,500 bacterial and archaeal, ~3,500 viral, and ~110 eukaryotic).¹²⁴ We used MaAsLin2 R package to normalize all microbiome variable and correlate them with metadata variable using linear regression models.¹²⁵

2.2.4 Intestinal Inflammation and Permeability Analysis

We tested stool samples for markers of intestinal inflammation and permeability using ELISA. The Biovender Alpha-1-antitrypsin in stool human ELISA was used to detect fecal Alpha-1-Antitrypsin (A1AT), a biomarker of intestinal permeability¹²⁶⁻¹²⁸. It is one of the principal serum proteins, and, in the context of intestinal permeability, A1AT can extravasate from the serum into the gut and be detected in the feces since it is highly resistant to proteolysis in the intestine¹²⁹. The Biovender Fecal calprotectin ELISA was used to detect fecal calprotectin, a sensitive marker of intestinal inflammation^{130,131}. It constitutes up to 60% of the cytosolic proteins in human neutrophil granulocytes, and, in the context of intestinal inflammation, activated granulocytes migrating into the intestinal wall will overexpress and release calprotectin into feces¹²⁹.

2.2.5 Diet Analysis

We assessed diet history using the Dietary Screener Questionnaire in the National Health and Nutrition Examination Survey. We analyzed the results of the survey using SAS statistical software to determine estimated intake of fiber, calcium, whole grains, sugar, dairy, fruits and vegetables, and sugar sweetened beverages.

2.2.6 APOE Genotyping

We collected oral swabs from all participants and placed them in Zymo DNA stabilization solution. We sent the oral swabs to the Core for Research Informatics at the University of Illinois Chicago for DNA extraction and amplification. The core performed PCR to amplify

and measure SNPs rs429358 and rs7412 that define the common allelic variants of Apolipoprotein E.

2.2.7 Imaging Analysis

MRI images were collected from all participants on a 3T Prisma MR scanner (Siemens, Germany) at UK's Magnetic Resonance Imaging & Spectroscopy Center. We collected the following sequences from participants: Turbo Gradient Spin Echo for Arterial Spin Labelling, resting state functional magnetic resonance imaging, magnetization-prepared 180 degrees radio-frequency pulses and rapid gradient-echo, diffusion tensor imaging, spectroscopy using chemical shift imaging sLASER sequence with a TE of 40ms, and Fluid-attenuated inversion recovery (FLAIR) imaging.

2.2.7.1 Arterial Spin Labeling

Quantitative CBF (with units of mL/g per minute) was measured using a pulsed arterial spin labeling (PASL) PICORE Q2T sequence with a TR=4400ms and a TE=20.8ms. We used FreeSurfer software to process relative cerebral blood flow (relCBF) data produced by the Siemens scanner. The automated software provides relCBF averages over the FreeSurferColorLUT.txt set of ROIs.

2.2.7.2 Structural Imaging

High-resolution, 3D anatomic images were acquired using an MP-RAGE sequence [repetition time (TR) = 2530 ms, echo time (TE) = 2.26 ms, flip angle (FA) = 7°, 1 mm isotropic voxels, 6:19 min]. We used the FreeSurfer Software Suite to segment and quantify brain volumes.

2.2.7.3 Diffusion Tensor Imaging

White matter integrity was measured using an axial double refocused spin echo, echo planar imaging ¹³² Diffusion Tensor Imaging (DTI) sequence with the following parameters: TR=3400 ms, TE=71 ms, field of view = 232 mm, 81 slices, 2 mm isotropic resolution. The DTI images were acquired with 128 noncollinear encoding directions (b=2000 s/mm²) and 6 images without diffusion weighting (b = 0 s/mm², b₀). DTI data were analyzed with FSL (Functional MRI of the Brain software library, FMRIB) to calculate fractional anisotropy (FA) values.

2.2.7.4 Fluid-attenuated inversion recovery (FLAIR) imaging

Hyperintensities were measured with fluid-attenuated inversion recovery (FLAIR) imaging [TR=5000ms, TE=388ms, FA=120°, 1mm isotropic voxels, 176 slices.] Vascular hyperintensity volumes will be calculated using the WMH cross-sectional kit, a combination of several programming tools and software, including Matlab, FSL, SPM, FreeSurfer, and Singularity container^{133,134}.

2.2.7.5 Magnetic Resonance Spectroscopy

Brain metabolites were measured with a chemical shift imaging (CSI) sequence that incorporates localization by adiabatic selective refocusing (LASER) for FOV-reduction¹³⁵. semi-laser sequence [TR=1700ms and TE=40ms]. All MRS slices were placed parallel to the anterior commissure-posterior commissure line. The volume of interest was centered to the medial to posterior part of the corpus callosum, with with VOI = 80 (l-r) × 80 (a-p) and field of view (FOV) = 160 × 160 mm³. The acquired matrix size was 10 × 10 × 15 mm. Two voxels that contained pure white matter were selected from each participant and averaged for analysis. Spectra were calculated using LCModel Software¹³⁶.

2.3 Functional Analysis

Functional analysis was measured using the Self-Care CARE Assessment from Section GG of the standardized patient assessment data elements in the following domains: Eating, Oral Hygiene, Toileting Hygiene, Shower/Bathe Self, Upper Body Dressing, Lower Body Dressing, Putting on/Taking off Footwear.³⁰ Stroke patients were graded on these domains for how independently they were able to perform them on a scale from 1 to 6, with 1 being dependent and 6 being independent.

2.4 NIH Toolbox

Cognitive, Emotional, and Sensation function was measured using assessments from the NIH toolbox. The picture vocabulary test was used to measure long-term or crystallized memory.¹³⁷ The list sorting test was used to measure short-term memory, attention, and executive function.¹³⁸ The sadness,¹³⁹ meaning and purpose,¹⁴⁰ self-efficacy,¹⁴¹ and support¹⁴² questionnaires were used to measure self-reported values of these emotional domains. The pain intensity scale¹⁴³ was used to measure sensation.

2.5 Statistical Analysis

All statistical analyses were completed using JMP Statistical Software (SAS, Cary, NC, USA) and R Statistical Software^{125,144}. For all chapters, two-sample t-test and 2-way ANOVA were used to determine differences between groups. The MaAsLin 2 R Package was used to normalize all variables and employ linear regression analysis to correlate

various variables with microbiome measures.¹⁴⁴ A false discovery rate of $q < 0.25$ was used in selecting significant variables to correct for multiple comparisons.

Table 2.1 Inclusion and Exclusion Criteria used to evaluate eligibility for acute stroke patients

<u>Inclusion Criteria</u>	<u>Exclusion Criteria</u>
<ul style="list-style-type: none"> • Ischemic stroke (small vessel lacunar stroke or cortical stroke <70 cc³) • Discharged from acute stroke service with NIHSS of 5-14 (moderate stroke) • Has diagnostic stroke MRI imaging available • Age 55-85 	<ul style="list-style-type: none"> • Any acute disease or chronic, clinically significant (unresolved, requiring ongoing medical management or medication) lung, bowel, skin, liver, kidney, or brain abnormality • Dementia, Cancer, HIV, hepatitis, immunosuppressed, major GI surgery in the past 5 years • Not MRI compatible • Participating in another research study

Table 2.2 Inclusion and Exclusion Criteria used to evaluate eligibility for no stroke patients with A) risk factors for stroke and B) no risk factors for stroke

A)	
<p><u>Inclusion Criteria</u></p> <ul style="list-style-type: none"> • Age 55-85 • Has at least one major risk factor for stroke (High blood pressure, Diabetes, Heart and blood vessel diseases, High LDL cholesterol levels, Smoking, Brain aneurysms or arteriovenous malformations (AVMs), Infections or conditions that cause inflammation, such as lupus or rheumatoid arthritis, birth control pills, or hormone replacement therapy) 	<p><u>Exclusion Criteria</u></p> <ul style="list-style-type: none"> • Any previous stroke • Any acute disease or chronic, clinically significant (unresolved, requiring ongoing medical management or medication) lung, bowel, skin, liver, kidney, or brain abnormality • Dementia, Cancer, HIV, hepatitis, immunosuppressed, major GI surgery in the past 5 years • Not MRI compatible • Participating in another research study
B)	
<p><u>Inclusion Criteria</u></p> <ul style="list-style-type: none"> • Age 55-85 	<p><u>Exclusion Criteria</u></p> <ul style="list-style-type: none"> • Any previous stroke • Any acute disease or chronic, clinically significant (unresolved, requiring ongoing medical management or medication) lung, bowel, skin, liver, kidney, or brain abnormality • Dementia, Cancer, HIV, hepatitis, immunosuppressed, major GI surgery in the past 5 years • Major risk factors for stroke (High blood pressure, Diabetes, Heart and blood vessel diseases, High LDL cholesterol levels, Smoking, Brain aneurysms or arteriovenous malformations (AVMs), Infections or conditions that cause inflammation, such as lupus or rheumatoid arthritis, birth control pills, or hormone replacement therapy) • Not MRI compatible • Participating in another research study

Table 2.3 Timeline of study visits and procedures

Table 1. Timeline of study visits and procedures					
Procedure	Participants with Acute Stroke			Control Participants (no stroke and chronic stroke)	
	Admission	Discharge	Outpatient follow up visit 3 months after admission	Baseline Visit	3-month follow up visit
Signing the consent form	X			X	
Stool Sample	X	X	X	X	X
Mouth Swab Sample	X	X	X	X	
MRI Scan			X	X	
Functional Recovery Testing	X	X	X	X	X

CHAPTER 3. THE GUT MICROBIOME IS ALTERED IN THE CONTEXT OF STROKE AND IS CORRELATED WITH IMPAIRED FUNCTION

3.1 Introduction

Over 795,000 people suffer a stroke every year in the United States alone¹. Recent advances in acute stroke therapies have lowered stroke mortality, but survivors are often left severely impaired¹². Rehabilitation therapies such as physical therapy, occupational therapy, and speech therapy are beneficial for inducing neuroplasticity to overcome these impairments²⁰, but over 40% of stroke survivors are left with moderate to severe disabilities that markedly reduce quality of life²¹. Novel multimodal approaches are needed to promote plasticity and sensorimotor function through a combination of current rehabilitation therapies with other treatments designed to foster neuroplasticity.

Accumulating evidence from animal studies suggests that gut microbes modulate brain plasticity via the bidirectional gut-brain axis and may play a role in stroke rehabilitation⁶⁷. A severely imbalanced microbial community, or dysbiosis, has been shown to occur following stroke, causing a systemic flood of neuro- and immunomodulatory substances due to increased gut permeability and decreased gut motility⁸⁵. These substances can impact neuroinflammation as commensal bacteria invade the bloodstream and as intestinal lymphocytes migrate from gut-associated lymphoid tissue to the brain⁹². Fecal microbiota transplant has been shown to normalize brain lesion-induced dysbiosis and to improve stroke outcome in mice⁹². The microbiome is modifiable as it is influenced by environmental factors such as diet and exercise and could potentially be a therapeutic target in stroke rehabilitation through nutritional and pharmacological interventions and physical therapy^{89,145}. Though it is unknown whether the findings from

the bidirectional gut-brain axis in animals translate the same way into humans. Human studies thus far have suggested that gut dysbiosis occurs shortly following stroke at a single time point and that this dysbiosis is associated with increased blood Apolipoprotein E¹⁰³ and IL-6¹⁰⁴, and decreased blood Trimethylamine-N-Oxide¹⁰⁷ and HDL¹¹⁴, plus poor early functional outcomes⁸⁰, and 180-day mortality¹¹⁸. However, no human studies have been performed to analyze changes in the microbiome over the first three-week course of stroke rehabilitation and whether these changes correlate with gut permeability and subsequent recovery as measured by functional testing, making it difficult to confirm whether the microbiome could be a therapeutic target in stroke rehabilitation.

Several markers have been developed to monitor stroke severity. Several recovery assessments have been created to monitor functional recovery over the course of rehabilitation. Among these is the Self-Care Assessment created by the American Occupational Therapy Association³⁰. The Self-Care Assessment determines how independently an individual can perform the following tasks related to daily living: eating, oral hygiene, toileting hygiene, shower/bathe self, upper body dressing, lower body dressing, and putting on/taking off footwear. The NIH Toolbox has been developed to assess cognitive, emotional, and sensation function in individuals using validated questionnaires³⁵. Changes in the brain associated with the gut microbiome and gut disorders have been documented with functional, cognitive, emotional, and sensation testing. Increased *Proteobacteria* and *Bacteroidetes* and decreased *Firmicutes* have been associated with poorer early functional outcomes following stroke⁸⁰ as measured by the modified Rankin Scale (mRS). Increased *Ruminococcaceae* and *Lachnospiraceae* families have been associated with good cognition^{81,82}. Microbiota-modulated metabolites such as

cholecystokinin have the ability to impact emotion in the brain⁸³. The abundance of *Streptococcus* species have been associated with heightened sensitivity to pain⁸⁴.

Here we document the gut-brain axis changes that occur following stroke in the first three weeks of rehabilitation and their associations with functional recovery measures in 12 stroke participants and 30 community dwelling adults. We measure the gut microbiome using whole genome shotgun sequencing on stool samples. We measure Self-Care CARE Assessment for function, the picture vocabulary and list sorting tasks for cognition, self-efficacy, sadness, support, meaning and purpose questionnaires for emotion, and pain intensity for sensation. We compare associations of tasks with the microbiome in the stroke population and control populations separately to provide a foundational knowledge of how the microbiome is associated with functional tasks in healthy and stroke populations.

3.2 Results

3.2.1 Participant Characteristics

We recruited 12 participants from the acute rehabilitation hospital setting upon admission and 30 control participants from a community dwelling sample divided into two categories: 1) controls at risk for stroke who have not had a stroke and 2) healthy controls. Participants were required to not have an acute disease or chronic, clinically significant (unresolved, requiring on-going medical management or medication) pulmonary, gastrointestinal, dermatologic, hepatic, or renal functional abnormality. Participants were required to not have had cancer or a positive test for HIV, HBV, or HCV. Participants were required to not be immunosuppressed or have had major surgery of the GI tract in the past five years. Participants also had to be MRI compatible. **Table 1** describes the basic

demographic characteristics of the participants. There were 12 participants in the acute stroke group, 18 in the at risk group, and 12 in the healthy control group. Those in the acute stroke group were slightly older than those in either control group. The healthy control group had a higher percentage of female participants. All of the groups were mostly white, with the at risk group containing two black participants and the healthy control group containing one Asian participant. The acute stroke group and healthy control group had over 20% APOE ϵ 2 carriers while the at risk group contained none. The participants in the acute stroke group were less educated than those in the control groups. The healthy group had a lower BMI than the stroke group and the at risk control group. The healthy control group by definition had no participants with diabetes, hypertension, or hyperlipidemia.

3.2.2 Stroke microbiome with pro-inflammatory and fewer butyrate producing taxa

Figure 3.1 shows the alpha diversity of the various groups using the Shannon diversity index. The acute stroke group had a diversity of 3.85 ± 0.385 , the at risk group had a diversity of 3.88 ± 0.273 , and the healthy control group had a diversity of 3.81 ± 0.392 . There were no significant differences between the groups on a pairwise Mann-Whitney test with an $\alpha=0.05$. **Figure 3.2** shows the beta diversity of the various groups using the Bray-Curtis dissimilarity index. An ANOSIM R test reveals a significant dissimilarity between the acute stroke and at risk groups ($R=0.405$, $p=0.001$) and a significant dissimilarity between the acute stroke and healthy control groups ($R=0.126$, $p=0.039$). The dissimilarity between the at risk and healthy control groups was not significant ($R=0.0381$, $p=0.228$). **Figure 3.3** shows the distribution of the most prevalent bacterial phyla amongst the participant groups. The acute stroke group was 39.4% *Bacteroidetes*, 2.44% *Verrucomicrobia*, 24.3% *Proteobacteria*, 7.1% *Actinobacteria*, and 25.2% *Firmicutes*. The

at risk group was 33.1% *Bacteroidetes*, 1.68% *Verrucomicrobia*, 21.9% *Proteobacteria*, 6.4% *Actinobacteria*, and 35.5% *Firmicutes*. The healthy control group was 35.4% *Bacteroidetes*, 3.0% *Verrucomicrobia*, 25.6% *Proteobacteria*, 4.7% *Actinobacteria*, and 29.7% *Firmicutes* (**Figure 3.3**). A detailed analysis of the microbial taxa shows significant decreases in butyrate producers (*Agathobaculum butyriciproducens*, *Lawsonibacter asaccharolyticus*, *Anaerostipes hadrus*, the genus *Roseburia*, and *Eubacterium rectale* (**Figure 3.4a-e**)), secondary bile acid producers (*Blautia obeum* and the genus *Ruminococcus* (**Figure 3.4f,g**)), equol producers (*Adlercreutzia equolifaciens* (**Figure 3.4h**)) and sulfate reducers (the family *Desulfovibrionaceae* (**Figure 3.4i**)). There was a significant increase in several pro-inflammatory taxa, including *Clostridium aldenense*, *Clostridium bolteae*, the genus *Anaeromassilibacillus*, *Ruthenibacterium lactatiformans*, and *Acidaminococcus intestini* (**Figure 3.4j-n**).

3.2.3 Stroke dysbiosis is associated with leaky gut markers

Figure 3.5 shows the average of the leaky gut markers amongst the groups. The calprotectin assay is a marker for intestinal inflammation and did not show differences among the groups (**Figure 3.5a**). Alpha-1-antitrypsin is a marker for intestinal permeability and was significantly increased in the acute stroke group (**Figure 3.5b**). **Table 3.2** shows the associations of alpha-1-antitrypsin with various microbial taxa. The presence of alpha-1-antitrypsin was inversely associated with several microbial taxa, including *Adlercreutzia equolifaciens*, *Lawsonibacter asaccharolyticus*, the genus *Anaerostipes*, *Blautia obeum*, *Coprococcus eutactus*, *Dorea longicatena*, *Lachnospira pectinoschiza*, the genus *Roseburia*, *Agathobaculum butyriciproducens*, and the genus *Ruminococcus*. (**Figure**

3.6a-j). Alpha-1-antitrypsin was positively associated with *Eggerthella lenta*, *Clostridium bolteae*, *Anaerotruncus colihominis*, and *Clostridium leptum*. (**Figure 3.6k-n**).

3.2.4 Some bacteria are associated with diet

Figure 3.7 shows the diet composition amongst the different participant groups. The stroke group ate significantly less fiber (**Figure 3.7a**) and fruits and vegetables (**Figure 3.7f**) and more sugar sweetened beverages (**Figure 3.7g**). We correlated diet composition with microbial taxa in the stroke group using linear correlation (**Table 3.3**). We found that an increase of fruits and vegetables was associated with a lower abundance of the genus *Bacteroides*, *Eisenbergiella massiliensis*, and *Holdemania filiformis* (**Figure 3.8a-c**) and a higher abundance of *Ruminococcus torques* and *Faecalibacterium prausnitzii* (**Figure 3.8d,e**). A higher intake of vegetables only was associated with an increase in the relative abundance of *Clostridium bolteae* (**Figure 3.8f**).

3.2.5 Microbiota are associated with markers of stroke recovery

3.2.5.1 Functional Testing

On the GG Self Care Assessment, the stroke group reported an average score of 25.4 out of 42 on admission to the hospital and an average score of 36.6 on discharge from the hospital (**Figure 3.9a**). *Collinsella aerofaciens* was positively correlated with self care scores (**Table 3.4, Figure 3.10a**).

3.2.5.1 Cognitive Testing

On average, the stroke group scored in the 35th percentile on the picture vocabulary test, the at risk group scored in the 52nd percentile, and the healthy control group scored in

the 53rd percentile. On the list sorting test, the stroke group scored in the 38th percentile, the at risk group scored in the 52nd percentile, and the healthy control group scored in the 57th percentile (**Figure 9b,c**). The genus *Roseburia* was positively correlated with scores on the picture vocabulary test for the stroke group (**Table 3.4, Figure 3.10b**).

3.2.5.1 Emotional Testing

On the self-efficacy test, the stroke group scored in the 45th percentile on average, the at risk group scored in the 54th percentile on average, and the healthy control group scored in the 57th percentile on average (**Figure 3.9d**). *Bacteroides uniformis* and *Alistipes putredinis* were positively correlated with self-efficacy score and *Escherichia coli* was negatively correlated with self-efficacy (**Table 3.4, Figure 3.10c**). On the sadness test, the stroke group scored in the 55th percentile on average, the at risk group scored in the 48th percentile on average, and the healthy control group scored in the 50th percentile on average (**Figure 3.9e**). On the meaning and purpose test, the stroke group scored in the 44th percentile on average, the at risk group scored in the 53rd percentile on average, and the healthy group scored in the 52nd percentile on average (**Figure 3.9f**). The family *Eubacteriaceae* was positively correlated with the score on the meaning and purpose questionnaire (**Table 3.4, Figure 3.10e**). On the support test, the stroke group reported support levels in the 47th percentile on average, the at risk group report support levels in the 51st percentile on average, and the healthy control group reported support levels in the 46th percentile on average (**Figure 3.9g**). From the *Actinobacteria* phylum, the class *Coriobacteriia* is positively correlated with support. From the *Bacteroidetes* phylum, the family *Odoribacteraceae* is positively correlated with support. From the *Firmicutes* phylum, the genus *Eubacterium*, the family *Acidaminococcaceae*, *Roseburia intestinalis*,

and *Phascolarctobacterium faecium* are positively correlated with support. From the *Bacteroidetes* phylum, *Bacteroides ovatus* is negatively correlated with support. From the *Firmicutes* phylum, *Erysipelatoclostridium ramosum* and *Flavonifractor plautii* were negatively correlated with support. From the *Proteobacteria* phylum, the family *Veillonellaceae* was negatively correlated with support (**Table 3.4, Figure 3.10d**).

3.2.5.1 Sensation Testing

On the pain questionnaire, the stroke group reported a 4.9 out of 10, the at risk group reported a 2 out of 10, and the healthy control group reported a 3.25 out of 10 (**Figure 3.9h**). In the stroke group, *Alistipes shahii* was positively correlated with pain scores (**Table 3.4, Figure 3.10f**).

3.3 Discussion

Here we measured the gut microbiome in the first three weeks of rehabilitation following stroke and its associations with functional recovery measures in 12 stroke participants and 30 community dwelling adults. We found significantly lower abundances of butyrate producers, secondary bile acid producers, equol producers, and sulfate reducers in the stroke group and significantly higher abundances of pro-inflammatory taxa.

Our work found no significant differences in alpha diversity between groups. This is consistent with a previous human study that found no differences in alpha diversity between cerebral infarction patients and healthy controls¹¹⁴. However, we did find significant dissimilarity between the groups on beta diversity which is consistent with previous human studies that found high dissimilarity between ischemic stroke patients and healthy controls^{102,115}. A detailed analysis of the relative abundance of the microbial taxa

revealed several taxa which were lower in the stroke group compared to either of the control groups. *Agathobaculum butyriciproducens* is a strictly anaerobic and butyric acid-producing bacteria that has had impressive success in restoring cognition in Alzheimer's disease mouse models¹⁴⁶. *Anaerostipes hadrus* can produce butyrate from carbohydrates or lactate^{147,148} and is often decreased in diabetes¹⁴⁹. *Eubacterium rectale* is also a butyrate producer¹⁵⁰ responsible for metabolizing dietary plant polysaccharides¹⁵¹; it is increased in obesity¹⁵² and reduces inflammatory dendritic cells¹⁵⁰. *Lawsonibacter asaccharolyticus* is also a butyrate producer¹⁵³. *Blautia obeum* is a natural producer of bile salt hydrolases¹⁵⁴ as well as lantibiotics that inhibit the growth of pathogenic bacteria¹⁵⁵; it has previously been shown to be decreased in acute cerebral infarction¹⁵⁶. *Roseburia* is a butyrate producer¹⁵⁷ that utilizes acetate¹⁴⁸ and increases serotonin and melatonin and is reduced in ulcerative colitis¹⁵⁸ and hypertension¹⁵⁹; treatment with *Roseburia hominis* in ulcerative colitis has been shown to strengthen gut barrier function and enhance T regulatory cells¹⁶⁰. *Ruminococcus* bacteria produce secondary bile acids¹⁶¹. *Adlercreutzia equolifaciens* is an equol producer¹⁶² and low abundances have been associated with primary sclerosing cholangitis¹⁶³. *Desulfovibrionaceae* reduces sulfate¹⁶⁴.

Several bacterial taxa were higher in the stroke group as compared to the control groups. *Ruthenibacterium lactatiformans* is an obligate anaerobe that is a major lactate producer and is also found to be increased in patients with multiple sclerosis¹⁶⁵. *Clostridium bolteae* is an obligate anaerobe commonly found to be increased in patients with autism¹⁶⁶, neuromyelitis optica spectrum disorders¹⁶⁷, multiple sclerosis^{168,169}, and spondyloarthritis¹⁷⁰. *Acidaminococcus intestini* has been associated with a pro-inflammatory diet¹⁷¹. Increased abundance of the genus *Lachnoclostridium* is associated

with ulcerative colitis¹⁷² and obesity¹⁷³. The genus *Anaeromassilibacillus* is associated with malnutrition¹⁷⁴.

Importantly, the healthy control group contained a significant percentage of APOE ϵ 2 carriers, which potentially shapes the gut microbiome characteristics for this group with a higher relative abundance of *Ruminococcaceae* and *Gemmiger* species and a lower abundance of *Prevotellaceae* species¹⁷⁵.

Alpha-1-antitrypsin can be a marker of increased intestinal permeability when it is found in the stool. Calprotectin can be a marker of intestinal inflammation. There was a large increase of fecal alpha-1-antitrypsin in our participants with stroke. Gut inflammatory and immune responses following stroke are central to this increased gut permeability. The bacteria that we found are disrupted following stroke which also correlate with alpha-1-antitrypsin include increased *Clostridium bolteae* and decreased *Adlercreutzia equolifaciens*, *Anaerostipes*, *Roseburia*, *Ruminococcus*, *Blautia obeum*, *Agathobaculum butyriciproducens*, and *Lawsonibacter asaccharolyticus*. *Roseburia* has consistently been associated with intestinal permeability both as a microbe that bolsters intestinal permeability¹⁷⁶ and as a microbe that changes in response to changes in the intestinal permeability¹⁷⁷⁻¹⁷⁹. We did not see a significant increase in calprotectin, likely because it is less stable at room temperature¹⁸⁰.

We found that certain dietary features are associated with the abundance of specific bacteria. This is congruent with other groups who have found that dietary modification is associated with gut microbiome composition¹⁸¹. In our study particularly, we found that most of the bacteria which were affected by stroke were not affected by diet, with the exception of a positive relationship *Clostridium bolteae* with vegetable intake. This is

interesting since *Clostridium bolteae* was increased in stroke. There are many studies that describe the effects of a vegetarian diet on the microbiome^{182,183}.

Our results indicate that the participants performed functionally better at discharge than at admission to the hospital. This is expected in the rehab setting. The species *Collinsella aerofaciens* was positively correlated with the Self Care Assessment. *Collinsella aerofaciens* is a natural bile salt hydrolase producer^{154,184} that is naturally increased in response to a cow milk supplemented diet^{185,186}. While *Collinsella aerofaciens* is generally considered to be a proinflammatory species that increases gut permeability¹⁸⁷, it has been associated with healthy clinical outcomes¹⁸⁸. While bile acids do not normally cross the blood brain barrier, in the context of a leaky blood brain barrier, they can accumulate in the hypothalamus and inhibit the hypothalamic-pituitary-adrenal axis, thereby suppressing the inflammatory response^{189,190}.

Participants in the stroke group perform more poorly on cognitive tests compared to those in the control groups. Cognitive impairment is common following stroke and is often the precursor to dementia and cognitive decline¹⁹¹. Amongst stroke participants, the genus *Roseburia* was positively correlated with performance on the picture vocabulary test. Previous groups have seen a correlation of memory performance with *Roseburia*^{192,193}. It is possible that *Roseburia* enhances memory performance through butyrate production since butyrate has been shown to be a cognitive enhancer of a weak memory¹⁹⁴.

We found that the stroke group reported lower self-efficacy than the control groups. *Bacteroides uniformis* and *Alistipes putredinis* were positively correlated with self-efficacy and *Escherichia coli* was negatively correlated with self-efficacy. The concept of self-efficacy encapsulates a person's perception of their capability for performance¹⁹⁵. Self-

efficacy has been shown to be a strong variable in impacting recovery following stroke¹⁹⁶. While it is not known why these taxa correlate with self-efficacy, it is possible that individuals with a higher self-efficacy are more likely to make healthy choices following stroke which would correlate with butyrate producing bacteria like *Bacteroides uniformis* as opposed to inflammatory species like *Escherichia coli*¹⁹⁷. The *Enterobacteriaceae* family, which *E. coli* is from, has previously been reported as being associated with bad outcomes in the context of stroke^{118,198,199}.

We found that the stroke group reported lower meaning and purpose than the control groups. The family *Eubacteriaceae* was positively correlated with scores on the meaning and purpose questionnaire. Depression is a common phenomenon following stroke²⁰⁰ and is characterized by low purpose in life. Increasing purpose in life has been proposed as a possible treatment for stroke^{201,202}. The gut microbiome has previously been implicated in the development of post-stroke depression and correlated with dysregulation of lipid metabolism¹¹³.

The stroke group reported similar levels of support to those of the control groups. The class *Coriobacteriia* was positively correlated with support. Social isolation stress has been shown to alter the gut-brain axis²⁰³. The class *Coriobacteriia* contains many species which are equol producers. Since equol producers and butyrate producers are associated with social support, it is possible that one mechanism by which people who have strokes who have more support do better is mediated by the microbiome.

The stroke group reported experiencing more pain than the control groups. Pain is a very common phenomenon following stroke and can include complex regional pain syndrome, musculoskeletal pain, spasticity-related pain, and post-stroke headache²⁰⁴. In

the stroke group, *Alistipes shahii* was positively associated with reported pain. The abundance of *Alistipes shahii* is highly positively correlated with trimethylamine-N-oxide (TMAO), a marker of poor cardiometabolic health²⁰⁵. While it is unknown how *Alistipes shahii* is associated with pain, many other studies have linked the microbiome with pain²⁰⁶, including other species of *Alistipes* with pain²⁰⁷.

While this study provides valuable insights into the associations of the composition of bacterial communities in the gut and various markers of stroke recovery, it has many limitations. As a prospective case control study, it cannot definitively say that the associations are causing stroke recovery to be altered. Future experiments should test the associations found here to determine causation. Additionally, our sample consists largely of older white adults from Kentucky. Larger studies comprising more diverse populations are needed to see whether these associations are generalizable. Furthermore, we used a false discovery rate of $q < 0.25$. This means that up to 25% of our found associations may be false positives. More targeted experiments are needed in the future to better characterize these associations.

Altogether, we found that stroke was associated with an increase of pro-inflammatory bacterial taxa and a decrease in taxa that produce butyrate and secondary bile acids necessary for healthy metabolic function. This shift towards inflammation is likely due to the activation of the sympathetic nervous system and hypothalamic-pituitary-adrenal axis in response to the stroke that increase gut permeability and decrease gut motility. While this inflammatory shift can help to mitigate the acute effects of stroke in the brain, the residual inflammation in the weeks and months following the stroke is likely undermining recovery. Previous studies have also found that butyrate-producing bacteria

were significantly reduced in cerebral ischemia patients and that this reduction is associated with poor outcomes^{115,208,209}. Future studies should explore treatments targeting the composition of microbial communities following stroke as a way to boost recovery from stroke in combination with other rehabilitation therapies. It is possible that optimizing butyrate producers, secondary bile acid producers, equol producers, and sulfate reducers in the gut could contribute to creating a rehabilitation environment where recovery is boosted.

Table 3.1 Participant Characteristics

	Acute Stroke	At Risk Controls	Healthy Controls
N	12	18	12
Age	68.5 ± 12.68	66.33 ± 6.53	64.75 ± 4.75
Sex (% Female)	83.33%	77.78%	91.67%
Race (% White)	100.00%	88.89%	91.67%
(% Black)	0.00%	11.11%	0.00%
(% Asian)	0.00%	0.00%	8.33%
Genotype (% APOE ε3/ε3)	41.67%	61.11%	41.47%
(% APOE ε3/ε4)	33.33%	33.33%	25.00%
(% APOE ε4/ε4)	0.00%	5.56%	0.00%
(% APOE ε2/ε4)	8.33%	0.00%	0.00%
(% APOE ε2/ε3)	16.67%	0.00%	33.33%
Education	13.27 ± 2.97	16.78 ± 1.52	17.92 ± 2.07
BMI	29.65 ± 7.78	28.43 ± 5.81	24.72 ± 3.95
Diabetes	33.33%	16.67%	0%
Hypertension	75%	72.22%	0%
Hyperlipidemia	81.82%	50.00%	0%

Table 3.2 Microbial Taxa Associated with fecal Alpha-1-Antitrypsin

Bacteria	Coefficient	Q-Value
Taxa Positively correlated with Alpha-1-Antitrypsin		
<i>Eggerthella lenta</i>	0.468	0.1731
<i>Clostridium bolteae</i>	0.274	0.1814
<i>Clostridium leptum</i>	0.344	0.2363
<i>Anaerotruncus colihominis</i>	0.456	0.1814
Taxa negatively correlated with Alpha-1-Antitrypsin		
<i>Adlercreutzia equolifaciens</i>	-0.307	0.1731
Genus <i>Anaerostipes</i>	-0.298	0.1731
Family <i>Lachnospiraceae</i>	-0.113	0.2074
<i>Lachnospira pectinoschiza</i>	-0.215	0.1731
Genus <i>Roseburia</i>	-0.42	0.07802
<i>Roseburia inulinivorans</i>	-0.299	0.1731
Genus <i>Ruminococcus</i>	-0.457	0.1814
<i>Blautia obeum</i>	-0.359	0.1440
<i>Dorea longicatena</i>	-0.473	0.1626
<i>Lawsonibacter asaccharolyticus</i>	-0.256	0.1854

Table 3.3 Diet Correlates with Microbial Taxa in Stroke Participants

Stroke Diet Feature	Microbial Taxa	Coef	<i>Q</i> Value
Fiber	<i>None</i>		
Calcium	<i>None</i>		
Whole Grains	<i>None</i>		
Sugar	<i>None</i>		
Dairy	<i>None</i>		
Fruits and Vegetables	<i>Ruminococcus torques</i>	1.00	0.04917
	<i>Eisenbergiella massiliensis</i>	-0.301	0.05379
	<i>Faecalibacterium prausnitzii</i>	0.0974	0.04917
	<i>Holdemania filiformis</i>	-0.385	0.04917
	Genus <i>Bacteroides</i>	-0.153	0.2464
Vegetables Only	<i>Clostridium bolteae</i>	0.578	0.1554
Sugar Sweetened Beverages	<i>None</i>		

Table 3.4 Microbial Taxa correlated with Markers of Stroke Recovery

Marker of Stroke Recovery	Bacteria	Coefficient	Q-Value
Self Care Assessment	<i>Collinsella aerofaciens</i>	0.772	0.01921
Picture Vocabulary Test	Genus <i>Roseburia</i>	0.593	0.1546
List Sorting Test	None		
Self-Efficacy Questionnaire	<i>Bacteroides uniformis</i>	0.337	0.2202
	Family <i>Enterobacteriaceae</i>	-0.766	0.1747
	<i>Escherichia coli</i>	-0.483	0.2202
Sadness Questionnaire	None		
Meaning and Purpose Questionnaire	Family <i>Eubacteriaceae</i>	1.29	0.1205
	Class <i>Coriobacteriia</i>	0.299	0.1691
	Family <i>Odoribacteraceae</i>	0.215	0.1888
	Genus <i>Eubacterium</i>	0.870	0.2258
	Family <i>Acidaminococcaceae</i>	0.133	0.2258
	<i>Roseburia intestinalis</i>	0.0584	0.2258
	<i>Phascolarctobacterium faecium</i>	0.0505	0.1691
	<i>Bacteroides ovatus</i>	-0.238	0.1888
	<i>Erysipelatoclostridium ramosum</i>	-0.375	0.2258
	<i>Flavonifractor plautii</i>	-0.437	0.1580
Support Questionnaire	Family <i>Veillonellaceae</i>	-0.683	0.2258
Pain Self-Rating	<i>Alistipes shahii</i>	0.311	0.04039

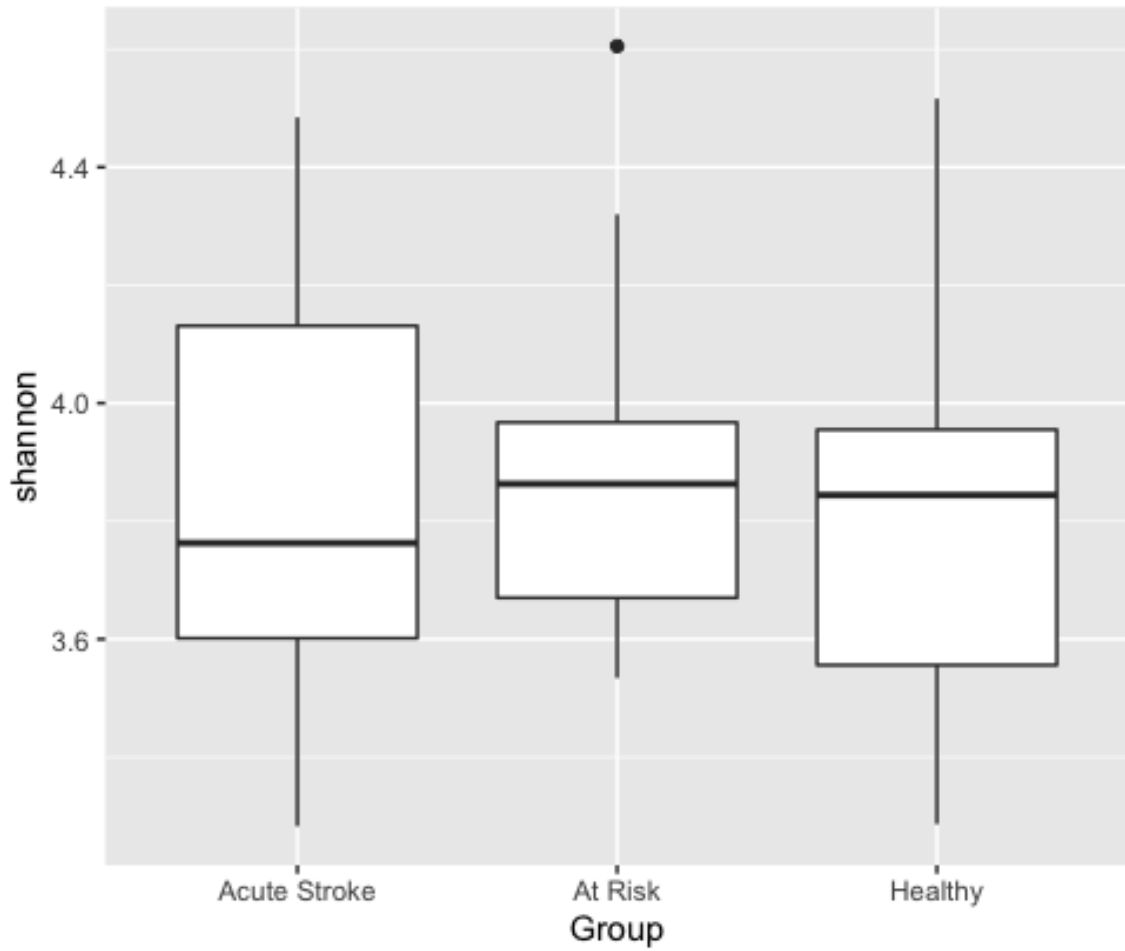


Figure 3.1 Alpha Diversity amongst the participants groups did not differ on Wilcoxon rank sum test

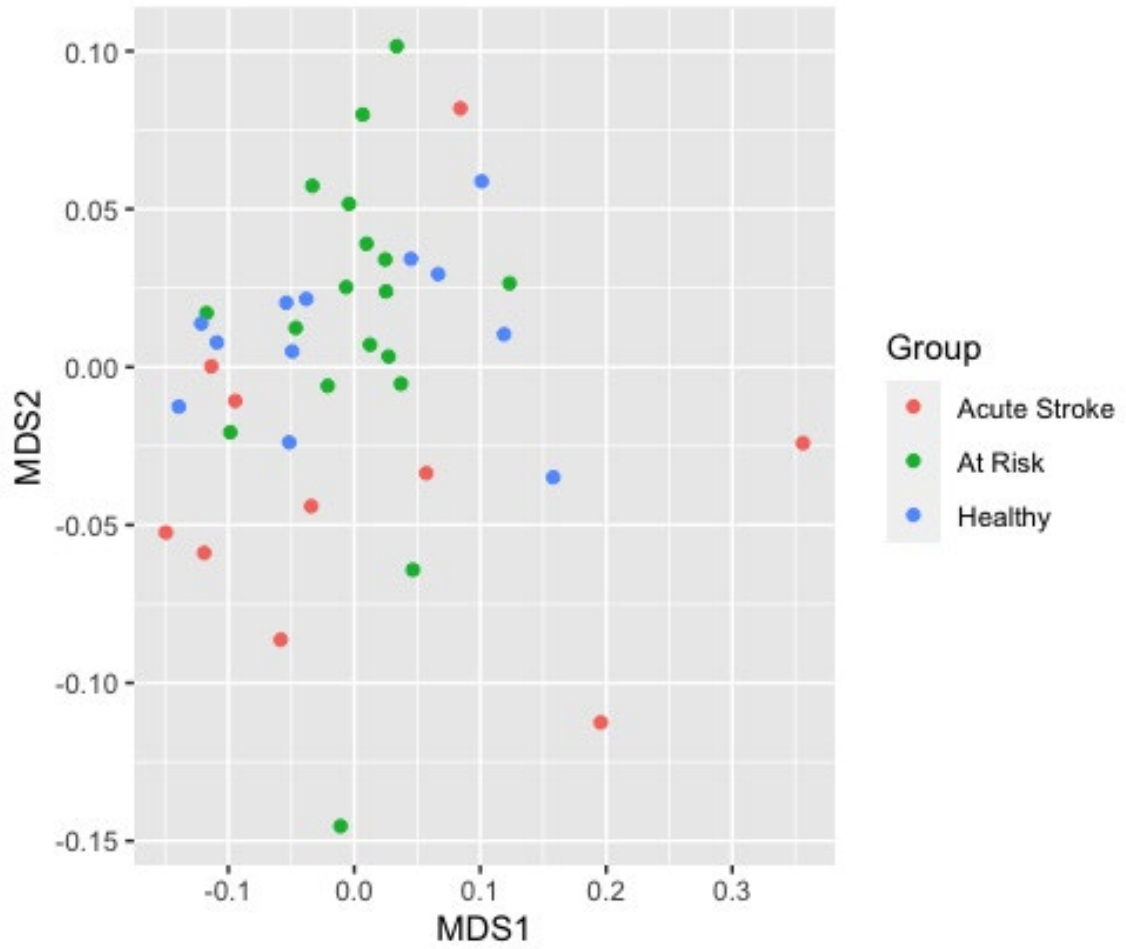


Figure 3.2 Beta Diversity amongst the groups

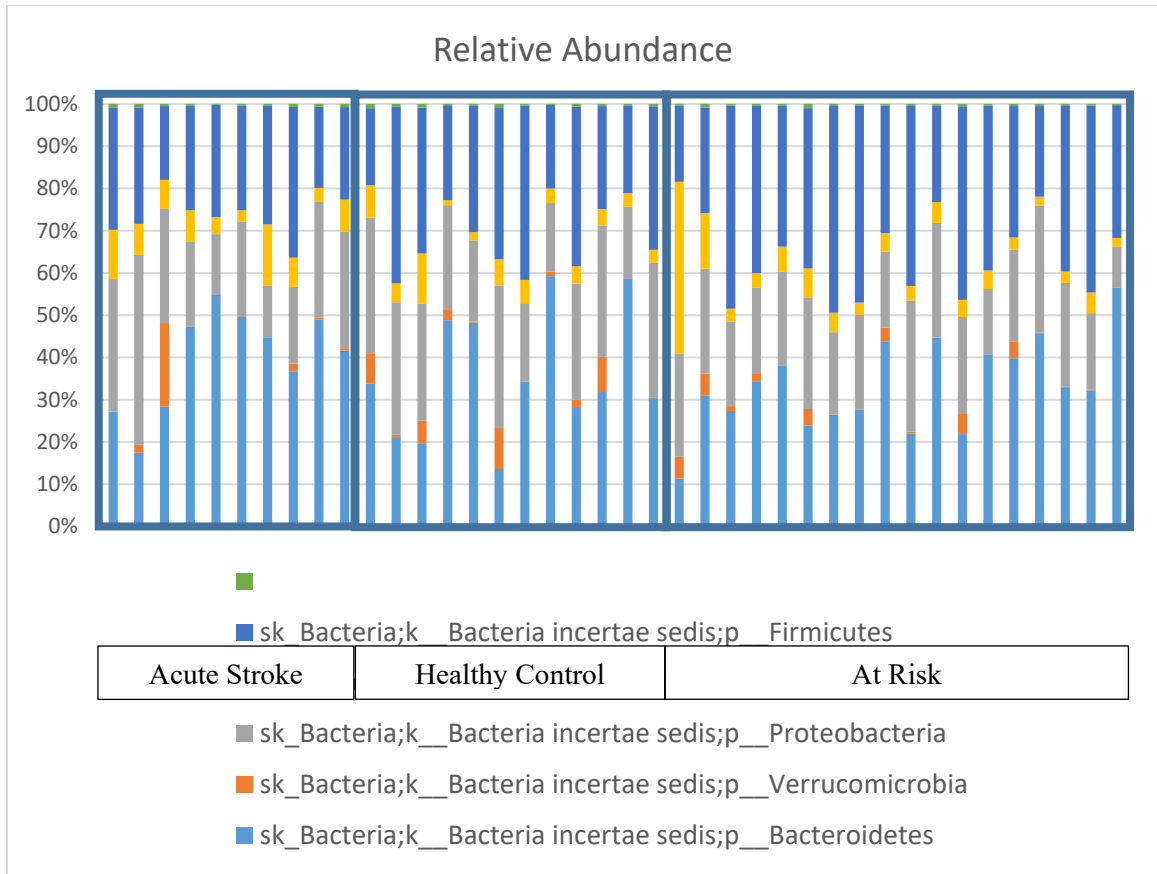


Figure 3.3 Relative Abundance of most prevalent phyla

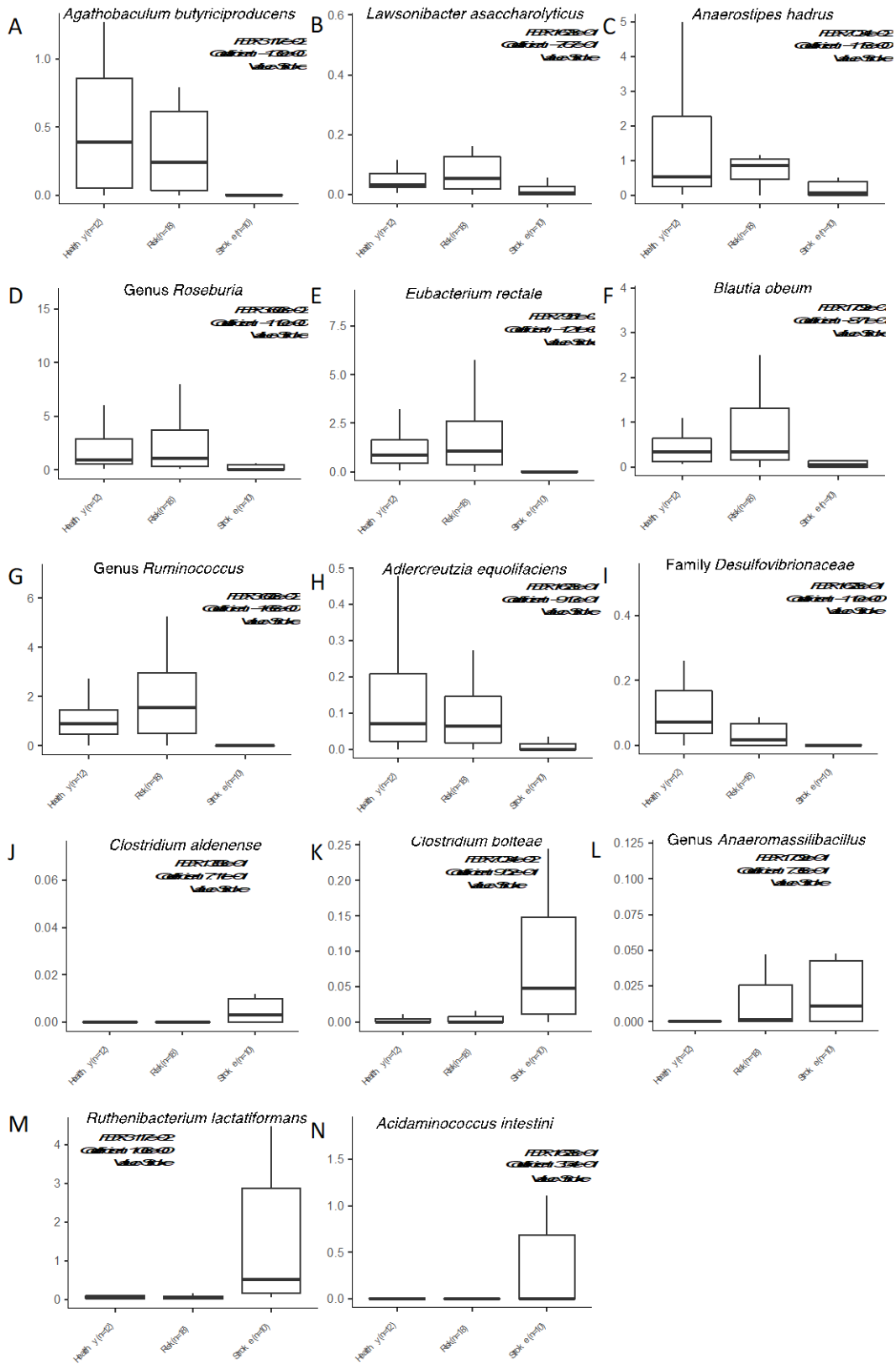


Figure 3.4 Significant Associations of Microbial Taxa with Stroke and At Risk Groups as compared to the healthy control group

The following taxa are lower in the stroke group: A) *Agathobaculum butyriciproducens*, B) *Lawsonibacter asaccharolyticus*, C) *Anaerostipes hadrus*, D) Genus *Roseburia*, E) *Eubacterium rectale*, F) *Blautia obeum*, G) Genus *Ruminococcus*, H) *Adlercreutzia equolifaciens*, I) Family *Desulfovibrionaceae*. The following taxa are higher in the stroke group: J) *Clostridium aldenense*, K) *Clostridium bolteae*, L) Genus *Anaeromassibacillus*, M) *Ruthenibacterium lactatiformans*, N) *Acidaminococcus intestini*

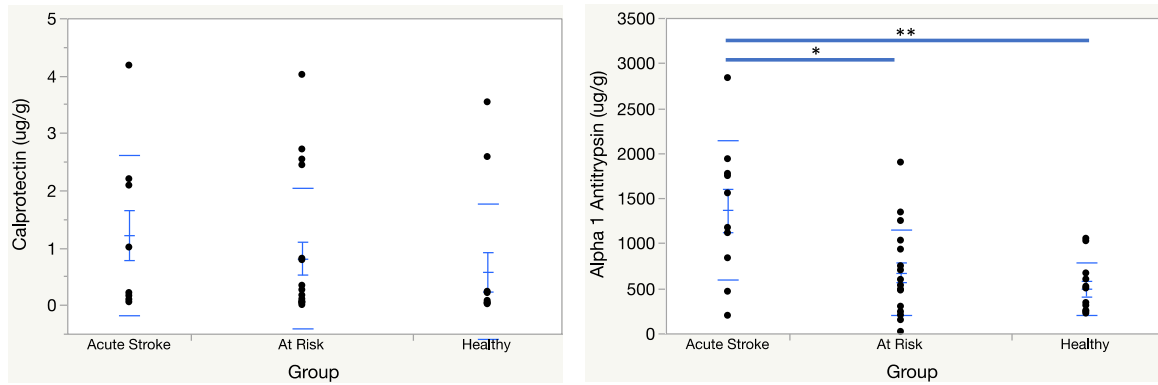


Figure 3.5 Leaky Gut Markers were compared amongst the participant groups using Kruskal-Wallis Test.

* p-value < 0.05

** p-value < 0.01

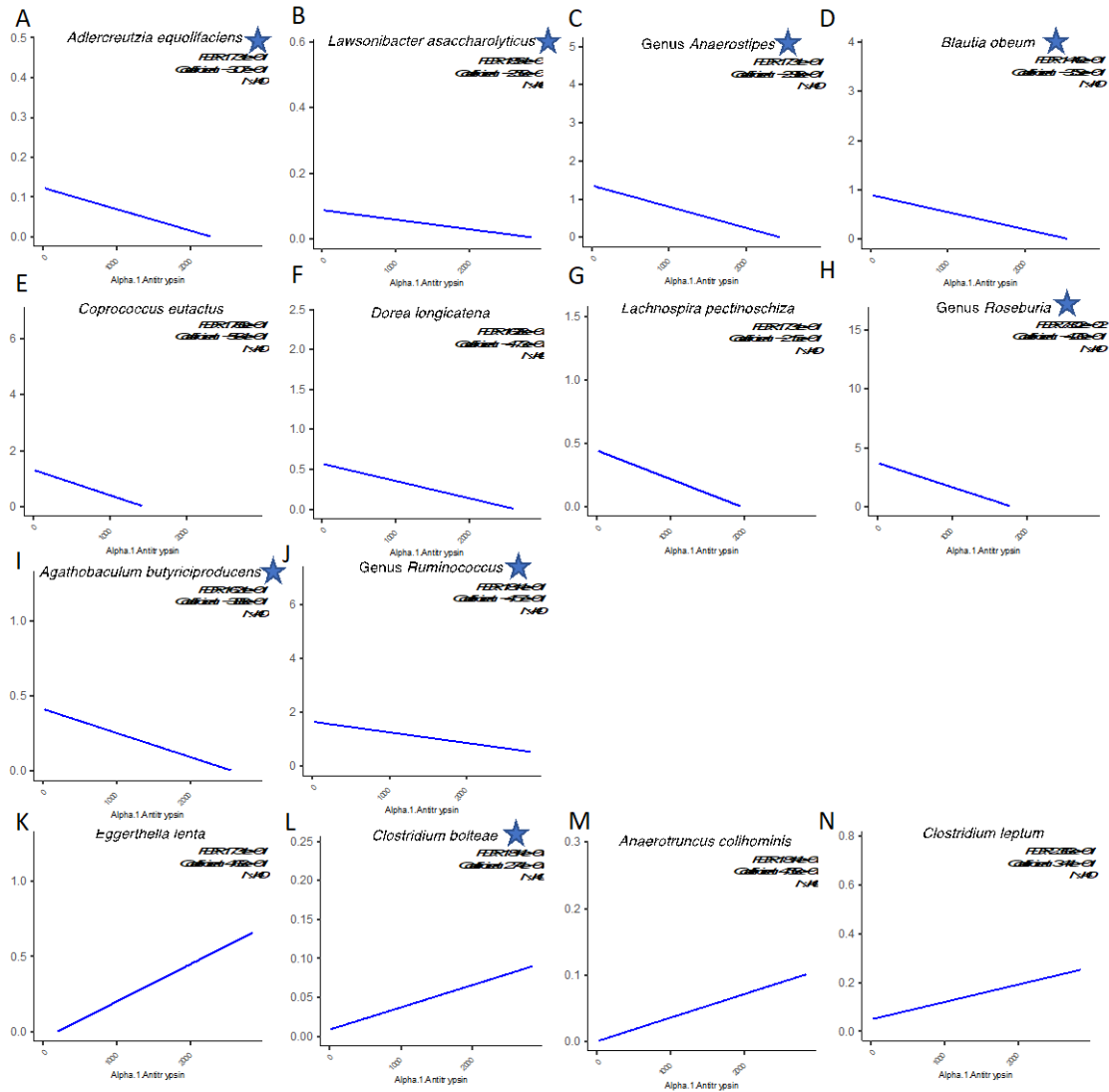


Figure 3.6 Microbial Taxa Associated with fecal Alpha-1-Antitrypsin.

Stars indicate bacteria which were also associated with stroke. Negative associations include A) *Adlercreutzia equolifaciens*, B) *Lawsonibacter asaccharolyticus*, C) the genus *Anaerostipes*, D) *Blautia obeum*, E) *Coprococcus eutactus*, F) *Dorea longicatena*, G) *Lachnospira pectinoschiza*, H) the genus *Roseburia*, I) *Agathobaculum butyriciproducens*, and J) the genus *Ruminococcus*. Positive associations include K) *Eggerthella lenta*, L) *Clostridium boltea*, M) *Anaerotruncus colihominis*, and N) *Clostridium leptum*.

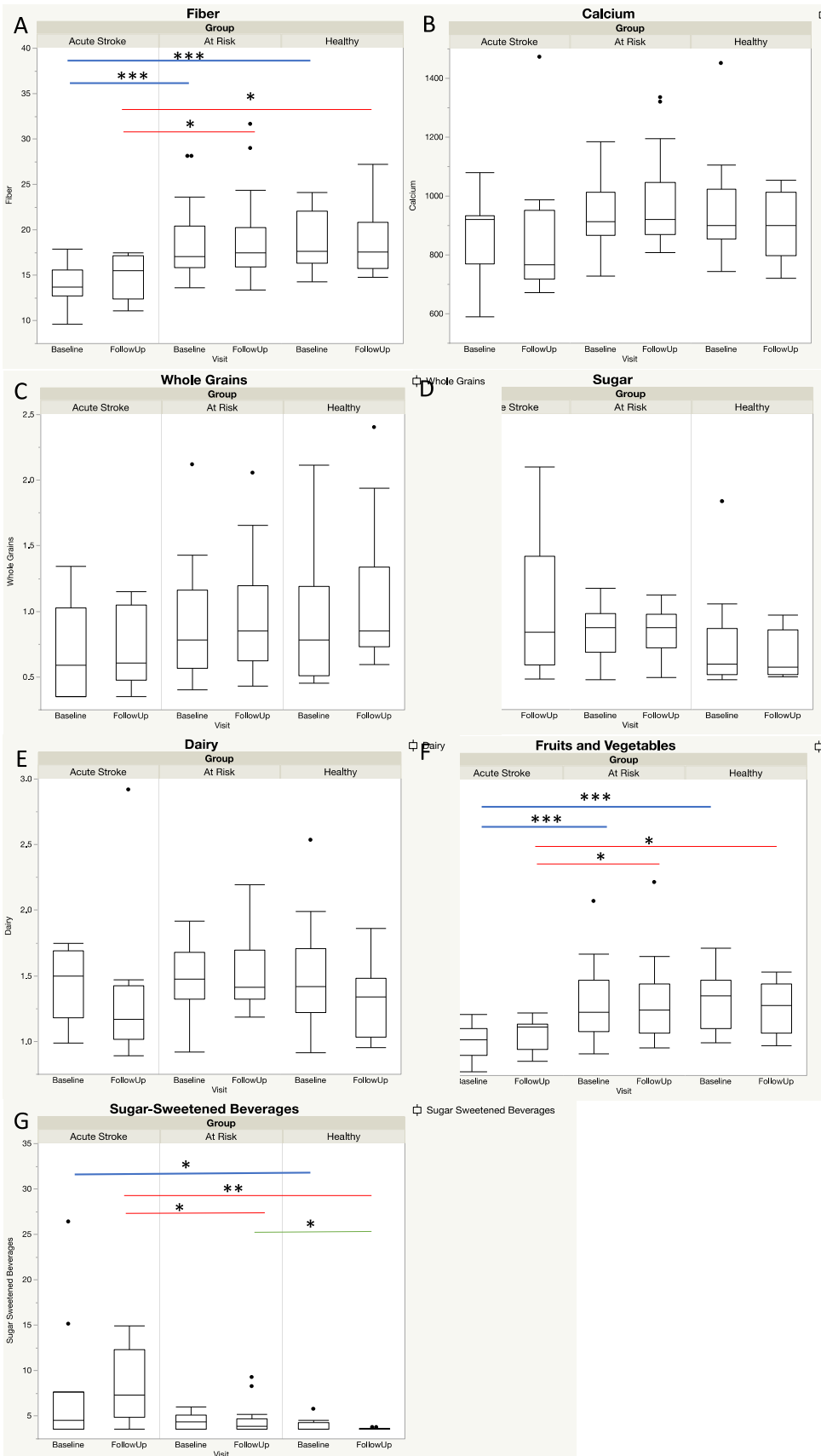


Figure 3.7 Diet composition amongst the groups.

Diet was compared between each of the groups using a Wilcoxon rank sum test in several components: A) fiber, B) calcium, C) whole grains, D) sugar, E) dairy, F) fruits and vegetables, and G) sugar-sweetened beverages

* p-value < 0.05

** p-value < 0.01

*** p-value < 0.001

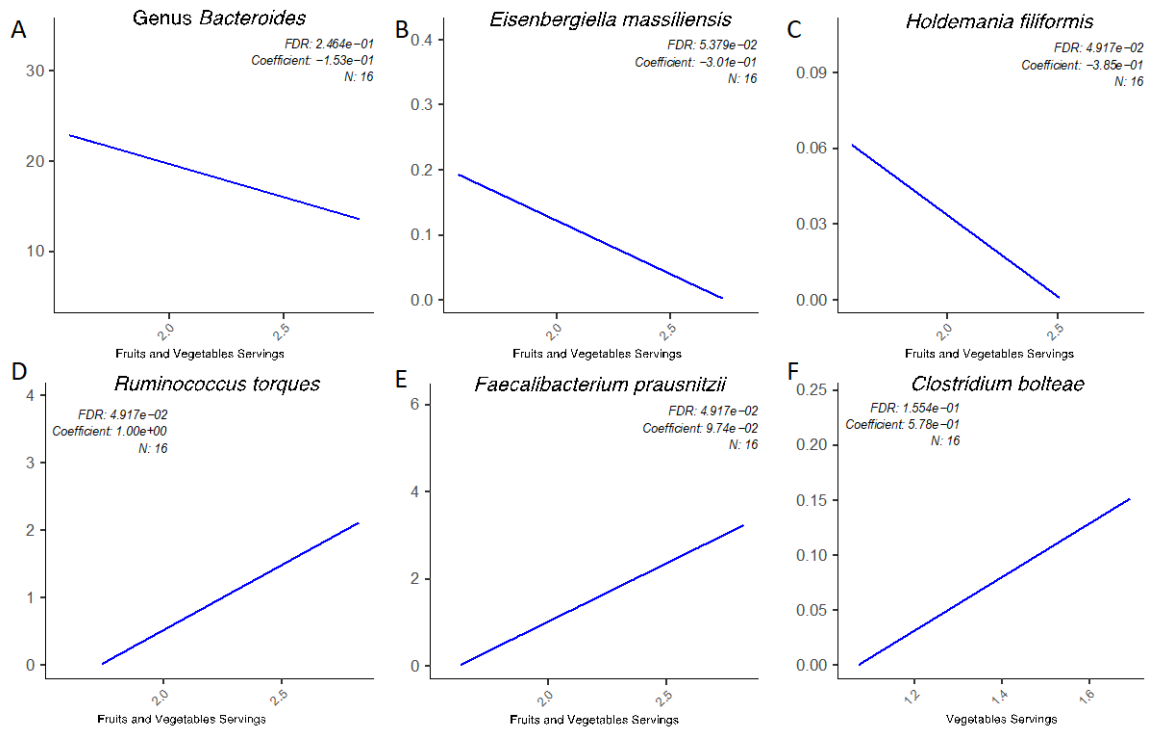


Figure 3.8 Microbial Taxa Associated with diet in stroke participants.

Negative associations with fruits and vegetables are with A) the genus *Bacteroides*, B) *Eisenbergiella massiliensis*, and C) *Holdemania filiformis*. Positive associations with fruits and vegetables are with D) *Ruminococcus torques*, E) *Faecalibacterium prausnitzii*, and F) *Clostridium bolteae*.

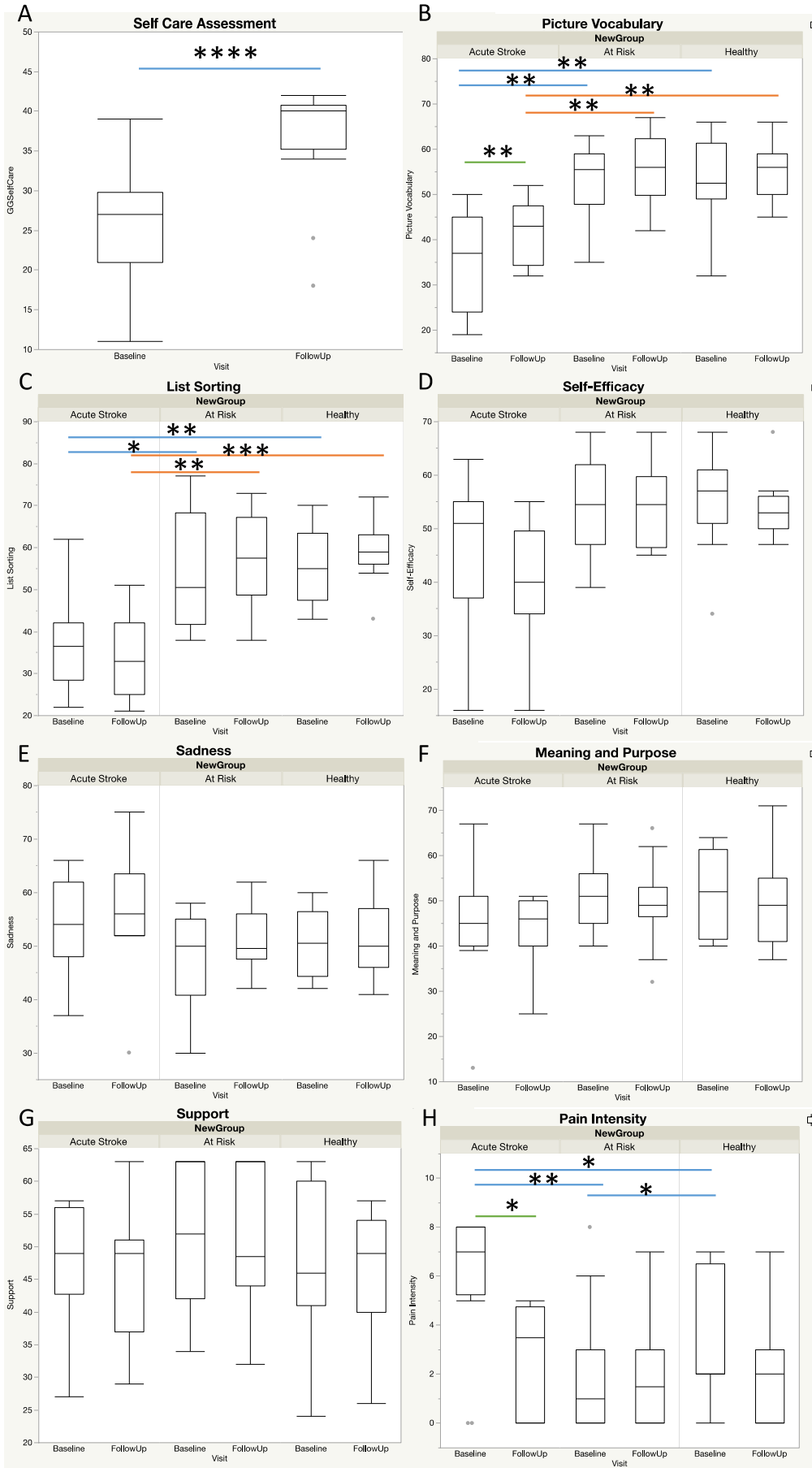


Figure 3.9 Markers of stroke function at baseline and follow up for acute stroke, at risk, and healthy participants.

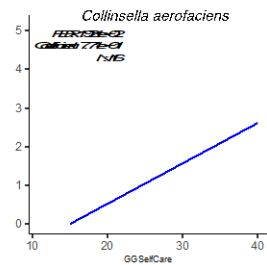
Assessments include A) Self Care Assessment, B) Picture Vocabulary, C) List Sorting, D) Self-Efficacy, E) Sadness, F) Meaning and Purpose, G) Support, and H) Pain Intensity.

* p-value < 0.05

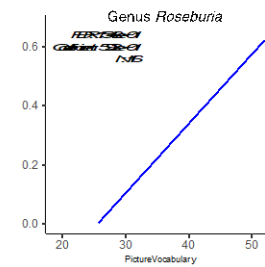
** p-value < 0.01

*** p-value < 0.001

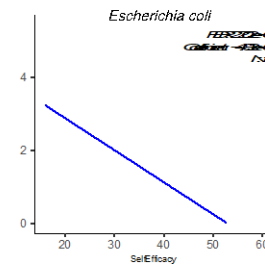
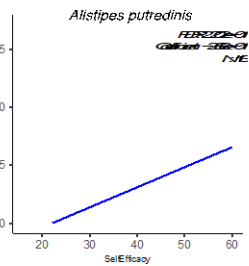
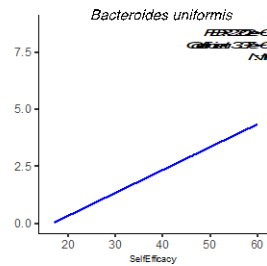
A) Self Care Assessment



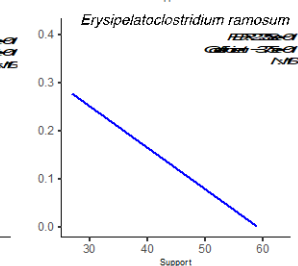
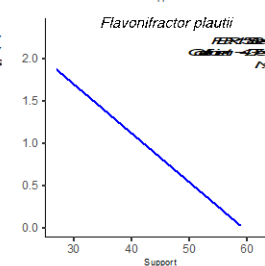
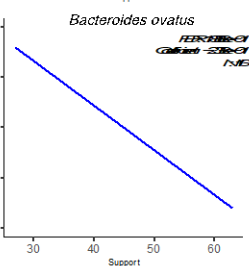
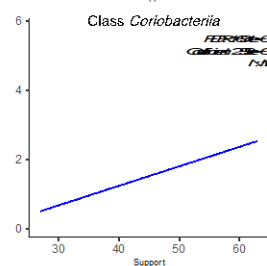
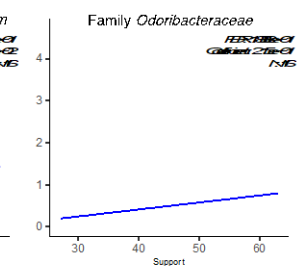
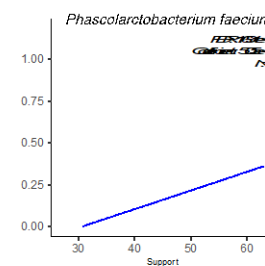
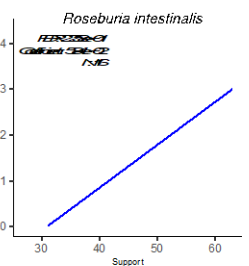
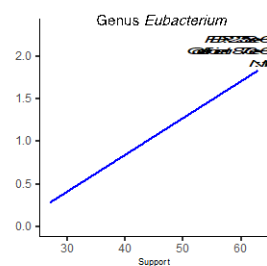
B) Picture Vocabulary Test



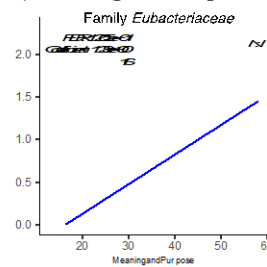
C) Self-Efficacy Questionnaire



D) Support Questionnaire



E) Meaning and Purpose Questionnaire



F) Pain Questionnaire

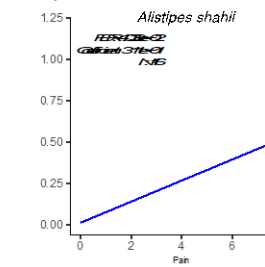


Figure 3.10 Microbial Taxa associations with Markers of Stroke recovery. Association plots depict the correlation between microbial taxa and A) Self Care Assessment, B) Picture Vocabulary Test, C) Self-Efficacy, D) Support, E) Meaning and Purpose, and F) Pain

CHAPTER 4. GUT MICROBIOME IS ASSOCIATED WITH BRAIN IMAGING IN COMMUNITY DWELLING OLDER ADULTS

4.1 Introduction

Healthy brain aging is a focus of many older adults trying to avoid age-related neuronal diseases. Popular dietary aids, cognitive puzzles, and exercise regimes have all been touted as lifestyle interventions to promote healthy aging. The popularity of these interventions suggests that there is much interest from the general population to achieve healthy aging and there is a need for a better understanding of the connection of these interventions with brain health. Accumulating evidence has implicated the gut microbiome in brain health. Microbial communities that inhabit the gut communicate with the brain through the vagus nerve in the nervous system, the peyers patches in the immune system, and metabolites in the circulatory system ⁶². It is possible that manipulation of the gut microbiome could lead to healthier brain aging.

Many imaging tools have been developed to measure brain health. T1 and T2 structural imaging is commonly used to calculate brain volume ³¹, but advanced imaging modalities such as diffusion tensor imaging ³², magnetic resonance spectroscopy ³³, and arterial spin labelling ³⁴ can be used to detect white matter integrity, brain metabolites, and cerebral blood flow, respectively. Many changes in the brain associated with the gut microbiome and gut disorders have been documented with imaging. Ulcerative colitis has been associated with a significantly reduced blood oxygen level-dependent signal in the amygdala, thalamic regions, and cerebellar regions ⁷². Irritable bowel syndrome has been associated with long-term white matter integrity changes in the brain, especially in regions associated with integration of sensory information and corticothalamic modulation ⁷³, and

lower volumes in the bilateral superior frontal gyrus, insula, amygdala, hippocampus, and middle orbital frontal gyrus ⁷⁴. Probiotic administration for 4 weeks has been associated with changes in brain activation patterns in response to emotional decision-making tasks ^{75,76}. Short chain fatty acids (SCFAs) are known to decrease blood brain barrier permeability and cerebral blood flow ⁷⁷. Finally, the gut microbiome is known to influence the transcriptional activity of genes involved in neuronal myelination, thereby altering white matter integrity ⁷⁹.

Here we document the association of brain imaging markers with the gut microbiome in 30 community dwelling older adults. We measure global and segmented brain volume, brain metabolites, cerebral blood flow, and white matter integrity using T1 MP-RAGE imaging, magnetic resonance spectroscopy, arterial spin labeling, and diffusion tensor imaging, respectively. We measure the gut microbiome using whole genome shotgun sequencing on stool samples. This analysis of aging subjects is foundational to understanding how gut microbes are associated with brain health as detected by imaging.

4.2 Results

4.2.1 Participant Characteristics

We recruited 30 participants aged 55-85 from a community dwelling sample. Participants were recruited from Research Match and advertisements posted online and in the community by the Center for Clinical and Translational Research at the University of Kentucky. Participants were required to not have an acute disease of chronic, clinically significant (unresolved, requiring on-going medical management or medication) pulmonary, gastrointestinal, dermatologic, hepatic or renal functional abnormality.

Participants were required to not have had cancer or a positive test for HIV, HBV, or HCV. Participants were required to not be immunosuppressed or have had major surgery of the GI tract in the past five years. Participants also had to be MRI compatible. **Table 4.1** describes the major demographic characteristics of our participants known to influence brain aging, with a mean age of 65.7, 17.23 years of education, and body mass index (BMI) of 26.95. Our population was 83.33% female, 90% white, and 10% had diabetes, 43.33% had hypertension, and 30% had hyperlipidemia. 53% were genotype APOE $\epsilon 3/\epsilon 3$, 33% were $\epsilon 4$ carriers, and 13% were $\epsilon 2$ carriers.

4.2.2 Microbiome Measurements

4.2.2.1 Gut microbiome is associated with sex, ApoE Genotype, Obesity, Diabetes, Hypertension

We measured the gut microbiome by performing whole genome shotgun sequencing on stool samples from the participants at baseline and at a three month follow up. We detected microbial taxa which were significantly associated ($q < 0.25$) with our demographic variables using the MaAsLin2 R package¹²⁵. While there were no significant associations with age, race, education, or hyperlipidemia, significant associations existed with sex, ApoE genotype, BMI, diabetes, and hypertension (**Table 4.2**). Microbial taxa were not significantly different between the baseline and three month follow up visit. *Bacteroides plebeius* and *Haemophilus parainfluenzae* were both significantly higher in males than females and the Genus *Clostridium* was significantly lower (**Figure 4.1a-c**). The *firmicutes* species *Eubacterium eligens*, *Oscillibacter*, and *Faecalibacterium prausnitzii* were all lower in the ApoE $\epsilon 2/\epsilon 3$ genotype and the *firmicutes* species *Blautia producta*, *Clostridium citroniae*, *Clostridium lavalense*, and *Clostridium symbiosum* were

all higher (**Figure 4.1d-g**). In the ApoE $\epsilon 3/\epsilon 4$ genotype, the firmicutes species *roseburia* and *Holdemania filiformis* were lower (**Figure 4.1h,i**). The *Verrucomicrobia* species *Akkermansia muciniphila* was lower in obesity and inversely associated with BMI and the *bacteroidetes* species *Bacteroides dorei* was higher (**Figure 4.1j,k**). The *Proteobacteria* species *Escherichia coli* and the *Bacteroidetes* species *Parabacteroides goldsteinii* were higher in participants with diabetes (**Figure 4.1l,m**). The *Firmicutes* genus *Phascolarctobacterium* was lower in participants with hypertension (**Figure 4.1n**).

4.2.2.1 Gut microbiome is associated with calcium intake and vegetables intake

We measured dietary intake over the previous month using the Dietary Screener Questionnaires (DSQ) in the National Health and Nutrition Examination Survey (NHANES) 2009-10. While there were no significant associations with fiber, whole grain, added sugar, dairy, or fruit and vegetables intake, significant associations existed with calcium intake (**Table 4.3**). An increased intake of calcium was associated a higher abundance of *Bifidobacterium adolescentis*, the family *Acidaminococcaceae*, *Eubacterium eligens*, and *Haemophilus parainfluenzae* (**Figure 4.2a-d**) and a lower abundance of *Clostridium asparagiforme*, *Eubacterium ventriosum*, and *Sellimonas intestinalis* (**Figure 4.2e-g**).

4.2.3 Imaging Measurements

We collected brain imaging on our participants to find associations between imaging features and markers of brain health as detected by imaging. We measured brain volume using structural T1 imaging, brain metabolites using magnetic resonance

spectroscopy, cerebral blood flow using arterial spin labeling, and white matter integrity using diffusion tensor imaging.

4.2.3.1 Gut microbiome is associated with Structural Imaging

Table 4.4 shows the microbial taxa that were associated with structural imaging features. Using a False Discovery Rate of 0.25, we found that *Bacteroides ovatus* was associated with the Thalamus Volume (**Figure 4.3a**) and *Bacteroides uniformis* was associated with White Matter Hypointensities (**Figure 4.3b**). The Family *Acidaminococcaceae* was positively associated the volume of the Mid Posterior portion of the Corpus Callosum (**Figure 4.3c**).

4.2.3.2 Gut microbiome is associated with Brain Metabolites

Table 4.5 shows the microbial taxa that were associated with brain metabolites recorded in the white matter of the posterior corpus callosum. *Collinsella aerofaciens* was negatively associated with GABA (**Figure 4.4a**) and *Parasutterella excrementihomis* were positively associated with GABA (**Figure 4.4b**). *Alistipes putredinis* and the Family *Acidaminococcaceae* were positively associated with Glycerophosphocholine (GPC) (**Figure 4.4c,d**). *Ruminococcus lactaris* was positively associated with N-acetylaspartate and N-acetylaspartylglutamate (NAA+NAAG) (**Figure 4.4e**) as well as several macromolecules. *Streptococcus thermophilus*, the Genus *Eubacterium*, and *Eubacterium eligens* were also associated with several macromolecules.

4.2.3.3 Equol producers are associated with Cerebral Blood Flow

Table 4.6 shows the microbial taxa that were associated with cerebral blood flow in various brain regions. Several taxa from the *Actinobacteria* phylum were implicated in

cerebral blood flow. These included the family *Eggerthellaceae*, which is negatively correlated with brain regions responsible for language. Specifically, *Adlercreutzia equolifaciens*, *Asaccharobacter celatus*, *Gordonibacter pamelaee* are all negatively correlated with language function and the limbic system (**Figure 4.5**) and *Collinsella stercoris* is positively correlated with language function and the limbic system. The Genera *Alistipes* and *Parabacteroides*, part of the *Bacteroidetes* phylum, are negatively correlated with cerebral blood flow in basal ganglia regions and hippocampal regions, both implicated in learning and memory (**Figure 4.6a-c**). The phylum *Firmicutes* is negatively correlated with blood flow in the primary auditory cortex. *Eubacterium siraeum*, a member of the phylum, is negatively correlated with the frontal eye fields and the primary somatosensory cortex. The genus *Haemophilus*, and specifically, *Haemophilus parainfluenzae*, are positively correlated with cerebral blood flow in memory and learning areas (**Figure 4.6d-f**), while the family *desulfovibrionaceae* is negatively correlated with blood flow in memory and learning areas (**Figure 4.6g**).

4.2.3.4 Equol producers are associated with White Matter Integrity

Table 4.7 shows the microbial taxa that were associated with white matter integrity. Several taxa from the *Actinobacteria* phylum were implicated in white matter integrity. These included the family *Eggerthellaceae*, which is positively correlated with white matter tracts in the middle cerebellar peduncle and the left external capsule, which contains corticocortical association fibers. Specifically, *Adlercreutzia equolifaciens*, *Asaccharobacter celatus*, *Gordonibacter pamelaee* are also positively correlated with several tracts that connects brain regions responsible for language function and the limbic system (**Figure 4.7**). Two members of the phylum *Bacteroidetes*, *Coprobacter fastidiosus*

and *Bacteroides uniformis*, are negatively correlated with the superior longitudinal fasciculus and the tapetum. The *firmicutes* phylum has several taxa that are positively correlated with white matter tracts, including *Eubacterium siraeum*, *Clostridium innocuum* (**Figure 4.8b**), the genus *Lactobacillus* (**Figure 4.8c**), *Lachnospira pectinoschiza* (**Figure 4.8d**), *Roseburia hominis* (**Figure 4.8e,f**), *Monoglobus pectinilyticus*, *Clostridium citroniae*, and the Genus *Flavonifractor*. The firmicutes taxa *Streptococcus thermophilus* and *Gemmiger formicilis* are negatively correlated with the superior longitudinal fasciculus connecting the parietal, occipital, and temporal lobes.

4.3 Discussion

Here we measured the gut microbiome of 30 community dwelling older adults and made associations with it and the imaging features of structural volume, brain metabolites, cerebral blood flow, and white matter integrity. We found that important butyrate producers are associated with the volume of the thalamus and corpus callosum which are superhighway regions of the brain, responsible for relaying and processing lots of information. We also found proinflammatory species to be associated with GABA production. Importantly, we found the family *eggerthellacaeae* to be highly associated with cerebral blood flow in areas of the brain related to language, memory, and learning and with the white matter integrity of the tracts connecting these areas.

There were bacterial taxa related to several of the demographic variables including sex, ApoE Genotype, BMI, Diabetes, and Hypertension. Males had more *Bacteroides plebeius* and *Haemophilus parainfluenzae*, and fewer of the genus *Clostridium*. *Bacteroides plebeius* contains a key enzyme for the digestions of agarose, a polymer derived from seaweed used in gelatin, ice cream, and other desserts^{210,211}. Sex hormones

are thought to play a role in microbiome differences between males and females, with ovariectomized rats showing higher levels of the genus *bacteroides*²¹². *Haemophilus parainfluenzae* is an infectious species that had lower abundance in conjunction with a plant-based diet²¹³. The ApoE $\epsilon 2/\epsilon 3$ genotype had higher *lachnospiridium* species and lower *Eubacterium eligens*, *Oscillibacter*, and *Faecalibacterium prausnitzii*; the ApoE $\epsilon 3/\epsilon 4$ genotype had lower *roseburia*. The ApoE $\epsilon 4/\epsilon 4$ genotype had higher *Sellimonas intestinalis*. *Eubacterium eligens* and *Faecalibacterium prausnitzii* both exert anti-inflammatory effects on the host, suggesting that individuals with ApoE $\epsilon 2/\epsilon 3$ genotype have less capability or need for these anti-inflammatory effects.²¹⁴ *Roseburia* is a famous butyrate producer that is decreased in a genotype known for being a risk factor for cognitive decline.²¹⁵ *Sellimonas intestinalis* is often found increased in inflammatory diseases and following recovery from dysbiosis²¹⁶. BMI was inversely associated with *Akkermansia muciniphila* and positively associated with *Bacteroides cellulosilyticus* and *Bacteroides dorei*. *A. muciniphila* has previously been found decreased in obesity and is thought to be protective against metabolic disorders via its excretion of endocannabinoids that control inflammation, the gut barrier, and gut peptide secretion²¹⁷. *B. cellulosilyticus* can degrade cellulose and produce short chain fatty acids²¹⁸. *B. dorei* can attenuate formation of atherosclerotic plaques by inhibiting lipopolysaccharide formation and a pro-inflammatory response²¹⁹. Diabetes is associated with increased *Escherichia coli* and *Parabacteroides goldsteinii*. *Escherichia coli* is a normal gut commensal that has many pathologic variants that can cause disease²²⁰. Increases in infectious *E. coli* have previously been reported in diabetes²²¹. *P. goldsteinii* has been inversely associated with a high fat diet²²² and is thought to have anti-inflammatory properties²²³. The genus *phascolarctobacterium* was

decreased in hypertension and is a producer of short chain fatty acids²²⁴ that has previously been shown to be decreased in high blood pressure²²⁵.

We found that certain dietary features are associated with the abundance of specific bacteria. This is congruent with other groups who have found that dietary modification is associated with gut microbiome composition¹⁸¹. We found an inverse relationship between calcium and *Clostridium asparagiforme*. *C. asparagiforme* has also been found to be reduced in smokers with hypertension²²⁶. Calcium was positively associated with the family *Acidaminococcaceae*, *Eubacterium eligens*, and the genera *Haemophilus* and *Phascolarctobacterium*. *Acidaminococcaceae* species can produce short chain fatty acids²²⁴. *Eubacterium eligens* has anti-inflammatory effects on the host²¹⁴. *Haemophilus* species are infectious²²⁷. *Phascolarctobacterium* species are producers of short chain fatty acids²²⁴. While it is unknown how calcium would affect these microbial taxa, it has previously been shown that a high calcium diet increases *firmicutes* species and lactic, acetic, and butyric acid levels²²⁸. We found a positive relationship of vegetables with *Agathobaculum butyriciproducens*, a butyrate producer, and a negative effect with *Eggerthella lenta*, an infectious species. There are many studies that describe the positive effects of a vegetarian diet on the microbiome by limiting inflammatory species and promoting SCFA-producing species^{182,183}.

Our results show that *Bacteroides ovatus* is inversely related to the Thalamus Volume and that *Bacteroides uniformis* is inversely related to White Matter Hypointensities. The Thalamus is an important relay station in the brain that communicates information from the spinal cord and cerebellum to the cerebral cortex²²⁹. *Bacteroides ovatus* is a commensal microbe that uses various carbohydrates and proteins as its fuel

source ²³⁰ and is a prominent inducer of IgA ²³¹ and promotes the reparative cytokine IL-22 ²³² thereby stimulating epithelial recovery ²³³. While it is not known why the presence of this particular bacteria would inversely correlate with thalamus size, a large thalamus size has previously been associated with irritable bowel syndrome ²³⁴. A reduced thalamus size has been associated with advanced chess players who have a more “streamlined” relay station allowing them to process information very quickly ²³⁵. White Matter Hypointensities are a value automatically detected by FreeSurfer from a T1 image that corresponds to the White Matter Hyperintensities typically found from a T2 image ²³⁶. White matter hyperintensities are a marker of vascular disease in the brain ²³⁷ and are often associated with cognitive impairment ²³⁸. *Bacteroides uniformis* prefers wheat bran extract as a fuel source and is a butyrate producer; it strengthens the first line of immune defense against unhealthy diets ²³⁹ and improves glucose tolerance ²⁴⁰. While it is not known why the presence of *Bacteroides uniformis* correlates inversely with White Matter Hypointensities, this microbe has been associated with increased dopamine transporters ²⁴¹ and normalizing the brain reward response to reduce anxiety in rats ²⁴². Interestingly, the microbiota-derived phenylacetylglutamine has previously been associated with the amount of white matter hyperintensities in the brain ¹⁰⁶. The Mid Posterior portion of the Corpus Callosum is responsible for connecting portions of the parietal and temporal cortices on each side of the brain. Many species of the family *Acidaminococcaceae* can produce short chain fatty acids ²²⁴, and it has been found to be increased in Major Depression ²⁴³. While it is unknown how *Acidaminococcaceae* can affect the corpus callosum volume, this taxa has previously been associated with memory performance ²⁴⁴.

We also found several taxa to be associated with metabolites in the corpus callosum. GABA is the main inhibitory neurotransmitter in the human brain ²⁴⁵. *Collinsella aerofaciens* is negatively associated with GABA production, and *Parasutterella excrementihominis* is positively associated with GABA. *Collinsella aerofaciens* is an obligate anaerobe ^{246,247} and a proinflammatory species associated with Crohn's Disease ^{248,249}. *Parasutterella excrementihominis* is strictly anaerobic ²⁵⁰ and has been associated with impaired GI health ²⁵¹. While *Collinsella aerofaciens* and *Parasutterella excrementihominis* have not previously been identified as GABA producers or consumers, *bacteroides* has been identified as a dominant GABA producer and *Pseudomonas* as a prominent GABA consumer ²⁵².

We also found *Alistipes putredinis* and the Family *Acidaminococcaceae* to be positively correlated with Glycerophosphocholine in the corpus callosum. Glycerophosphocholine is a precursor to the phospholipids used in lipid bilayers and is a natural source of choline ²⁵³. Glycerophosphocholine has been associated with white matter microstructure and processing speed ²⁵⁴. *Alistipes putredinis* has been shown to be protective against ulcerative colitis ²⁵⁵ and is generally associated with a healthy microbiome ²⁵⁶. While it is unknown why *Alistipes putredinis* has a positive association with glycerophosphocholine, taxa such as parabacteroides, ruminococcus, and bacteroides have been shown to have a positive association with glycerophosphocholine ²⁵⁷.

We also found *Ruminococcus lactaris* to be associated with N-acetyl aspartate and N-acetyl aspartylglutamate. N-acetyl aspartate correlates with neuronal mitochondrial function and survival ²⁵⁸, and N-acetyl aspartyl glutamate has procognitive properties ²⁵⁹. *Ruminococcus lactaris* is a butyrate producer ²⁶⁰ and is negatively correlated with the

inflammatory IL-8 ²⁶¹. A previous group found a link between *Ruminococcus* and N-acetylaspartate thought to be mediated by ruminococcus decreasing cortisol, which impacts brain N-acetyl aspartate ²⁶².

Ruminococcus lactaris, *Streptococcus thermophilus*, and *Eubacterium eligens* were also positively associated with various macromolecules. While the specific identification of these macromolecules isn't defined, *S. thermophilus* is a popular species found in yogurt that is known to decrease uremic toxins ²⁶³, and *E. eligens* has anti-inflammatory properties ²¹⁴.

Several bacteria were also associated with cerebral blood flow in various brain areas. The family *Eggerthellaceae* negatively correlated with cerebral blood flow in the banks of the superior temporal sulcus and the left pars triangularis. The superior temporal sulcus is commonly referred to as Wernicke's area as is a central area for speech recognition and processing.²⁶⁴ The left pars triangularis is commonly referred to as Broca's area and is a central part for speech production.²⁶⁵ Members of the family *Eggerthellaceae* are able to convert the isoflavone daidzein (a soy product) into equol, an estrogen.²⁶⁶ Specific members of this family, including *Adlercreutzia equolifaciens*, *Asaccharobacter celatus*, and *Gordonibacter pamelaiae* all have negative associations with these same areas responsible for language circuits, in addition to areas of the brain responsible to memory, learning, and reward processing. Equol supplementation has been shown to improve long and short term memory in rats by increasing brain antioxidant activity and improving blood pressure.^{267,268} Interestingly, equol has previously been reported to increase cerebral blood flow in rats.²⁶⁹ Previous studies have implicated a role of soy consumption in regulating hypertension via its consumption by the gut microbiome.²⁷⁰ *Collinsella stercoris* is also a

member of the *coriobacteriia* class, and positively correlates with cerebral blood flow in the same areas of the brain that correlate with language, memory, and learning. Interestingly, *Collinsella stercoris* is also highly positively correlated with Chronic Kidney Disease.²⁷¹ Interestingly, disruptions to the gut microbiome has previously been linked to impaired cerebral blood flow via its reduction of endothelial nitric oxide synthase (eNOS) activity²⁷². The genera *Alistipes* and *Parabacteroides*, part of the order *bacteroidales* are inversely correlated with cerebral blood flow in the putamen, accumbens, and hippocampus, all part of the limbic/rewards circuit. *Alistipes* species are highly correlated with cholesterol levels and are short chain fatty acid producers^{273,274}. *Parabacteroides* species alter dopaminergic signaling²⁷⁵

The phylum *firmicutes* and, more specifically, the order *clostridiales*, are inversely correlated with blood flow in the left transverse temporal cortex. The transverse temporal cortex is the site of the primary auditory cortex.²⁷⁶ Members of the *clostridiales* order are obligate anaerobes²⁷⁷. *Eubacterium siraeum* is a member of this order and is positively correlated with HDL cholesterol levels²⁷⁸.

The genus *Haemophilus* and the family *desulfovibrionaceae* are both part of the phylum *proteobacteria*. *Haemophilus* is infectious and is positively associated with blood flow in the cingulate and entorhinal cortices, both part of the limbic system²⁷⁹. The family *desulfovibrionaceae* are sulfate reducing bacteria and are inversely associated with blood flow in the limbic system²⁸⁰.

The Family *eggerthellaceae* was also positively correlated with the white matter integrity of the middle cerebellar peduncle and the left external capsule, which connects the frontal and parietal cortices with the temporal cortex.²⁸¹ Members of the family

eggerthellaceae, including *Adlrecreutzia equolifaciens*, *Asaccharobacter celatus*, and *Gordonibacter pamelaee* have an inverse correlation with these same tracts in addition to the pontine crossing tracts, the corticospinal tracts, the tapetum, the fornix, and the inferior fronto occipital fasciculus. These tracts are important for connecting the structures whose blood flow was altered as explained in the previous paragraph. Interestingly, the relative abundance of the Actinobacteria phylum has previously been linked to diffusion tensor imaging measurements in the thalamus, hypothalamus, and amygdala.²⁸²

The genus *Bifidobacterium* is comprised of several commensal short chain fatty acid producers²⁸³. It is inversely correlated with the white matter integrity of the corticospinal tract, while *Clostridium innocuum*, an infectious pathogen²⁸⁴, and the equol producers *Gordonibacter pamelaee*, *Asaccharobacter celatus*, and *Adlrecreutzia equolifaciens* were also positively correlated with the white matter integrity of the corticospinal tract.

The genus *Lactobacillus* strengthens the gut barrier²⁸⁵. It is positively associated with white matter integrity in the medial lemniscus along with *Lachnospira pectinoschiza*, a pectin degrading microbe. *Monoglobus pectinilyticus* also degrades pectin and is positively associated with white matter integrity in the superior longitudinal fasciculus^{286,287}.

While this study provides foundational understanding of the gut-brain axis, it has many limitations. Chief among these is that the observational nature of this study helps us to make many associations between gut bacteria and markers of brain health on imaging, but we are unable to determine causation. Additionally, the relatively small sample size for a human study with a heterogeneous population potentially leaves the study underpowered to detect smaller associations and changes in the microbiome. Future work should investigate the long-term nature of the gut microbiome following stroke.

This foundational study improves scientific knowledge of the bidirectional microbiome-brain axis by highlighting the gut microbiome changes associated with markers of brain health as detected by imaging. Future studies should examine potential mechanisms of association; these mechanisms could be exploited to bolster brain health. The gut is much easier to target therapeutically than the brain because the brain is protected by the skull and the blood brain barrier. Potential gut microbiome modifiers include dietary changes, prebiotics, probiotics, fecal transplants, or other pharmacologic therapies and could be developed to bolster brain health. Specific methods to employ would be butyrate and equol supplementation and a probiotic intervention of butyrate and equol producers, including roseburia. These types of interventions would be easily implemented, would be inexpensive, and would provide patients with additional tools to optimize healthy brain aging.

Table 4.1 Participant Characteristics

N	30
Age	65.7 ± 5.79
Sex (% Female)	83.33%
Race (% White)	90.00%
(% Black)	6.67%
(% Asian)	3.33%
Genotype (% APOE ε3/ε3)	53.33%
(% APOE ε3/ε4)	30.00%
(% APOE ε4/ε4)	3.33%
(% APOE ε2/ε3)	13.33%
Education	17.23 ± 1.80
BMI	26.95 ± 5.36
Diabetes	10.00%
Hypertension	43.33%
Hyperlipidemia	30.00%

Table 4.2 Microbial Taxa associated with Demographic Features

Demographic Feature	Bacterial Taxa	Taxa Key Characteristics	β	Q-Value
Age	None			
Sex (Male)	<i>Bacteroides plebeius</i>	Metabolizes agarose	0.969	0.01641
	Genus <i>Clostridium</i>	Also inhabits female reproductive tract	-1.12	0.04952
	Genus <i>Haemophilus</i>	Infectious, inversely associated with plant based diet	0.611	0.06091
Race	None			
ApoE ϵ 2 carriers	<i>Eubacterium eligens</i>	Anti-inflammatory	-1.44	0.1697
	<i>Blautia producta</i>		0.587	0.0827
	Genus <i>Lachnoclostridium</i>		1.59	0.1171
	Genus <i>Oscillibacter</i>		-2.75	0.1808
	<i>Faecalibacterium prausnitzii</i>	Anti-inflammatory	-1.26	0.1808
ApoE ϵ 4 carriers	Genus <i>Roseburia</i>	Butyrate producer	-0.638	0.2134
	<i>Holdemania filiformis</i>		-0.658	0.2049
Education	None			
Obese	<i>Akkermansia muciniphila</i>	Decreased in obesity	-0.663	0.1205
	<i>Bacteroides dorei</i>	Anti-inflammatory	1.62	0.0703
Diabetes	<i>Escherichia coli</i>	Normal gut commensal with capacity to cause extraintestinal infections	1.76	0.1169
	<i>Parabacteroides goldsteinii</i>	Anti-inflammatory	1.34	0.2214
Hypertension	Genus <i>Phascolarctobacterium</i>	Produce SCFAs	-1.26	0.06803
Hyperlipidemia	None			

Table 4.3 Diet correlates with microbial taxa

Diet Feature	Microbial Taxa	Taxa Key Characteristics	Coef	Q Value
Fiber	<i>None</i>			
	<i>Clostridium asparagiforme</i>		-0.247	0.1906
	Family <i>Acidaminococcaceae</i>	Produce SCFAs	0.201	0.1906
Calcium	<i>Eubacterium eligens</i>	Anti-inflammatory	0.312	0.2166
	Genus <i>Haemophilus</i>	Infectious, inversely associated with plant based diet	0.176	0.2166
	Genus <i>Phascolarctobacterium</i>	Produce SCFAs	0.203	0.2421
Whole Grains	<i>None</i>			
Added Sugars	<i>None</i>			
Dairy	<i>None</i>			
Fruits	<i>None</i>			
	<i>Eggerthella lenta</i>	Infectious	-0.347	0.1405
Vegetables	<i>Agathobaculum butyriciproducens</i>	Butyrate producer	0.311	0.1405

Table 4.4 Microbial taxa associated with imaging features

Microbial Taxa	Taxa Key Characteristics	Imaging Feature Volume	Coef	<i>Q</i> Value
<i>Bacteroides ovatus</i>	Induces IgA Promotes IL-22	Thalamus	-0.672	0.169
<i>Bacteroides uniformis</i>	Butyrate Producer	White Matter Hypointensities	-0.376	0.1578
Family <i>Acidaminococcaceae</i>	SCFA Producer	Corpus Callosum Mid Posterior	0.364	0.2157

Table 4.5 Microbial taxa associated with brain metabolites

Microbial Taxa	Taxa Key Characteristics	Metabolite	Coef	Q Value
<i>Collinsella aerofaciens</i>	Proinflammatory Bile-Acid Conjugator	GABA	- 0.357	0.0615 2
<i>Parasutterella excrementihominis</i>		GABA	0.703	0.0739 1
<i>Alistipes putredinis</i>		GPC	0.956	0.2127
Family <i>Acidaminococcaceae</i>	SCFA Producer	GPC	0.338	0.2127
		NAA+NAAG	0.653	0.0965 8
<i>Ruminococcus lactaris</i>	Butyrate Producer Inhibits IL-8	MM09	0.688	0.0351 9
		MM12	0.612	0.0916 0
<i>Streptococcus thermophilus</i>	Decreases uremic toxins	MM09	0.526	0.1315
		MM12	0.547	0.0714 3
<i>Eubacterium eligens</i>	Anti-inflammatory	MM14+Lip13 a+Lip13b+M M12	0.484	0.2314

Table 4.6 Microbial Taxa associated with Cerebral Blood Flow

Microbial Taxa	Taxa Key Characteristics	Perfusion Imaging Feature	Coef	Q Value
Family <i>Eggerthellaceae</i>	Equol Producers	Banks of Superior Temporal Sulcus	-0.364	0.1261
		Left Pars Triangularis	-0.219	0.09265
<i>Adlercreutzia equolifaciens</i>	Equol Producer	Banks of Superior Temporal Sulcus	-0.551	0.1261
		Total Middle Temporal Cortex	-0.356	0.2146
		Left Pars Triangularis	-0.355	0.09821
<i>Asaccharobacter celatus</i>	Equol Producer	Total Banks of Superior Temporal Sulcus	-0.573	0.07049
		Left Middle Temporal Cortex	-0.595	0.0489
		Total Middle Temporal Cortex	-0.652	0.01391
		Total Insula	-0.527	0.2112
		Left Pars Triangularis Cortex	-0.518	0.09265
		Right Pars Opercularis Cortex	-0.630	0.02800
<i>Gordonibacter pamelaee</i>	Equol Producer	Total Putamen	-0.577	0.08859
		Left Pars Triangularis Cortex	-0.525	0.09265
		Left Posterior Cingulate Cortex	-0.594	0.1455
		Total Posterior Cingulate Cortex	-0.635	0.0503
<i>Collinsella stercoris</i>	Bile-Acid Conjugator	Right Banks of Superior Temporal Sulcus	0.460	0.00409
		Total Middle Temporal Cortex	0.340	0.1678
		Left Pars Triangularis	0.327	0.09401
		Left Transverse Temporal	0.339	0.2098
Genus <i>Alistipes</i>	SCFA Producer	Left Putamen	-0.485	0.00174
		Left Accumbens area	-0.406	0.1063
Genus <i>Parabacteroides</i>	Alter dopamine signaling	Right Hippocampus	-0.753	0.00210
Order <i>Clostridiales</i>		Left Transverse Temporal Cortex	-0.900	0.2098
<i>Eubacterium siraeum</i>	Positively correlated with HDL cholesterol	Total Middle Temporal Cortex	-0.715	0.1352
		Right Caudal Middle Frontal Cortex	-0.770	0.1239
		Right Post Central Cortex	-0.674	0.1691
Genus <i>Haemophilus</i>	Infectious	Total Rostral Anterior Cingulate	0.267	0.09848
		Total Posterior Cingulate Cortex	0.240	0.1928
<i>Haemophilus parainfluenzae</i>		Right Entorhinal	0.281	0.02571
Family <i>Desulfovibrionaceae</i>	Sulfate reducers	Right Entorhinal Cortex	-0.449	0.1875

Table 4.7 Microbial taxa associated with white matter integrity

Microbial Taxa	Taxa Key Characteristics	White Matter Integrity Imaging Feature	Coef	Q Value
Family <i>Eggerthellaceae</i>	Equol Producers	Middle Cerebellar Peduncle	0.245	0.05163
		Left External Capsule	0.252	0.09284
<i>Gordonibacter pamelaiae</i>	Equol Producer	Middle Cerebellar Peduncle	0.720	0.004926
		Pontine Crossing Tract	0.646	0.05013
		Left Corticospinal Tract	0.613	0.1115
<i>Assacharobacter celatus</i>	Equol Producer	Left Tapetum	0.662	0.02824
		Left Corticospinal Tract	0.468	0.1821
<i>Adlercreutzia equolifaciens</i>	Equol Producer	Left Corticospinal Tract	0.324	0.2284
		Left Fornix	0.396	0.1751
		Left Inferior Frontal Occipital Fasciculus	0.437	0.06521
Genus <i>Bifidobacterium</i>	SCFA Producer	Left Corticospinal Tract	- 0.547	0.1115
<i>Coprobacter fastidiosus</i>		Right Superior Longitudinal Fasciculus	- 0.473	0.2484
<i>Bacteroides uniformis</i>	Butyrate Producer	Right Tapetum	0.469	0.03213
<i>Eubacterium siraeum</i>	Positively correlated with HDL cholesterol	Middle Cerebellar Peduncle	0.645	0.1392
<i>Clostridium innocuum</i>	Infectious	Left Corticospinal Tract	0.423	0.2468
Genus <i>Lactobacillus</i>	Strengthen gut barrier	Left Medial Lemniscus	0.380	0.2285
<i>Lachnospira pectinoschiza</i>	Degrades pectin	Left Medial Lemniscus	0.296	0.2285
<i>Roseburia hominis</i>	Butyrate Producer	Left Cingulum	0.544	0.09441
		Left Inferior Frontal Occipital Fasciculus	0.503	0.06636

Genus <i>Streptococcus</i>	Decreases uremic toxins	Right Superior Longitudinal Fasciculus	- 0.416	0.2484
<i>Monoglobus pectinilyticus</i>	Degrades pectin	Right Superior Longitudinal Fasciculus Tapetum	0.609 0.626	0.2484 0.1934
<i>Clostridium citroniae</i>		Right Superior Longitudinal Fasciculus	0.384	0.2484
Genus <i>Flavonifractor</i>		Right Superior Longitudinal Fasciculus	0.369	0.2484
<i>Gemmiger formicilis</i>		Superior Longitudinal Fasciculus	- 0.447	0.2047

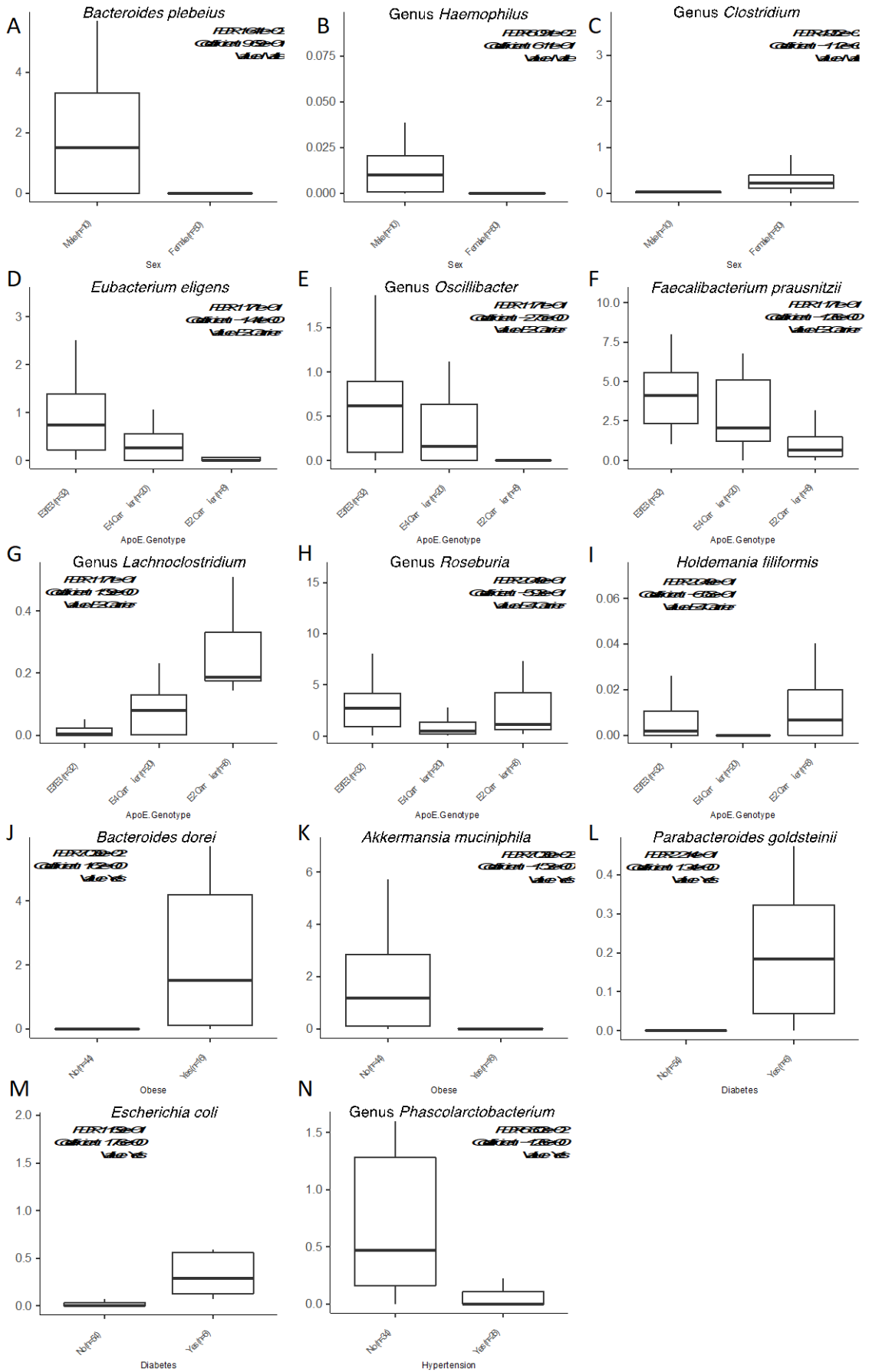


Figure 4.1 Microbial taxa associated with demographic features.

Male sex was associated with higher A) *Bacteroides plebeius* and B) the genus *Haemophilus* and lower C) genus *Clostridium*. The Apolipoprotein E (ApoE) ϵ 2 genotype was associated with lower D) *Eubacterium eligens*, E) the genus *Oscillibacter*, and F) *Faecalibacterium prausnitzii* and higher G) genus *Lachnoclostridium*. The ApoE ϵ 4 genotype was associated with lower H) genus *Roseburia* and I) *Holdemania filiformis*. Obesity was associated with higher J) *Bacteroides dorei* and lower K) *Akkermansia muciniphila*. Diabetes was associated with higher L) *Parabacteroides goldsteinii* and M) *Escherichia coli*. Hypertension was associated with lower N) genus *Phascolarctobacterium*.

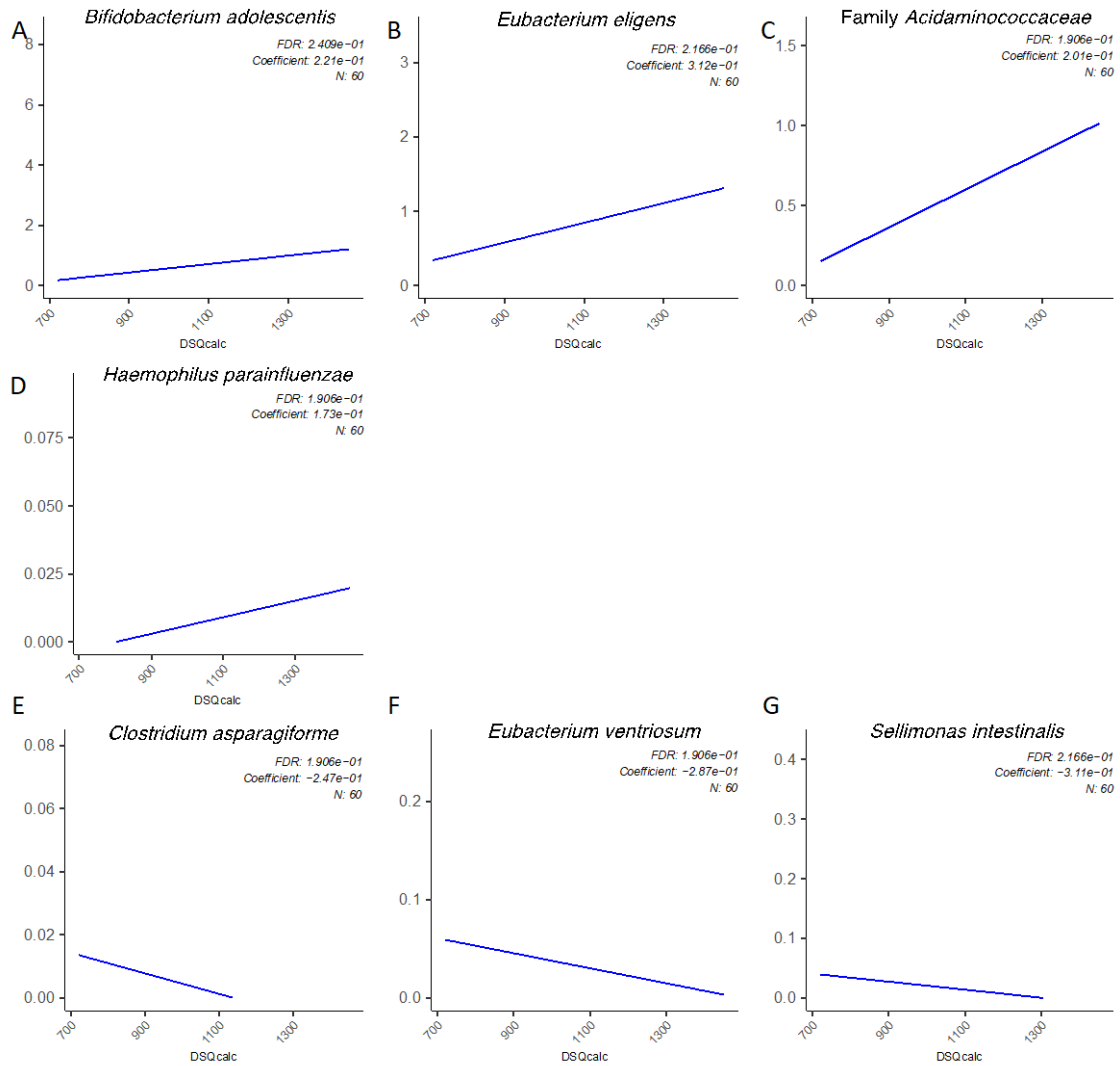


Figure 4.2 Microbial Taxa Associations with Dietary Calcium Intake.

The following taxa were positively associated with calcium intake: A) *Bifidobacterium adolescentis*, B) *Eubacterium eligens*, C) family *Acidaminococcaceae*, and D) *Haemophilus parainfluenzae*. The following taxa were negatively associated with calcium intake: E) *Clostridium asparagiforme*, F) *Eubacterium ventriosum*, and G) *Sellimonas intestinalis*.

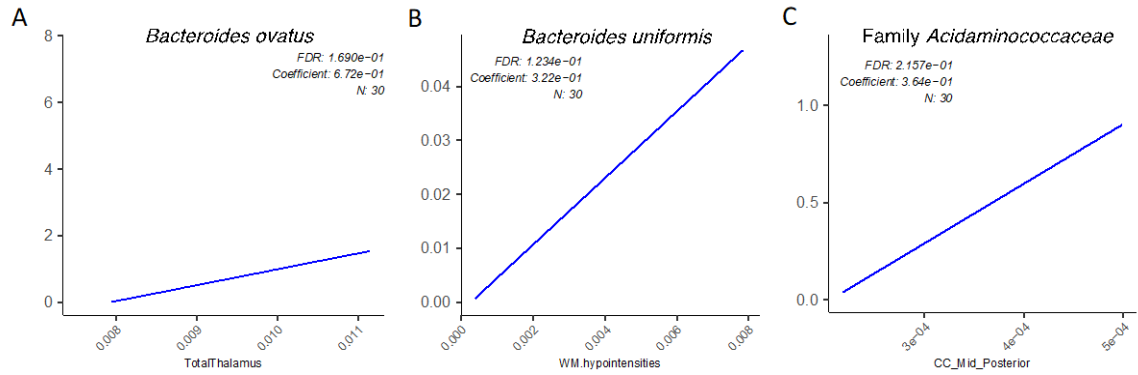


Figure 4.3 Microbial Taxa Associations with Structural Imaging Features.

A) The thalamus volume is positively associated with *Bacteroides ovatus* abundance. B) White Matter (WM) hypointensities are positively associated with *Bacteroides uniformis* abundance. C) The volume of the mid-posterior portion of the corpus callosum (CC_Mid_Posterior) is positively associated with the family *acidaminococcaceae* abundance.

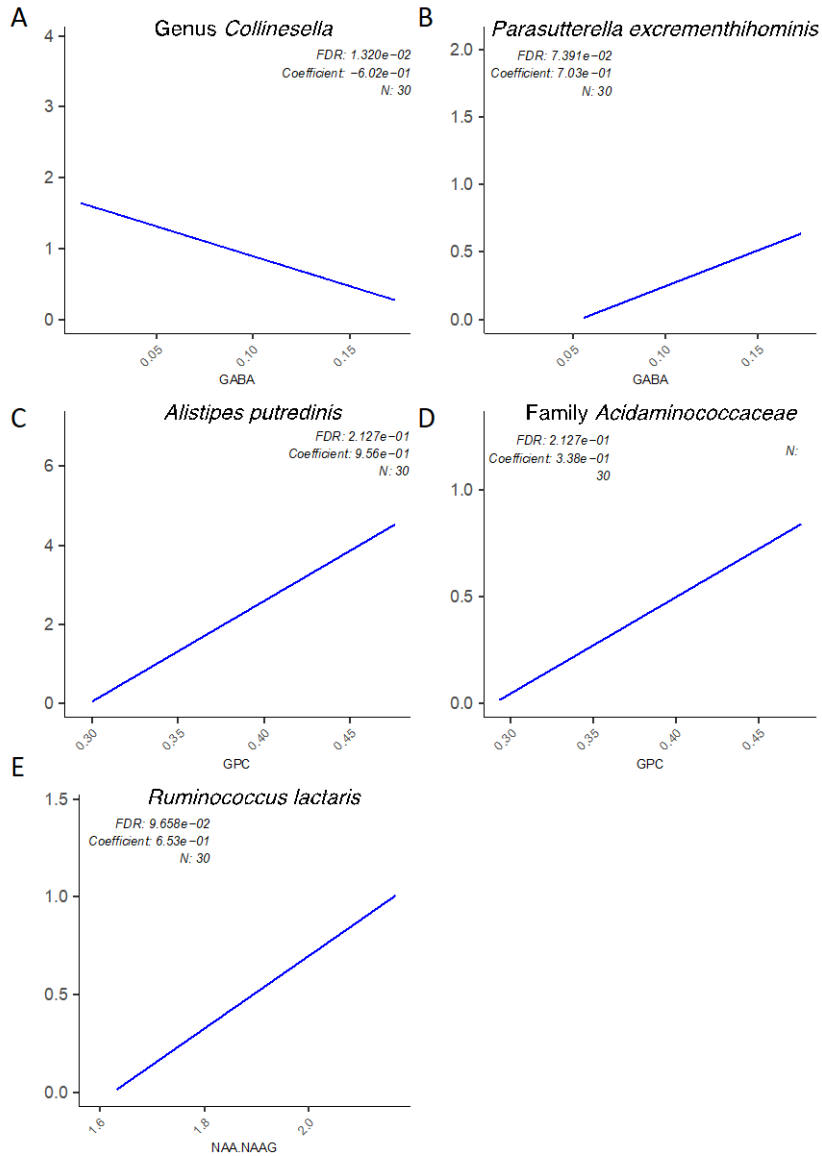


Figure 4.4 Notable Microbial Taxa Associations with Brain Metabolites in the white matter of the corpus callosum.

A) GABA is negatively associated with the genus *Collinsella* and B) positively associated with *Parasutterella excrementihominis*. C) Glycerophosphorylcholine (GPC) is positively associated with *Alistipes putredinis* and D) the family *Acidaminococcaceae*. E) N-acetyl aspartate (NAA) or N-acetyl aspartyl glutamate (NAAG) is positively associated with *Ruminococcus lactaris*.

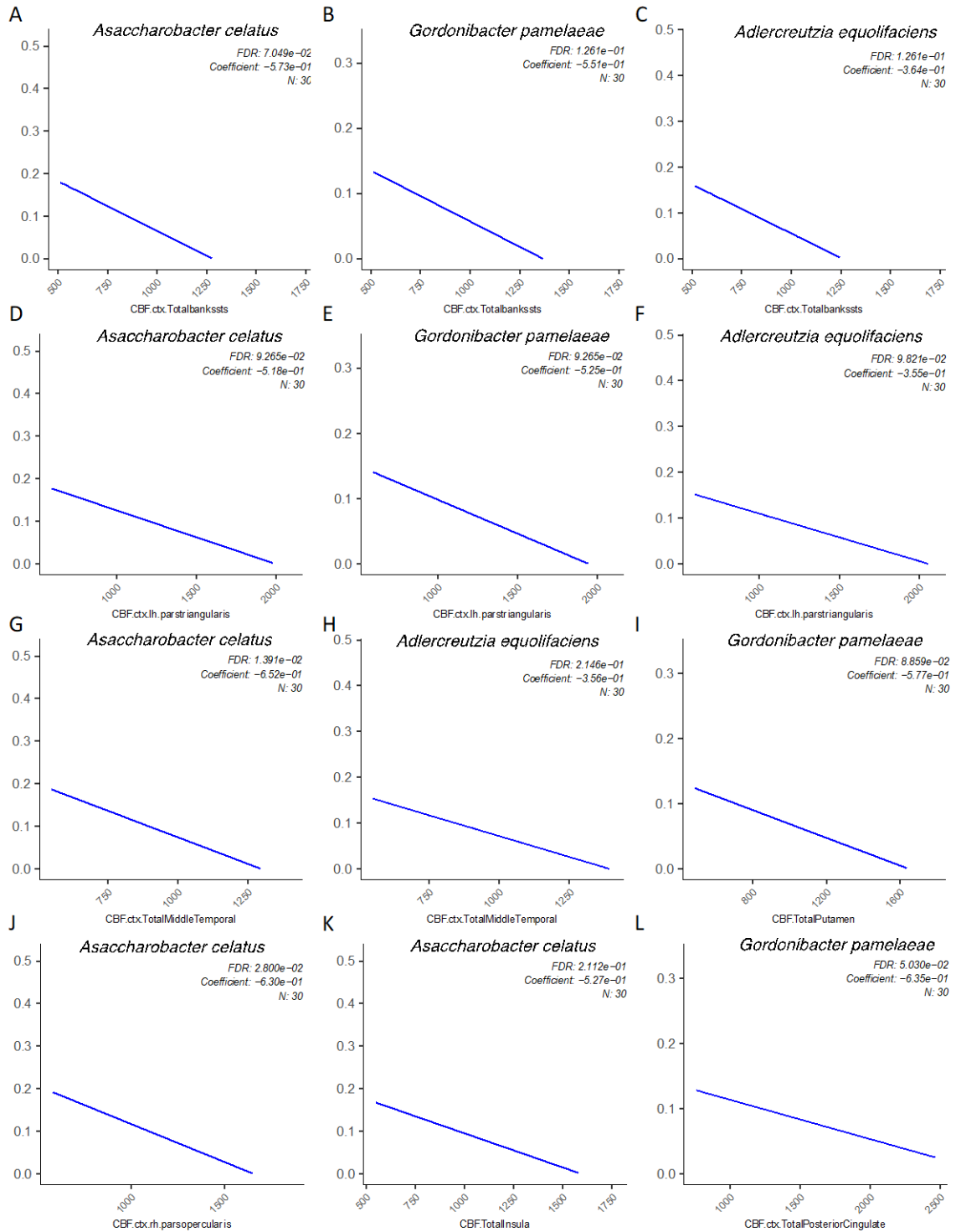


Figure 4.5 Species from the *eggerthellaceae* family are negatively associated with cerebral blood flow (CBF) in language, memory, and limbic brain areas. *Eggerthellaceae* spp. are negatively associated with CBF in A-C) the banks of the superior of the superior temporal sulcus, D-F) the pars triangularis, G,H) the middle temporal gyrus, I) the putamen, J) the pars opercularis, K) the insula, and L) the posterior cingulate.

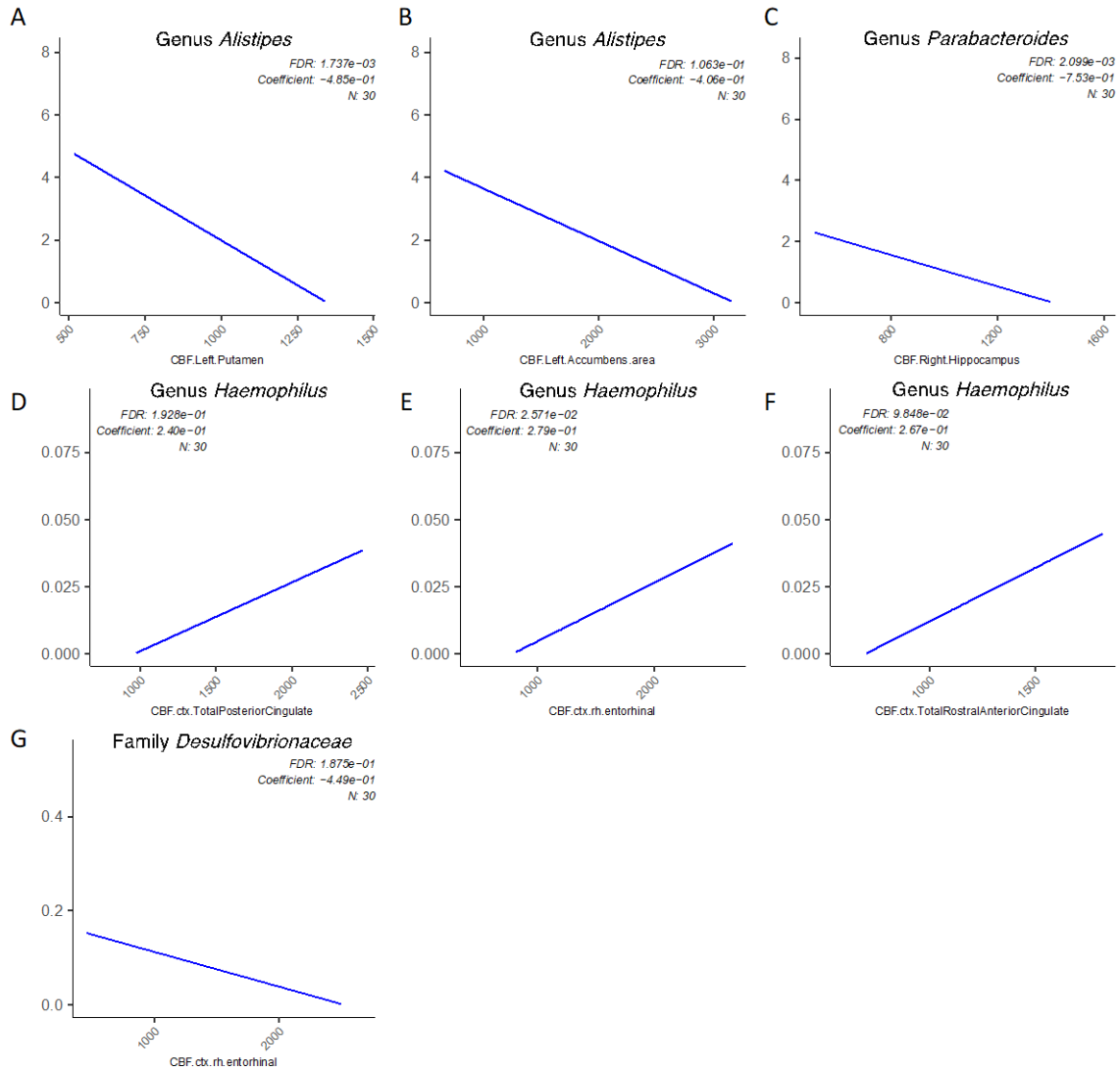


Figure 4.6 Notable Microbial Taxa Associations with cerebral blood flow (CBF) in limbic and memory regions.

The genus *Alistipes* is negatively associated with CBF in the A) Putamen and B) Accumbens area. The genus *Parabacteroides* is negatively associated with CBF in the C) Hippocampus. The genus *Haemophilus* is positively associated with CBF in the D) posterior cingulate cortex, E) entorhinal cortex, and F) rostral anterior cingulate cortex. The family *Desulfovibrionaceae* is negatively associated with G) the entorhinal cortex.

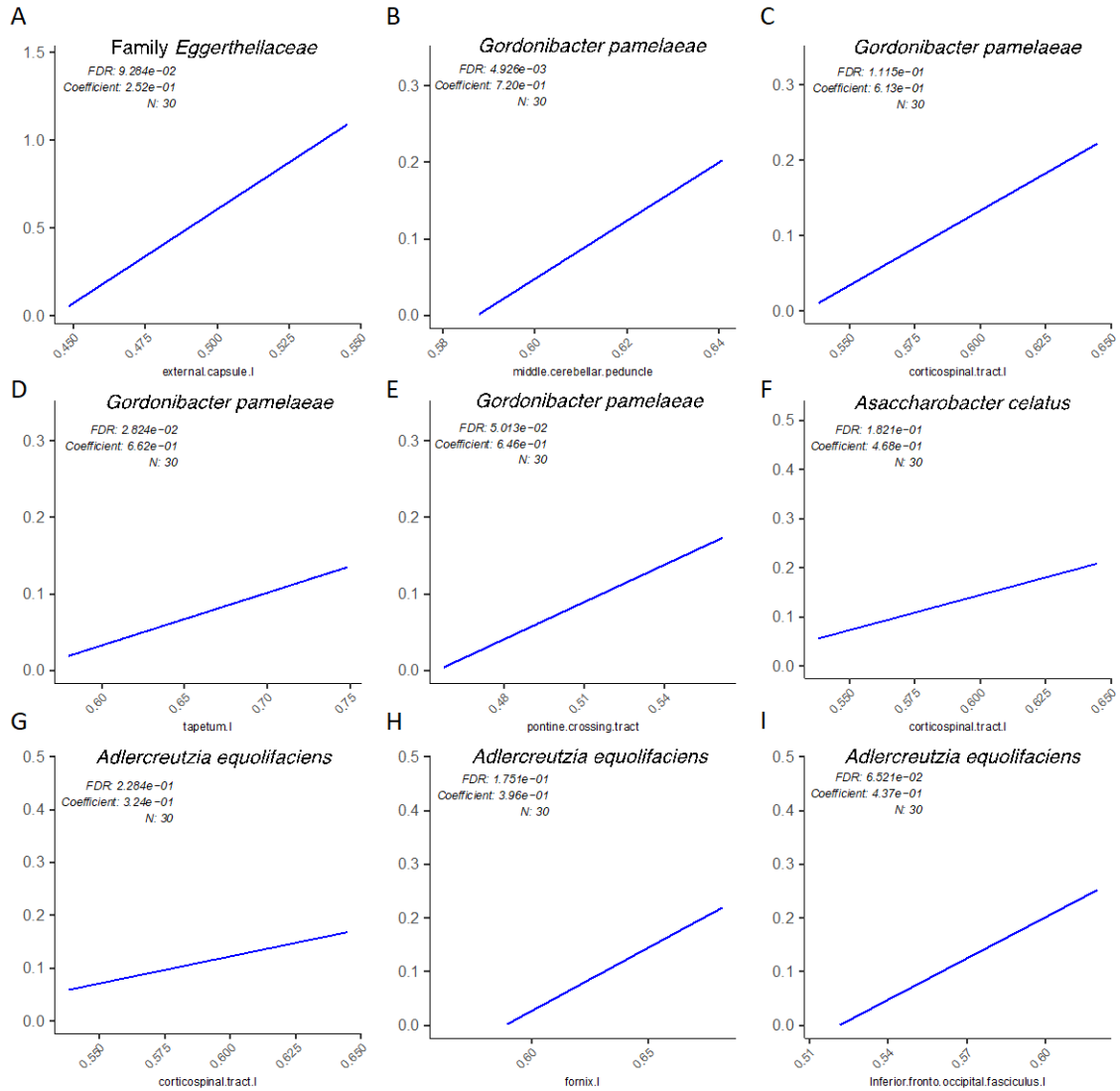


Figure 4.7 Species from the *eggerthellaceae* family are positively correlated with white matter integrity (WMI) in language, memory, and limbic brain circuits. *Eggerthellaceae* spp. Are positively associated with WMI in A) the external capsule, B) the middle cerebellar peduncle, C,F,G) the corticospinal tract, D) the tapetum, E) the pontine crossing tract, H) the fornix, and I) the Inferior fronto-occipital fasciculus.

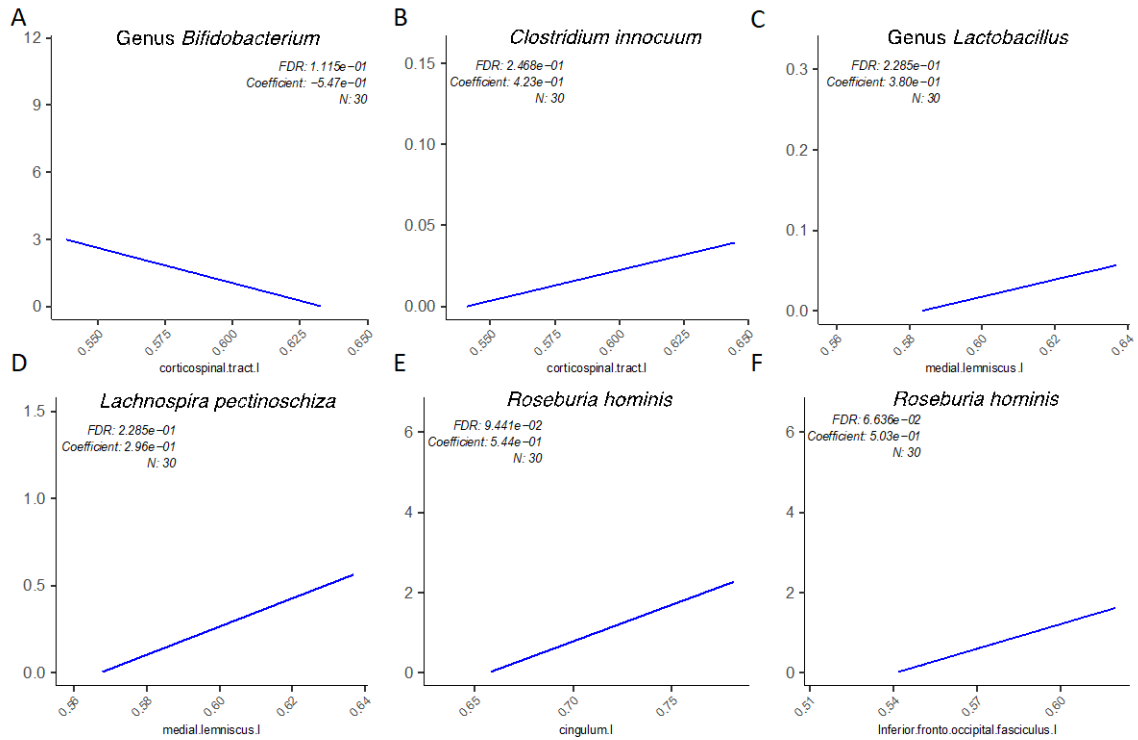


Figure 4.8 Notable Microbial Taxa Associations with cerebral blood flow (CBF) in limbic and memory regions.

A) The Genus *Bifidobacterium* is negatively associated with WMI in the corticospinal tract. B) *Clostridium innocuum* is positively associated with WMI in the corticospinal tract. C) The Genus *Lactobacillus* is positively associated with WMI in the medial lemniscus. D) *Lachnospira pectinoschiza* is positively associated with WMI in the medial lemniscus. *Roseburia hominis* is positively associated with WMI in E) the cingulum and F) the Inferior fronto-occipital fasciculus.

CHAPTER 5. GENERAL DISCUSSION

In summary, we found that stroke was associated with an increase of pro-inflammatory bacterial taxa and a decrease in taxa that produce butyrate and secondary bile acids necessary for healthy metabolic function. *Roseburia*, an important butyrate producer, had a lower relative abundance in association with a leaky gut. In individuals with the APOE $\epsilon 2/\epsilon 3$ genotype, bacteria with anti-inflammatory properties were reduced and in individuals with APOE $\epsilon 3/\epsilon 4$ genotype, *roseburia* was reduced.

On imaging analysis, we found that butyrate producers are associated with the volume of the thalamus and corpus callosum which are superhighway regions of the brain, responsible for relaying and processing mass information. Proinflammatory species were associated with GABA production. Importantly, the family *eggerthellacaeae* was highly associated with cerebral blood flow in areas of the brain related to language, memory, and learning and with the white matter integrity of the tracts connecting these areas.

Finally, many functional tasks were associated with gut microbiome levels. Recovery from stroke was associated with *Collinsella aerofaciens*, a bile-salt conjugator that may inhibit the hypothalamic-pituitary-adrenal axis in the context of a leaky blood brain barrier. Long-term memory performance in stroke is associated with *roseburia* abundance. *Bacteroides uniformis*, a butyrate producer, is positively correlated with self-efficacy, while *Enterobacteriaceae*, a classically inflammatory family, is negatively correlated with self-efficacy. *Eubacteriaceae* is positively associated with meaning and purpose. *Coriobacteriia*, an equol producer, is positively correlated with social support. *Alistipes shahii*, a TMAO producer is correlated with perceived pain.

Butyrate-producing bacteria continuously emerged as being decreased in the context of stroke and inversely related to stroke severity markers. Previous studies have also found a reduction of butyrate-producing bacteria in the context of stroke.²⁰⁸ Butyrate is a histone deacetylase inhibitor and a ligand for a subset of G protein-coupled receptors that has the power to affect gene expression and have many downstream applications.²⁸⁸ Butyrate treatment in stroke has been associated with an increase in the number of cells expressing markers of developing and migrating neurons and synaptogenesis.²⁸⁹ In rats, administration of butyrate following stroke reduces infarct volume and improves neurological function at 24 and 72 hours after middle cerebral artery occlusion by ameliorating the apoptosis caused by the stroke by binding to G-protein coupled receptors that regulate apoptosis and inflammation.⁹⁵

While many butyrate producing bacteria appeared important in the context of stroke, the genus *roseburia* was continuously hallmarked as one of the most important butyrate producers. We found that *roseburia* was decreased in our stroke participants in association with the leaky gut marker fecal alpha-1-antitrypsin. Additionally, *roseburia* was decreased in individuals with the ApoE $\epsilon 3/\epsilon 4$ genotype, a risk factor for severe stroke and post-stroke cognitive impairment. Finally, long term memory performance was associated with *roseburia* abundance. A previous study found that individuals with a higher abundance of *roseburia* generally experienced strokes that were more mild compared with their counterparts with a lower abundance who experienced more severe strokes, suggesting a neuroprotective effect of *roseburia*.²⁹⁰ *Roseburia* uses its flagella to penetrate the colonic mucus layer to interact with the epithelium and is therefore one of the most abundant butyrate-producing bacteria that adhere to intestinal mucin, positioning it well for use as a

probiotic.²⁹¹ Beyond its function as a butyrate producer, *roseburia* is also a powerful stimulator of the gut immune system to produce IL-22, a cytokine involved in wound healing and protection against microbes,^{292,293} and reduce IL-6 and IL-17, both proinflammatory factors.²⁹⁴

A surprising role of members of the class *coriobacteriia* in the phylum *actinobacteria* was found in our markers of stroke severity. *Collinsella aerofaciens* was found to be positively associated with functional recovery in the rehabilitation setting. It was also found to be negatively associated with GABA abundance in the corpus callosum. While *C. aerofaciens* is commonly considered to be a pro-inflammatory species in the context of inflammatory bowel disease,^{248,249} in the context of a leaky blood brain barrier like that found in stroke, it has been reported as a bile-salt conjugator that may inhibit the hypothalamic-pituitary-adrenal axis via bile acid deposition in the hypothalamus and reduce CNS and systemic inflammation.^{189,190} The family *eggerthellaceae* containing the species *Asaccharobacter celatus*, *Adlercreutzia equolifaciens*, and *Gordonibacter pamelaee* were all inversely associated with cerebral blood flow in brain regions related to language, memory, and learning, and positively associated with the white matter integrity connecting these regions. Additionally *A. equolifaciens* was inversely associated with leaky gut and *coriobacteriia* as a whole was positively associated with social support. One of the hallmark features of these bacteria is their role as equol producers. Equol is an estrogen metabolized from soy that possesses antiatherogenic properties and improves arterial stiffness.²⁹⁵ One group found that plasma levels of equol were reduced in response to stroke in proportion to the severity of the stroke.²⁹⁶ A separate study found that equol administration in rats is able to inhibit the activation of Src and the upregulation of

gp91(phox) thought to play a prominent role in mediating ischemic alteration in neurons following stroke.²⁹⁷

While this study provides foundational understanding of the gut-brain axis in the context of stroke rehabilitation, it has many limitations. Chief among these is that the observational nature of this study helps us to make many associations between gut bacteria and markers of stroke severity, but we are unable to determine causation. Additionally, the relatively small sample size for a human study with a heterogeneous population potentially leaves the study underpowered to detect smaller associations and changes in the microbiome. Finally, due to the challenges of the COVID-19 pandemic, many of our stroke subjects were lost to follow-up making a longitudinal study challenging. Future work should investigate the long-term nature of the gut microbiome following stroke.

This foundational study improves scientific knowledge of the bidirectional microbiome-brain axis by highlighting the gut microbiome changes associated with stroke in humans and how these changes are associated with markers of stroke severity. Future studies should examine potential therapies targeting the microbiome after stroke in order to optimize functional recovery. The gut is much easier to target therapeutically than the brain because the brain is protected by the skull and the blood brain barrier. Potential gut microbiome modifiers include dietary changes, prebiotics, probiotics, fecal transplants, or other pharmacologic therapies and could be developed to target the specific microbial community imbalances seen following stroke. Specific methods to employ would be butyrate and equol supplementation and a probiotic intervention of butyrate and equol producers, including roseburia. These types of interventions would be easily implemented,

would be inexpensive, and would provide patients with additional tools to optimize neuroplasticity in their difficult rehabilitation journey.

CHAPTER 6. [SUPPLEMENT] β -AMYLOID AND TAU DRIVE EARLY ALZHEIMER'S DISEASE DECLINE WHILE HYPOMETABOLISM DRIVES LATE DECLINE

6.1 Summary

Clinical trials focusing on therapeutic candidates that modify β -amyloid ($A\beta$) have repeatedly failed to treat Alzheimer's disease (AD), suggesting that $A\beta$ may not be the optimal target for treating AD. The evaluation of $A\beta$, tau, and neurodegenerative (A/T/N) biomarkers has been proposed for classifying AD. However, it remains unclear whether disturbances in each arm of the A/T/N framework contribute equally throughout the progression of AD. Here, using the random forest machine learning method to analyze participants in the Alzheimer's Disease Neuroimaging Initiative dataset, we show that A/T/N biomarkers show varying importance in predicting AD development, with elevated biomarkers of $A\beta$ and tau better predicting early dementia status, and biomarkers of neurodegeneration, especially glucose hypometabolism, better predicting later dementia status. Our results suggest that AD treatments may also need to be disease stage-oriented with $A\beta$ and tau as targets in early AD and glucose metabolism as a target in later AD.

6.2 Introduction

Alzheimer's disease (AD) is the most common form of dementia worldwide and is defined biologically as the pathologic deposition of folded β -amyloid ($A\beta$) plaques and hyperphosphorylated neurofibrillary tau tangles in the brain leading to neurodegeneration²⁹⁸⁻³⁰⁰. Clinically, AD presents as a syndrome of progressive episodic memory and executive functioning problems across a cognitive continuum ranging through cognitively unimpaired (CU), mild cognitive impairment (MCI), and AD. While there are

currently five drugs approved by the FDA to treat the symptoms of AD, there are no disease-modifying therapies that alter the course of the disease. Over the past few decades, the development of treatments for AD has been largely focused on compounds which aim to reduce A β plaques, either by directly targeting A β itself through antibodies or by targeting the enzymes that cleave amyloid precursor protein (APP) to produce it^{301,302}. However, clinical trials of drugs targeting A β had a 99.6% failure rate between 2002 and 2012³⁰³, and two more A β -focused drug trials failed in phase three in 2019³⁰⁴. This failure rate is among the highest of any disease area. The high failure rate for AD drug candidates focused on A β indicates that A β may not be the optimal therapeutic target to combat AD.

Careful analysis of AD biomarkers may give important insights into underlying AD pathogenesis and clues about appropriate AD treatments since these biomarkers exist as proxies for AD neuropathologic changes. Furthermore, an understanding of how the biomarkers correlate with clinical symptoms of AD could inform clinicians making AD management decisions to improve patient quality of life. The A/T/N biomarker framework promulgated by the National Institute on Aging-Alzheimer's Association was created to be an unbiased classification scheme for the three arms of biomarkers known to underlie AD pathology, namely neuropathological loads of A β (A) and tau (T), and neurodegeneration (N, including hypometabolism and brain atrophy)^{305,306}. Indeed, some research groups have demonstrated that the distribution of tau tangles³⁰⁷ and hypometabolism (due to low glucose uptake) are more strongly correlated with cognitive performance than A β ³⁰⁸. Moreover, brain atrophy is also suggested to be highly correlated with AD progression³⁰⁹. However, it remains unclear whether disturbances in each arm of the A/T/N framework contribute equally to the progression of AD symptoms or if these factors instead have

varying impacts at different stages of AD progression. Understanding this stage-dependent nature of the biomarkers could lead to important clues in preventing and treating AD.

In order to determine the nature of the association of AD biomarkers with the progression of AD symptoms, in this study we assessed the statistical importance of each arm of the A/T/N framework in predicting three progressive clinical statuses of cognitive performance: cognitively unimpaired (CU), late mild cognitive impairment (LMCI), and AD³⁰⁵. To do so, we used data from the Alzheimer's Disease Neuroimaging Initiatives (ADNI) database, relating to four biomarkers: A β (assessed from ¹⁸Florbetapir-positron emission tomography (PET)), phosphorylated tau (pTau181, assessed from cerebrospinal fluid), glucose uptake (assessed from ¹⁸fluorodeoxyglucose (FDG)-PET), and volumetric measures (assessed from MRI). We used a random forest machine learning algorithm to rank the importance of each biomarker in predicting clinical dementia status. We chose the random forest machine learning method because it not only has the ability to fit models with high prediction accuracy due to its use of multiple decision trees that combine to yield a consensus prediction, but also is very interpretable due to its ranking capability of the relative importance of predictors used in the classification (AD biomarkers in our case). We also analyzed the relationship between A/T/N biomarkers and memory composite and executive functioning composite scores in order to assess more directly their association with cognitive performance. We show that A/T/N biomarkers have differing contributions in predicting clinical dementia status based on the stage of cognitive impairment, with A β and pTau having higher contribution in predicting early cognitive impairment (LMCI vs CU) and glucose uptake having higher contribution in predicting later cognitive impairment (AD vs LMCI and AD vs. CU). Our findings could help real-world patient

populations by informing clinicians to make AD management decisions according to disease stage based on the expression of the relevant A/T/N biomarkers and by informing drug development teams to design treatments to target the pathophysiology underlying the expression of the biomarkers at the appropriate stage of disease progression.

6.3 Results

6.3.1 Participant characterizations and data selection

Participant data was extracted from the ADNI database for inclusion in the analysis. Participants were required to have baseline A β imaging biomarkers (from ¹⁸Florbetapir PET), glucose uptake imaging biomarkers (from ¹⁸FDG PET), brain volume imaging biomarkers (from T1-weighted structural MRI), and cognitive testing to be included in the analysis. Participants with three or more missing values were excluded from the analysis. As tau imaging was not available for most participants in the ADNI database, we used a phosphorylated tau biomarker (pTau) from cerebrospinal fluid (CSF) as a measure of tau levels. These criteria yielded a final sample of 405 participants clinically diagnosed as being either cognitively unimpaired (CU; n = 148) or with late mild cognitive impairment (LMCI; n = 147) or Alzheimer's disease (AD; n = 110) (**Table 6.1**).

The three study groups were balanced in terms of gender, race, and ethnicity, but not age or education, across clinical status, with the AD group being significantly older than LMCI subjects and less educated than CU and LMCI subjects; accordingly, we adjusted the features for age before applying them to the random forest model since age is known to affect brain volumetric measures. Notably, the groups differed in terms of the expression of the $\epsilon 4$ allele of apolipoprotein E (*APOE* $\epsilon 4$), the largest genetic risk factor for Alzheimer's disease³¹⁰, and cognitive testing scores, with the AD group being

significantly more likely to carry *APOE* $\epsilon 4$ and to have lower cognitive testing scores than CU and LMCI subjects. The cognitive tests completed included the Mini-Mental State Examination (MMSE), Clinical Dementia Rating Sum of Boxes (CDRSB), Alzheimer’s Disease Assessment Scale-Cognitive Subscale (ADAS-cog 13), composite memory score (ADNI_MEM), and composite executive functioning score (ADNI_EF). The biomarkers were further stratified into 16 features classified according to the A/T/N framework, comprising $A\beta$ measures from 6 brain regions (frontal lobe, cingulate gyrus, parietal lobe, temporal lobe, precuneus, and hippocampus), glucose uptake (FDG) data from 3 brain regions (angular gyrus, temporal lobe, and posterior cingulum), volumetric measures from 6 regions (ventricles, whole brain, entorhinal cortex, hippocampus, gray matter, white matter), and pTau levels from the CSF (**Table 6.2**). We show the correlation of the 16 features with each other using a heatmap. It shows that the $A\beta$ measures were highly correlated with each other, as were the FDG measures, and the volumetric measures, while $A\beta$ and pTau were negatively correlated with FDG and volumetric measures.

6.3.2 Relative importance of AD biomarkers in early and late AD

We first sought to determine the relative importance of each biomarker feature in predicting clinical dementia status in three participant group pairings: CU vs LMCI, LMCI vs AD, and CU vs AD. **Table 6.3** shows the descending order ranking of the relative importance of the 16 features in predicting clinical dementia status based on the random forest method, a machine-learning algorithm that utilizes multiple decision trees to classify and rank variables according to their accuracy in predicting outcomes. Notably, the top half (top 8) of the features made up the majority of the relative importance (69.1%, 75.45%, and 86.74%) for each cognitive state classification. In CU vs LMCI, hippocampal volume

ranked highest in relative prediction accuracy with a relative importance of 12.69%, followed by four A β features, pTau, FDG in the angular gyrus (FDG-Angular), and entorhinal cortex volume; thus, features from all three arms of the A/T/N framework were represented in the top 8 features in the CU vs LMCI comparison. In contrast, in LMCI vs AD, neurodegeneration, i.e., the N component of the framework, dominated the top 8 features, with all three FDG glucose uptake measurements (temporal lobe = 18.88% relative importance) and entorhinal cortex, hippocampal and ventricle volumes represented. In particular, the three FDG features were ranked as the top three contributors in the LMCI vs AD comparison. Moreover, the contribution of FDG was weighted even higher in CU vs AD, with FDG-Angular making up 23.78%, and FDG in the posterior cingulum (FDG-CingulumPost) making up 16.99% of the relative importance. Another N component, hippocampal volume, also had an increased relative importance in the CU vs AD comparison relative to the other comparisons. The findings suggest that, overall, A β and pTau are important contributors to the progression from normal cognitive functioning to LMCI, but that neurodegeneration, especially glucose hypometabolism, emerges as a more important contributor when progressing from LMCI to AD. Glucose hypometabolism also serves as a prominent distinguishing feature between normal cognitive functioning and AD. We replicated our analysis using the SHapley Additive exPlanations (SHAP) technique and obtained a feature ranking analysis consistent with those from the random forest analysis.

6.3.3 Accuracy of the top 8 features vs all 16 features

We next determined the prediction accuracy of all 16 features in classifying the three participant group pairs. For all 16 features, accuracies of 73.17%, 71.01%, and

90.34% were obtained for the CU vs LMCI, LMCI vs AD, and CU vs AD comparisons, respectively (**Table 6.4**). To ensure that our cognitive status classification model was robust, the F_1 score was also used to evaluate the precision and recall of the model. The results show that the 16 features were able to classify the three group pairs with high accuracy. Knowing that the top 8 biomarker features have high relative importance in predicting cognitive status, we also explored whether the classification accuracy of the top 8 features was comparable to that of all 16 features. Using the top 8 features only, accuracies of 72.74%, 70.15%, and 91.63% were obtained for the CU vs LMCI, LMCI vs AD, and CU vs AD comparisons, respectively, thus confirming that the accuracy of the top 8 features was similar to that of all 16 features. **Figure 6.1** depicts the comparison of the receiver operating characteristic curves with five-fold cross validation³¹¹ between all 16 features and between the top 8 features. We found similar results in accuracy when using three- and ten-fold cross validations for comparison. The ROCs show that the top 8 features performed slightly better than all 16 features in distinguishing CU vs LMCI and LMCI vs AD. Precision recall (PR) curves verified similar levels of accuracy. These results suggest that there may be feature redundancy present when all 16 features are used to predict cognitive state: indeed, we found some of the features to be insignificant for cognitive state classification, especially those with the lowest ranking. Our findings suggest that the accuracy of the cognitive state prediction model does not depend strictly on the number of features used in the model, and that the top 8 features may be sufficient to accurately classify the three clinical cognitive statuses.

6.3.4 Correlation of AD biomarkers with cognitive performance

To understand if the Top 8 features in classifying the three participant group pairs are associated with performance on memory and executive functioning tests, we performed a correlation analysis of each feature on a memory composite score³¹² and on an executive functioning composite score³¹³. These composite scores are validated, psychometrically sophisticated composite scores based on the ADNI battery of neuropsychological tests described above. Ranking the biomarker features based on their r correlation value, we found that the pattern of biomarker correlation with performance on memory and executive functioning tests across participant groups was similar to the pattern found in the feature ranking analysis. When comparing the CU and LMCI groups (**Figure 6.2A**), memory performance was inversely correlated with $A\beta$ biomarkers, especially $A\beta$ in the temporal ($A\beta$ -Temporal), $A\beta$ in the precuneus ($A\beta$ -Precuneus) and $A\beta$ in the frontal lobe ($A\beta$ -Frontal). Hippocampal volume was also highly positively correlated and pTau was highly negatively correlated with memory when comparing CU and LMCI. However, when comparing LMCI and AD data (**Figure 6.2B**), in all three brain areas assessed, glucose uptake (FDG) was the feature most highly positively correlated with memory, showing larger correlation coefficients (r values) than those in the CU vs LMCI analysis. A similar correlation pattern was observed when comparing CU and AD data (**Figure 6.2C**), with the correlation constants being even larger for the FDG measurements than in the LMCI and AD comparison. These results suggest that FDG biomarkers become increasingly predictive of memory performance as cognitive decline progresses from LMCI to AD. In particular, FDG-Angular appears to be an especially important predictor of memory function, as it has the highest correlation coefficient of the three FDG biomarkers in these

memory correlation analyses. A similar pattern to that observed in the memory performance analyses emerged when correlating executive functioning with the top 8 biomarkers with FDG biomarkers becoming increasingly predictive of executive functioning as cognitive decline progresses (**Figure 6.3**). Notably, however, pTau and A β -Precuneus were more highly correlated with memory than executive functioning in the CU vs LMCI group (**Figure 6.2A and Figure 6.3A**). Interestingly, out of all the features, pTau showed the smallest correlation with executive functioning in each group (**Figure 6.3, A-C**).

6.3.5 Biomarker quantification for predicting LMCI and AD

Having shown through ranking and correlation that the top 8 features from each participant group may be used as effective biomarkers to predict disease progression from CU to LMCI and AD, we next sought to assess the average values for each biomarker feature in each diagnosis group that can be used for the clinical diagnosis of these three cognitive statuses. **Table 6.5** summarizes the values of each of the top 8 features that can be used to distinguish CU, LMCI and AD.

6.4 Discussion

We demonstrated three novel aspects in this study. First, we employed AD biomarkers from all arms of the newly developed A/T/N framework in a random forest machine learning analysis powerful enough to accurately predict an AD diagnosis of CU, LMCI, or AD and to rank biomarkers in order of their importance in the prediction. Second, we showed that biomarkers from the A/T/N framework have differing importance in predicting clinical dementia status across the disease progression, with A β and pTau having higher importance in predicting early cognitive impairment (CU vs LMCI) and glucose

uptake having higher importance in predicting later cognitive impairment (LMCI vs AD and CU vs AD) (**Figure 6.4**). Our findings suggest that A β and pTau accumulation contribute to the cognitive decline that leads to LMCI, but may not be sufficient to lead to clinical AD. Instead, neurodegeneration, especially in the form of glucose hypometabolism, appears to be crucial for exacerbating cognitive decline and furthering its progression to clinical AD. Additionally, we found that A β and pTau are more strongly correlated with cognitive performance in LMCI, while glucose hypometabolism is more strongly correlated with cognitive performance in AD, with FDG biomarkers becoming increasingly predictive of memory and executive functioning as cognitive decline progresses. While others have previously documented the temporal ordering of biomarkers preceding clinical symptomatology of Alzheimer's disease³¹⁴, the real strength of our analysis is in creating algorithms for computational analyses that are consistent with available clinical and imaging data from data that has been collected over many years. The challenge moving forward will be to translate these algorithms into usable tools to that can assess the capacity of patients in a clinically-friendly manner. Finally, we demonstrated that the top 8 features used in classifying the three participant group pairs were just as accurate in predicting clinical dementia status as all 16 features combined. The top 8 biomarker features that can be used to distinguish between stages of cognitive impairment, which may prove useful for the future prediction and diagnosis of LMCI and AD.

Machine learning techniques have previously been used to predict cognitive status in AD using several separate biomarkers, including those measured by FDG-PET^{315,316}, structural MRI^{315,317-319}, amyloid-PET^{317,320,321}, and CSF-phosphorylated tau^{318,319}. However, this is the first study to our knowledge to combine biomarkers from all arms of

the A/T/N framework into one integrated analysis using a machine learning method capable of classifying clinical dementia status and ranking the biomarker features according to their relative importance in the prediction model. Consistent with our findings, a previous study showed that A β was more highly associated with cognitive decline in cognitively normal participants, while glucose hypometabolism was more closely linked with cognitive decline in moderate and later stages of the disease (LMCI/AD)³²². Additionally, another study showed that FDG-PET, which assesses glucose uptake, is more highly correlated to cognitive ability than A β levels in patients with MCI and AD³⁰⁸. These studies, in conjunction with our findings strongly support the argument that cognitive decline in AD is initially propagated by A β and tau aggregation but is further exacerbated by glucose hypometabolism as cognitive decline progresses. Our findings could better inform clinical AD management decisions and may shift the targets of therapies to treat and prevent AD in future drug development.

We found that A β and pTau accumulation are more highly correlated with cognitive test scores in the CU vs LMCI comparison than other biomarker features. In particular, A β deposition in the temporal cortex, precuneus, and frontal cortex, as well as increased hippocampal volume, appear to be the most important features in predicting memory and executive functioning performance in early stage disease. Indeed, these areas play a central role in a wide spectrum of highly integrated tasks that are noticeably disturbed in patients with MCI. For example, the temporal cortex is involved in memory, auditory cognition and semantics³²³; the precuneus is involved in visuo-spatial image processing and episodic memory retrieval³²⁴; the frontal lobe is involved in executive function, attention, memory, and language³²⁵; and the hippocampus is important for declarative memory³²⁶.

Additionally, we found that increased levels of pTau were associated with memory performance but not executive functioning in LMCI, which is consistent with previous findings³²⁷. We note that some groups have found a high correlation between tau levels and cognitive decline across the entire AD spectrum^{328,329}; even so, our results align with those of Mielke *et al.*, who found a significant association between tau and cognitive performance in MCI, but a nonsignificant association between these factors in AD³³⁰. We also noticed that the atrophy of the hippocampus and entorhinal cortex (measures of neurodegeneration) were highly correlated in the CU vs LMCI comparison of cognitive test scores; in addition to A β and pTau burden, brain atrophy in these two regions may thus substantially contribute to progression from CU to LMCI status, as other groups have reported³³¹.

We observed that impaired glucose uptake is most highly correlated with cognitive test scores in LMCI vs AD and CU vs AD groups. In particular, we found glucose uptake in the angular gyrus (FDG-Angular) to be the most important feature for predicting memory and executive functioning performance in later stages of AD, which is consistent with other groups who have found reduced glucose uptake in the angular gyrus in later cognitive decline³³². This area is involved in semantic processing, word comprehension, number processing, memory retrieval, attention, spatial and social cognition, and reasoning³³³, all of which are known to decline later in disease progression. Sustained deficits in glucose uptake in key brain areas dramatically impair cognitive functions by reducing proper support of neuronal activity and functional processes³³⁴⁻³³⁶, and it is therefore unsurprising that we found that impaired glucose uptake is highly correlated with advancing cognitive decline.

Notably, the individuals with AD that were included in the current study were older and less educated than individuals in other groups, and a higher percentage of AD patients carried the *APOE* ϵ 4 allele, the largest genetic risk factor for AD, than LMCI and CU patients. Interestingly, all three of these factors are linked to metabolic function³³⁷⁻³⁴¹. A widely accepted cause of the functional losses that accompany aging is decreased brain metabolic function.^{342,343} Indeed, mitochondrial function declines with age in the brain and, thus, neural ATP production decreases, which has been proposed to be a major factor in the aging-associated loss of brain function^{337,340,343}. Moreover, a recent study demonstrated that regional brain metabolism and functional connectivity as measured by fMRI differed with years of education³³⁸: relative to less educated participants, highly educated participants had higher glucose metabolism in the ventral areas of the cerebrum, which are mainly involved in memory, language, and neurogenesis, and functional connectivity experiments illustrated that the brains of the highly educated individuals were overall more efficient and resilient to aging³³⁸. The *APOE* gene plays a role in cholesterol and A β homeostasis³³⁶, and the *APOE* ϵ 4 allele is the strongest genetic risk factor for AD. Two recent studies showed that disturbances in cholesterol metabolism, such as alterations in bile acid metabolism, are highly associated with AD^{344,345}. Notably, the bile acid composition signatures were much more highly associated with brain hypometabolism and atrophy (i.e., the “N” component of the A/T/N framework) than with A β and tau. Moreover, cross-sectional FDG-PET studies found that cognitively unimpaired carriers of the *APOE* ϵ 4 allele have abnormally low glucose uptake in the same brain regions that show hypometabolism in AD patients. Indeed, these metabolic abnormalities were observed in late-middle-aged (40-60 years of age) and young (20-39 years of age) *APOE* ϵ 4 carriers,

who had intact memory and were free of A β or tau pathology³⁴⁶⁻³⁵⁰. These neuroimaging results suggest that *APOE* ϵ 4 carriers develop functional brain abnormalities several decades before the possible onset of dementia, and the results are in line with our finding that a high percentage of those with clinical AD were *APOE* ϵ 4 carriers.

There are many plausible reasons to explain why we found glucose hypometabolism to be an important biomarker in predicting progressive cognitive decline in clinical AD. For example, impairments in brain glucose metabolism are associated with insulin resistance, which, in turn, exacerbates A β deposition^{336,351}. Indeed, AD is characterized by impaired brain insulin signaling³⁵². In line with this finding, type 2 diabetes mellitus, hyperlipidemia, obesity, and other metabolic diseases increase the risk of developing AD^{309,336}. Indeed the metabolic abnormalities present in AD are often likened to a form of diabetes of the brain³⁵³. The preservation of normal brain glucose metabolism is, thus, highly associated with cognitive resilience. A recent study showed that FDG-PET uptake in the bilateral anterior cingulate cortex and anterior temporal pole was positively associated with global cognition in cognitively unimpaired individuals over 80 years of age, despite the fact that they were A β -positive and *APOE* ϵ 4-positive³⁴¹. The results also suggest that normal cognitive performance can be preserved even in the presence of A β and *APOE* ϵ 4 in 80+ year-old individuals. Another study using deep learning methods showed that FDG-PET imaging can be used to predict AD an average of 75.8 months prior to its final diagnosis with 82% specificity and 100% sensitivity³¹⁶.

Taken together, our current findings and those of previous reports suggest that maintaining normal brain glucose metabolism is critical for cognitive resilience; therefore, therapeutic strategies for preventing or treating AD may need to shift focus from A β toward

the preservation and restoration of normal brain metabolism. Interventions with this therapeutic strategy have been reported that use intranasal insulin administration and a ketogenic diet. Specifically, intranasal insulin therapy provides rapid delivery of insulin to the central nervous system via bulk flow along olfactory and trigeminal perivascular channels without adversely affecting blood insulin or glucose levels and has been shown to improve AD symptomology, although individual patient responses may depend on gender, *APOE* genotype and insulin formulation³⁵⁴⁻³⁵⁶. With regards to the potential benefits of a ketogenic diet, ketone bodies can function as an alternative fuel substrate in the brain when glucose is unavailable or when glucose metabolism is impaired due to insulin resistance^{340,357-359}. One study showed that a ketogenic diet can modulate deposition of A β and Tau in the CSF of MCI patients in conjunction with its modulation of the gut microbiome and the production of short-chain fatty acids³⁶⁰. This finding is consistent with an animal study showing that a ketogenic diet enhanced A β clearance across the blood-brain barrier and improved the composition of the gut microbiome³⁶¹. The gut microbiome produces secondary bile acids, and, as mentioned above, alterations of bile acid production have been observed in AD patients due to gut microbiome imbalances, suggesting another mechanism by which AD patients may benefit from therapeutic strategies aiming to restore normal brain metabolism like the ketogenic diet^{344,345}. Another animal study showed that by modulating the gut microbiome with a prebiotic diet, mice with the human *APOE* ϵ 4 gene had enhanced systemic metabolism and reduced neuroinflammatory gene expression, another hallmark of AD pathology³⁶². Collectively, modulating metabolic function and the gut microbiome may have a profound impact on reducing the risk of AD.

Future efforts should include the continued collection of the A/T/N framework biomarkers to fill critical gaps in our understanding of how their expression is associated with AD and aging. In our model construction and analysis, we used CSF-pTau to fulfill the “T” component of the A/T/N framework³⁰⁶; however, imaging-derived biomarkers provide information about the location of the pathology in the brain that CSF-derived markers do not³⁰⁵. Therefore, future work is needed to incorporate Tau-PET imaging into the model³⁶³. In addition, glucose metabolism is tightly coupled with cerebral blood flow (CBF)^{364,365}, and neurovascular dysfunction also plays a critical role in cognitive impairment; thus, it will also be important to include CBF-MRI measures in the future for a more thorough representation of AD pathology. Indeed, Tau and CBF imaging data are currently available for only a small subset of the ADNI cohort, and thus could not be incorporated into our model. Additionally, while the available dataset from ADNI has more male participants, it should be noted that AD disproportionately affects women³⁶⁶. Future efforts may be needed to re-evaluate the outcome when data from the female participants become more available.

In summary, we show that A/T/N biomarkers have cognitive impairment stage-dependent roles in AD, with A β and pTau better predicting LMCI and neurodegeneration (especially low glucose uptake) better predicting clinical AD. Our findings may partly explain the repeated failures of clinical trials attempting to treat AD by modifying the A β load: it may be too late to gain therapeutic benefit from the treatment of A β when patients have already progressed to the clinical AD stage. Therefore, our results imply that treatments for AD may also need to be disease stage-oriented: A β and tau may be appropriate targets early in the disease course, but the restoration of brain glucose

metabolism should be explored as a treatment strategy for clinical AD. Our findings may influence the thinking in the field regarding AD progression and therapeutics.

6.5 Methods

6.5.1 Data pre-processing

Study data were obtained from the ADNI database, a longitudinal multicenter study designed to develop clinical, imaging, genetic, and biochemical biomarkers for the early detection and tracking of Alzheimer's disease. Specifically, data were downloaded from the ADNI2 dataset within the ADNI database since these data contained all the biomarkers of interest for the present study. Specific details about the acquisition of the imaging measures have been reported elsewhere^{367,368}. Briefly, all subjects were consented under the approval of the IRB at each testing site and scanned at 3T for 3D T1-weighted volume, FLAIR, a long TE gradient echo volumetric acquisition for micro hemorrhage detection, arterial spin-labeling perfusion, resting state functional connectivity, and diffusion tensor imaging; all enrolled subjects were also scanned for [¹⁸F]fluorodeoxyglucose PET (FDG-PET) glucose uptake and [¹⁸F]florbetapir PET for amyloid imaging. The data were merged from five subset datasets within the ADNI2 dataset to achieve a final dataset for analysis consisting of demographic information, structural MRI volumes, FDG-PET SUVs, amyloid-PET SUVs, White Matter Hyperintensities, and CSF-ptau measurements. Age, gender, education, *APOE* ϵ 4 carrier status, cognitive scores, and diagnosis and the structural MRI variables of ventricle volume, whole brain volume, entorhinal cortex volume, and hippocampal volume were extracted from the ADNIMERGE subset dataset. FDG-Angular, FDG-Temporal, and FDG-CingulumPost were extracted from the UC Berkeley FDG subset dataset. A β -Frontal, A β -Cingulate, A β -Parietal, A β -Temporal, A β -

Precuneus, and A β -Hippocampus were extracted from the UC Berkeley AV45 subset dataset. Gray matter volume, White matter volume, and White matter hyperintensity were extracted from the UC Davis White Matter Hyperintensity Volumes subset dataset. pTau concentration was extracted from the UPENN CSF Biomarkers Elecsys subset dataset. Missing values were imputed by selecting the twenty closest patients based on Euclidean distance with non-missing values in the same group and averaging these values. Most of the missing values appeared in the structural MRI data. Data imputation was performed on patients who had less than three missing values. Patients with three or more missing values were deleted to avoid bias caused by excessive imputation.

6.5.2 Machine learning analysis

The random forest (RF) classification algorithm was used to assess the importance of all seventeen biomarker features in predicting the AD clinical diagnosis, as determined by the progression of cognitive impairment as a result of the disease process (CU, LMCI, or AD) (**Table 7.2**). The algorithm was chosen, as opposed to other traditional statistical (e.g., ANOVA) and machine learning methods, because (i) it is a robust classification method and (ii) it enables feature ranking. An RF is trained by fitting multiple decision trees, each to a different random subset of the examples and features of the full dataset. The predictions of these decision trees are then combined to yield a single consensus classification prediction. Given the trained RF, each feature is considered more important if decision trees constructed from subsets that include the feature give predictions that are more accurate. This is calculated by averaging the out-of-bag accuracy (i.e., the accuracy on examples there were not used when training the tree) of the individual decision trees that were trained using the corresponding feature.

We acknowledge that some of the features (e.g., brain volumetric measures) are impacted with age; therefore, we adjusted the feature values for age accordingly. Specifically, we used CU group dataset and performed a linear regression with the seven brain volumetric measures used in our model as the feature variables and age as the target regression variable. We applied the derived beta coefficients from the regression model to the brain volumetric measures of the whole dataset and trained these balanced brain volumetric measure values in our RF model. In the implementation, we used the function *sklearn.linear_model.LinearRegression* of the ‘scikit-learn’ package to calculate the linear regression coefficients between brain volumetric measures and age.

Figure 6.5A illustrates the workflow of the feature ranking and accuracy performance using the random forest machine learning method. K-fold cross validation (k = 5) was used to evaluate the performance of the RF classification algorithm in predicting the AD clinical diagnosis. Using this strategy, the dataset was randomly partitioned into 5 equal parts, and 5 RF models were trained, each on a dataset consisting of 4 parts. Each of the trained RF models was evaluated based on the prediction performance on the corresponding omitted validation set. For evaluation, each complete data copy was forwarded into a random forest classifier model utilizing the Python scikit-learn library v0.21.3⁶⁹. All default parameters were used for the *sklearn.ensemble.RandomForestClassifier* function, with the exception of the criterion parameter, where we used the *entropy* option. Specifically, decision trees are classified in a binary fashion where the split in the trees are from either true or false responses to feature thresholds. The *RandomForestClassifier* decides the thresholds based on Gini Impurity. “Purity” is a measure as to how homogenous the samples are, with “0” as maximal purity,

and “1” as maximal impurity. As the decision tree progresses down, the Gini values eventually decrease to 0 (**Figure 6.5B**). Final predictions were calculated and features were ranked based on the prediction of the majority of trees within that training dataset. The resulting predictions were evaluated on their ability to correctly predict the AD clinical diagnosis in the validation dataset.

The cross-validated model prediction accuracy, receiver operating characteristic curve (ROC) and F₁ score were used to assess model performance.

The accuracy is calculated with the following equation [1]:

$$Accuracy = \frac{TP+TN}{TP+TN+FP+FN} \quad [1]$$

where TP = true positives, TN = true negatives, FP = false positives, and FN = false negatives.

The F₁ score is calculated by the following equation [2]:

$$F_1 = 2 \cdot \frac{precision \cdot recall}{precision+recall} \quad [2]$$

where precision = $TP / (TP+FP)$ and recall = $TP / (TP+ FN)$. ROC curves compare the true positive rate (TPR) and false positive rate (FPR) at different decision thresholds and are often used to judge the performance of binary classifiers. F₁ scores combine precision and recall and are often used to evaluate models on imbalanced dataset, since it is possible to obtain high accuracy on imbalanced datasets simply by predicting the most common class. A high F₁ score indicates low false positives and low false negatives.

6.5.3 Statistics and Reproducibility

In the **Table 6.1**, the overall dataset was initially evaluated for group differences in age, gender, education, *APOE* genotype, ethnicity, race, and cognitive test differences using non-parametric Kruskal-Wallis tests comparing the groups CU, LMCI, and AD using JMP 1.4 software. η^2 -approximate values and p-values were documented to identify statistical significance. η^2 values for effect sizes were calculated using the ‘rcompanion’ package in R statistical software.

To verify the reproducibility of five-fold validation used in the RF analysis, we compared the results of accuracy and F_1 score from those using three- and ten-fold cross validations.

To verify the accuracy measurements validated using ROC, we also performed precision recall (PR) curves calculation. Precision-Recall Curve is another method to evaluate classification models, especially binary classification models where the dataset is imbalanced. The Average of Precision (AP) is calculated to determine the average precision score under different possible thresholds. We used the scikit learn package `sklearn.model_selection.RandomizedSearchCV` for hyperparameters optimization. The hyperparameters of the RF model is as follows: `'n_estimators'=3600`, `'min_samples_split'=5`, `'min_samples_leaf'=8`, `'max_features'='auto'`, `'max_depth'=50`, and `'bootstrap'=False`.

We also used the SHapley Additive exPlanations (SHAP) technique to implement an additional feature ranking analysis. In our experiments, we applied the SHAP on Random Forest Classifier. Using the SHAP method as a reference for feature ranking analysis, the results showed similar feature importance ranking as RF.

Gradient tree boosting (GTB), another classification method from the *scikit-learn* package, was used as a comparison for the RF classification method. The same tree estimators from the RF method were used for GTB with all other default function parameters. The accuracies for the GTB method were similar to the RF method. The accuracy of the GTB classifiers were 72.30%, 71.26%,

and 91.87% respectively for CU vs LMCI, LMCI vs AD, and CU vs AD clinical diagnosis. The model was also trained with 3- and 10-fold cross validation for comparison. There were minor difference in the feature rankings estimated using the GTB model as compared to the RF model but the same general patterns hold true: A β and pTau are important contributors to the prediction of early AD decline, but neurodegeneration, especially glucose hypometabolism, is a more important predictor of later AD decline.

6.5.4 Pearson correlation analysis of cognitive performance

Pearson correlation was used to evaluate linear relationships between individual biomarker features and cognitive function using the JMP 1.4 software (**Figures 6.2 and 6.3**). Pearson correlation coefficient is calculated by the covariance of two variables over the product of their standard deviation. The value range of Pearson correlation coefficient is from -1 to 1 with a higher absolute value indicating a stronger association and the sign indicating a positive or negative association between the two variables.

6.5.5 Calculation of biomarker values

In the **Table 6.5**, biomarker Values were calculated for the different diagnosis groups and compared using two-sided Wilcoxon rank-sum tests. Z-score test statistics were calculated using JMP 1.4 software and effect sizes r were calculated with $r (= Z/(\sqrt{N_{\text{obs}}}))$. Amyloid standard uptake values (SUVs) were intensity normalized to the whole cerebellum and volume was normalized by dividing by the region of interest (ROI) in cubic centimeters (cm³). FDG SUVs were normalized according to metaROIs described elsewhere³⁷⁰. Briefly, a set of pre-defined regions of interest (FDG-ROIs) were developed by identifying regions cited frequently in FDG-PET studies of AD and MCI patients. All coordinates of significant voxels were transformed into MNI space. Intensity values were generated for coordinates that reflected a combination of the Z-scores associated with the coordinate. The volumes were intensity normalized using the maximum value, and volume was normalized by dividing by the ROI in cubic centimeters (cm³).

6.5.6 Data Availability

The datasets analyzed during the current study are available in the Alzheimer's Disease Neuroimaging Initiative (ADNI) repository.

Table 6.1 Demographic and cognitive data for the cross-sectional study population

	CU	LMCI	AD	χ^2 - approx	ε^2	P-value
Subject characteristics						
n	148	147	110			
Age (years)	73.43 ± 6.29	71.98 ± 7.42	74.46 ± 8.39	7.207	0.0178	0.0272*
Gender (% Male)	51%	54%	60%	2.236	0.00554	0.3268
Education (years)	16.63 ± 2.53	16.70 ± 2.45	15.61 ± 2.55	13.395	0.0332	0.0012*
<i>APOE</i> ε 4 carriers (%)	27%	57%	69%	53.653	0.133	<0.0001*
Ethnicity (% Hispanic)	5.4%	1.4%	3.6%	3.673	0.00909	0.1594
Race (% White)	89%	95%	92%	2.799	0.00693	0.2467
(% Black)	7%	3%	4%			
(% Asian)	2%	1%	4%			
Cognitive data						
MMSE	29.06 ± 1.14	27.61 ± 1.82	23.14 ± 2.03	246.414	0.61	<0.0001*
CDRSB	0.03 ± 0.13	1.71 ± 1.00	4.60 ± 1.61	351.755	0.871	<0.0001*
ADAS-cog 13	9.08 ± 4.58	18.57 ± 7.08	30.16 ± 9.70	239.827	0.594	<0.0001*
ADNI_MEM	1.06 ± 0.63	-0.03 ± 0.66	-0.89 ± 0.54	266.260	0.63	<0.0001*
ADNI_EF	0.94 ± 0.81	0.16 ± 0.85	-0.83 ± 0.93	161.477	0.388	<0.0001*

Values are displayed as the mean \pm SD. The χ^2 -approx test statistic is calculated from a Kruskal-Wallis test comparing the groups CU, LMCI, and AD. ϵ^2 is the effect size calculated from a Kruskal-Wallis test. Asterisk (*) next to P-value indicates statistical significance. DF=2 for all comparisons. CU = cognitively unimpaired; LMCI = late mild cognitive impairment; AD = Alzheimer's disease; MMSE = Mini-Mental State Examination; CDRSB = Clinical Dementia Rating Sum of Boxes; ADAS-cog = Alzheimer's Disease Assessment Scale-Cognitive Subscale; ADNI_MEM = Composite memory score; ADNI_EF = Composite executive functioning score.

Table 6.2 Biomarkers used in the feature analysis

Data Source	Biomarker Measure	Features	A/T/N classification
Positron emission tomography (PET)	Amyloid-beta (AV45; ¹⁸ Florbetapir)	1. A β -Frontal	A
		2. A β -Cingulate	
		3. A β -Parietal	
		4. A β -Temporal	
		5. A β -Precuneus	
		6. A β -Hippocampus	
	Glucose uptake (¹⁸ FDG)	7. FDG-Angular	N
		8. FDG-Temporal	
		9. FDG-CingulumPost	
Magnetic resonance imaging (MRI)	Volumetric measures	10. Ventricle volume	
		11. Whole brain volume (WBV)	
		12. Entorhinal cortex volume	
		13. Hippocampal volume	
		14. Gray matter volume (GMV)	
		15. White matter volume (WMV)	
Cerebrospinal fluid (CSF)	phosphor-Tau (¹⁸¹ P)	16. Phosphorylated tau (pTau)	T

¹⁸FDG = Fluorodeoxyglucose

Amyloid-beta measures include A β from the frontal lobe (A β -Frontal), cingulate cortex (A β -Cingulate), parietal lobe (A β -Parietal), temporal lobe (A β -Temporal), precuneus (A β -Precuneus), and hippocampus (A β -Hippocampus).

Glucose uptake measures include FDG from the angular gyrus (FDG-Angular), temporal lobe (FDG-Temporal), and posterior cingulum (FDG CingulumPost).

Table 6.3 Ranking of each biomarker feature importance to prediction of diagnosis classification from the random forest analysis

	CU vs LMCI		LMCI vs AD		CU vs AD		
	Rank	Biomarker Feature	Relative Importance	Biomarker Feature	Relative Importance	Biomarker Feature	Relative Importance
Top half	1	Hippocampus Volume	12.69%	FDG-Temporal	18.88%	FDG-Angular	23.78%
	2	A β -Frontal	11.51%	FDG-Angular	17.36%	FDG-CingulumPost	16.99%
	3	A β -Temporal	8.57%	FDG-CingulumPost	12.11%	Hippocampus Volume	12.93%
	4	FDG-Angular	8.32%	Hippocampus Volume	7.49%	FDG-Temporal	10.00%
	5	Entorhinal Cortex Volume	7.88%	A β -Precuneus	5.14%	A β -Temporal	8.11%
	6	A β -Precuneus	7.78%	A β -Temporal	4.97%	A β -Precuneus	6.20%
	7	pTau	7.60%	pTau	4.82%	Entorhinal Cortex Volume	4.81%
	8	A β -Cingulate	4.75%	Entorhinal Cortex Volume	4.76%	pTau	3.92%
	Subtotal		69.1%		75.45%		86.74%
Bottom Half	9	A β -Hippocampus	4.48%	A β -Parietal	4.71%	A β -Frontal	3.81%
	10	Ventricles	4.35%	A β -Frontal	3.98%	A β -Parietal	3.32%
	11	FDG-CingulumPost	4.29%	Ventricles	3.69%	A β -Hippocampus	3.17%
	12	GMV	4.20%	A β -Hippocampus	3.14%	A β -Cingulate	0.99%
	13	WMV	3.56%	A β -Cingulate	2.63%	Ventricles	0.65%
	14	FDG-Temporal	3.48%	GMV	2.59%	GMV	0.60%
	15	WBV	3.45%	WBV	2.46%	WMV	0.38%
	16	A β -Parietal	3.10%	WMV	1.29%	WBV	0.32%
	Subtotal		30.9%		24.55%		13.26%
Sum			100%		100%		100%

CU = cognitively unimpaired; LMCI = late mild cognitive impairment; AD = Alzheimer's disease

FDG = fluorodeoxyglucose; GMV = gray matter volume; WMV = white matter volume; WBV = whole brain volume

Table 6.4 Accuracy of all 16 features and of the top 8 features in predicting diagnosis for each participant group comparison

All 16 features			
	CU vs LMCI	LMCI vs AD	CU vs AD
Accuracy (%)	73.17	71.01	90.34
F ₁ Score (%)	73.09	70.84	90.32
Top 8 features			
	CU vs LMCI	LMCI vs AD	CU vs AD
Accuracy (%)	72.74	70.15	91.63
F ₁ Score (%)	72.59	70.02	91.59

Table 6.5 Average values of the top 8 biomarker features for each diagnosis group that can be used to predict cognitive status

Features	CU	LMCI	AD	A/T/N arm
A β -Precuneus (SUV cm ⁻³)	0.0715 \pm 0.0154	0.0873 \pm 0.0231	0.107 \pm 0.0272	A
		Z=5.79, p<0.0001** r=0.34	Z=9.89, p<0.0001†† r= 0.62	
A β -Frontal (SUV cm ⁻³)	0.00949 \pm 0.00187	0.0114 \pm 0.00260	0.0129 \pm 0.00286	
		Z=6.75, p<0.0001** r=0.39	Z=9.07, p<0.0001†† r=0.56	
A β -Cingulate (SUV cm ⁻³)	0.0692 \pm 0.00111	0.0787 \pm 0.00181	0.0892 \pm 0.00192	
		Z=4.87, p<0.0001** r=0.28	Z=8.03, p<0.0001†† r=0.50	
A β -Temporal (SUV cm ⁻³)	0.0259 \pm 0.00523	0.0302 \pm 0.00678	0.0331 \pm 0.00672	
		Z=6.76, p<0.0001** r=0.39	Z=9.92, p<0.0001†† r=0.62	
pTau (pg ml ⁻¹)	21.50 \pm 8.87	29.70 \pm 14.01	38.50 \pm 16.52	T
		Z=5.62, p<0.0001** r=0.33	Z=9.56, p<0.0001†† r=0.60	
FDG-Angular (SUV cm ⁻³)	1.21 \pm 0.104	1.13 \pm 0.149	0.956 \pm 0.159	N
		Z=5.31, p<0.0001** r=0.31	Z=11.46, p<0.0001†† r=0.71	
FDG-CingulumPost (SUV cm ⁻³)	3.03 \pm 0.324	2.84 \pm 0.391	2.47 \pm 0.343	
		Z=4.72, p<0.0001** r=0.27	Z=10.69, p<0.0001†† r=0.67	
FDG-Temporal (SUV cm ⁻³)	8.24 \pm 0.706	7.78 \pm 0.983	6.73 \pm 0.924	
		Z=4.54, p<0.0001** r=0.26	Z=10.82, p<0.0001†† r=0.67	
Hippocampus volume (cm ³)	7.49 \pm 0.827	6.67 \pm 1.11	5.91 \pm 0.923	

		Z=6.62, p<0.0001** r=0.39	Z=10.59, p<0.0001## r=0.66
Entorhinal cortex volume (cm ³)	3.85 ± 0.587	3.39 ± 0.710	2.92 ± 0.622
		Z=5.51, p<0.0001** r=0.32	Z=9.40, p<0.0001## r=0.59

Values are displayed as the mean ± SD.

**P<0.0001 calculated with a Wilcoxon rank-sum test comparing CU vs LMCI

P<0.0001 calculated with a Wilcoxon rank-sum test comparing CU vs AD

SUV = standard uptake value; Z = Z-score test statistic for Wilcoxon rank-sum test; r = effect size for Wilcoxon rank-sum test

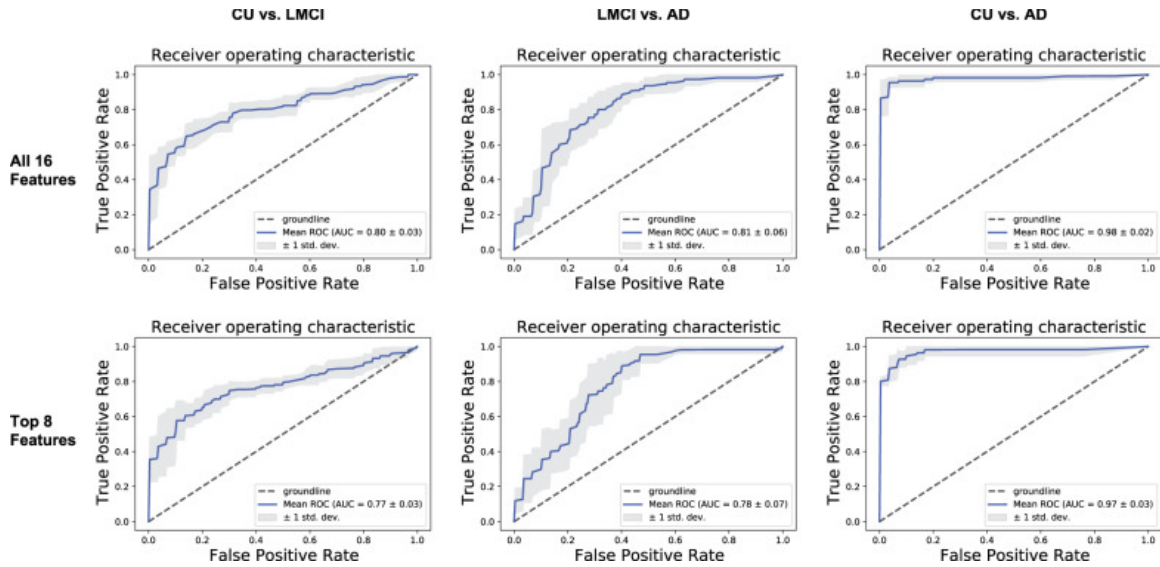
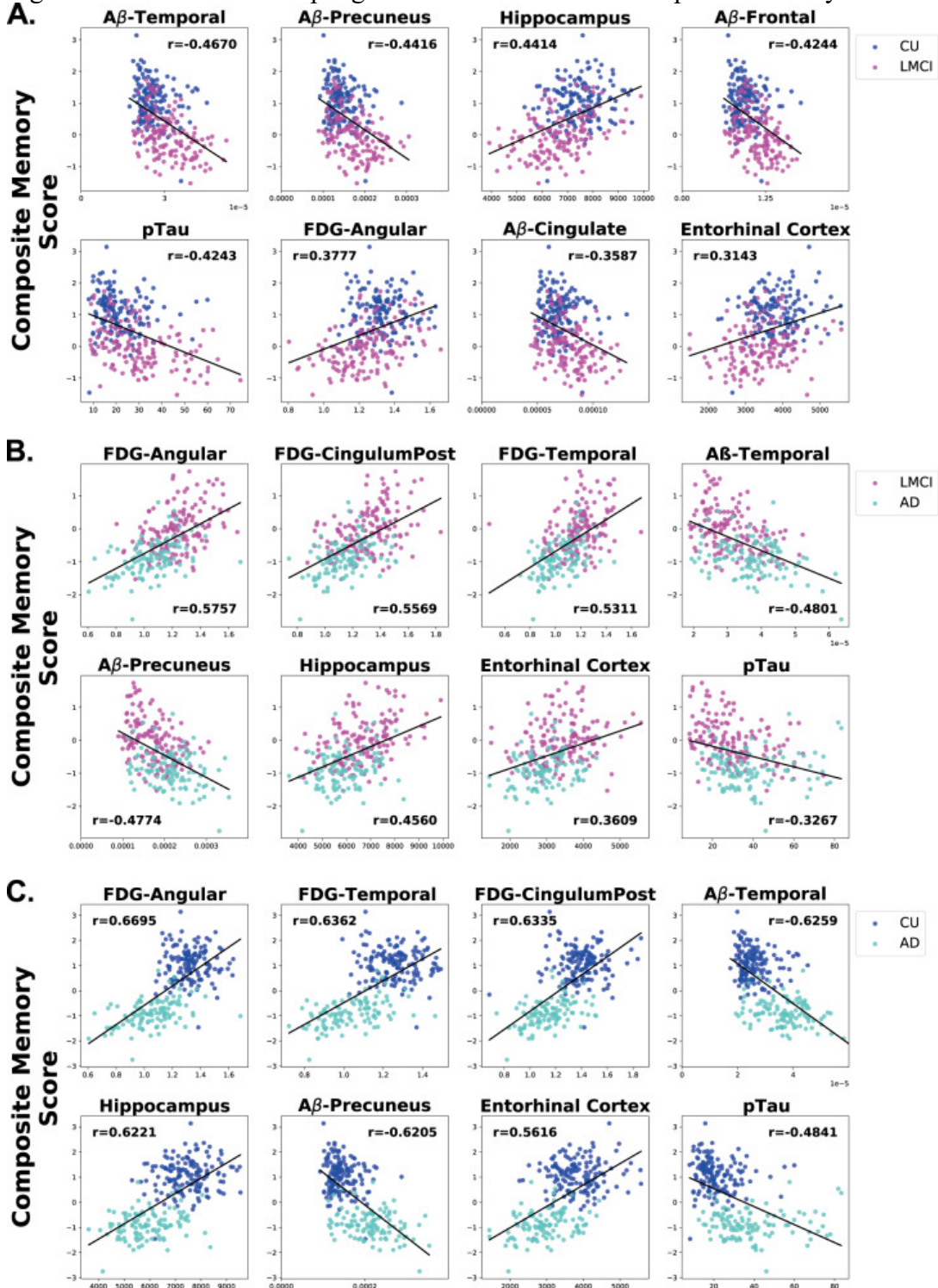


Figure 6.1 Receiver operating characteristic (ROC) curves depicting the accuracy of all 16 biomarker features (top) vs. the top 8 biomarker features (bottom).

Comparison of receiver operating characteristic¹⁴ curves between all 16 biomarker features (top) and the top 8 biomarker features (bottom) from the three diagnosis participant group comparisons: cognitively unimpaired (CU) vs. late mild cognitive impairment (LMCI), LMCI vs. Alzheimer's disease (AD), and CU vs. AD. Groundline refers to a model that cannot predict better than random chance. The mean ROC is calculated from the average of the five ROC curves produced from the k-fold cross validation.

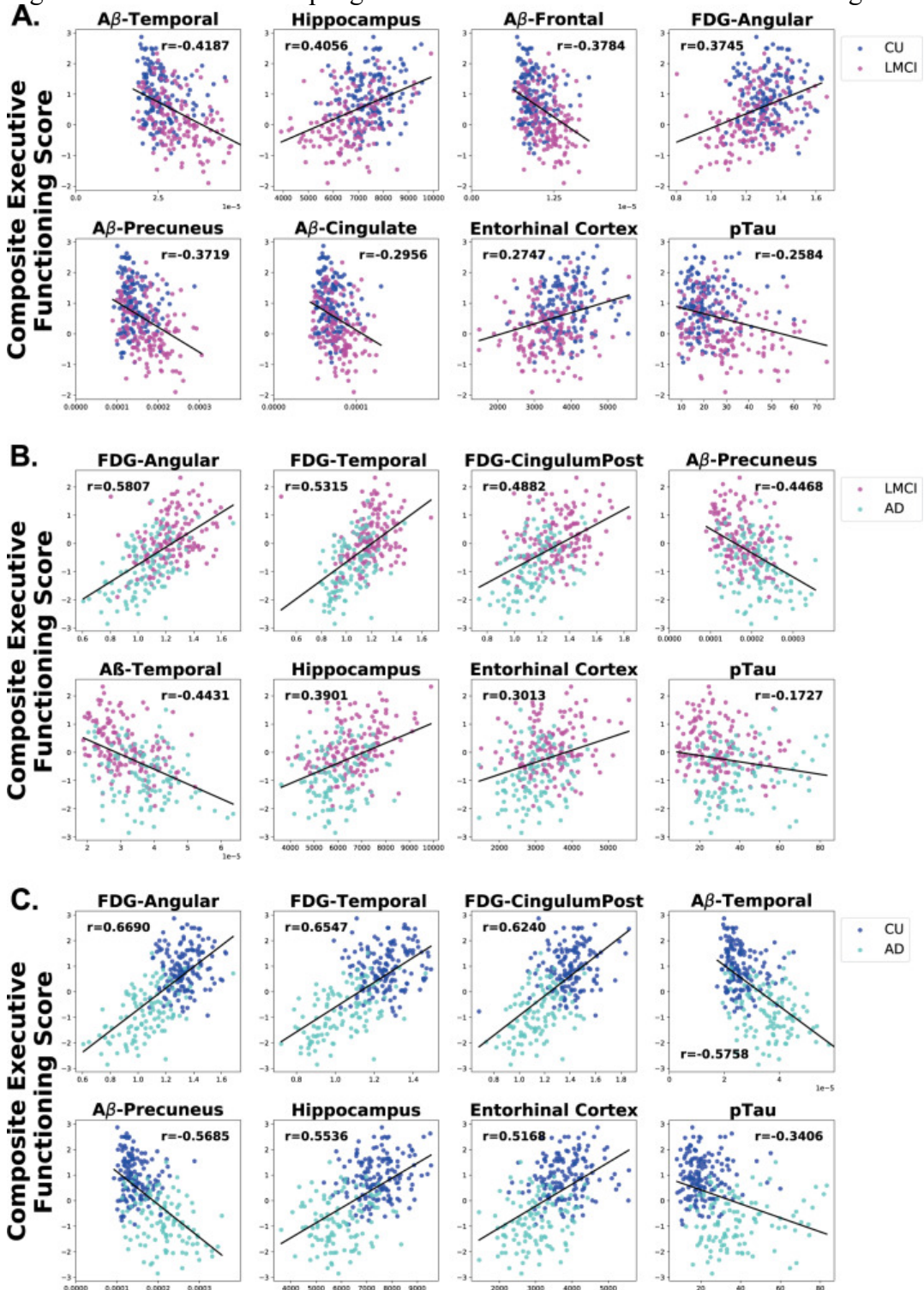
Figure 6.2 Correlation of top eight AD biomarkers with composite memory scores.



Scatter plots showing the correlations of the top eight features with performance on composite memory tests in each pairwise analysis among the cognitive statuses. (a) CU vs. LMCI. (b) LMCI vs. AD. (c) CU vs. AD. The order of the scatter plots in each panel is according to the rank of the r correlation value when compared to composite memory score. The x -axis refers to the indicated biomarker score and the y -axis

refers to the composite memory score. Each dot refers to the indicated biomarker score and composite memory score of a single participant.

Figure 6.3 Correlation of top eight AD biomarkers with executive functioning scores.



Scatter plots showing the correlations of the top eight features with performance on composite executive functioning tests in each pairwise analysis among the cognitive statuses (a) CU vs. LMCI, (b) LMCI vs. AD, (c) CU vs. AD. The order of the scatter plots in each panel is according to the rank of the r correlation

value when compared to composite executive functioning score. The x -axis refers to the indicated biomarker score and the y -axis refers to the composite memory score. Each dot refers to the indicated biomarker score and composite executive functioning score of a single participant.

Figure 6.4 Relative importance of biomarkers predicting AD clinical diagnosis.

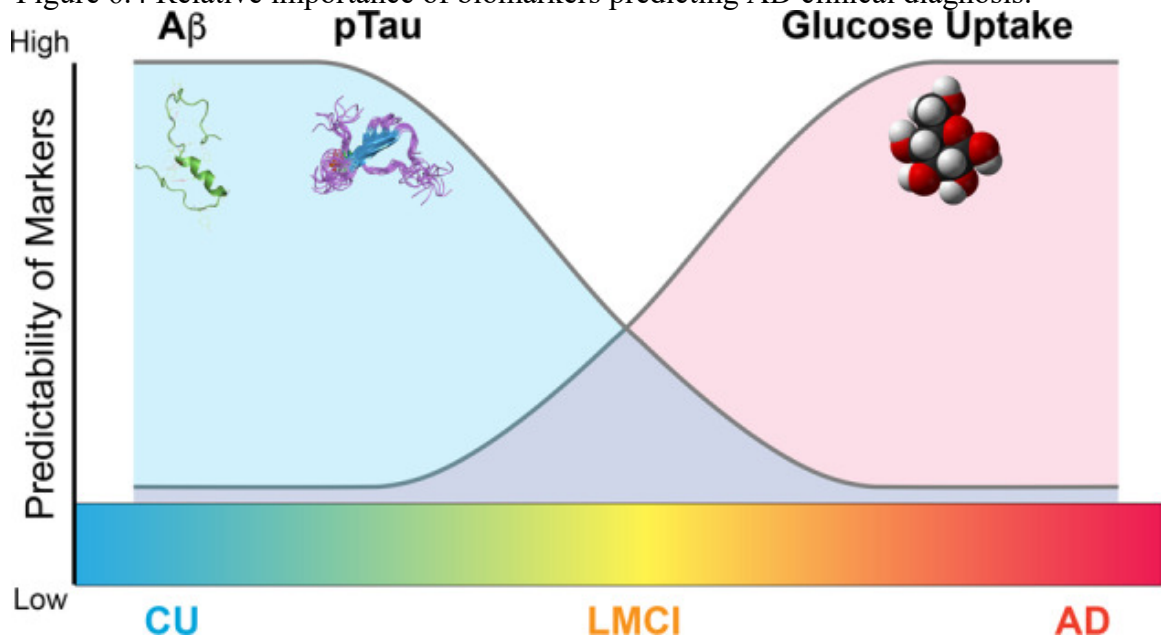
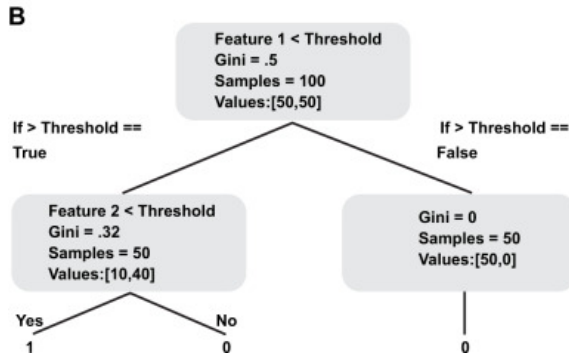
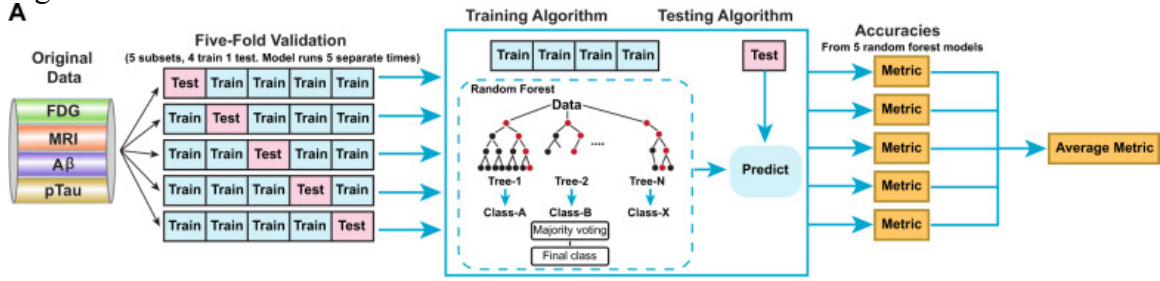


Diagram depicting the relative importance of biomarkers in predicting AD clinical diagnosis (predictability). In early AD, A β and pTau deposition in the brain have higher relative importance in predicting AD clinical diagnosis. In late disease low glucose uptake in the brain has higher relative importance in predicting AD clinical diagnosis.

Figure 6.5 Flow chart of the random forest method used.



a Flow chart depicting the analysis used with the random forest method. The AD biomarkers from the original dataset were randomly split into five equal-sized subsets. For evaluation, each complete data copy was forwarded into a random forest (decision tree; see **b**) classifier model. Final predictions were calculated and features were ranked based on the prediction of the majority of trees within that training dataset. **b** Decision trees are classified in a binary fashion, where the split in the trees are from either true or false responses to feature thresholds based on Gini Impurity. “Purity” is a measure homogeneity, with “0” as maximal purity, and “1” as maximal impurity.

CHAPTER 7. [SUPPLEMENT] HUMAN GRAY AND WHITE MATTER METABOLOMICS TO DIFFERENTIATE APOE AND STAGE DEPENDENT CHANGES IN ALZHEIMER'S DISEASE

7.1 Summary

Alzheimer's disease (AD) is the most common form of dementia with hallmarks of β -amyloid ($A\beta$) plaques, tau tangles and neurodegeneration. Studies have shown that neurodegeneration components, especially brain metabolic deficits, are more predictable for AD severity than $A\beta$ and tau. However, a detailed knowledge of the biochemical composition of AD brain tissue vs normal brain tissue remains unclear. In this study, we performed a metabolomics analysis on the brain tissue of 158 community-based older adults in the University of Kentucky AD Research Center brain bank to characterize the biochemical profiles of brains with and without AD based on white/gray matter type, apolipoprotein E genotype ($\epsilon 3$ vs $\epsilon 4$ variants), and disease stage (early vs late) as all these factors influence metabolic processes. We also used machine learning to rank the top metabolites that separates controls and AD in gray and white matter. Compared with control samples, we found that glutamate and creatine metabolism were more important for predicting AD in the gray matter, while glycine, fatty acid, pyrimidine, tricarboxylic acid (TCA) cycle, and phosphatidylcholine metabolism were more important in the white matter. In $\epsilon 4$ carriers, metabolites associated with the TCA cycle and oxidative phosphorylation were prominent in advanced stages compared to the early stages. In $\epsilon 3$ carriers, metabolites associated with oxidative DNA damage, changes in inhibitory neurotransmitters, and disruptions of neuronal membranes were prominent in advanced stages compared to the early stages. In early disease, $\epsilon 4$ carriers had metabolites related to

poor kidney function and altered neuronal sterol metabolism compared to $\epsilon 3$ carriers, but there were few differences between genotypes in late disease. Our results indicate that metabolism plays a pivotal role in differentiating *APOE*- and stage-dependent changes in AD and may facilitate precision lifestyle and dietary interventions to mitigate AD risk in the early stages, especially for $\epsilon 4$ carriers.

7.2 Introduction

Alzheimer's disease (AD) is a leading cause of death and morbidity in the United States³⁷¹. The hallmarks of AD are β -amyloid ($A\beta$) and tau. However, studies have indicated that metabolic dysfunction may play a more pivotal role in the progression of AD³⁷². Glucose hypometabolism and mitochondrial dysfunction are well-known features of AD³⁷². These irregularities are likely influenced by Apolipoprotein E (*APOE*) genotype, the most common genetic risk factor for AD. *APOE* is a lipid transport carrier with direct impact on metabolism whose function is dependent on the structure of the protein variant (whether it is $\epsilon 2$, $\epsilon 3$, or $\epsilon 4$). Those who are carriers of the *APOE* $\epsilon 4$ allele have two to four-fold increased risk for developing AD^{373,374}.

AD progresses differently in the white matter than the gray matter. While most research has been focused on reporting changes in the gray matter of cortex, many studies are now reporting changes in white matter tracts³⁷⁵. Metabolism is different in gray versus white matter due to the unique composition of each type (more lipid metabolism in the white matter³⁷⁶ and more glucose metabolism in the gray matter³⁷⁷). There is also evidence to suggest that there is more glycolytic metabolism in the white matter and more oxidative

metabolism in the gray matter³⁷⁸. Understanding the metabolic demands of the two different brain environments could give important clues about the progression of AD.

A detailed knowledge of the biochemical composition of AD brain tissue vs normal brain tissue will be key in understanding the metabolic processes underlying AD. To our knowledge, only three reports have been published describing a brain metabolomics signature of AD. These reports demonstrated that the top metabolites that classify AD in brain tissue include glycerophospholipids, spermidine, sphingolipids, and changes in bile acids³⁷⁹⁻³⁸¹. These reports analyzed between 15 and 111 samples per group to develop brain metabolomics signature based on targeted assays of lipids or bile acids. The analyses were based on gray-enriched matter only. While these reports provide an introductory analysis of brain metabolomics, a more complete understanding is needed that factors a larger patient population, an untargeted assay, and samples that are enriched for both gray and white matter. Furthermore, a better understanding of how AD progresses based on *APOE* genotype is needed to eventually develop therapeutics for AD based on precision medicine.

Here we performed a metabolomics analysis on the brain tissue of a large cohort of community-based participants in the University of Kentucky Alzheimer's Disease Research Center (UK-ADRC) brain bank. We used machine learning to identify the differences between the biochemical profiles of white-enriched matter and gray-enriched matter and identified the metabolites which were the top predictors in differentiating AD from normal brain tissue. We proceeded to characterize the biochemical profiles of brains with and without AD and other pathologies based on *APOE* genotype and disease stage.

7.3 Methods

7.3.1 Participant Characteristics

Details of UK-ADC research volunteers' recruitment, inclusion/exclusion criteria, and clinical and pathological assessments have been described previously³⁸². Briefly, community-based older adult volunteers agreed to be followed annually for cognitive, physical, and neurological examination and to donate their brain at the time of death. Protocols were approved by the UK Institutional Review Board, and all participants provided written informed consent. Included subjects were ≥ 70 years of age at death. Research subjects with relatively rare dementia syndromes (e.g. prions, trinucleotide repeat diseases, or Frontotemporal lobar degeneration (FTLD)), or any brain tumor were excluded. Additionally, since our research questions focused on the association between *APOE* and tau pathology, cases also had to have *APOE* genotyping available and were dichotomized into *APOE* $\epsilon 4$ carriers and *APOE* $\epsilon 3$ homozygotes. Demographic information included about our participants included age at death (years), sex, race (nonwhite or white), and years of education. We describe diagnosed cognitive status (normal cognition, impaired not mild cognitive impairment [MCI], MCI, dementia), and primary clinical diagnosis (normal cognition, AD, LBD/Parkinson disease; vascular disease, other) at the participant's last visit before death. Using Braak NFT staging³⁸³, we defined those as early stage with a Braak NFT score 0-III and those as late stage with a braak score IV-VI. Participant characteristics are listed in **Table 8.1**.

Human brain tissue samples were collected and snap-frozen in liquid nitrogen at brain autopsy. For the present study, samples were obtained from Brodmann's area 9 (the

dorsolateral prefrontal cortex) of the left hemisphere of 158 community-based older adult volunteers. Brain tissue samples were further dissected into gray-enriched matter and white-enriched matter samples, yielding a total of 316 brain samples. The education level was the same across stage and genotype. Age differed between only late $\epsilon 3$ and late $\epsilon 4$ groups (87.97 ± 6.96 vs 82.76 ± 8.45). We profiled the brain tissue metabolomics using Metabolon's (Durham, NC) global screening platform. We separated our analyses by Braak NFT stages (early 0-III vs late IV-VI) and *APOE* genotype ($\epsilon 3$ and $\epsilon 4$) (**Table 8.2**).

7.3.2 Metabolon Platform

We sent samples to Metabolon (Durham, NC) for a global metabolic profile for each sample. All samples were maintained at -80°C until processed. Samples were prepared using the automated MicroLab STAR® system from Hamilton Company. Proteins were precipitated with methanol under vigorous shaking for 2 min (Glen Mills GenoGrinder 2000) followed by centrifugation. The resulting extract was divided into five fractions: two for analysis by two separate reverse phase (RP)/UPLC-MS/MS methods with positive ion mode electrospray ionization (ESI), one for analysis by RP/UPLC-MS/MS with negative ion mode ESI, one for analysis by HILIC/UPLC-MS/MS with negative ion mode ESI, and one sample was reserved for backup. Samples were placed briefly on a TurboVap® (Zymark) to remove the organic solvent.

7.3.2.1 Ultra-high performance Liquid Chromatography-Tandem Mass Spectroscopy

All methods utilized a Waters ACQUITY ultra-performance liquid chromatography (UPLC) and a Thermo Scientific Q-Exactive high resolution/accurate mass spectrometer

interfaced with a heated electrospray ionization (HESI-II) source and Orbitrap mass analyzer operated at 35,000 mass resolution. The sample extract was dried then reconstituted in solvents compatible to each of the four methods. Each reconstitution solvent contained a series of standards at fixed concentrations to ensure injection and chromatographic consistency. One aliquot was analyzed using acidic positive ion conditions, chromatographically optimized for more hydrophilic compounds. In this method, the extract was gradient eluted from a C18 column (Waters UPLC BEH C18-2.1x100 mm, 1.7 μ m) using water and methanol, containing 0.05% perfluoropentanoic acid (PFPA) and 0.1% formic acid (FA). Another aliquot was also analyzed using acidic positive ion conditions, however it was chromatographically optimized for more hydrophobic compounds. In this method, the extract was gradient eluted from the same afore mentioned C18 column using methanol, acetonitrile, water, 0.05% PFPA and 0.01% FA and was operated at an overall higher organic content. Another aliquot was analyzed using basic negative ion optimized conditions using a separate dedicated C18 column. The basic extracts were gradient eluted from the column using methanol and water, however with 6.5mM Ammonium Bicarbonate at pH 8. The fourth aliquot was analyzed via negative ionization following elution from a HILIC column (Waters UPLC BEH Amide 2.1x150 mm, 1.7 μ m) using a gradient consisting of water and acetonitrile with 10mM Ammonium Formate, pH 10.8. The MS analysis alternated between MS and data-dependent MSⁿ scans using dynamic exclusion. The scan range varied slightly between methods but covered 70-1000 m/z.

7.3.2.2 Bioinformatics

The informatics system consisted of four major components, the Laboratory Information Management System (LIMS), the data extraction and peak-identification software, data processing tools for QC and compound identification, and a collection of information interpretation and visualization tools for use by data analysts. The hardware and software foundations for these informatics components were the LAN backbone, and a database server running Oracle 10.2.0.1 Enterprise Edition.

7.3.2.3 LIMS

The purpose of the Metabolon LIMS system was to enable fully auditable laboratory automation through a secure, easy to use, and highly specialized system. The scope of the Metabolon LIMS system encompasses sample accessioning, sample preparation and instrumental analysis and reporting and advanced data analysis. All of the subsequent software systems are grounded in the LIMS data structures. It has been modified to leverage and interface with the in-house information extraction and data visualization systems, as well as third party instrumentation and data analysis software.

7.3.2.4 Data Extraction and Compound Identification

Raw data was extracted, peak-identified and QC processed using Metabolon's hardware and software. These systems are built on a web-service platform utilizing Microsoft's .NET technologies, which run on high-performance application servers and fiber-channel storage arrays in clusters to provide active failover and load-balancing. Compounds were identified by comparison to library entries of purified standards or recurrent unknown entities. Metabolon maintains a library based on authenticated standards that contains the retention time/index (RI), mass to charge ratio (m/z), and chromatographic data (including

MS/MS spectral data) on all molecules present in the library. Furthermore, biochemical identifications are based on three criteria: retention index within a narrow RI window of the proposed identification, accurate mass match to the library +/- 10 ppm, and the MS/MS forward and reverse scores between the experimental data and authentic standards. The MS/MS scores are based on a comparison of the ions present in the experimental spectrum to the ions present in the library spectrum. While there may be similarities between these molecules based on one of these factors, the use of all three data points can be utilized to distinguish and differentiate biochemicals. More than 3300 commercially available purified standard compounds have been acquired and registered into LIMS for analysis on all platforms for determination of their analytical characteristics. Additional mass spectral entries have been created for structurally unnamed biochemicals, which have been identified by virtue of their recurrent nature (both chromatographic and mass spectral). These compounds have the potential to be identified by future acquisition of a matching purified standard or by classical structural analysis.

7.3.2.5 Metabolite Quantification and Data Normalization

Peaks were quantified using area-under-the-curve. For studies spanning multiple days, a data normalization step was performed to correct variation resulting from instrument inter-day tuning differences. Essentially, each compound was corrected in run-day blocks by registering the medians to equal one (1.00) and normalizing each data point proportionately (termed the “block correction”; Figure 2). For studies that did not require more than one day of analysis, no normalization is necessary, other than for purposes of data visualization. In certain instances, biochemical data may have been normalized to an additional factor (e.g., cell counts, total protein as determined by Bradford assay, osmolality, etc.) to account

for differences in metabolite levels due to differences in the amount of material present in each sample.

7.3.3 Statistical and Analytical Methods

7.3.3.1 Statistical Calculations

For many studies, two types of statistical analysis are usually performed: (1) significance tests and (2) classification analysis. Standard statistical analyses are performed in ArrayStudio on log transformed data. For those analyses not standard in ArrayStudio, the programs R or JMP are used. Below are examples of frequently employed significance tests and classification methods followed by a discussion of p- and q-value significance thresholds.

7.3.3.1 Machine Learning Classification

Random forest was used as a supervised classification technique to identify the relative importance of the different biochemicals in predicting gray-enriched matter vs. white-enriched matter, Alzheimer's disease vs control, APOE ϵ 4 vs APOE ϵ 3 genotype in early stage and late stage, early stage vs late stage in APOE E4 and APOE E3 genotype, and Vascular dementia vs. control based on an ensemble of decision trees. For a given decision tree, a random subset of the data with identifying true class information was selected to build the tree, and the remaining data, the "out-of-bag" (OOB) variables, were passed down the tree to obtain a class prediction for each sample. This process was repeated thousands of times to produce the forest. The final classification of each sample was determined by computing the class prediction frequency ("votes") for the OOB variables over the whole forest. This method is unbiased since the prediction for each sample is based on trees built

from a subset of samples that do not include that sample. When the full forest is grown, the class predictions are compared to the true classes, generating the “OOB error rate” as a measure of prediction accuracy. Thus, the prediction accuracy is an unbiased estimate of how well one can predict sample class in a new data set. Random forest has several advantages – it makes no parametric assumptions, variable selection is not needed, it does not overfit, it is invariant to transformation, and it is fairly easy to implement with R.

To determine which variables (biochemicals) make the largest contribution to the classification, a “variable importance” measure is computed. We use the “Mean Decrease Accuracy” (MDA) as this metric. The MDA is determined by randomly permuting a variable, running the observed values through the trees, and then reassessing the prediction accuracy. If a variable is not important, then this procedure will have little change in the accuracy of the class prediction (permuting random noise will give random noise). By contrast, if a variable is important to the classification, the prediction accuracy will drop after such a permutation, which we record as the MDA. Thus, the random forest analysis provides an “importance” rank ordering of biochemicals; we typically output the top 30 biochemicals in the list as potentially worthy of further investigation.

7.4 Results

7.4.1 Metabolomics differences in gray and white-enriched matters

In total, 540 of the 776 detected metabolites were either increased or decreased in the white-enriched matter vs gray-enriched matter. White-enriched matter has more lipid metabolites associated with myelin than gray-enriched matter.

Using a random forest analysis, we found that the model was able to predict whether a sample was gray-enriched matter or white-enriched matter based on the metabolomics profile with 91.77% accuracy (**Table 7.3A**). Heat map of statistically significant biochemicals profiled when comparing groups are labeled as follows: Red and green shaded cells indicate $p \leq 0.05$ (red specifies that the mean values are significantly higher for that comparison; green values significantly lower). The top 10 predictors were all lipids, which play a major role in the brain as structural components of membranes and signaling molecules. Notably, there was an increase in prominent hexosylceramides, some phosphatidylcholines, lysoplasmalogen, some plasmalogens, and phosphatidylserine, whereas there was a decrease in other phosphatidylcholines, phosphatidylethanolamine, and some plasmalogen metabolites. Most of the observed changes correlated with the known differences in white and gray-enriched matter lipid populations due to the diverse functions of neuron cell biology. All analyses were performed in both gray-enriched matter and white-enriched matter to account for these differences.

7.4.2 Machine learning to classify AD from normal with metabolomics

Using random forest analysis, we found that the model predicted whether a sample came from AD brain tissue or normal brain tissue based on the metabolomics profile with 80.0% accuracy in the gray-enriched matter (**Table 7.3B**) and an 81.54% accuracy in the white-enriched matter (**Table 7.3C**). The top 9 predictors in gray-enriched matter mainly consisted of increases in phospholipid and creatine metabolism, and decreases in amino acid metabolism, and the monohydroxy fatty acid 13-HODE + 9-HODE. The top 12 predictors in white-enriched matter mainly consisted of increases in phospholipid metabolism and decreases in amino acid metabolism, phosphatidylcholine, and some

monohydroxy fatty acids. Glycerophosphocholine is formed in the breakdown of phosphatidylcholine and is increased in both the gray-enriched matter and white-enriched matter. N-acetylasparagine is a breakdown product of asparagine and is decreased in both the gray-enriched matter and white-enriched matter. The human body produces dimethylglycine when metabolizing choline into glycine, and it is decreased in the gray-enriched matter. NAAG is a neuropeptide that is an agonist at mGluR3 receptors and an antagonist at NMDA receptors and is decreased in the gray-enriched matter. Pipecolic acid originates mainly from the catabolism of dietary lysine by intestinal bacteria rather than by direct food intake, and it is decreased in both the gray-enriched matter and the white-enriched matter. Ureidopropionic acid is a urea compound and is an intermediate in the metabolism of uracil; it is decreased in the white-enriched matter.

Taken together, our findings indicate that glutamate and creatine metabolism are more important for predicting disease in the gray matter, and glycine, fatty acid, pyrimidine, TCA cycle, and phosphatidylcholine metabolism are more important for predicting disease in the white matter.

7.4.3 Gray and white matter metabolomics between early and late in *APOE* ϵ 4

We next investigated the differences between late stage and early stage disease in the ϵ 4 genotype (**Table 7.4**). We found that, compared with the early stage, late-stage APOE4 carriers had significantly reduced metabolite levels in the gray matter. Notable changes were found in pathways associated with mitochondrial function, glucose metabolism, and neurotransmitters, including tricarboxylic acid (TCA) cycle, oxidative phosphorylation, pentose metabolism, and acetyl-CoA and glutamate metabolism. We

observed lower levels of *serine* and *aspartate*, whose declines are known to correlate with the amount of A β plaques and neuronal pathology³⁸⁴, as well as *tyrosine* and *leucine*, which are known to reduce atherosclerosis by improving the lipid profile and reducing systemic inflammation³⁸⁵. Further, metabolites related to mitigating oxidative stress, such as *cysteine*, *arginine*, *gamma-glutamyl amino acid*, *pentose* were also lower in gray matter in the late stage. We also saw lipid decreases in seven lysophospholipid (LPL) species. LPL receptor ligands are known to bind to and activate their cognate receptors located in the cell membrane with a wide range of effects on the cell; these include the primary effects of inhibition of adenylyl cyclase and the release of calcium from the endoplasmic reticulum, as well as the secondary effects of preventing apoptosis and increasing cell proliferation³⁸⁶.

In white matter, reductions were found in biochemicals related to glutamate, tyrosine, leucine and methionine/cysteine metabolism. Interestingly, *diacylglycerol* was increased in the white matter in later disease similar to levels found in the e3 genotype. Since diacylglycerol has been shown to reduce atherosclerosis in an APOE-deficient mouse model³⁸⁷, the increase in diacylglycerol in the e4 genotype could be a compensatory mechanism to combat rising levels of atherosclerosis.

The results show that with the disease progression, APOE4 carriers had alterations in metabolites that are associated with increased A β retention, reducing atherosclerosis, and the impaired TCA cycle and oxidative phosphorylation.

7.4.4 Gray and white matter metabolomics between early and late in APOE ϵ 3

We further investigated the differences between late stage and early stage in APOE ϵ 3 genotype (**Table 7.5**). Individuals with ϵ 3 variants had similar changes in the gray and white matters.

However, unlike ϵ 4, which involves mitochondrial and glucose metabolism, notable key reductions in ϵ 3 carriers were found in *glycolysis*, *glutamate*, *tryptophan*, and *tyrosine* metabolism. Glutamate is an excitatory neurotransmitter, which plays a critical role in learning and memory³⁸⁸ and *N-acetyl-aspartyl-glutamate (NAAG)* has been shown to have precognitive effects by binding to metabotropic glutamate receptors²⁵⁹. *Tryptophan* metabolism is known to be altered in patients with AD³⁸⁹, and *tryptophan*-derived metabolites can inhibit A β fibril formation in neurons and neuroblastoma cells³⁹⁰. Tryptophan is an essential amino acid and is the precursor of serotonin. Indole-3-propionic acid, a tryptophan-derived metabolite, can inhibit A β fibril formation in neurons and neuroblastoma cells³⁹⁰. Metabolites that play a role in tyrosine metabolism including phenol sulfate, phenol glucuronide, and p-cresol glucuronide are associated with inflammation³⁹¹. We observed lower levels of *dimethylglycine*, which is linked to increased oxidative DNA damage associated with A β deposition³⁹², and *homocarnosine*, which is part of the histidine pathway and generally declines with age³⁹³. Neuronal histamine, phenylalanine, and tryptophan have a role on memory, reinforcement, and emotions³⁹⁴⁻³⁹⁶. We also found lower levels of *fatty acids*, which are often found as oxidized linoleic acid metabolites (OXLAMs) in the serum of AD patients³⁹⁷ and *phosphatidylcholine*, which provides a reservoir of choline that can be used for acetylcholine synthesis. Notable key increases were found in *myo-inositol* metabolism,

urea cycle, lysine, nucleotide sugar, inositol, and phospholipid. Myo-inositol, a neuroinflammatory marker, is negatively correlated with visuospatial working memory³⁹⁸. Lysine can act as neurotransmitter modulating GABAergic transmission. Phospholipid is known to be raised in AD by disrupting neural cell membranes and causing cell death³⁹⁹.

Taken together, our findings indicate that increases in metabolites linked to oxidative DNA damage, changes in inhibitory neurotransmitters, and disruptions of neuronal membranes and decreases in metabolites related to acetylcholine synthesis drive the differences between early and late stage of AD among *APOE* ϵ 3 carriers.

7.4.5 Gray and white metabolomics between *APOE* ϵ 3 and ϵ 4

We next compared the differences between *APOE* ϵ 4 and ϵ 3 carriers at early-stage disease (**Table 7.6**). Notable changes were found in pathways associated with leucine, glycine, arginine, gamma-glutamyl amino acid, pentose, and secondary bile acid metabolism in *APOE* ϵ 4 carriers compared to non-carriers. *N,N,N-trimethyl-alanylproline betaine* (TMAP), part of arginine metabolism, was found to be lower in ϵ 4, and is associated with poor kidney function⁴⁰⁰. We also found decreases in *glutathione*, commonly decreased with age⁴⁰¹, *eicosanoid*, and *sterol* - carriers of the *APOE* ϵ 3/ ϵ 4 allele are known to exhibit altered neuronal sterol metabolism.

Unique differences in gray-enriched matter include an amino acid increase of histamine and 1-carboxyethylisoleucine (part of isoleucine metabolism), a peptide increase of gamma-glutamylisoleucine, a lipid increase of arachidonate (a long chain polyunsaturated fatty acid) and docosahexaenoyl ethanolamide (an endocannabinoid implicated in the pathology of neurodegenerative diseases).

Other differences were found only in the white-enriched matter. Unique differences include amino acid decreases in formiminoglutamate (part of histidine metabolism) and increases of 2-aminoadipate (part of lysine metabolism), lipid decreases in 1,2-dipalmitoyl-GPE (a phosphatidylethanolamine) and palmitoyl-docosahexaenoyl-glycerol (a diacylglycerol), and increases in 1,2-dioleoyl-GPG (a phosphatidylglycerol), 1-(1-enyl-oleoyl)-2-oleoyl-GPE (a lysoplasmalogen), glycosyl-N-stearoyl-sphingadienine and glycosyl ceramide (both hexosylceramides), sphingomyelin, and sphingosine 1-phosphate.

Taken together, our findings indicate that increased metabolites in *APOE* $\epsilon 4$ carriers related to poor kidney function and altered neuronal sterol metabolism drive the differences between the genotypes at early stage.

There were four detected metabolites that were detected to be increased between *APOE* $\epsilon 4$ and $\epsilon 3$ carriers at late stages of AD. At an $\alpha=0.01$, random chance would be expected to generate ~8 significant observations. Since our results do not surpass this threshold, our analyses did not identify metabolic differences between $\epsilon 3$ and $\epsilon 4$ carriers at late stages of AD.

7.5 Discussion

We analyzed frontal cortical tissue from subjects across a spectrum of AD severity, with different genotypes (*APOE* $\epsilon 3/3$ or *APOE* $\epsilon 3/4$) (summary of results are in **Figure 7.2**). We found distinct changes in the white versus gray-enriched matter of subjects as demonstrated through peptide alterations and lipid changes that have been associated with brain matter. There were increases in phospholipid metabolism and decreases in amino acid metabolism in AD brains compared with normal brains. Taken together, our findings

indicated that glutamate and creatine metabolism were more important for predicting disease in the gray matter, and glycine, fatty acid, pyrimidine, TCA cycle, and phosphatidylcholine metabolism are more important for predicting disease in the white matter. As disease progressed in the *APOE* ϵ 4 genotype, brains were characterized by decreases in metabolites responsible for reducing atherosclerosis, and the TCA cycle and oxidative phosphorylation. With disease progression in the *APOE* ϵ 3 genotype, brains were characterized by increases in metabolites related to oxidative DNA damage, changes in inhibitory neurotransmitters, and disruptions of neuronal membranes and decreases in metabolites related to acetylcholine synthesis. In early disease, the *APOE* ϵ 4 genotype was associated with increased metabolites related to poor kidney function and altered neuronal sterol metabolism, but there were few metabolic differences between *APOE* ϵ 3 and ϵ 4 genotypes in more severe AD.

The major differences between the metabolite composition of white-enriched matter and gray-enriched matter were characterized mainly by the metabolite components inherent to the myelin sheath present in the white-enriched matter. The myelin sheath is mainly comprised of lipids which insulate axons to speed action potentials, and it is not surprising that our data show that the top predictors for distinguishing gray-enriched matter from white-enriched matter were all lipids. Alpha-hydroxylated cerebroside are the most abundant lipids in the myelin sheath⁴⁰² and the myelin sheath has a lower phosphatidylcholine to phosphatidylethanolamine ratio compared with grey matter due to its unique composition of myelin, which are all consistent with our data. It is important to separate white-enriched matter from gray-enriched matter in brain metabolomics analyses

so that differences found between samples aren't confounded by the inherent differences between tissue types (and sample-to-sample differences in ratios of white and gray matter).

Previous studies investigating metabolomics changes in AD reported changes in phosphatidylcholine and acylcarnitine metabolism⁴⁰³, taurine transport, bile acid synthesis, and cholesterol metabolism^{380,381,404}, lipids, sphingolipids (notably GM₃ gangliosides) and lipid classes previously associated with cardiometabolic disease (phosphatidylethanolamine and triglycerides)^{405,406}. Results using Metabolon's untargeted assay showed changes in not only phospholipid, phosphatidylcholine, and fatty acid metabolism, but also the TCA cycle, pyrimidine, and several amino acids including aspartate, lysine, glycine, glutamate, creatine, histidine. In addition to the lipid changes found by others, these important amino acid, energy, and nucleotide changes could give important clues about the underlying disease mechanism of AD.

Separating our analysis by Braak NFT stages and *APOE* genotype allowed us to better understand the nuances of metabolite changes unique to disease stage and genotype. As disease progresses in the *APOE* ε4 carriers, metabolites associated with reducing atherosclerosis and the TCA cycle and oxidative phosphorylation appeared to correlate with (and perhaps to drive) the differences between early and late stage AD. Previous studies have reported that age-related vascular changes accompany or even precede the development of AD pathology⁴⁰⁷, and a plant based diet can reduce atherosclerosis⁴⁰⁸. Further, it has been observed that the TCA cycle can regulate the pathogenesis of neuroinflammation and neurodegeneration⁴⁰⁹. It is interesting that TCA cycle metabolite decreases are statistically more significant in the gray matter than the white matter in the ε4 genotype, but that the machine learning analysis revealed TCA cycle metabolites to be

more important in predicting AD in the white matter. While TCA cycle decreases are more commonly seen in late stage gray matter E4 as a whole, when TCA cycle decreases are seen in white matter, they are more likely to be predictive of AD, whereas other metabolites in the gray matter are more predictive of AD.

As AD progresses in the *APOE* ϵ 3 genotype, metabolites linked to oxidative DNA damage, changes in inhibitory neurotransmitters, disruptions of neuronal membranes, and decreases in metabolites related to acetylcholine synthesis correlated best with the differences between early and late stage AD. Oxidative stress may participate in the development of AD by promoting A β deposition, tau hyperphosphorylation, and the subsequent loss of synapses and neurons⁴¹⁰. There is evidence that the Mediterranean diet is protective against oxidative DNA damage⁴¹¹. There is growing evidence in support of GABAergic remodeling in the AD brain, potentially beginning in early stages of disease pathogenesis⁴¹². Alterations of fatty acids at the level of lipid rafts and cerebral lipid peroxidation were found in the early stage of AD⁴¹³. Cholinergic neurons located in the basal forebrain, including the neurons comprising the nucleus basalis of Meynert, are severely lost in AD⁴¹⁴.

Separating by *APOE* genotype was an important part of our analysis as the *APOE* ϵ 4 genotype is the most common genetic risk factor for developing AD. At the early stage of disease, *APOE* ϵ 4 carriers differed from *APOE* ϵ 3/3 in metabolites related to poor kidney function and altered neuronal sterol metabolism. Older patients on hemodialysis are at substantial risk of diagnosis with dementia and Alzheimer's disease⁴¹⁵. *APOE* ϵ 4-expressing cultured astrocytes and neurons have reduced cholesterol and phospholipid secretion, decreased lipid-binding capacity, and increased intracellular degradation⁴¹⁶. This

is likely due to the changed domain interaction with cholesterol receptors and less stable conformation of the *APOE* $\epsilon 4$ genotype that changes its involvement in lipid metabolism and neurobiology, thereby impacting neuronal repair, remodeling, and degeneration⁴¹⁷. There were far fewer metabolic differences between *APOE* $\epsilon 3$ and $\epsilon 4$ genotype in later disease stages. It is possible that genotype differences are pronounced during early disease, but that the disease course causes both genotypes to exhibit a similar biochemical profile as the disease progresses and neurons are lost. These genotype differences should be further explored to determine whether precision interventions, like the consumption of inulin or the administration of rapamycin, could be implemented for $\epsilon 4$ carriers^{418,419}.

Taken together, our current findings and those of previous reports suggest that maintaining normal brain glucose metabolism is critical for cognitive resilience; therefore, therapeutic strategies for preventing or treating AD may need to shift focus from $A\beta$ toward the preservation and restoration of normal brain metabolism. Recently, aducanumab, an $A\beta$ directed antibody, was granted accelerated approval to verify its clinical benefit for use in early AD after decades of failed drugs targeted at $A\beta$; it is possible that metabolic interventions could be used across the disease course to provide clinical benefit to patients. Interventions with a metabolic therapeutic strategy have been reported that use intranasal insulin administration and a ketogenic diet. With regards to the potential benefits of a ketogenic diet, ketone bodies can function as an alternative fuel substrate in the brain when glucose is unavailable or when glucose metabolism is impaired due to insulin resistance^{340,357-359}. One study showed that a ketogenic diet can modulate deposition of $A\beta$ and Tau in the CSF of MCI patients in conjunction with its modulation of the gut microbiome and the production of short-chain fatty acids³⁶⁰. This finding is consistent with

an animal study showing that a ketogenic diet enhanced A β clearance across the blood-brain barrier and improved the composition of the gut microbiome³⁶¹.

The gut microbiome produces secondary bile acids, and, as mentioned above, alterations of bile acid production have been observed in AD patients due to gut microbiome imbalances, suggesting another mechanism by which AD patients may benefit from therapeutic strategies aiming to restore normal brain metabolism like the ketogenic diet^{344,345}. Another animal study showed that by modulating the gut microbiome with a prebiotic diet, mice with the human *APOE* ϵ 4 gene had enhanced systemic metabolism and reduced neuroinflammatory gene expression, another hallmark of AD pathology^{362,418}. Collectively, modulating metabolic function and the gut microbiome may have a profound impact on reducing the risk of AD.

Implication of gut microbiome changes; we have shown that prebiotic diet inulin can increase tryptophan and tyrosine level in the APOE3 mice. (our recent inulin study shows to reduce DNA damage in the E3 mice).

Future studies that evaluate the serum of subjects may be helpful to evaluate potential systemic metabolomic changes in subjects and if the changes observed here are limited to brain tissue. Similarly, analyses of cell-sorted tissue could give additional resolution into the results. Furthermore, minimizing drug usage in subjects (about 9% of biochemicals in named dataset were pharmaceuticals which included AD therapies such as donepezil and memantine and the anti-diabetic medication metformin) may provide some additional clarity in the above observations.

In conclusion, our study shows that metabolite differences are associated with disease stage, genotype, and cognitive decline in AD. Further study in AD metabolomics may elucidate new insights into disease mechanism and therapeutics.

Table 7.1 Participant Characteristics

Number of Participants	158
Age	85.6 (84.4, 86.9)
APOE (% ε4 carriers)	36.7%
Braak Stage 0-3	51.3%
Braak Stage 4-6	48.7%
Gender (% Female)	58.9%
Race (% White)	94.9%
Race (% Black)	5.1%
MMSE	22.2 (20.8, 23.6)
Postmortem Interval	3.7 (3.36, 4.02)
Consensus Diagnosis (% AD)	10.8%
Consensus Diagnosis (% Mixed AD)	42.7%
Consensus Diagnosis (% Other Dementia)	17.2%
Consensus Diagnosis (% Normal)	29.3%
TDP-43 (% Positive)	27.9%

Table 7.2 Number of samples belonging to APOE genotypes and Braak Stages

	APOE $\epsilon 3/\epsilon 3$	APOE $\epsilon 3/\epsilon 4$	Total
Braak Stage 0-3	64	17	81
Braak Stage 4-6	36	41	77
Total	100	58	158

Table 7.3 Top ranked biochemicals in (A) predicting gray vs white matter all belong to the lipid superclass, (B) in predicting AD vs Normal brain tissue in Gray and (C) White Matter

A) Gray Matter vs White Matter				
Accuracy: 91.77%				
Rank Order	Super Pathway	Sub Pathway	Biochemical Name	Fold Change
1	Lipid	Hexosylceramides (HCER)	glycosyl ceramide (d18:2/24:1, d18:1/24:2)*	2.35
2	Lipid	Phosphatidylcholine (PC)	1,2-dipalmitoyl-GPC (16:0/16:0)	0.38
3	Lipid	Phosphatidylcholine (PC)	1,2-dioleoyl-GPC (18:1/18:1)	2.61
4	Lipid	Lysoplasmalogen	1-(1-enyl-oleoyl)-2-oleoyl-GPE (P-18:1/18:1)*	3.01
5	Lipid	Plasmalogen	1-(1-enyl-palmitoyl)-2-oleoyl-GPE (P-16:0/18:1)*	2.37
6	Lipid	Hexosylceramides (HCER)	glycosyl ceramide (d18:2/25:1, d18:1/25:2)	2.01
7	Lipid	Phosphatidylethanolamine (PE)	1-palmitoyl-2-docosahexaenoyl-GPE (16:0/22:6)*	0.41
8	Lipid	Phosphatidylserine (PS)	1-stearoyl-2-oleoyl-GPS (18:0/18:1)	2.11
9	Lipid	Phosphatidylethanolamine (PE)	1-oleoyl-2-docosahexaenoyl-GPE (18:1/22:6)*	0.54
10	Lipid	Plasmalogen	1-(1-enyl-palmitoyl)-2-palmitoyl-GPC (P-16:0/16:0)*	0.58
B) Gray Matter AD vs Normal				
Accuracy: 80.00%				
Rank Order	Super Pathway	Sub Pathway	Biochemical Name	Fold Change
1	Lipid	Phospholipid Metabolism	glycerophosphorylcholine (GPC)	1.51
2	Amino Acid	Alanine and Aspartate Metabolism	N-acetylasparagine	0.67
3	Lipid	Fatty Acid, Monohydroxy	13-HODE + 9-HODE	0.50
4	Amino Acid	Lysine Metabolism	pipecolate	0.47
5	Lipid	Phospholipid Metabolism	glycerophosphoethanolamine	1.26
6	Amino Acid	Glycine, Serine and Threonine Metabolism	dimethylglycine	0.58
7	Amino Acid	Glutamate Metabolism	N-acetyl-aspartyl-glutamate (NAAG)	0.75
8	Amino Acid	Creatine Metabolism	Guanidinoacetate	1.49
9	Amino Acid	Histidine Metabolism	N-acetylhistidine	0.57
C) White Matter AD vs Normal				
Accuracy: 81.54%				
Rank Order	Super Pathway	Sub Pathway	Biochemical Name	Fold Change
1	Lipid	Fatty Acid, Monohydroxy	13-HODE + 9-HODE	0.56
2	Lipid	Phospholipid Metabolism	glycerophosphorylcholine (GPC)	1.47
3	Amino Acid	Lysine Metabolism	pipecolate	0.48
4	Amino Acid	Glycine, Serine and Threonine Metabolism	betaine	0.74
5	Amino Acid	Histidine Metabolism	N-acetylhistidine	0.62
6	Lipid	Fatty Acid, Monohydroxy	2-hydroxyheptanoate*	0.81
7	Lipid	Phospholipid Metabolism	glycerophosphoethanolamine	1.25
8	Nucleotide	Pyrimidine Metabolism, Uracil containing	3-ureidopropionate	0.56
9	Energy	TCA Cycle	2-methylcitrate/homocitrate	0.80
10	Lipid	Phosphatidylcholine (PC)	1,2-dilinoleoyl-GPC (18:2/18:2)	0.74
11	Amino Acid	Alanine and Aspartate Metabolism	N-acetylasparagine	0.69
12	Amino Acid	Glycine, Serine and Threonine Metabolism	dimethylglycine	0.59

Heat map of statistically significant biochemicals profiled when comparing groups are labeled as follows: Red and green shaded cells indicate $p \leq 0.05$ (red specifies that the mean values are significantly higher for that comparison; green values significantly lower).

Table 7.4 Gray and white matter metabolomics between early and late stage in APOE4

Super Pathway	Sub Pathway	Biochemical Name	E4 Late Stage vs Early Stage	
			Gray Matter	White Matter
Amino Acid	Glycine, Serine and Threonine Metabolism	N-acetyls erine	0.84	0.91
	Alanine and Aspartate Metabolism	N-acetylasparagine	0.74	0.80
	Glutamate Metabolism	N-acetyl-aspartyl-glutamate (NAAG)	0.72	0.70
	Tyrosine Metabolism	4-hydroxyphenylpyruvate	0.81	0.67
	Leucine, Isoleucine and Valine Metabolism	methysuccinate	0.65	0.70
		methysuccinoylcarnitine	0.73	0.72
	Methionine, Cysteine, SAM and Taurine Metabolism	cystathionine	0.80	0.72
Urea cycle; Arginine and Proline Metabolism	N-acetylarginine	0.80	0.93	
Peptide	Gamma-glutamyl Amino Acid	gamma-glutamylisoleucine*	0.63	0.95
		gamma-glutamylmethionine	0.68	0.73
		gamma-glutamylthreonine	0.81	0.96
Carbohydrate	Pentose Metabolism	ribitol	0.73	0.77
	Fructose, Mannose and Galactose Metabolism	galactose 1-phosphate	0.40	1.01
Energy	TCA Cycle	fumarate	0.80	0.86
		malate	0.81	0.89
	Oxidative Phosphorylation	phosphate	0.94	0.92
Lipid	Fatty Acid Metabolism	acetyl CoA	0.69	0.66
	Phospholipid Metabolism	choline phosphate	0.83	0.79
	Lysophospholipid (LPL)	1-palmitoleoyl-GPC (16:1)*	0.81	0.94
		1-stearoyl-GPC (18:0)	0.88	0.92
		1-oleoyl-GPC (18:1)	0.82	0.91
		1-linoleoyl-GPC (18:2)	0.79	0.88
		1-arachidonoyl-GPC (20:4n6)*	0.82	1.01
		1-linoleoyl-GPE (18:2)*	0.77	0.94
		1-arachidonoyl-GPE (20:4n6)*	0.80	0.98
Diacylglycerol	palmitoyl-docosahexaenoyl-glycerol (16:0/22:6) [1]*	1.26	1.69	

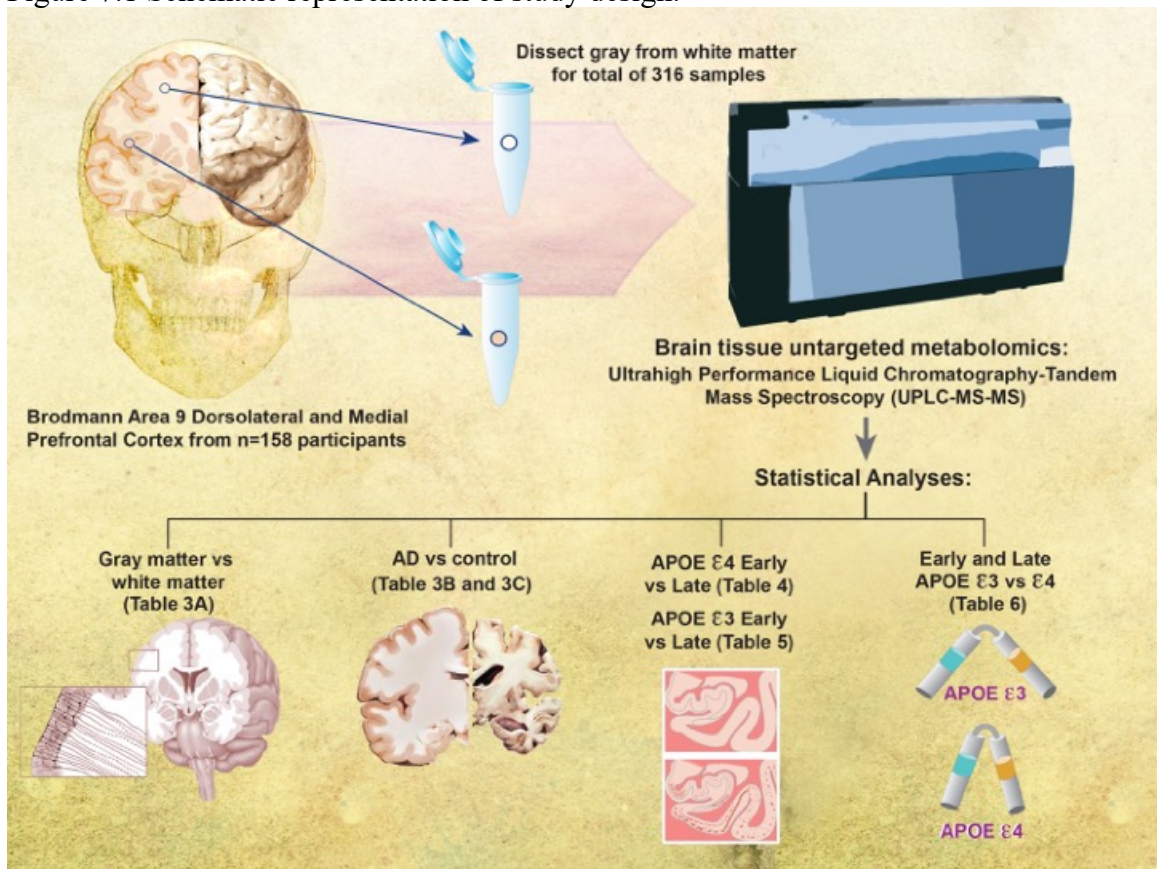
Table 7.5 Gray and white matter metabolomics between early and late stage in APOE3

Super Pathway	Sub Pathway	Biochemical Name	E3 Late Stage vs Early Stage	
			Gray Matter	White Matter
Amino Acid	Glycine, Serine and Threonine Metabolism	N-acetylglycine	1.75	1.62
		dimethylglycine	0.61	0.59
		betaine	0.71	0.69
	Alanine and Aspartate Metabolism	N-acetylasparagine	0.69	0.70
	Glutamate Metabolism	N-acetyl-aspartyl-glutamate (NAAG)	0.80	0.88
		beta-citrylglutamate	0.73	0.85
	Histidine Metabolism	N-acetylhistidine	0.62	0.67
		N-acetyl-3-methylhistidine*	1.48	1.48
		homocarnosine	0.67	0.74
		1-methylhistamine	0.65	0.67
	Lysine Metabolism	1-methyl-4-imidazoleacetate	0.63	0.82
		2-aminoadipate	1.21	1.24
		pipecolate	0.51	0.56
		N-acetyl-2-aminoadipate	1.05	1.15
	Tyrosine Metabolism	3-methoxytyramine sulfate	0.26	0.33
	Tryptophan Metabolism	tryptophan betaine	0.45	0.44
		8-methoxykynurenate	0.64	0.67
		5-hydroxyindoleacetate	0.62	0.72
	Urea cycle; Arginine and Proline Metabolism	argininate*	1.21	1.14
	Polyamine Metabolism	N-acetylputrescine	0.76	0.74
N1,N12-diacetylspermine		0.21	0.32	
Glutathione Metabolism	S-lactoylglutathione	0.70	0.94	
Carbohydrate	Glycolysis, Gluconeogenesis, and Pyruvate Metabolism	fructose 1,6-diphosphate/glucose 1,6-diphosphate/myo-inositol diphosphates	0.51	0.92
		dihydroxyacetone phosphate (DHAP)	0.57	0.79
	Nucleotide Sugar	UDP-galactose	1.51	1.47
Lipid	Long Chain Polyunsaturated Fatty Acid (n3 and n6)	tetradecadienoate (14:2)*	0.75	0.69
	Fatty Acid, Dicarboxylate	octadecenedioate (C18:1-DC)	0.55	0.59
	Fatty Acid Metabolism (Acyl Carnitine, Short Chain)	acetylcarnitine (C2)	0.86	0.70
	Fatty Acid Metabolism (Acyl Carnitine, Polyunsaturated)	arachidonoylcarnitine (C20:4)	0.65	0.84
		docosahexaenoylcarnitine (C22:6)*	0.52	0.53
	Fatty Acid, Monohydroxy	2-hydroxyheptanoate*	0.76	0.78
		13-HODE + 9-HODE	0.62	0.54
	Inositol Metabolism	myo-inositol	1.15	1.21
	Phospholipid Metabolism	glycerophosphorylcholine (GPC)	1.34	1.34
		glycerophosphoethanolamine	1.18	1.20
Phosphatidylcholine (PC)	1-palmitoyl-2-linoleoyl-GPC (16:0/18:2)	0.96	0.90	
	1,2-dilinoleoyl-GPC (18:2/18:2)	0.79	0.62	

Table 7.6 Gray and white matter metabolomics between APOE3 and APOE4 at early and late stages

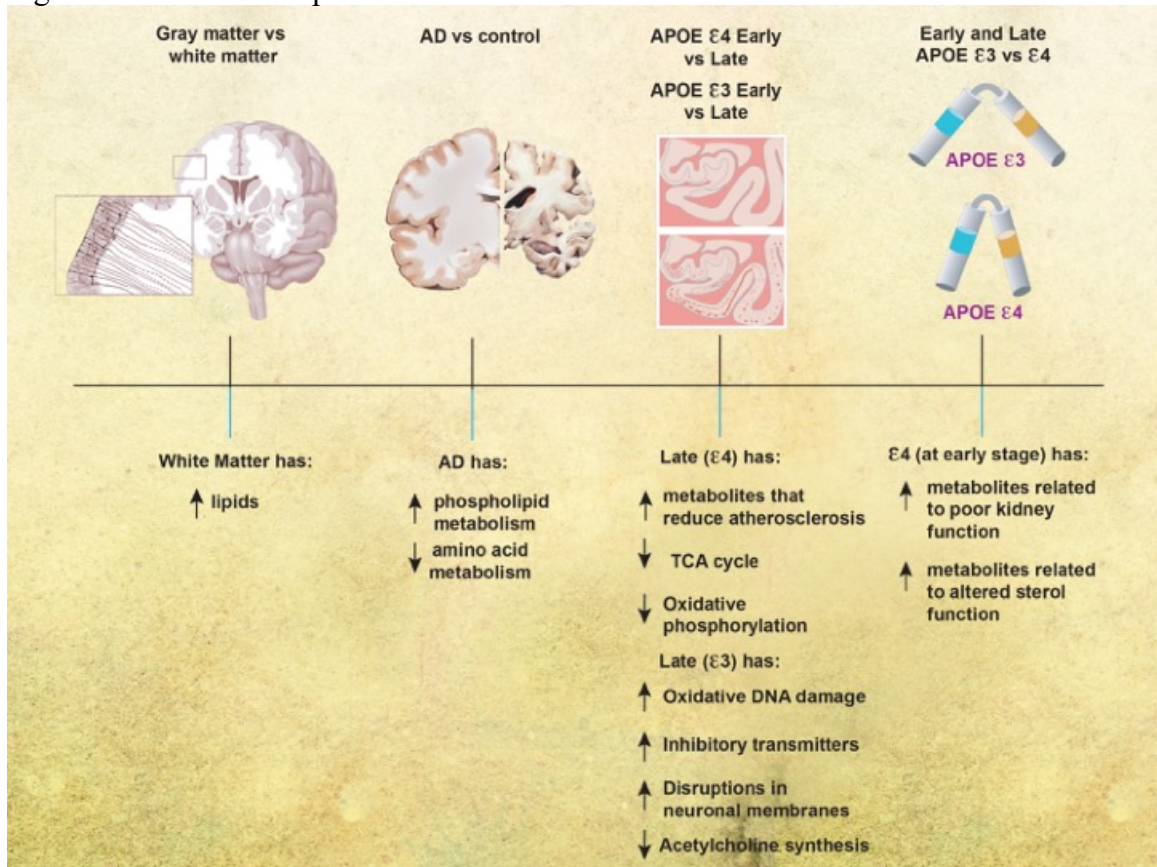
Early Stage					
			E4/E3 Fold Change		
Super Pathway	Sub Pathway	Biochemical Name	Gray Matter	White Matter	
Amino Acid	Glycine, Serine and Threonine Metabolism	dimethylglycine	0.60	0.57	
		Histidine Metabolism	formiminoglutamate	0.03	0.02
			histamine	1.28	1.15
		1-methyl-4-imidazoleacetate	0.64	0.53	
	Lysine Metabolism	2-aminoadipate	1.27	1.28	
	Leucine, Isoleucine and Valine Metabolism	1-carboxyethylisoleucine	1.40	1.22	
		methylsuccinate	1.38	1.41	
		methylsuccinoylcarnitine	1.36	1.42	
	Urea cycle; Arginine and Proline Metabolism	N,N,N-trimethyl-alanylproline betaine (TMAP)	0.52	0.49	
		argininate*	1.38	1.29	
Glutathione Metabolism	4-hydroxy-nonenal-glutathione	0.55	0.49		
Peptide	Gamma-glutamyl Amino Acid	gamma-glutamylisoleucine*	1.81	1.31	
		gamma-glutamylmethionine	1.31	1.24	
		gamma-glutamylthreonine	1.54	1.47	
Carbohydrate	Pentose Metabolism	ribitol	1.30	1.23	
Energy	Oxidative Phosphorylation	phosphate	1.06	1.09	
Lipid	Long Chain Polyunsaturated Fatty Acid (n3 and n6)	arachidonate (20:4n6)	1.19	1.09	
		Eicosanoid	15-HETE	0.54	0.50
	Endocannabinoid	docosahexaenoyl ethanolamide	1.32	0.99	
	Phosphatidylethanolamine (PE)	1,2-dipalmitoyl-GPE (16:0/16:0)*	0.94	0.73	
	Phosphatidylglycerol (PG)	1,2-dioleoyl-GPG (18:1/18:1)	0.55	1.25	
		Lysophospholipid	1-oleoyl-GPC (18:1)	1.11	1.09
			1-palmitoyl-GPS (16:0)*	1.36	0.96
	Sterol	7-hydroxycholesterol (alpha or beta)	0.42	0.42	
Secondary Bile Acid Metabolism	glycodeoxycholate	0.46	0.59		
Late Stage					
			E4/E3 Fold Change		
Super Pathway	Sub Pathway	Biochemical Name	Gray Matter	White Matter	
Amino Acid	Tryptophan Metabolism	indolelactate	2.58	1.76	
	Urea cycle; Arginine and Proline Metabolism	homoarginine	1.66	1.53	
		Polyamine Metabolism	N1,N12-diacetylspermine	6.95	10.26
Lipid	Primary Bile Acid Metabolism	glycochenodeoxycholate	2.67	3.68	

Figure 7.1 Schematic representation of study design.



We took brain tissue from Brodmann Area 9 of 158 participants in the University of Kentucky Alzheimer's Disease Center brain bank. We divided the samples into gray matter and white matter and performed untargeted metabolomics. We compared 1) Gray matter vs White matter, 2) AD vs control, 3) APOE 4 Early vs Late, 4) APOE 3 Early vs Late, and 5) Early and Late APOE 3 vs 4

Figure 7.2 Schematic representation of overall results.



Overall results from analysis of matter type, disease diagnosis, Braak stage, and APOE genotype.

CHAPTER 8. [SUPPLEMENT] GUT MICROBIAL DYSBIOSIS IS CORRELATED WITH STROKE SEVERITY MARKERS IN AGED RATS FOLLOWING STROKE

8.1 Summary

An imbalanced gut microbial community, or dysbiosis, has been shown to occur following stroke. It is possible that this dysbiosis negatively impacts stroke recovery and rehabilitation. Species level resolution measurements of the gut microbiome following stroke are needed to develop and test precision interventions such as probiotic or fecal microbiota transplant therapies that target the gut microbiome following stroke. Previous studies have used 16S rRNA amplicon sequencing in young male mice to obtain broad profiling of the gut microbiome at the genus level following stroke, but further investigations will be needed with whole genome shotgun sequencing in aged rats of both sexes to obtain species level resolution in a model which will better translate to the demographics of human stroke patients.

39 aged male and female rats underwent middle cerebral artery occlusion. Fecal samples were collected before stroke and three days post stroke to measure gut microbiome. Machine learning was used to identify the top ranked bacteria which were changed following stroke. MRI imaging was used to obtain infarct and edema size and cerebral blood flow (CBF). ELISA was used to obtain inflammatory markers.

Dysbiosis was demonstrated by an increase in pathogenic bacteria such as *Butyricimonas virosa* (15.52 fold change, $p < 0.0001$), *Bacteroides vulgatus* (7.36 fold change, $p < 0.0001$), and *Escherichia coli* (47.67 fold change, $p < 0.0001$). These bacteria were positively associated with infarct and edema size and with the inflammatory markers Ccl19, Ccl24, IL17a, IL3, and complement C5; they were negatively correlated with CBF. Conversely,

beneficial bacteria such as *Ruminococcus flavefaciens* (0.14 fold change, $p < 0.0001$), *Akkermansia muciniphila* (0.78 fold change, $p < 0.0001$), and *Lactobacillus murinus* (0.40 fold change, $p < 0.0001$) were decreased following stroke and associated with all the previous parameters in the opposite direction of the pathogenic species. There were not significant microbiome differences between the sexes.

The species level resolution measurements found here can be used as a foundation to develop and test precision interventions targeting the gut microbiome following stroke. Probiotics that include *Ruminococcus flavefaciens*, *Akkermansia muciniphila*, and *Lactobacillus murinus* should be developed to target the deficit following stroke to measure the impact on stroke severity.

8.2 Introduction

Over 795,000 people suffer a stroke every year in the United States alone¹. Recent advances in acute stroke therapies have lowered stroke mortality, but survivors are often left severely impaired¹². Rehabilitation therapies are beneficial at inducing neuroplasticity to overcome these impairments, but over 40% of stroke survivors are left with moderate to severe disabilities that markedly reduce quality of life²¹. Novel multimodal approaches are needed to promote plasticity and sensorimotor function through a combination of current rehabilitation therapies with other treatments designed to foster neuroplasticity.

Accumulating evidence suggests that gut microbes modulate brain plasticity via the bidirectional gut-brain axis and may play a role in stroke rehabilitation⁶⁷. A severely imbalanced microbial community, or dysbiosis, has been shown to occur following stroke, causing a systemic flood of neuro- and immunomodulatory substances due to increased gut

permeability and decreased gut motility⁸⁵. These substances can impact neuroinflammation as commensal bacteria invade the bloodstream and as intestinal lymphocytes migrate from gut-associated lymphoid tissue to the brain⁹². Fecal microbiota transplant has been shown to normalize brain lesion-induced dysbiosis and to improve stroke outcome in mice⁹². The microbiome is modifiable as it is influenced by environmental factors such as diet and exercise and could potentially be a therapeutic target in stroke rehabilitation through nutritional and pharmacological interventions and physical therapy^{89,145}. To our knowledge, no studies have measured the species level resolution necessary to develop precision interventions such as probiotics or fecal microbiota transplants that target the gut microbiota following stroke. Furthermore, no microbiome studies have been performed on aged rats of both sexes, which are better matched to the demographics of human stroke patient than the young male mice used in most studies. The microbiome changes found in this study need to be examined and correlated with clinical imaging markers of stroke and inflammatory markers to understand better whether the microbiome could be a therapeutic target in stroke rehabilitation.

Here we identify the gut-brain axis changes that occur following stroke in aged rats using high resolution whole genome shotgun sequencing and correlate them with clinical imaging markers of stroke including MRI-based infarct size, edema size, and cerebral blood flow (CBF) as well as inflammatory markers. We found that microbial communities are disrupted in an aged rat population following stroke, showing significantly different beta diversity, increased alpha diversity, and changes in the relative abundance of 5 of the 6 major phyla found in the gut. Changes in thirteen bacterial species as detected by machine learning were highly associated with stroke and changes in these species were also

associated with increased infarct and edema size and decreased CBF. Changes in the microbiome due to stroke were also associated with increases in 49 inflammatory markers.

8.3 Results

We performed a middle cerebral artery occlusion on a sample of 39 aged rats of both sexes (age 15-18 months). Half of the rats underwent a permanent occlusion and half underwent a transient 5-hour occlusion. We analyzed male and female rats. We analyzed all rats before and after middle cerebral artery occlusion and considered sex, surgery type, and treatment with LIF or PBS in the analysis. We administered a leukemia inhibitory factor (LIF) treatment on half of the rats based on previous work suggesting that LIF is an anti-inflammatory that regulates the immune/inflammatory response to stroke⁴²⁰. The rats had an average of 96.50 mm³ infarct size, 131.0 mm³ edema size, and 1.31 ml/g/min CBF from a permanent occlusion and 31.46 mm³ infarct size, 102.1 mm³ edema size, and 2.16 ml/g/min CBF from a transient occlusion. Infarct and edema volumes were not significantly different between sex, treatment group, or occlusion type. No significant difference in CBF was detected between sex or treatment, but, as expected, a significant difference occurred between permanent and transient occlusion in CBF (**Fig. 8.1**). We used four tests to determine motor function skills before and after stroke. 76% of the rats circled following stroke (**Fig. 8.2a**), there was a swing bias of 8 (**Fig. 8.2b**), there was a step bias of 9.3 (**Fig. 8.2c**), and only 26.5% of the rats extended their paw (**Fig 8.2d**).

8.3.1 The aged rat gut microbiome is disrupted following stroke

We performed an analysis on the gut microbial communities of the rats by running whole genome shotgun sequencing using DNA quantification services provided by

CosmosID. We collected fecal samples 24 hours before stroke and within 72 hours following stroke. Comparing the alpha diversity before and after stroke, we found that richness and evenness increased from 3.818 on the Shannon diversity index⁴²¹ to 4.178 (**Fig. 8.3A**). There were no differences in the change of alpha diversity between sex, treatment, or occlusion type. Comparing the beta diversity before and after stroke, we found that the microbial communities were significantly different between baseline and stroke ($p=0.0001$), but no significant microbial community differences were detected based on sex, treatment, or occlusion type. (**Fig. 8.3B**).

We investigated specific differences in the relative abundance of the major bacterial phyla in the gut (**Fig. 8.4**). We found increases in proteobacteria and Bacteroidetes and decreases in firmicutes, verrucomicrobia, and actinobacteria following stroke. This translates to a sharp decrease in the firmicutes to bacteroidetes ratio. Using linear regression, the major bacterial phyla predict infarct size with an $R^2=0.3866$ and edema size with an $R^2=0.6022$.

8.3.2 The top 13 disrupted bacterial species following stroke

We investigated specific differences in the relative abundance of the major bacterial species in the gut. There was a total of 29 species increased and 23 species decreased following stroke (**Table 8.1**). Using random forest machine learning classification, we found the most important bacterial species that predict stroke verse baseline with an 85.14% accuracy. They include an increase in *Butyricimonas virosa*, *Bacteroides vulgatus*, *Escherichia coli*, *Bacteroides uniformis*, *Bacteroides dorei*, *Parabacteroides distasonis*, and *Alistipes indistinctus* and a decrease in *Ruminococcus flavefaciens*, *Akkermansia muciniphila*, *Ruminococcus_u_s*, *[Clostridium] clostridioforme*, *Lactobacillus murinus*, and *Lachnospiraceae bacterium 3-1*. Using linear regression with backwards elimination

(Table 8.2), we found that increases in *Ruminococcus_u_s* and *Alistipes indistinctus* and decreases in *Lachnospiraceae bacterium 3-1* predict infarct volume with an $R^2=0.4433$. Increases in *Butyricinomas virosa*, *Bacteroides uniformis*, and *Ruminococcus_u_s* and decreases in *Ruminococcus flavefaciens* predict edema with an $R^2=0.6230$. Finally, decreases in *Alistipes indistinctus* predict CBF with an $R^2=0.1825$.

We investigated potential interactions between bacterial species in predicting infarct size, edema size, and CBF. Using a feasible solution algorithm (FSA) for finding interactions, we found that decreases in *Lachnospiraceae bacterium A2* and *Lactobacillus murinus* predict infarct size, but a combination of the two predicts a dramatic increase in the prediction value with an $R^2=0.6206$. Decreases in *Lachnospiraceae bacterium A4* and *Lactobacillus murinus* predict edema size, but a combination of the two have stronger predictive ability with an $R^2=0.6454$. Decreases in *Adlercreutzia equolifaciens* and *Desulfovibrio desulfuricans* predict CBF, but again, a combination of the two has a stronger prediction with an $R^2=0.8093$.

8.3.3 Bacterial disruptions following stroke are correlated with stroke severity

We investigated the correlation of all the bacterial species with infarct size and edema size (Table 8.3). Using the MaAsLin 2 R package⁴²², which automatically normalizes and transforms all variables in preparation for linear regression, we correlated metagenomic sequencing with imaging variables of stroke severity. Twenty-seven bacterial species were positively correlated and 19 negatively correlated with infarct volume. Thirty species were positively correlated, and 31 species were negatively correlated with edema volume. No species were correlated with CBF.

8.3.4 Bacterial disruptions following stroke are correlated with inflammation

We investigated the correlation of all the bacterial species with infarct size and edema size (**Table 8.3**). Using the MaAsLin 2 R package⁴²², which automatically normalizes and transforms all variables in preparation for linear regression, we correlated metagenomic sequencing with imaging variables of stroke severity. Twenty-seven bacterial species were positively correlated and 19 negatively correlated with infarct volume. Thirty species were positively correlated, and 31 species were negatively correlated with edema volume. No species were correlated with CBF.

8.4 Discussion

To our knowledge, we are the first to report on the gut microbial changes with species level resolution in aged male and female rats and to correlate these changes with clinical MRI imaging markers of stroke and inflammatory markers. Following stroke, we found that alpha diversity significantly increased, beta diversity significantly changed, and 5 of the 6 major bacterial phyla were altered. Using machine learning, the top 13 bacterial species that predict whether a sample came from the baseline or post-stroke time point. These bacterial species had independent significant correlations with infarct size, edema size, and CBF. We also identified several species whose interactions with one another were significant in correlating with stroke imaging outcomes. Finally, we found 49 inflammatory markers that correlated with the changes in microbiome from stroke. These changes are representative of a shift from beneficial to pathogenic bacterial species following stroke which results in an increased inflammatory response.

Figure 8.5 summarizes the changes in gut microbial communities in response to stroke. Following stroke there is a significant shift in the gut microbiome, with alterations to 52 major bacterial species. These bacterial fluctuations shift the environment to a more inflammatory state that adversely affect injury. The microbial community dysbiosis is likely due to the increased gut permeability and decreased gut motility in addition to the immunodepression caused by the amplified stress response (increased sympathetic nervous system response and hypothalamic-pituitary-adrenal (HPA) axis response) following stroke ⁴²³. Previous groups have reported a decrease in alpha diversity following stroke in a mouse model⁹² and an increase in a human model ¹⁰⁷. Our findings are consistent with others who have seen that microbial communities differ before and after stroke based on measures of beta diversity ⁴²⁴. We did not find any significant differences in the microbiome between males and females. Some groups have found sex differences in the microbiome that are largely attributed to hormone differences ⁴²⁵. It is possible that we did not see these differences because the female rats we used are aged and reproductively senescent.

We saw increases in proteobacteria following stroke. In previous studies, proteobacteria have been associated with increased cognitive impairment following stroke ¹⁹⁸. Dysbiosis related to metabolic disorders, inflammation, and cancer is often related to an increase in proteobacteria ^{426,427}. This is possibly due to increased oxygen content in the gut following increases in inflammation, providing an optimal environment for these facultative anaerobes ⁴²⁸. We also saw decreases in firmicutes and increases in bacteroidetes species. Decreased firmicutes have also been associated with Alzheimer's disease ⁴²⁹. Obesity is often characterized by a significantly increased firmicutes to

bacteroidetes (F/B) ratio ⁴³⁰; interestingly, our study found that stroke has the opposite effect on F/B ratio. Actinobacteria was significantly decreased following stroke. Actinobacteria downregulates inflammation by production of IL-4 and IL-13 ⁴³¹ and is known to have anti-biofilm properties against pathogenic bacteria ⁴³². It is possible that a decrease in actinobacteria allows other pathogenic bacteria to flourish.

Of the bacteria we found that are increased following stroke, many were of the bacteroides species. Bacteroides species have the ability to reduce oxygen levels and breakdown food products to liberate fucose and sialic acid residues from glycoproteins that can be consumed by other microorganisms, including pathogens. Higher bacteroides species are associated with type I diabetes ⁴³³. *Bacteroides vulgatus* and *Bacteroides dorei* reduce gut microbial lipopolysaccharide production and inhibit atherosclerosis ²¹⁹, but they are also associated with insulin resistance, altered bile acid metabolism, and reduced interleukin-22 secretion ⁴³⁴. *Butyricimonas virosa*, *Escherichia coli*, and *Parabacteroides distasonis* were also elevated following stroke. An increase of *Butyricimonas virosa* has also been seen in divers with high occupational exposure to a hyperoxic environment ⁴³⁵, which is very different from the hypoxic environment of stroke. *Escherichia coli* is a very common commensal bacteria that has the potential to cause extraintestinal infections based on its genome content and phenotypic traits ²²⁰ and is famous for causing post-stroke infections, especially pneumonia. *Parabacteroides distasonis* has been shown to alleviate obesity and metabolic dysfunctions via production of succinate and secondary bile acids ⁴³⁶, which is interesting since stroke is often associated with obesity and metabolic dysfunctions.

Many bacteria which are generally considered beneficial were decreased following stroke including *Akkermansia*, *Lactobacillus*, and *Ruminococcus* species. *Akkermansia muciniphila* is a mucin-degrading bacterium⁴³⁷ that can be increased with fasting⁴³⁸ that is known to improve host metabolic functions and immune responses⁴³⁹. *Lactobacillus murinus* can combat inflammaging⁴⁴⁰, and a reduction of *L. murinus* due to high salt consumption has been associated with an increase in proinflammatory TH17 cells⁴⁴¹, which have been correlated with post stroke dysbiosis and secondary injury⁴⁴². *Lactobacillus reuteri* was also significantly reduced following stroke. A randomized control trial in children showed administration of *L. reuteri* as a probiotic to be useful in treating constipation in children⁴⁴³. Constipation is a common morbidity in stroke, and administration of this species could help to alleviate symptoms. *Ruminococcus flavefaciens* has also been shown to decrease the therapeutic effects of antidepressants, having implications for the treatment of post-stroke depression.

Many of the bacterial changes were associated with increases in inflammatory markers. The major markers that were increased were CCL19, CCL24, IL-17A, IL-3, and complement factor C5. CCL19 is a chemokine that is commonly upregulated as a result of viral infections⁴⁴⁴, and attracts dendritic cells and T lymphocytes⁴⁴⁵; it promotes thymocyte development, secondary lymphoid organogenesis, high affinity antibody responses, regulatory and memory T cell function, and lymphocyte egress from tissues organs^{446,447}. CCL19 suppresses angiogenesis and can inhibit proliferation, migration, and sprouting responses of tumors⁴⁴⁸. CCL19 has previously been found to be upregulated following stroke after damage to the intestinal epithelium⁴⁴⁹ and has been shown to facilitate T-cell migration to the insult site and microglial activation following stroke⁴⁵⁰.

CCL24 plays an important role in pathological processes of skin and lung inflammation and fibrosis ⁴⁵¹ and regulates inflammatory and fibrotic activities through its receptor, CCR3 ⁴⁵². CCR3 is a mediator of neural cell death ⁴⁵³. In host defense, IL-17A has been shown to be mostly beneficial against infection caused by extracellular bacteria and fungi ⁴⁵⁴ and IL-17A has been shown to be increased following stroke, especially in males ⁴⁵⁵. IL3 is strongly associated with brain volume variation and plays pivotal roles in the expansion and maintenance of the neural progenitor pool and the number of surviving neurons ⁴⁵⁶; our work has previously identified IL3 increased in the spleen with our aged rat model of stroke ⁴²⁰. Activation of complement C5 generates the potent anaphylatoxin C5a and leads to pathogen lysis, inflammation, and cell damage ⁴⁵⁷. Activated C5 complement components are a part of the cerebral tissue inflammation following ischemia ⁴⁵⁸.

This study lays an important foundation upon which precision interventions can be developed to target the gut microbiome in stroke rehabilitation. Future studies should attempt to manipulate the microbiome to change stroke outcomes. This could be achieved through diet interventions, antibiotic therapy, probiotics, or fecal microbiota transplant. For example, a future probiotics study should include the use of *Ruminococcus flavefaciens*, *Akkermansia muciniphila*, and *Lactobacillus murinus* as these were deficient in our population. Stroke severity measures from imaging and inflammatory markers could be used as outcomes to compare to the current study. While the present study identified associations of various inflammatory markers with changes in gut microbial composition, it would also be useful to perform mechanistic studies to determine how the microbiota change the expression of these markers and what their downstream effects are. Finally,

human studies will be needed to determine whether the microbial changes seen in animals following stroke are similar to the changes seen in animals. Such results can then be used to alter the gut microbiome to favor positive clinical outcomes after stroke.

8.5 Methods

8.5.1 Ethics approval and animals

Details of ethics approval and animals have been reported previously⁴⁵⁹. Briefly, aged male and female rats (18-month-old Sprague-Dawley rats (ENVIGO, Indianapolis, IN) were used for all procedures. The aged female rats on average weighed between 245g and 425g, and aged male rats approximately weighed between 505g and 705g. The study was conducted in accordance with the National Institutes of Health Guide for the Care and Use of Laboratory Animals and study protocols were approved by University of Kentucky's (UK) Institutional Animal Care and Use Committee. Reporting in this manuscript follows the recommendations in the ARRIVE guidelines. Animals were housed in a climate-controlled room on a 12-hr light and dark cycle (0700–1900) with access to food and water. Per Division of Laboratory Animal Resources (DLAR) cage requirements at UK's vivarium facility, the animals can be paired in one cage if the animal weight is under 650 grams. We typically house two animals (males or females) per cage upon arrival to DLAR. Once the rats are over 650 grams, they are then split into a separate cage by themselves. Fecal samples were collected for all animals at 24 hours before surgery and 72 hours post-surgery and for 4 animals at 30 days post-surgery. The rats underwent MRI at 72 hours to measure infarct and edema volumes and CBF then euthanized.

8.5.2 Middle cerebral artery occlusion

Details of the middle cerebral artery occlusion have been reported previously⁴⁵⁹. Briefly, 22 of the rats received a permanent Middle Cerebral Artery Occlusion (p-MCAO) and 17 of the rats received a 5-hour transient Middle Cerebral Artery Occlusion (5t-MCAO). All animals were induced with oxygen containing 5% isoflurane, then shaved, prepped with Hibiclens (chlorohexidine scrub) prior to 70% EtOH and then a betadine solution. Maintenance isoflurane was maintained at 2.5% in O₂ was delivered via a nosecone placed in line with the binner tubeQ (gas delivery tube) of the anesthesia circuit. Under bnear sterileQ conditions and with the use of a Zeiss operating microscope (Carl Zeiss AG, Gottingen, Germany) at 4 to 25 magnification, the procedure was performed. First, the skin was opened with a midline vertical incision, and the underlying submandibular gland bluntly dissected in the midline to produce left and right lobes, which were retracted laterally. Division of the omohyoid muscle, then dissection medial to the right sternocleidomastoid (SCM) muscle was used to expose the common carotid artery (CCA), which was separated from the vagus nerve. Elastic hooks (Lone Star Medical Products, Houston, TX, USA) tethered to metal stays on the customized surgery table were used to retract the skin and the SCM muscle. In the p-MCAO, a hand-held electrocautery (Aaron Medical, St. Petersburg, FL, USA) is used to cauterize the superior thyroid artery (STA), a collateral off the ECA, and the occipital artery (OA), a collateral off the ICA. Two 5-0 silk sutures (Surgical Specialties, Reading, PA, USA) were used to ligate the external carotid artery (ECA) as distal as possible to the ECA/ICA bifurcation, and a second tie that was applied just proximal to the first, leaving enough space in between the two ties to cut the artery with micro scissors. At this point, blunt dissection was used to

isolate the internal carotid artery (ICA) and its collateral, the pterygopalatine artery. Next, microvascular aneurysm clips (Mizuho, Beverly, MA, USA) were applied to the CCA and the ICA. A 5-0 PDS II monofilament embolus (Ethicon, Cornelia, GA, USA), was introduced into an arteriotomy hole—produced with a 26-gauge hypodermic needle—in the reflected ECA stump and fed distally into the ICA. At this time, a collar suture at the base of the ECA stump was tightened around the embolus, and the ICA clamp was removed. The embolus was advanced 20 mm from the carotid bifurcation, with care taken to avoid entrance into the pterygopalatine artery.

For the transient occlusion, the same steps were done as stated with the pMCAO, with the exception that Docol Corporation silicone rubber-coated monofilaments were used for the occlusion of the middle cerebral artery (MCA). Multiple sized Docol monofilaments are used in the MCAO surgery depending on the sex and weight of the rat. Two 18-inch length of 5-0 silk suture were used for the ligation of the external carotid artery (ECA) to secure the ECA stump, and the entry point of the monofilament into the ECA/ICA bifurcation. The third 5-0 silk suture was used to secure the monofilament within the ECA. A micro-serrefines arterial clamp (FST, Fine Science Tools, #18055-01) was used to occlude the internal carotid artery (ICA) and common carotid artery (CCA) prior to advancement of the monofilament into the MCA. After 5 hours, the embolus was gently removed and the collar suture at the base of the ECA stump tightened. The skin was closed with 3-0 nylon suture (Ethicon, Cornelia, GA, USA), anesthesia discontinued, and the animal allowed to recover. Animals used for control underwent a neck dissection and coagulation of the external carotid artery, but no manipulation or occlusion of the common or internal carotid arteries.

8.5.3 Post-surgical fluid management and pain control

Details of the post-surgical fluid management and pain control have been reported previously⁴⁵⁹. Briefly, immediately post-operatively the animals received 2 ml of sterile saline (0.9%) subcutaneous. An additional 1 ml of saline was given if extra blood loss occurred during surgery. The animals were injected with sterile filtered PBS pH 7.4 at 6 (for the p-MCAO), 24, 48, and 72 hours post-MCAO. The animals were weighed every morning post-MCAO to determine dehydration. Hydration status was checked by pinching up or “tenting” the skin over the nape of the neck. The skin should immediately relax into its normal position. If the skin remains tented longer than normal, the rat was deemed dehydrated, and saline was given. Per DLAR guidelines, rats can receive up to 10 ml at a time and no more than 2 ml at any one location per 6 hr. If warranted, additional saline (1–2 ml) will be given in addition to 6, 24, 48, and 72 hr. Also, we added an additional water bottle in each cage to allow more availability to free water for the rats to consume and moistened food was provided on the bottom of the cage to encourage feeding and additional water intake. Post-surgical pain control was managed with carprofen, which is based on weight of the animal. Animal weights are taken prior to surgery (pMCAO) and daily until animals are euthanized at 72 hr. (post MRI). The animals received a dosage of carprofen 5mg/kg prior to surgery and every 24 hr. for three days post-pMCAO until 72 hr. when they were euthanized (post MRI). Termination of survival criteria include that all animals were weighed and monitored, especially for dehydration and pain, each morning post surgery. This includes specific attention to the animal as a whole, as well as incision sights. If symptoms such as pain, fatigue, loss of energy, excess energy, ruffled hair coat, reluctance to move, failure to groom or feed, hypoactivity, hyperactivity, restlessness, self-

trauma, aggressiveness, ataxia, pale mucous membranes, cyanosis, rapid, shallow and/or labored breathing, cachexia, porphyria, soiled anogenital area, inactivity, failure to respond to stimuli, lack of inquisitiveness, vocalization, and/or hunched posture were observed, the research team obtained advice from the vivarium veterinary staff on how best to intervene to alleviate discomfort; if that was not possible the animal was euthanatized. Additional checks were made in the afternoon if there was any rat of concern. The animals were removed from the study if adverse signs persisted despite carprofen and treatment past 24 hr. If the signs fail to resolve, the vivarium veterinarian was consulted and decided the time course when such animals were euthanized. Additionally, weight loss greater than 20% (emaciated appearance, rapid weight loss over two days) was considered an endpoint. Rapid weight loss was considered greater than 10% a day for two days.

8.5.4 Microbiome Sequencing

Fecal samples were collected for all animals at 24 hours before surgery and 72 hours post-surgery and for 4 animals at 30 days post-surgery. Genomic DNA were extracted from 0.25 grams of stool using ZymoBIOMICS™ DNA Mini Kit and shipped to CosmosID for DNA quantification using fluorometer Qubit 3.0. Libraries were constructed and the PCR products were purified using 1.0X speed beads and eluted in 15 µL of nuclease-free water and quantified by PicoGreen fluorometric assay (100X final dilution). The libraries were pooled and loaded onto a high sensitivity chip run on the Caliper LabChipGX (Perkin Elmer, Waltham, MA) for size estimation and sequenced using Illumina NextSeq/HiSeq platform. Unassembled sequencing reads were analyzed by CosmosID bioinformatics platform (CosmosID Inc., Rockville, MD) ⁴⁶⁰⁻⁴⁶³ for microbiome analysis. Heatmaps, stacked bar graphs, and Principal Component Analysis (PCA) plots were generated to

visualize the diversity and abundance of each microbial taxa. Alpha- and beta-diversity were calculated to determine the number of species present in a cohort and diversity similarities between groups.

8.5.5 Magnetic resonance imaging

MRI images were acquired on a 7T Bruker Clinscan horizontal bore system (7.0T, 30 cm, 300 Hz) equipped with a triple-axis gradient system (630 mT/m and 6,300 T m⁻¹ s⁻¹) with a closed cycle. PCASL (pseudo continuous arterial spin labelling) images were acquired coronally to determine CBF with a fat saturated, double refocused echo planar sequence: TR 4000 ms, TE 26 ms, Matrix 74 x 56, FOV 26 mm x 19.7 mm, Slice 1.2 mm, Slices 6, 120 Tagged-Untagged Pairs, 10 M₀ Images, Tagging Plane Offset 12mm, Bolus duration 1.86sec, Post Labeling Delay 0sec, and Acquisition Time of 10 min. T2 weighted images were acquired coronally with a RARE sequence: TR 6000 ms, TE 29 ms, Turbo Factor 5, Matrix 190 x 190, FOV 240 mm x 240 mm, Slice 0.4 mm, Slices 44, and Acquisition Time of 9 min. Male rats were anesthetized with an average of 2.25% isoflurane in oxygen, while female rats were anesthetized with an average of 1.75% isoflurane in oxygen using an MRI compatible CWE Inc. equipment (Ardmore, PA). They were held in place on a Bruker scanning bed with a tooth bar, ear bars, and tape. Body temperature, heart rate, and respiratory rate were continuously monitored throughout the MRI scans (SA Instruments, Inc., Stony Brook, NY). The animal's body temperatures were maintained at 37°C with a water heating system built into the scanning bed. The scanning procedure took approximately 40-60 mins. per animal.

The MR images were analyzed by a blinded neuroradiologist who visually identified infarct volume and edema volume. These volumes were counted, and this number was

normalized to the number of images counted to provide a per section count. The volume of brain parenchyma demonstrating infarct volume visibly affected was calculated by manual segmentation using ITK-SNAP software⁴⁶⁴. The volume of brain parenchyma visibly affected by T2 hyperintensity (edema volume) was calculated in a similar fashion. The data are given as absolute volume in cubic millimeters. The calculation was based on all slices from each MR sequence. Cerebral perfusion values of the area of lesion within the ipsilateral hemisphere, and the equivalent region within the contralateral hemisphere were generated using the quantification as previously described.^{358,419}

8.5.6 Biochemical analysis

In following STAIR guidelines, clinically relevant biomarkers were determined in our aged male and female rats⁴⁶⁵. Blood was taken from the jugular vein at three different time points: immediately prior to MCAO surgery and 5 mins after reperfusion of the MCA in the pMCAO, and 5 hours post MCAO procedure in the 5t-MCAO. Blood was immediately placed on ice and centrifuged at 2000 g for 15 minutes. Plasma was extracted and stored separately, both pellet and plasma were frozen at -80°C for later analysis. RNA extraction and Amplification followed the methods of Martha et.al 2020⁴⁶⁶. Briefly, total RNA was extracted from the pellet portion via a Nucleospin Blood Kit (Macherey-Nagel, Düren, Germany), RNA quantity was estimated using a Qubit 4 Fluorometer (Thermo-Fisher; Waltham, MA), cDNA was synthesized using a RT² PreAMP cDNA synthesis Kit from Qiagen and expression of 84 genes were measured using an ABI StepOne Plus (Germantown, MD) and a RT² Profiler Rat Chemokine and Receptor Array from Qiagen. Delta Delta CT was calculated using the fold change of the gene expression measurement from pre to 3-day.

8.5.7 Statistical analysis

Descriptive microbiome analyses were performed with CosmosID bioinformatics software to generate alpha diversity, beta diversity, and relative abundance data. Alpha diversities amongst groups were compared using Wilcoxon Rank Sum test. Beta diversities amongst groups were compared using PerMANOVA. Relative abundance data was compared to measures of stroke severity as determined by imaging (infarct size, edema size, CBF) using general linear models within the MaAsLin 2 R package⁴²². Random forest was used to determine top bacterial species that were changed following stroke using the randomForest R package⁴⁶⁷. All imaging variables in the study were transformed to meet assumptions of normality. The transformation procedures began with Shapiro-Wilks and for measures with $p < 0.05$, the variables were square root transformed. A p-value of 0.05 was set a priori to determine statistical significance.

Table 8.1 Top 13 bacterial species changes following stroke as detected by random forest

Bacterial Species	Change in Relative Abundance	Gram Stain	Phylum
<i>Butyrivimonas virosa</i>	15.52	(-)	Bacteroides
<i>Ruminococcus flavefaciens</i>	0.14	(+)	Firmicutes
<i>Akkermansia muciniphila</i>	0.78	(-)	Verrucomicrobia
<i>Bacteroides vulgatus</i>	7.36	(-)	Bacteroidetes
<i>Escherichia coli</i>	47.67	(-)	Proteobacteria
<i>Bacteroides uniformis</i>	5.15	(-)	Bacteroidetes
<i>Bacteroides dorei</i>	5.29	(-)	Bacteroidetes
<i>Ruminococcus_u_s</i>	0.25	(+)	Firmicutes
<i>Parabacteroides distasonis</i>	10.84	(-)	Bacteroidetes
<i>[Clostridium] clostridioforme</i>	0.42	(+)	Firmicutes
<i>Alistipes indistinctus</i>	335.73	(-)	Bacteroidetes
<i>Lactobacillus murinus</i>	0.36	(+)	Firmicutes
<i>Lachnospiraceae bacterium 3-1</i>	0.40	(+)	Firmicutes

Predictive Accuracy of Random Forest Model: 85.14%

Table 8.2 Linear Regression models predicting infarct, edema, and CBF by top 13 species

Parameter	Estimate	DF	SS	F-Ratio	P-value
Predicting Infarct					
Intercept	10.41	1	0	0	1
<i>Ruminococcus_u_s</i>	5.34	1	201.66	11.85	0.0015
<i>Alistipes indistinctus</i>	3.05	1	122.20	7.18	0.0112
<i>Lachnospiraceae bacterium 3-1</i>	-24.97	1	141.01	8.28	0.0068
Predicting Edema					
Intercept	3.05	1	0	0	1
<i>Butyrivimonas virosa</i>	35.48	1	73.77	5.68	0.0229
<i>Ruminococcus flavefaciens</i>	-6.50	1	276.79	21.30	<0.0001
<i>Bacteroides uniformis</i>	12.93	1	59.99	4.62	0.0394
<i>Ruminococcus_u_s</i>	4.92	1	152.28	11.72	0.0016
Predicting Cerebral Blood Flow					
Intercept	1.48	1	0	0	1
<i>Alistipes indistinctus</i>	-0.46	1	3.53	7.82	0.008

Model parameters selected using backward elimination from top 13 list in Table 1

Table 8.3 Correlation of bacterial species with infarct and edema

Bacteria	Coefficient	Bacteria	Coefficient
Species Increase associated with infarct		Species Increase associated with edema	
<i>Alistipes finegoldii</i>	0.32	<i>Alistipes finegoldii</i>	0.35
<i>Alistipes indistinctus</i>	0.29	<i>Alistipes indistinctus</i>	0.34
<i>Alistipes sp HGB5</i>	0.33	<i>Alistipes sp HGB5</i>	0.38
<i>Alistipes timonensis</i>	0.16	<i>Alistipes timonensis</i>	0.17
<i>Bacteroides caccae</i>	0.29	<i>Bacteroides caccae</i>	0.32
<i>Bacteroides dorei</i>	0.38	<i>Bacteroides dorei</i>	0.43
<i>Bacteroides eggerthii</i>	0.30	<i>Bacteroides eggerthii</i>	0.34
<i>Bacteroides fragilis</i>	0.09	<i>Bacteroides fragilis</i>	0.11
<i>Bacteroides intestinalis</i>	0.17	<i>Bacteroides intestinalis</i>	0.25
<i>Bacteroides massiliensis</i>	0.25	<i>Bacteroides massiliensis</i>	0.26
<i>Bacteroides ovatus</i>	0.10	<i>Bacteroides ovatus</i>	0.12
<i>Bacteroides sartorii</i>	0.19	<i>Bacteroides rodentium</i>	0.15
<i>Bacteroides sp 3.1.40A</i>	0.24	<i>Bacteroides sartorii</i>	0.22
<i>Bacteroides uniformis</i>	0.35	<i>Bacteroides sp 3.1.40A</i>	0.26
<i>Bacteroides vulgatus</i>	0.47	<i>Bacteroides uniformis</i>	0.41
<i>Butyrivibrio virosa</i>	0.41	<i>Bacteroides vulgatus</i>	0.53
<i>Desulfovibrio_u_s</i>	0.23	<i>Butyrivibrio virosa</i>	0.48
<i>Enterococcus_u_s</i>	0.15	<i>Desulfovibrio_u_s</i>	0.26
<i>Enterococcus faecalis</i>	0.22	<i>Enterococcus faecalis</i>	0.26
<i>Escherichia coli</i>	0.52	<i>Escherichia coli</i>	0.60
<i>Parabacteroides_u_s</i>	0.33	<i>Parabacteroides_u_s</i>	0.34
<i>Parabacteroides distasonis</i>	0.49	<i>Parabacteroides distasonis</i>	0.55
<i>Parabacteroides goldsteinii</i>	0.18	<i>Parabacteroides goldsteinii</i>	0.21
<i>Parabacteroides merdae</i>	0.13	<i>Parabacteroides merdae</i>	0.17
<i>Parabacteroides sp D13</i>	0.21	<i>Parabacteroides sp D13</i>	0.24
<i>Porphyromonas sp 31.2</i>	0.15	<i>Porphyromonas sp 31.2</i>	0.19
		<i>Proteus mirabilis</i>	0.13
Species decrease associated with infarct		Species decrease associated with edema	
<i>Bifidobacterium animalis</i>	-0.21	<i>Bifidobacterium animalis</i>	-0.24
<i>Bifidobacterium bifidum</i>	-0.13	<i>Bifidobacterium bifidum</i>	-0.12
<i>Bifidobacterium pseudolongum</i>	-0.14	<i>Bifidobacterium pseudolongum</i>	-0.16
<i>Eubacterium plexicaudatum</i>	-0.15	<i>Clostridium saudiense</i>	-0.08
<i>Lachnospiraceae bacterium 10-1</i>	-0.21	<i>Eubacterium plexicaudatum</i>	-0.16
<i>Lachnospiraceae bacterium 28-4</i>	-0.19	<i>Imtechella halotolerans</i>	-0.12
<i>Lachnospiraceae bacterium 3-1</i>	-0.38	<i>Lachnospiraceae bacterium A4</i>	-0.35
<i>Lachnospiraceae bacterium A2</i>	-0.23	<i>Lachnospiraceae bacterium COE1</i>	-0.26
<i>Lachnospiraceae bacterium A4</i>	-0.31	<i>Lactobacillus animalis</i>	-0.16
<i>Lachnospiraceae bacterium COE1</i>	-0.23	<i>Lactobacillus johnsonii</i>	-0.23
<i>Lactobacillus murinus</i>	-0.37	<i>Lactobacillus murinus</i>	-0.42
<i>Oscillibacter sp 1-3</i>	-0.13	<i>Lactobacillus reuteri</i>	-0.20
<i>Ruminococcus flavefaciens</i>	-0.45	<i>Oscillibacter sp 1-3</i>	-0.11
<i>Clostridium clostridioforme</i>	-0.20	<i>Ruminococcus bromii</i>	-0.09
		<i>Ruminococcus flavefaciens</i>	-0.56
		<i>Clostridium clostridioforme</i>	-0.20

P<0.01 for all bacteria

Table 8.4 Association of Inflammatory Markers and Bacterial Species

Feature	Coef	Q value	Inflammatory Marker	Coef	Q Value
Aerococcus.urinaeequi	-0.272821	0.008123	Ccl11	-0.20556	1.94E-10
			Ccl24	-0.20162	0.004625
			Ccl4	-0.19439	1.15E-06
			Ccl5	-0.19492	2.35E-09
			Ccl6	-0.19490	1.57E-09
			Cxcl9	-0.18666	0.005476
			Cxcr1	-0.19420	0.002162
			Cxcr5	-0.19052	0.000588
			Il10ra	-0.19083	0.000597
			IL11	-0.19497	2.08E-10
			Il13	-0.19468	9.21E-08
			Il16	-0.19442	1.19E-06
			Il3	-0.21801	8.19E-07
			Il4	-0.19464	4.19E-07
			RGD1561905	-0.20264	0.003346
Aerococcus.viridans	-0.2502272	0.00710756	Ccl11	-0.29201	1.94E-10
			Ccl12	-0.27568	1.57E-05
			Ccl2	-0.27670	1.43E-06
			Ccl22	-0.27693	2.58E-09
			Ccl24	-0.28641	0.004625
			Ccl4	-0.27615	1.15E-06
			Ccl5	-0.27689	2.35E-09
			Ccl6	-0.27687	1.57E-09
			Cxcl9	-0.26517	0.005476
			Cxcr1	-0.27587	0.002162
			Cxcr5	-0.27065	0.000588
			Il10ra	-0.27109	0.000597
			IL11	-0.27697	2.08E-10
			Il13	-0.27655	9.21E-08
Il16	-0.27619	1.19E-06			
Il3	-0.30971	8.19E-07			
Il4	-0.27650	4.19E-07			
			RGD1561905	-0.28786	0.003346
Alistipes.indistinctus	0.49548605	0.00010758	Il17a	0.190118	3.32E-05
Bacteroides.caccae	0.55294244	2.70E-05	Lfng	0.592807	0.008044
Bacteroides.intestinalis	0.39545256	0.00090266	Ccl19	0.21675248	0.0014087
			Cxcl1	0.23004667	0.00219959
Imtechella.halotolerans	-0.2698021	0.00513494	Tnfrsf11b	-0.3915736	7.93E-16
Parabacteroides.goldsteinii	0.36960675	0.00061701	Il2rb	0.51806	0.00364866
			Il3	0.55259618	2.34E-20
			Il6st	0.52789004	0.00072493
			Tnfsf4	0.51998756	0.00362087
Parabacteroides.sp..D13	0.37087382	0.00010987	Ccl24	0.36028464	0.00462557
Porphyromonas.sp..31_2	0.36233409	0.00022155	Ccl24	0.35003715	0.00462557

Q-Value<0.01 for all bacteria and inflammatory markers

Negative coefficients for bacteria with negative coefficients for inflammatory markers indicate increase in inflammatory marker

Positive coefficients for bacteria with positive coefficients for inflammatory markers indicate increase in inflammatory marker

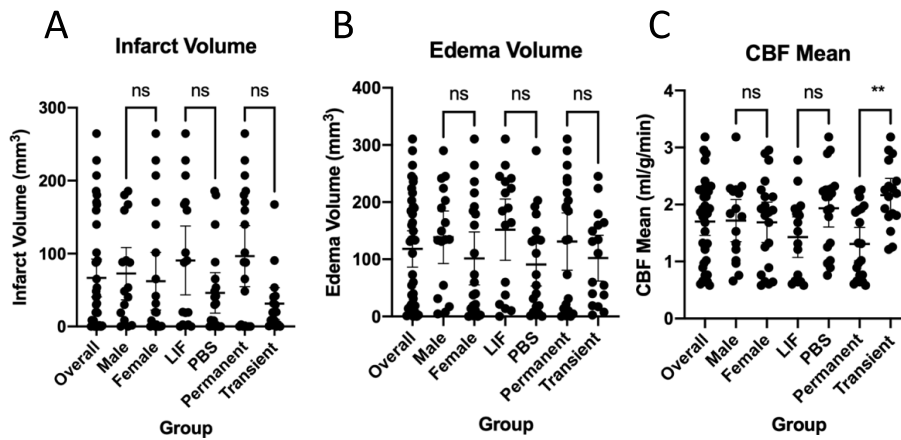


Figure 8.1 Imaging features following stroke

A) Infarct volume, B) Edema volume, and C) Cerebral Blood Flow (CBF) Mean following stroke in overall rats and separated by male, female, LIF, PBS, Permanent, and Transient.

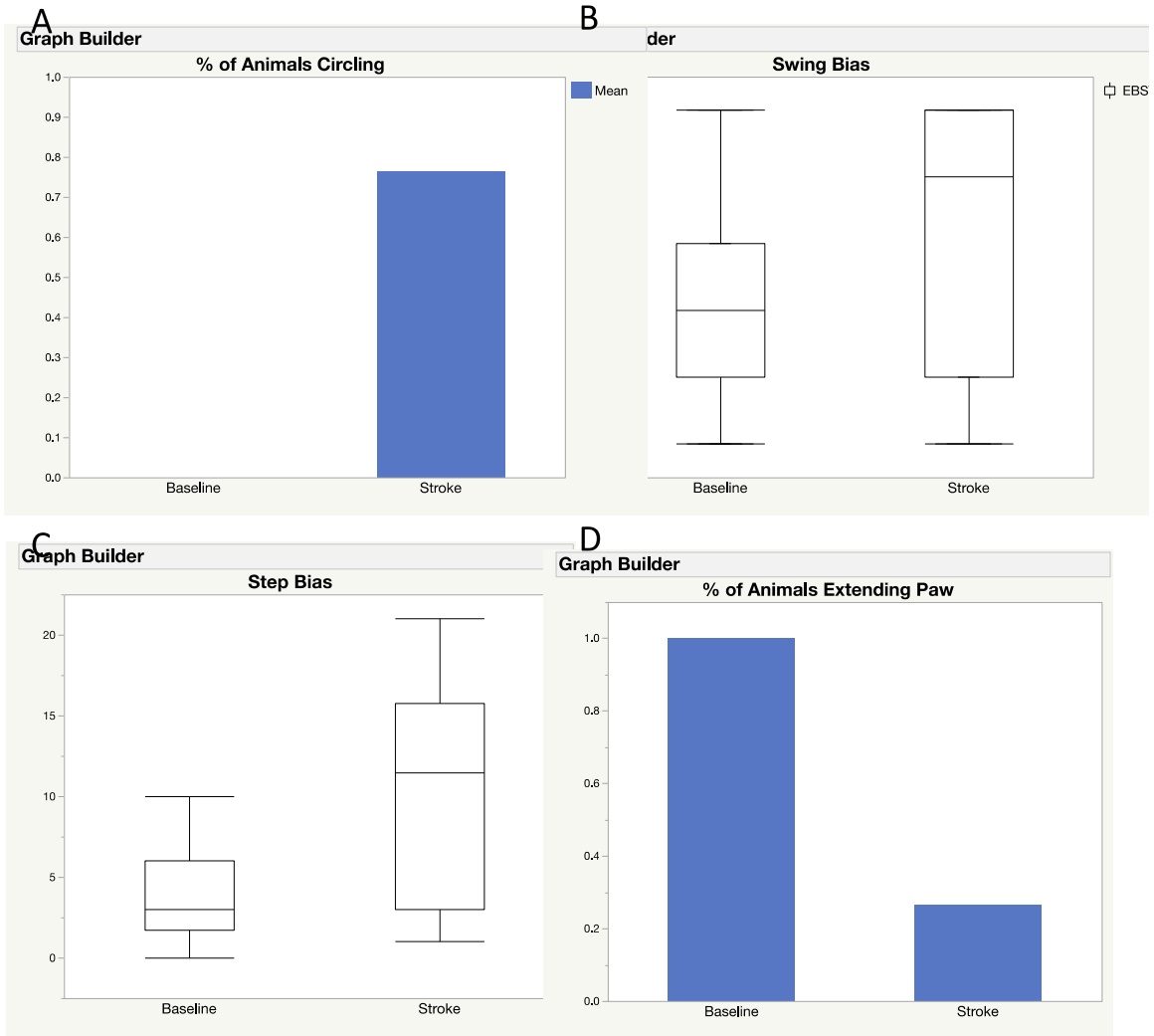


Figure 8.2 Motor function skills before and after stroke

Four test were used to measure motor function before and after stroke: A) circling, B) elevated body swing test, C) step test, D) paw extension test.

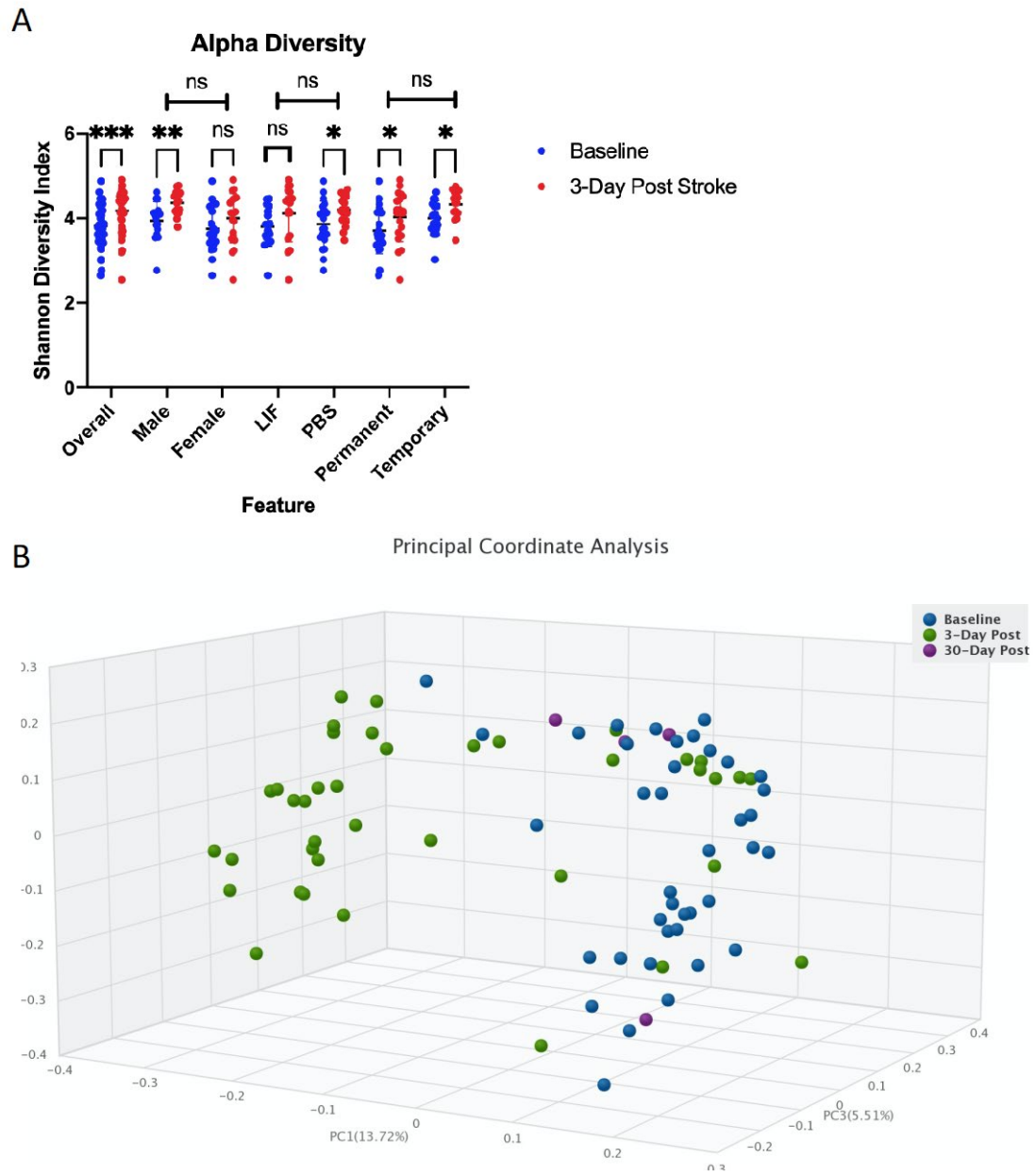


Figure 8.3 Diversity changes following stroke.

A) Alpha diversity as measured by the Shannon diversity index detecting species richness and evenness is increased following stroke. There is no difference in change across sex, treatment, or stroke type. **B)** Beta Diversity as measured by Bray-Curtis method comparing how different samples are

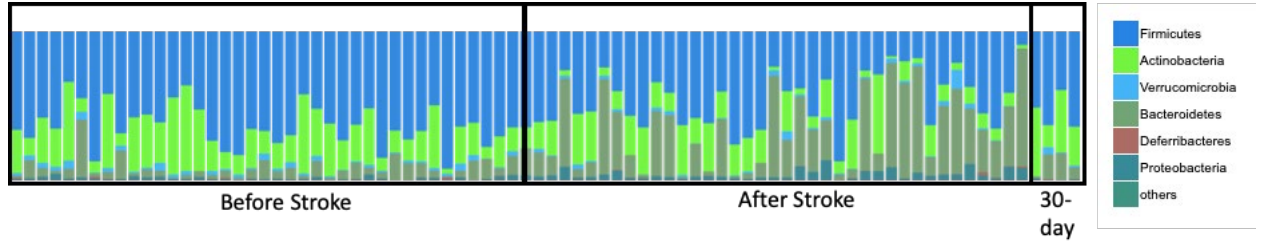


Figure 8.4 Phyla changes as a result of stroke.
Relative Abundance shows phyla composition before and after stroke.

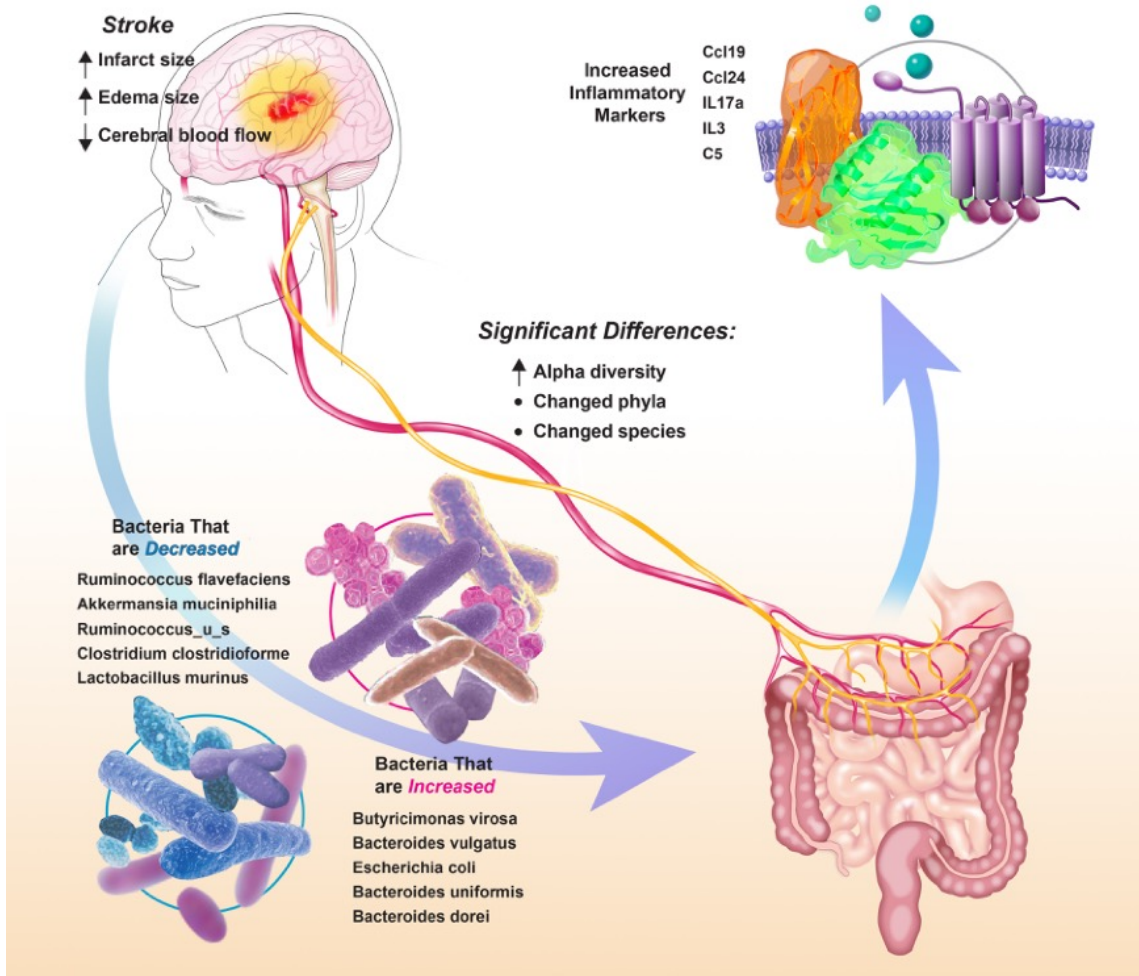


Figure 8.5 Summary figure depicting changes in gut microbial communities in response to stroke

BIBLIOGRAPHY

1. Benjamin, E.J., *et al.* Heart Disease and Stroke Statistics-2017 Update: A Report From the American Heart Association. *Circulation* **135**, e146-e603 (2017).
2. Sacco, R.L., *et al.* An updated definition of stroke for the 21st century: a statement for healthcare professionals from the American Heart Association/American Stroke Association. *Stroke* **44**, 2064-2089 (2013).
3. van der Zwan, A. & Hillen, B. Review of the variability of the territories of the major cerebral arteries. *Stroke* **22**, 1078-1084 (1991).
4. Hasso, A.N., Stringer, W.A. & Brown, K.D. Cerebral ischemia and infarction. *Neuroimaging Clin N Am* **4**, 733-752 (1994).
5. Jolugbo, P. & Ariens, R.A.S. Thrombus Composition and Efficacy of Thrombolysis and Thrombectomy in Acute Ischemic Stroke. *Stroke* **52**, 1131-1142 (2021).
6. Murtagh, B. & Smalling, R.W. Cardioembolic stroke. *Curr Atheroscler Rep* **8**, 310-316 (2006).
7. Kuriakose, D. & Xiao, Z. Pathophysiology and Treatment of Stroke: Present Status and Future Perspectives. *Int J Mol Sci* **21**(2020).
8. Wu, F., *et al.* Circular RNA TLK1 Aggravates Neuronal Injury and Neurological Deficits after Ischemic Stroke via miR-335-3p/TIPARP. *The Journal of neuroscience : the official journal of the Society for Neuroscience* **39**, 7369-7393 (2019).
9. Spacek, M., Zemanek, D., Hutyra, M., Sluka, M. & Taborsky, M. Vulnerable atherosclerotic plaque - a review of current concepts and advanced imaging. *Biomed Pap Med Fac Univ Palacky Olomouc Czech Repub* **162**, 10-17 (2018).
10. Libby, P., *et al.* Atherosclerosis. *Nat Rev Dis Primers* **5**, 56 (2019).
11. Wei, L.K., *et al.* Polymorphisms of MTHFR, eNOS, ACE, AGT, ApoE, PON1, PDE4D, and Ischemic Stroke: Meta-Analysis. *J Stroke Cerebrovasc Dis* **26**, 2482-2493 (2017).
12. Moy, E., *et al.* Leading Causes of Death in Nonmetropolitan and Metropolitan Areas- United States, 1999-2014. *Morbidity and mortality weekly report. Surveillance summaries (Washington, D.C. : 2002)* **66**, 1-8 (2017).
13. Prabhakaran, S., Ruff, I. & Bernstein, R.A. Acute stroke intervention: a systematic review. *JAMA* **313**, 1451-1462 (2015).
14. Derex, L. & Cho, T.H. Mechanical thrombectomy in acute ischemic stroke. *Rev Neurol (Paris)* **173**, 106-113 (2017).
15. Katan, M. & Luft, A. Global Burden of Stroke. *Semin Neurol* **38**, 208-211 (2018).
16. Dhir, N., *et al.* Pre-clinical to Clinical Translational Failures and Current Status of Clinical Trials in Stroke Therapy: A Brief Review. *Curr Neuropharmacol* **18**, 596-612 (2020).
17. Cassidy, J.M. & Cramer, S.C. Spontaneous and Therapeutic-Induced Mechanisms of Functional Recovery After Stroke. *Transl Stroke Res* **8**, 33-46 (2017).
18. Cramer, S.C. Repairing the human brain after stroke: I. Mechanisms of spontaneous recovery. *Ann Neurol* **63**, 272-287 (2008).
19. Langhorne, P., Bernhardt, J. & Kwakkel, G. Stroke rehabilitation. *Lancet* **377**, 1693-1702 (2011).

20. Brewer, L., Horgan, F., Hickey, A. & Williams, D. Stroke rehabilitation: recent advances and future therapies. *QJM : monthly journal of the Association of Physicians* **106**, 11-25 (2013).
21. Carandang, R., *et al.* Trends in incidence, lifetime risk, severity, and 30-day mortality of stroke over the past 50 years. *Jama* **296**, 2939-2946 (2006).
22. Nahum, M., Lee, H. & Merzenich, M.M. Principles of neuroplasticity-based rehabilitation. *Prog Brain Res* **207**, 141-171 (2013).
23. Gulyaeva, N.V. Molecular Mechanisms of Neuroplasticity: An Expanding Universe. *Biochemistry (Mosc)* **82**, 237-242 (2017).
24. Sasmita, A.O., Kuruvilla, J. & Ling, A.P.K. Harnessing neuroplasticity: modern approaches and clinical future. *Int J Neurosci* **128**, 1061-1077 (2018).
25. Feng, Z., *et al.* The neuroprotective mechanisms of ginkgolides and bilobalide in cerebral ischemic injury: a literature review. *Mol Med* **25**, 57 (2019).
26. Ramaholimihaso, T., Bouazzaoui, F. & Kaladjian, A. Curcumin in Depression: Potential Mechanisms of Action and Current Evidence-A Narrative Review. *Front Psychiatry* **11**, 572533 (2020).
27. Novak, P., *et al.* AADvac1, an Active Immunotherapy for Alzheimer's Disease and Non Alzheimer Tauopathies: An Overview of Preclinical and Clinical Development. *J Prev Alzheimers Dis* **6**, 63-69 (2019).
28. Kurisu, K. & Yenari, M.A. Therapeutic hypothermia for ischemic stroke; pathophysiology and future promise. *Neuropharmacology* **134**, 302-309 (2018).
29. Elias, G.J.B., Namasivayam, A.A. & Lozano, A.M. Deep brain stimulation for stroke: Current uses and future directions. *Brain Stimul* **11**, 3-28 (2018).
30. Li, C.Y., *et al.* Characterizing Standardized Functional Data at Inpatient Rehabilitation Facilities. *J Am Med Dir Assoc* (2022).
31. Baird, A.E. & Warach, S. Magnetic resonance imaging of acute stroke. *J Cereb Blood Flow Metab* **18**, 583-609 (1998).
32. Labayru, G., *et al.* White matter integrity changes and neurocognitive functioning in adult-late onset DM1: a follow-up DTI study. *Sci Rep* **12**, 3988 (2022).
33. Wardlaw, J.M., *et al.* Studies of acute ischemic stroke with proton magnetic resonance spectroscopy: relation between time from onset, neurological deficit, metabolite abnormalities in the infarct, blood flow, and clinical outcome. *Stroke* **29**, 1618-1624 (1998).
34. Fan, H., *et al.* Simultaneous Hemodynamic and Structural Imaging of Ischemic Stroke With Magnetic Resonance Fingerprinting Arterial Spin Labeling. *Stroke*, STROKEAHA121037066 (2022).
35. Meier, E.L., Kelly, C.R., Goldberg, E.B. & Hillis, A.E. Executive control deficits and lesion correlates in acute left hemisphere stroke survivors with and without aphasia. *Brain Imaging Behav* (2021).
36. Weintraub, S., *et al.* The cognition battery of the NIH toolbox for assessment of neurological and behavioral function: validation in an adult sample. *J Int Neuropsychol Soc* **20**, 567-578 (2014).
37. Sidhu, M. & van der Poorten, D. The gut microbiome. *Aust Fam Physician* **46**, 206-211 (2017).
38. Barko, P.C., McMichael, M.A., Swanson, K.S. & Williams, D.A. The Gastrointestinal Microbiome: A Review. *J Vet Intern Med* **32**, 9-25 (2018).

39. Jandhyala, S.M., *et al.* Role of the normal gut microbiota. *World J Gastroenterol* **21**, 8787-8803 (2015).
40. Quigley, E.M. Gut bacteria in health and disease. *Gastroenterol Hepatol (N Y)* **9**, 560-569 (2013).
41. Weiss, G.A. & Hennet, T. Mechanisms and consequences of intestinal dysbiosis. *Cell Mol Life Sci* **74**, 2959-2977 (2017).
42. Theriot, C.M. & Young, V.B. Interactions Between the Gastrointestinal Microbiome and *Clostridium difficile*. *Annu Rev Microbiol* **69**, 445-461 (2015).
43. Kostic, A.D., Xavier, R.J. & Gevers, D. The microbiome in inflammatory bowel disease: current status and the future ahead. *Gastroenterology* **146**, 1489-1499 (2014).
44. Pimentel, M. & Lembo, A. Microbiome and Its Role in Irritable Bowel Syndrome. *Dig Dis Sci* **65**, 829-839 (2020).
45. John, G.K. & Mullin, G.E. The Gut Microbiome and Obesity. *Curr Oncol Rep* **18**, 45 (2016).
46. Safari, Z. & Gerard, P. The links between the gut microbiome and non-alcoholic fatty liver disease (NAFLD). *Cell Mol Life Sci* **76**, 1541-1558 (2019).
47. Vindigni, S.M. & Surawicz, C.M. Fecal Microbiota Transplantation. *Gastroenterol Clin North Am* **46**, 171-185 (2017).
48. Rohlke, F., Surawicz, C.M. & Stollman, N. Fecal flora reconstitution for recurrent *Clostridium difficile* infection: results and methodology. *J Clin Gastroenterol* **44**, 567-570 (2010).
49. Ferrer, M., Mendez-Garcia, C., Rojo, D., Barbas, C. & Moya, A. Antibiotic use and microbiome function. *Biochem Pharmacol* **134**, 114-126 (2017).
50. Kim, S.K., *et al.* Role of Probiotics in Human Gut Microbiome-Associated Diseases. *J Microbiol Biotechnol* **29**, 1335-1340 (2019).
51. Dahl, W.J., Rivero Mendoza, D. & Lambert, J.M. Diet, nutrients and the microbiome. *Prog Mol Biol Transl Sci* **171**, 237-263 (2020).
52. Holscher, H.D. Dietary fiber and prebiotics and the gastrointestinal microbiota. *Gut Microbes* **8**, 172-184 (2017).
53. Dalton, A., Mermier, C. & Zuhl, M. Exercise influence on the microbiome-gut-brain axis. *Gut Microbes* **10**, 555-568 (2019).
54. Milani, C., *et al.* The First Microbial Colonizers of the Human Gut: Composition, Activities, and Health Implications of the Infant Gut Microbiota. *Microbiol Mol Biol Rev* **81**(2017).
55. Pannaraj, P.S., *et al.* Association Between Breast Milk Bacterial Communities and Establishment and Development of the Infant Gut Microbiome. *JAMA Pediatr* **171**, 647-654 (2017).
56. Cotozzolo, E., *et al.* Characterization of Bacterial Microbiota Composition along the Gastrointestinal Tract in Rabbits. *Animals (Basel)* **11**(2020).
57. Donaldson, G.P., Lee, S.M. & Mazmanian, S.K. Gut biogeography of the bacterial microbiota. *Nat Rev Microbiol* **14**, 20-32 (2016).
58. Ranjan, R., Rani, A., Metwally, A., McGee, H.S. & Perkins, D.L. Analysis of the microbiome: Advantages of whole genome shotgun versus 16S amplicon sequencing. *Biochem Biophys Res Commun* **469**, 967-977 (2016).

59. Schmidt, P.J., Cameron, E.S., Muller, K.M. & Emelko, M.B. Ensuring That Fundamentals of Quantitative Microbiology Are Reflected in Microbial Diversity Analyses Based on Next-Generation Sequencing. *Front Microbiol* **13**, 728146 (2022).
60. Dubinkina, V.B., Ischenko, D.S., Ulyantsev, V.I., Tyakht, A.V. & Alexeev, D.G. Assessment of k-mer spectrum applicability for metagenomic dissimilarity analysis. *BMC Bioinformatics* **17**, 38 (2016).
61. Lin, Y., Gifford, S., Ducklow, H., Schofield, O. & Cassar, N. Towards Quantitative Microbiome Community Profiling Using Internal Standards. *Appl Environ Microbiol* **85**(2019).
62. Cox, L.M. & Weiner, H.L. Microbiota Signaling Pathways that Influence Neurologic Disease. *Neurotherapeutics* **15**, 135-145 (2018).
63. Furness, J.B. The enteric nervous system and neurogastroenterology. *Nat Rev Gastroenterol Hepatol* **9**, 286-294 (2012).
64. Fung, T.C. The microbiota-immune axis as a central mediator of gut-brain communication. *Neurobiol Dis* **136**, 104714 (2020).
65. Di Paola, M., *et al.* Oleoylethanolamide treatment affects gut microbiota composition and the expression of intestinal cytokines in Peyer's patches of mice. *Sci Rep* **8**, 14881 (2018).
66. Liu, F., *et al.* Communications Between Peripheral and the Brain-Resident Immune System in Neuronal Regeneration After Stroke. *Front Immunol* **11**, 1931 (2020).
67. Leung, K. & Thuret, S. Gut Microbiota: A Modulator of Brain Plasticity and Cognitive Function in Ageing. *Healthcare (Basel, Switzerland)* **3**, 898-916 (2015).
68. O'Mahony, S.M., Clarke, G., Borre, Y.E., Dinan, T.G. & Cryan, J.F. Serotonin, tryptophan metabolism and the brain-gut-microbiome axis. *Behav Brain Res* **277**, 32-48 (2015).
69. Banskota, S., Ghia, J.E. & Khan, W.I. Serotonin in the gut: Blessing or a curse. *Biochimie* **161**, 56-64 (2019).
70. Tan, J., *et al.* The role of short-chain fatty acids in health and disease. *Adv Immunol* **121**, 91-119 (2014).
71. Sadler, R., *et al.* Short-Chain Fatty Acids Improve Poststroke Recovery via Immunological Mechanisms. *The Journal of neuroscience : the official journal of the Society for Neuroscience* **40**, 1162-1173 (2020).
72. Agostini, A., *et al.* Brain functional changes in patients with ulcerative colitis: a functional magnetic resonance imaging study on emotional processing. *Inflamm Bowel Dis* **17**, 1769-1777 (2011).
73. Ellingson, B.M., *et al.* Diffusion tensor imaging detects microstructural reorganization in the brain associated with chronic irritable bowel syndrome. *Pain* **154**, 1528-1541 (2013).
74. Labus, J.S., *et al.* Irritable bowel syndrome in female patients is associated with alterations in structural brain networks. *Pain* **155**, 137-149 (2014).
75. Bagga, D., *et al.* Probiotics drive gut microbiome triggering emotional brain signatures. *Gut Microbes* **9**, 486-496 (2018).

76. Tillisch, K., *et al.* Consumption of fermented milk product with probiotic modulates brain activity. *Gastroenterology* **144**, 1394-1401, 1401 e1391-1394 (2013).
77. Braniste, V., *et al.* The gut microbiota influences blood-brain barrier permeability in mice. *Sci Transl Med* **6**, 263ra158 (2014).
78. Bell, R.D., *et al.* Apolipoprotein E controls cerebrovascular integrity via cyclophilin A. *Nature* **485**, 512-516 (2012).
79. Ong, I.M., *et al.* Gut microbiome populations are associated with structure-specific changes in white matter architecture. *Transl Psychiatry* **8**, 6 (2018).
80. Xia, G.H., *et al.* Stroke Dysbiosis Index (SDI) in Gut Microbiome Are Associated With Brain Injury and Prognosis of Stroke. *Front Neurol* **10**, 397 (2019).
81. Bajaj, J.S., *et al.* Colonic mucosal microbiome differs from stool microbiome in cirrhosis and hepatic encephalopathy and is linked to cognition and inflammation. *Am J Physiol Gastrointest Liver Physiol* **303**, G675-685 (2012).
82. Gareau, M.G. Cognitive Function and the Microbiome. *Int Rev Neurobiol* **131**, 227-246 (2016).
83. Lach, G., Schellekens, H., Dinan, T.G. & Cryan, J.F. Anxiety, Depression, and the Microbiome: A Role for Gut Peptides. *Neurotherapeutics* **15**, 36-59 (2018).
84. Boer, C.G., *et al.* Intestinal microbiome composition and its relation to joint pain and inflammation. *Nat Commun* **10**, 4881 (2019).
85. Stanley, D., Moore, R.J. & Wong, C.H.Y. An insight into intestinal mucosal microbiota disruption after stroke. *Scientific reports* **8**, 568 (2018).
86. Wen, S.W. & Wong, C.H.Y. An unexplored brain-gut microbiota axis in stroke. *Gut microbes* **8**, 601-606 (2017).
87. Rundek, T., *et al.* Gut permeability and cognitive decline: A pilot investigation in the Northern Manhattan Study. *Brain Behav Immun Health* **12**(2021).
88. Wei, M., Huang, Q., Liu, Z., Luo, Y. & Xia, J. Intestinal Barrier Dysfunction Participates in the Pathophysiology of Ischemic Stroke. *CNS Neurol Disord Drug Targets* **20**, 401-416 (2021).
89. Winek, K., Meisel, A. & Dirnagl, U. Gut microbiota impact on stroke outcome: Fad or fact? *Journal of cerebral blood flow and metabolism : official journal of the International Society of Cerebral Blood Flow and Metabolism* **36**, 891-898 (2016).
90. Durgan, D.J., Lee, J., McCullough, L.D. & Bryan, R.M., Jr. Examining the Role of the Microbiota-Gut-Brain Axis in Stroke. *Stroke* **50**, 2270-2277 (2019).
91. Chen, Y., *et al.* Persistence of Gut Microbiota Dysbiosis and Chronic Systemic Inflammation After Cerebral Infarction in Cynomolgus Monkeys. *Front Neurol* **10**, 661 (2019).
92. Singh, V., *et al.* Microbiota Dysbiosis Controls the Neuroinflammatory Response after Stroke. *The Journal of neuroscience : the official journal of the Society for Neuroscience* **36**, 7428-7440 (2016).
93. Lee, J., *et al.* Gut Microbiota-Derived Short-Chain Fatty Acids Promote Poststroke Recovery in Aged Mice. *Circ Res* **127**, 453-465 (2020).
94. Wang, H., *et al.* Fecal Transplantation from db/db Mice Treated with Sodium Butyrate Attenuates Ischemic Stroke Injury. *Microbiol Spectr* **9**, e0004221 (2021).

95. Zhou, Z., *et al.* Sodium butyrate attenuated neuronal apoptosis via GPR41/Gbetagamma/PI3K/Akt pathway after MCAO in rats. *J Cereb Blood Flow Metab* **41**, 267-281 (2021).
96. Chen, R., *et al.* Transplantation of fecal microbiota rich in short chain fatty acids and butyric acid treat cerebral ischemic stroke by regulating gut microbiota. *Pharmacol Res* **148**, 104403 (2019).
97. Feng, Y., *et al.* Effect of intestinal microbiota transplantation on cerebral ischemia reperfusion injury in aged mice via inhibition of IL-17. *Neurogastroenterol Motil*, e14313 (2022).
98. Silva de Carvalho, T., *et al.* Post-ischemic protein restriction induces sustained neuroprotection, neurological recovery, brain remodeling, and gut microbiota rebalancing. *Brain Behav Immun* **100**, 134-144 (2022).
99. Yuan, Q., *et al.* Lactulose Improves Neurological Outcomes by Repressing Harmful Bacteria and Regulating Inflammatory Reactions in Mice After Stroke. *Front Cell Infect Microbiol* **11**, 644448 (2021).
100. Huang, J.T., *et al.* Calorie restriction conferred improvement effect on long-term rehabilitation of ischemic stroke via gut microbiota. *Pharmacol Res* **170**, 105726 (2021).
101. Kingsbury, C., *et al.* Inflammation-relevant microbiome signature of the stroke brain, gut, spleen, and thymus and the impact of exercise. *J Cereb Blood Flow Metab* **41**, 3200-3212 (2021).
102. Dang, Y., *et al.* Distinctive Gut Microbiota Alteration Is Associated with Poststroke Functional Recovery: Results from a Prospective Cohort Study. *Neural Plast* **2021**, 1469339 (2021).
103. Wang, W., Li, X., Yao, X., Cheng, X. & Zhu, Y. The characteristics analysis of intestinal microecology on cerebral infarction patients and its correlation with apolipoprotein E. *Medicine* **97**, e12805 (2018).
104. Yamashiro, K., *et al.* Gut dysbiosis is associated with metabolism and systemic inflammation in patients with ischemic stroke. *PloS one* **12**, e0171521 (2017).
105. Yu, F., *et al.* Phenylacetylglutamine, a Novel Biomarker in Acute Ischemic Stroke. *Front Cardiovasc Med* **8**, 798765 (2021).
106. Yu, F., *et al.* Gut-Derived Metabolite Phenylacetylglutamine and White Matter Hyperintensities in Patients With Acute Ischemic Stroke. *Front Aging Neurosci* **13**, 675158 (2021).
107. Yin, J., *et al.* Dysbiosis of Gut Microbiota With Reduced Trimethylamine-N-Oxide Level in Patients With Large-Artery Atherosclerotic Stroke or Transient Ischemic Attack. *Journal of the American Heart Association* **4**(2015).
108. Xu, D.J., *et al.* Compositional and functional alterations of gut microbiota in patients with stroke. *Nutr Metab Cardiovasc Dis* **31**, 3434-3448 (2021).
109. Sharma, V., *et al.* At the Intersection of Gut Microbiome and Stroke: A Systematic Review of the Literature. *Front Neurol* **12**, 729399 (2021).
110. Zhu, W., *et al.* Gut microbes impact stroke severity via the trimethylamine N-oxide pathway. *Cell Host Microbe* **29**, 1199-1208 e1195 (2021).
111. Zhang, J., *et al.* Gut microbial metabolite TMAO portends prognosis in acute ischemic stroke. *J Neuroimmunol* **354**, 577526 (2021).

112. Xia, G.H., *et al.* Dysbiosis of Gut Microbiota Is an Independent Risk Factor of Stroke-Associated Pneumonia: A Chinese Pilot Study. *Front Cell Infect Microbiol* **11**, 715475 (2021).
113. Jiang, W., Gong, L., Liu, F., Ren, Y. & Mu, J. Alteration of Gut Microbiome and Correlated Lipid Metabolism in Post-Stroke Depression. *Front Cell Infect Microbiol* **11**, 663967 (2021).
114. Li, N., *et al.* Change of intestinal microbiota in cerebral ischemic stroke patients. *BMC Microbiol* **19**, 191 (2019).
115. Haak, B.W., *et al.* Disruptions of Anaerobic Gut Bacteria Are Associated with Stroke and Post-stroke Infection: a Prospective Case-Control Study. *Transl Stroke Res* **12**, 581-592 (2021).
116. Chang, Y., *et al.* Microbiota dysbiosis and functional outcome in acute ischemic stroke patients. *Sci Rep* **11**, 10977 (2021).
117. Tan, C., *et al.* Dysbiosis of Gut Microbiota and Short-Chain Fatty Acids in Acute Ischemic Stroke and the Subsequent Risk for Poor Functional Outcomes. *JPEN J Parenter Enteral Nutr* **45**, 518-529 (2021).
118. Xu, R., *et al.* Dysbiosis of the intestinal microbiota in neurocritically ill patients and the risk for death. *Crit Care* **23**, 195 (2019).
119. Tian, X., *et al.* Effect of Enteral Nutrition on the Intestinal Microbiome and Risk of Death in Ischemic Stroke Patients. *JPEN J Parenter Enteral Nutr* (2022).
120. Roth, W. & Mohamadzadeh, M. Vitamin B12 and gut-brain homeostasis in the pathophysiology of ischemic stroke. *EBioMedicine* **73**, 103676 (2021).
121. Benjamin, E.J., *et al.* Heart Disease and Stroke Statistics-2017 Update: A Report From the American Heart Association. *Circulation* **135**, e146-e603 (2017).
122. Harris, A.D., *et al.* The use and interpretation of quasi-experimental studies in medical informatics. *Journal of the American Medical Informatics Association : JAMIA* **13**, 16-23 (2006).
123. Zhou, H., Taber, C., Arcona, S. & Li, Y. Difference-in-Differences Method in Comparative Effectiveness Research: Utility with Unbalanced Groups. *Appl Health Econ Health Policy* **14**, 419-429 (2016).
124. Beghini, F., *et al.* Integrating taxonomic, functional, and strain-level profiling of diverse microbial communities with bioBakery 3. *Elife* **10**(2021).
125. Mallick, H., *et al.* Multivariable association discovery in population-scale metagenomics studies. *PLoS Comput Biol* **17**, e1009442 (2021).
126. Crossley, J.R. & Elliott, R.B. Simple method for diagnosing protein-losing enteropathies. *Br Med J* **1**, 428-429 (1977).
127. Laine, L., *et al.* Protein-losing enteropathy and hypoalbuminemia in AIDS. *AIDS* **7**, 837-840 (1993).
128. Alam, A.N., Sarker, S.A., Wahed, M.A., Khatun, M. & Rahaman, M.M. Enteric protein loss and intestinal permeability changes in children during acute shigellosis and after recovery: effect of zinc supplementation. *Gut* **35**, 1707-1711 (1994).
129. Wang, L., *et al.* Methods to determine intestinal permeability and bacterial translocation during liver disease. *J Immunol Methods* **421**, 44-53 (2015).

130. Konikoff, M.R. & Denson, L.A. Role of fecal calprotectin as a biomarker of intestinal inflammation in inflammatory bowel disease. *Inflamm Bowel Dis* **12**, 524-534 (2006).
131. Langhorst, J., *et al.* Noninvasive markers in the assessment of intestinal inflammation in inflammatory bowel diseases: performance of fecal lactoferrin, calprotectin, and PMN-elastase, CRP, and clinical indices. *Am J Gastroenterol* **103**, 162-169 (2008).
132. Yang, T., *et al.* Gut dysbiosis is linked to hypertension. *Hypertension* **65**, 1331-1340 (2015).
133. Bahrani, A.A., *et al.* White Matter Hyperintensity Associations with Cerebral Blood Flow in Elderly Subjects Stratified by Cerebrovascular Risk. *J Stroke Cerebrovasc Dis* **26**, 779-786 (2017).
134. Bahrani, A.A., *et al.* Post-acquisition processing confounds in brain volumetric quantification of white matter hyperintensities. *J Neurosci Methods* **327**, 108391 (2019).
135. McNab, J.A. & Bartha, R. Quantitative short echo-time 1H LASER-CSI in human brain at 4 T. *NMR in biomedicine* **19**, 999-1009 (2006).
136. Provencher, S.W. Estimation of metabolite concentrations from localized in vivo proton NMR spectra. *Magn Reson Med* **30**, 672-679 (1993).
137. Parsey, C.M., Bagger, J.E., Trittschuh, E.H. & Hanson, A.J. Utility of the iPad NIH Toolbox Cognition Battery in a clinical trial of older adults. *J Am Geriatr Soc* **69**, 3519-3528 (2021).
138. Tulskey, D.S., *et al.* NIH Toolbox Cognition Battery (NIHTB-CB): list sorting test to measure working memory. *J Int Neuropsychol Soc* **20**, 599-610 (2014).
139. Pilkonis, P.A., *et al.* Assessment of self-reported negative affect in the NIH Toolbox. *Psychiatry Res* **206**, 88-97 (2013).
140. Salsman, J.M., *et al.* Assessing psychological well-being: self-report instruments for the NIH Toolbox. *Qual Life Res* **23**, 205-215 (2014).
141. Kupst, M.J., *et al.* Assessment of stress and self-efficacy for the NIH Toolbox for Neurological and Behavioral Function. *Anxiety Stress Coping* **28**, 531-544 (2015).
142. Cyranowski, J.M., *et al.* Assessing social support, companionship, and distress: National Institute of Health (NIH) Toolbox Adult Social Relationship Scales. *Health Psychol* **32**, 293-301 (2013).
143. Cook, K.F., *et al.* Pain assessment using the NIH Toolbox. *Neurology* **80**, S49-53 (2013).
144. R Core Team. R: A language and environment for statistical computing. *R Foundation for Statistical Computing, Vienna, Austria* (2020).
145. Mailing, L.J., Allen, J.M., Buford, T.W., Fields, C.J. & Woods, J.A. Exercise and the Gut Microbiome: A Review of the Evidence, Potential Mechanisms, and Implications for Human Health. *Exerc Sport Sci Rev* **47**, 75-85 (2019).
146. Go, J., *et al.* Human gut microbiota *Agathobaculum butyriciproducens* improves cognitive impairment in LPS-induced and APP/PS1 mouse models of Alzheimer's disease. *Nutr Res* **86**, 96-108 (2021).
147. Allen-Vercoe, E., *et al.* *Anaerostipes hadrus* comb. nov., a dominant species within the human colonic microbiota; reclassification of *Eubacterium hadrum* Moore *et al.* 1976. *Anaerobe* **18**, 523-529 (2012).

148. Louis, P. & Flint, H.J. Formation of propionate and butyrate by the human colonic microbiota. *Environ Microbiol* **19**, 29-41 (2017).
149. Balvers, M., *et al.* Analyzing Type 2 Diabetes Associations with the Gut Microbiome in Individuals from Two Ethnic Backgrounds Living in the Same Geographic Area. *Nutrients* **13**(2021).
150. Islam, S.M.S., *et al.* Eubacterium rectale Attenuates HSV-1 Induced Systemic Inflammation in Mice by Inhibiting CD83. *Front Immunol* **12**, 712312 (2021).
151. David, L.A., *et al.* Diet rapidly and reproducibly alters the human gut microbiome. *Nature* **505**, 559-563 (2014).
152. Gomes, A.C., Hoffmann, C. & Mota, J.F. The human gut microbiota: Metabolism and perspective in obesity. *Gut Microbes* **9**, 308-325 (2018).
153. Sakamoto, M., Iino, T., Yuki, M. & Ohkuma, M. Lawsonibacter asaccharolyticus gen. nov., sp. nov., a butyrate-producing bacterium isolated from human faeces. *Int J Syst Evol Microbiol* **68**, 2074-2081 (2018).
154. Mullish, B.H., *et al.* Microbial bile salt hydrolases mediate the efficacy of faecal microbiota transplant in the treatment of recurrent *Clostridioides difficile* infection. *Gut* **68**, 1791-1800 (2019).
155. Hatziioanou, D., *et al.* Discovery of a novel lantibiotic nisin O from *Blautia obeum* A2-162, isolated from the human gastrointestinal tract. *Microbiology (Reading)* **163**, 1292-1305 (2017).
156. Huang, L., *et al.* Analysis of microbiota in elderly patients with Acute Cerebral Infarction. *PeerJ* **7**, e6928 (2019).
157. Song, L., *et al.* Roseburia hominis Increases Intestinal Melatonin Level by Activating p-CREB-AANAT Pathway. *Nutrients* **14**(2021).
158. Machiels, K., *et al.* A decrease of the butyrate-producing species *Roseburia hominis* and *Faecalibacterium prausnitzii* defines dysbiosis in patients with ulcerative colitis. *Gut* **63**, 1275-1283 (2014).
159. Calderon-Perez, L., *et al.* Gut metagenomic and short chain fatty acids signature in hypertension: a cross-sectional study. *Sci Rep* **10**, 6436 (2020).
160. Patterson, A.M., *et al.* Human Gut Symbiont *Roseburia hominis* Promotes and Regulates Innate Immunity. *Front Immunol* **8**, 1166 (2017).
161. Sinha, S.R., *et al.* Dysbiosis-Induced Secondary Bile Acid Deficiency Promotes Intestinal Inflammation. *Cell Host Microbe* **27**, 659-670 e655 (2020).
162. Vazquez, L., Florez, A.B., Rodriguez, J. & Mayo, B. Heterologous expression of equol biosynthesis genes from *Adlercreutzia equolifaciens*. *FEMS Microbiol Lett* **368**(2021).
163. Bajer, L., *et al.* Distinct gut microbiota profiles in patients with primary sclerosing cholangitis and ulcerative colitis. *World J Gastroenterol* **23**, 4548-4558 (2017).
164. Van Hecke, T., *et al.* Combined Consumption of Beef-Based Cooked Mince and Sucrose Stimulates Oxidative Stress, Cardiac Hypertrophy, and Colonic Outgrowth of *Desulfovibrionaceae* in Rats. *Mol Nutr Food Res* **63**, e1800962 (2019).
165. Shkoporov, A.N., *et al.* *Ruthenibacterium lactatiformans* gen. nov., sp. nov., an anaerobic, lactate-producing member of the family *Ruminococcaceae* isolated from human faeces. *Int J Syst Evol Microbiol* **66**, 3041-3049 (2016).

166. Pequegnat, B. & Monteiro, M.A. Carbohydrate Scaffolds for the Study of the Autism-associated Bacterium, *Clostridium bolteae*. *Curr Med Chem* **26**, 6341-6348 (2019).
167. Pandit, L., *et al.* *Clostridium bolteae* is elevated in neuromyelitis optica spectrum disorder in India and shares sequence similarity with AQP4. *Neurol Neuroimmunol Neuroinflamm* **8**(2021).
168. Cox, L.M., *et al.* Gut Microbiome in Progressive Multiple Sclerosis. *Ann Neurol* **89**, 1195-1211 (2021).
169. Song, Y., *et al.* *Clostridium bolteae* sp. nov., isolated from human sources. *Syst Appl Microbiol* **26**, 84-89 (2003).
170. Wang, L., *et al.* Gut microbiota changes in patients with spondyloarthritis: A systematic review. *Semin Arthritis Rheum* **52**, 151925 (2022).
171. Zheng, J., *et al.* Dietary inflammatory potential in relation to the gut microbiome: results from a cross-sectional study. *Br J Nutr* **124**, 931-942 (2020).
172. Wang, C.S., *et al.* VSL#3 can prevent ulcerative colitis-associated carcinogenesis in mice. *World J Gastroenterol* **24**, 4254-4262 (2018).
173. Zhou, L., *et al.* Correlation Between Fecal Metabolomics and Gut Microbiota in Obesity and Polycystic Ovary Syndrome. *Front Endocrinol (Lausanne)* **11**, 628 (2020).
174. Guilhot, E., Tidjani Alou, M., Diallo, A., Raoult, D. & Khelaifia, S. *Anaeromassilibacillus senegalensis* gen. nov., sp. nov., isolated from the gut of a child with kwashiorkor. *New Microbes New Infect* **12**, 59-60 (2016).
175. Tran, T.T.T., *et al.* APOE genotype influences the gut microbiome structure and function in humans and mice: relevance for Alzheimer's disease pathophysiology. *FASEB J* **33**, 8221-8231 (2019).
176. Seo, B., *et al.* *Roseburia* spp. Abundance Associates with Alcohol Consumption in Humans and Its Administration Ameliorates Alcoholic Fatty Liver in Mice. *Cell Host Microbe* **27**, 25-40 e26 (2020).
177. Plaza-Diaz, J., *et al.* The Gut Barrier, Intestinal Microbiota, and Liver Disease: Molecular Mechanisms and Strategies to Manage. *Int J Mol Sci* **21**(2020).
178. Khanna, S., Bishnoi, M., Kondepudi, K.K. & Shukla, G. Synbiotic (*Lactiplantibacillus pentosus* GSSK2 and isomalto-oligosaccharides) supplementation modulates pathophysiology and gut dysbiosis in experimental metabolic syndrome. *Sci Rep* **11**, 21397 (2021).
179. Singh, D.P., *et al.* Isomalto-oligosaccharides, a prebiotic, functionally augment green tea effects against high fat diet-induced metabolic alterations via preventing gut dysbacteriosis in mice. *Pharmacol Res* **123**, 103-113 (2017).
180. Haisma, S.M., van Rheenen, P.F., Wagenmakers, L. & Muller Kobold, A. Calprotectin instability may lead to undertreatment in children with IBD. *Arch Dis Child* **105**, 996-998 (2020).
181. Hills, R.D., Jr., *et al.* Gut Microbiome: Profound Implications for Diet and Disease. *Nutrients* **11**(2019).
182. Sakkas, H., *et al.* Nutritional Status and the Influence of the Vegan Diet on the Gut Microbiota and Human Health. *Medicina (Kaunas)* **56**(2020).

183. Tang, Z.Z., *et al.* Multi-Omic Analysis of the Microbiome and Metabolome in Healthy Subjects Reveals Microbiome-Dependent Relationships Between Diet and Metabolites. *Front Genet* **10**, 454 (2019).
184. Wegner, K., *et al.* Rapid analysis of bile acids in different biological matrices using LC-ESI-MS/MS for the investigation of bile acid transformation by mammalian gut bacteria. *Anal Bioanal Chem* **409**, 1231-1245 (2017).
185. Rettedal, E.A., Altermann, E., Roy, N.C. & Dalziel, J.E. The Effects of Unfermented and Fermented Cow and Sheep Milk on the Gut Microbiota. *Front Microbiol* **10**, 458 (2019).
186. Jacobi, S.K., *et al.* Dietary Isomers of Sialyllactose Increase Ganglioside Sialic Acid Concentrations in the Corpus Callosum and Cerebellum and Modulate the Colonic Microbiota of Formula-Fed Piglets. *J Nutr* **146**, 200-208 (2016).
187. Balakrishnan, B., Luckey, D. & Taneja, V. Autoimmunity-Associated Gut Commensals Modulate Gut Permeability and Immunity in Humanized Mice. *Mil Med* **184**, 529-536 (2019).
188. Slanzon, G.S., *et al.* Fecal microbiome profiles of neonatal dairy calves with varying severities of gastrointestinal disease. *PLoS One* **17**, e0262317 (2022).
189. Ni Dhonnabhain, R., Xiao, Q. & O'Malley, D. Aberrant Gut-To-Brain Signaling in Irritable Bowel Syndrome - The Role of Bile Acids. *Front Endocrinol (Lausanne)* **12**, 745190 (2021).
190. McMillin, M., *et al.* Suppression of the HPA Axis During Cholestasis Can Be Attributed to Hypothalamic Bile Acid Signaling. *Mol Endocrinol* **29**, 1720-1730 (2015).
191. Lo Coco, D., Lopez, G. & Corrao, S. Cognitive impairment and stroke in elderly patients. *Vasc Health Risk Manag* **12**, 105-116 (2016).
192. Sadovnikova, I.S., *et al.* Nrf2/ARE Activators Improve Memory in Aged Mice via Maintaining of Mitochondrial Quality Control of Brain and the Modulation of Gut Microbiome. *Pharmaceuticals (Basel)* **14**(2021).
193. Gu, C., *et al.* ZiBuPiYin recipe improves cognitive decline by regulating gut microbiota in Zucker diabetic fatty rats. *Oncotarget* **8**, 27693-27703 (2017).
194. Vinarskaya, A.K., Balaban, P.M., Roshchin, M.V. & Zuzina, A.B. Sodium butyrate as a selective cognitive enhancer for weak or impaired memory. *Neurobiol Learn Mem* **180**, 107414 (2021).
195. Cervone, D. Thinking about self-efficacy. *Behav Modif* **24**, 30-56 (2000).
196. Nott, M., *et al.* Stroke self-management and the role of self-efficacy. *Disabil Rehabil* **43**, 1410-1419 (2021).
197. Lieber, A.C., *et al.* Nutrition, Energy Expenditure, Dysphagia, and Self-Efficacy in Stroke Rehabilitation: A Review of the Literature. *Brain Sci* **8**(2018).
198. Ling, Y., *et al.* Gut Microbiome Signatures Are Biomarkers for Cognitive Impairment in Patients With Ischemic Stroke. *Front Aging Neurosci* **12**, 511562 (2020).
199. Ling, Y., *et al.* Structural Change of Gut Microbiota in Patients with Post-Stroke Comorbid Cognitive Impairment and Depression and Its Correlation with Clinical Features. *J Alzheimers Dis* **77**, 1595-1608 (2020).
200. Robinson, R.G. & Jorge, R.E. Post-Stroke Depression: A Review. *Am J Psychiatry* **173**, 221-231 (2016).

201. Kaplin, A. & Anzaldi, L. New Movement in Neuroscience: A Purpose-Driven Life. *Cerebrum* **2015**, 7 (2015).
202. Crego, A., Yela, J.R., Gomez-Martinez, M.A., Riesco-Matias, P. & Petisco-Rodriguez, C. Relationships between Mindfulness, Purpose in Life, Happiness, Anxiety, and Depression: Testing a Mediation Model in a Sample of Women. *Int J Environ Res Public Health* **18**(2021).
203. Donovan, M., *et al.* Social isolation alters behavior, the gut-immune-brain axis, and neurochemical circuits in male and female prairie voles. *Neurobiol Stress* **13**, 100278 (2020).
204. Harrison, R.A. & Field, T.S. Post stroke pain: identification, assessment, and therapy. *Cerebrovasc Dis* **39**, 190-201 (2015).
205. Li, J., *et al.* Interplay between diet and gut microbiome, and circulating concentrations of trimethylamine N-oxide: findings from a longitudinal cohort of US men. *Gut* **71**, 724-733 (2022).
206. Freidin, M.B., *et al.* An association between chronic widespread pain and the gut microbiome. *Rheumatology (Oxford)* **60**, 3727-3737 (2021).
207. Saulnier, D.M., *et al.* Gastrointestinal microbiome signatures of pediatric patients with irritable bowel syndrome. *Gastroenterology* **141**, 1782-1791 (2011).
208. Li, H., *et al.* Dysbiosis characteristics of gut microbiota in cerebral infarction patients. *Transl Neurosci* **11**, 124-133 (2020).
209. Sun, H., Gu, M., Li, Z., Chen, X. & Zhou, J. Gut Microbiota Dysbiosis in Acute Ischemic Stroke Associated With 3-Month Unfavorable Outcome. *Front Neurol* **12**, 799222 (2021).
210. Park, N.J., Yu, S., Kim, D.H., Yun, E.J. & Kim, K.H. Characterization of BpGH16A of *Bacteroides plebeius*, a key enzyme initiating the depolymerization of agarose in the human gut. *Appl Microbiol Biotechnol* **105**, 617-625 (2021).
211. Munoz-Munoz, J., *et al.* Sulfation of Arabinogalactan Proteins Confers Privileged Nutrient Status to *Bacteroides plebeius*. *mBio* **12**, e0136821 (2021).
212. Cox-York, K.A., *et al.* Ovariectomy results in differential shifts in gut microbiota in low versus high aerobic capacity rats. *Physiol Rep* **3**(2015).
213. Stanford, J., *et al.* Associations Among Plant-Based Diet Quality, Uremic Toxins, and Gut Microbiota Profile in Adults Undergoing Hemodialysis Therapy. *J Ren Nutr* **31**, 177-188 (2021).
214. Chung, W.S.F., *et al.* Prebiotic potential of pectin and pectic oligosaccharides to promote anti-inflammatory commensal bacteria in the human colon. *FEMS Microbiol Ecol* **93**(2017).
215. Jin, X., *et al.* Association of APOE epsilon4 genotype and lifestyle with cognitive function among Chinese adults aged 80 years and older: A cross-sectional study. *PLoS Med* **18**, e1003597 (2021).
216. Munoz, M., *et al.* Comprehensive genome analyses of *Sellimonas intestinalis*, a potential biomarker of homeostasis gut recovery. *Microb Genom* **6**(2020).
217. Everard, A., *et al.* Cross-talk between *Akkermansia muciniphila* and intestinal epithelium controls diet-induced obesity. *Proceedings of the National Academy of Sciences of the United States of America* **110**, 9066-9071 (2013).

218. Robert, C., Chassard, C., Lawson, P.A. & Bernalier-Donadille, A. *Bacteroides cellulosilyticus* sp. nov., a cellulolytic bacterium from the human gut microbial community. *Int J Syst Evol Microbiol* **57**, 1516-1520 (2007).
219. Yoshida, N., *et al.* *Bacteroides vulgatus* and *Bacteroides dorei* Reduce Gut Microbial Lipopolysaccharide Production and Inhibit Atherosclerosis. *Circulation* **138**, 2486-2498 (2018).
220. Leimbach, A., Hacker, J. & Dobrindt, U. *E. coli* as an all-rounder: the thin line between commensalism and pathogenicity. *Curr Top Microbiol Immunol* **358**, 3-32 (2013).
221. Suri, R.S., *et al.* Relationship between *Escherichia coli* O157:H7 and diabetes mellitus. *Kidney Int Suppl*, S44-46 (2009).
222. Wu, T.R., *et al.* Gut commensal *Parabacteroides goldsteinii* plays a predominant role in the anti-obesity effects of polysaccharides isolated from *Hirsutella sinensis*. *Gut* **68**, 248-262 (2019).
223. Lai, H.C., *et al.* Gut microbiota modulates COPD pathogenesis: role of anti-inflammatory *Parabacteroides goldsteinii* lipopolysaccharide. *Gut* **71**, 309-321 (2022).
224. Wu, F., *et al.* *Phascolarctobacterium faecium* abundant colonization in human gastrointestinal tract. *Exp Ther Med* **14**, 3122-3126 (2017).
225. Wan, C., *et al.* Analysis of Gut Microbiota in Patients with Coronary Artery Disease and Hypertension. *Evid Based Complement Alternat Med* **2021**, 7195082 (2021).
226. Wang, P., *et al.* Cigarette smoking status alters dysbiotic gut microbes in hypertensive patients. *J Clin Hypertens (Greenwich)* **23**, 1431-1446 (2021).
227. Musher, D.M. *Haemophilus* Species. in *Medical Microbiology* (eds. Th & Baron, S.) (Galveston (TX), 1996).
228. Fuhren, J., *et al.* Dietary calcium phosphate strongly impacts gut microbiome changes elicited by inulin and galacto-oligosaccharides consumption. *Microbiome* **9**, 218 (2021).
229. Sherman, S.M. The thalamus is more than just a relay. *Curr Opin Neurobiol* **17**, 417-422 (2007).
230. Fultz, R., *et al.* Unraveling the Metabolic Requirements of the Gut Commensal *Bacteroides ovatus*. *Front Microbiol* **12**, 745469 (2021).
231. Yang, C., *et al.* Fecal IgA Levels Are Determined by Strain-Level Differences in *Bacteroides ovatus* and Are Modifiable by Gut Microbiota Manipulation. *Cell Host Microbe* **27**, 467-475 e466 (2020).
232. Ihekweazu, F.D., *et al.* *Bacteroides ovatus* Promotes IL-22 Production and Reduces Trinitrobenzene Sulfonic Acid-Driven Colonic Inflammation. *Am J Pathol* **191**, 704-719 (2021).
233. Ihekweazu, F.D., *et al.* *Bacteroides ovatus* ATCC 8483 monotherapy is superior to traditional fecal transplant and multi-strain bacteriotherapy in a murine colitis model. *Gut Microbes* **10**, 504-520 (2019).
234. Mao, C.P., *et al.* Larger regional volume of the thalamus in diarrhea-predominant irritable bowel syndrome: a cross-sectional study. *Brain Imaging Behav* **14**, 2302-2310 (2020).

235. Wang, Y., Zuo, C., Wang, D., Tao, S. & Hao, L. Reduced Thalamus Volume and Enhanced Thalamus and Fronto-Parietal Network Integration in the Chess Experts. *Cereb Cortex* **30**, 5560-5569 (2020).
236. Wei, K., *et al.* White matter hypointensities and hyperintensities have equivalent correlations with age and CSF beta-amyloid in the nondemented elderly. *Brain Behav* **9**, e01457 (2019).
237. Graff-Radford, J., *et al.* White matter hyperintensities: relationship to amyloid and tau burden. *Brain* **142**, 2483-2491 (2019).
238. Hu, H.Y., *et al.* White matter hyperintensities and risks of cognitive impairment and dementia: A systematic review and meta-analysis of 36 prospective studies. *Neurosci Biobehav Rev* **120**, 16-27 (2021).
239. Lopez-Almela, I., *et al.* Bacteroides uniformis combined with fiber amplifies metabolic and immune benefits in obese mice. *Gut Microbes* **13**, 1-20 (2021).
240. Fabersani, E., *et al.* Bacteroides uniformis CECT 7771 alleviates inflammation within the gut-adipose tissue axis involving TLR5 signaling in obese mice. *Sci Rep* **11**, 11788 (2021).
241. Hartstra, A.V., *et al.* Infusion of donor feces affects the gut-brain axis in humans with metabolic syndrome. *Mol Metab* **42**, 101076 (2020).
242. Agusti, A., *et al.* Bacteroides uniformis CECT 7771 Modulates the Brain Reward Response to Reduce Binge Eating and Anxiety-Like Behavior in Rat. *Mol Neurobiol* **58**, 4959-4979 (2021).
243. Cheung, S.G., *et al.* Systematic Review of Gut Microbiota and Major Depression. *Front Psychiatry* **10**, 34 (2019).
244. Khine, W.W.T., *et al.* Mental awareness improved mild cognitive impairment and modulated gut microbiome. *Aging (Albany NY)* **12**, 24371-24393 (2020).
245. Petroff, O.A. GABA and glutamate in the human brain. *Neuroscientist* **8**, 562-573 (2002).
246. Qin, P., *et al.* Characterization a Novel Butyric Acid-Producing Bacterium Collinsella aerofaciens Subsp. Shenzhenensis Subsp. Nov. *Microorganisms* **7**(2019).
247. Bag, S., Ghosh, T.S. & Das, B. Complete Genome Sequence of Collinsella aerofaciens Isolated from the Gut of a Healthy Indian Subject. *Genome Announc* **5**(2017).
248. Joossens, M., *et al.* Dysbiosis of the faecal microbiota in patients with Crohn's disease and their unaffected relatives. *Gut* **60**, 631-637 (2011).
249. Kalinkovich, A. & Livshits, G. A cross talk between dysbiosis and gut-associated immune system governs the development of inflammatory arthropathies. *Semin Arthritis Rheum* **49**, 474-484 (2019).
250. Nagai, F., Morotomi, M., Sakon, H. & Tanaka, R. Parasutterella excrementihominis gen. nov., sp. nov., a member of the family Alcaligenaceae isolated from human faeces. *Int J Syst Evol Microbiol* **59**, 1793-1797 (2009).
251. Fart, F., *et al.* Differences in Gut Microbiome Composition between Senior Orienteering Athletes and Community-Dwelling Older Adults. *Nutrients* **12**(2020).
252. Strandwitz, P., *et al.* GABA-modulating bacteria of the human gut microbiota. *Nat Microbiol* **4**, 396-403 (2019).

253. Narukawa, M., *et al.* Efficacy of Long-Term Feeding of alpha-Glycerophosphocholine for Aging-Related Phenomena in Old Mice. *Gerontology* **66**, 275-285 (2020).
254. Syme, C., *et al.* Visceral fat-related systemic inflammation and the adolescent brain: a mediating role of circulating glycerophosphocholines. *Int J Obes (Lond)* **43**, 1223-1230 (2019).
255. Nomura, K., *et al.* Bacteroidetes Species Are Correlated with Disease Activity in Ulcerative Colitis. *J Clin Med* **10**(2021).
256. Mohandas, S., *et al.* Differences in Gut Microbiome in Hospitalized Immunocompetent vs. Immunocompromised Children, Including Those With Sickle Cell Disease. *Front Pediatr* **8**, 583446 (2020).
257. Wang, Z., *et al.* The Nutritional Supplement L-Alpha Glycerylphosphorylcholine Promotes Atherosclerosis. *Int J Mol Sci* **22**(2021).
258. Paslakis, G., Traber, F., Roberz, J., Block, W. & Jessen, F. N-acetyl-aspartate (NAA) as a correlate of pharmacological treatment in psychiatric disorders: a systematic review. *Eur Neuropsychopharmacol* **24**, 1659-1675 (2014).
259. Neale, J.H. & Olszewski, R. A role for N-acetylasparylglutamate (NAAG) and mGluR3 in cognition. *Neurobiol Learn Mem* **158**, 9-13 (2019).
260. Sato, N., *et al.* Metagenomic profiling of gut microbiome in early chronic kidney disease. *Nephrol Dial Transplant* **36**, 1675-1684 (2021).
261. Shintouo, C.M., *et al.* Is inflammageing influenced by the microbiota in the aged gut? A systematic review. *Exp Gerontol* **141**, 111079 (2020).
262. Mudd, A.T., Berding, K., Wang, M., Donovan, S.M. & Dilger, R.N. Serum cortisol mediates the relationship between fecal Ruminococcus and brain N-acetylasparylglutamate in the young pig. *Gut Microbes* **8**, 589-600 (2017).
263. Vitetta, L., Llewellyn, H. & Oldfield, D. Gut Dysbiosis and the Intestinal Microbiome: Streptococcus thermophilus a Key Probiotic for Reducing Uremia. *Microorganisms* **7**(2019).
264. Nourski, K.V., *et al.* Electrophysiology of the Human Superior Temporal Sulcus during Speech Processing. *Cereb Cortex* **31**, 1131-1148 (2021).
265. Foundas, A.L., Leonard, C.M., Gilmore, R.L., Fennell, E.B. & Heilman, K.M. Pars triangularis asymmetry and language dominance. *Proceedings of the National Academy of Sciences of the United States of America* **93**, 719-722 (1996).
266. Soukup, S.T., *et al.* Metabolism of Daidzein and Genistein by Gut Bacteria of the Class Coriobacteria. *Foods* **10**(2021).
267. Liu, T.H. & Tsai, T.Y. Effects of equol on deoxycorticosterone acetate salt-induced hypertension and associated vascular dementia in rats. *Food Funct* **7**, 3444-3457 (2016).
268. Caliskan, G., *et al.* Depletion of dietary phytoestrogens reduces hippocampal plasticity and contextual fear memory stability in adult male mouse. *Nutr Neurosci* **24**, 951-962 (2021).
269. Yu, W., *et al.* Equol increases cerebral blood flow in rats via activation of large-conductance Ca(2+)-activated K(+) channels in vascular smooth muscle cells. *Pharmacol Res* **107**, 186-194 (2016).

270. Shah, R.D., Tang, Z.Z., Chen, G., Huang, S. & Ferguson, J.F. Soy food intake associates with changes in the metabolome and reduced blood pressure in a gut microbiota dependent manner. *Nutr Metab Cardiovasc Dis* **30**, 1500-1511 (2020).
271. Wu, I.W., *et al.* Gut Microbiota as Diagnostic Tools for Mirroring Disease Progression and Circulating Nephrotoxin Levels in Chronic Kidney Disease: Discovery and Validation Study. *Int J Biol Sci* **16**, 420-434 (2020).
272. Rustia, A.J., Paterson, J.S., Best, G. & Sokoya, E.M. Microbial disruption in the gut promotes cerebral endothelial dysfunction. *Physiol Rep* **9**, e15100 (2021).
273. Le Roy, T., *et al.* The intestinal microbiota regulates host cholesterol homeostasis. *BMC Biol* **17**, 94 (2019).
274. Parker, B.J., Wearsch, P.A., Veloo, A.C.M. & Rodriguez-Palacios, A. The Genus *Alistipes*: Gut Bacteria With Emerging Implications to Inflammation, Cancer, and Mental Health. *Front Immunol* **11**, 906 (2020).
275. Noble, E.E., *et al.* Gut microbial taxa elevated by dietary sugar disrupt memory function. *Transl Psychiatry* **11**, 194 (2021).
276. Ong, W.Y. & Garey, L.J. Neuronal architecture of the human temporal cortex. *Anat Embryol (Berl)* **181**, 351-364 (1990).
277. Morvan, C., Folgosa, F., Kint, N., Teixeira, M. & Martin-Verstraete, I. Responses of Clostridia to oxygen: from detoxification to adaptive strategies. *Environ Microbiol* **23**, 4112-4125 (2021).
278. Newman, T.M., *et al.* Diet, obesity, and the gut microbiome as determinants modulating metabolic outcomes in a non-human primate model. *Microbiome* **9**, 100 (2021).
279. Calderazzo, S.M., Busch, S.E., Moore, T.L., Rosene, D.L. & Medalla, M. Distribution and overlap of entorhinal, premotor, and amygdalar connections in the monkey anterior cingulate cortex. *J Comp Neurol* **529**, 885-904 (2021).
280. Kushkevych, I., *et al.* Recent Advances in Metabolic Pathways of Sulfate Reduction in Intestinal Bacteria. *Cells* **9**(2020).
281. Ribas, E.C., Yagmurlu, K., de Oliveira, E., Ribas, G.C. & Rhoton, A. Microsurgical anatomy of the central core of the brain. *J Neurosurg* **129**, 752-769 (2018).
282. Fernandez-Real, J.M., *et al.* Gut Microbiota Interacts With Brain Microstructure and Function. *J Clin Endocrinol Metab* **100**, 4505-4513 (2015).
283. O'Callaghan, A. & van Sinderen, D. Bifidobacteria and Their Role as Members of the Human Gut Microbiota. *Front Microbiol* **7**, 925 (2016).
284. Cherny, K.E., Muscat, E.B., Reyna, M.E. & Kociolek, L.K. Clostridium innocuum: Microbiological and clinical characteristics of a potential emerging pathogen. *Anaerobe* **71**, 102418 (2021).
285. Heeney, D.D., Gareau, M.G. & Marco, M.L. Intestinal Lactobacillus in health and disease, a driver or just along for the ride? *Curr Opin Biotechnol* **49**, 140-147 (2018).
286. Cornick, N.A., Jensen, N.S., Stahl, D.A., Hartman, P.A. & Allison, M.J. *Lachnospira pectinoschiza* sp. nov., an anaerobic pectinophile from the pig intestine. *Int J Syst Bacteriol* **44**, 87-93 (1994).
287. Kim, C.C., *et al.* Genomic insights from *Monoglobus pectinilyticus*: a pectin-degrading specialist bacterium in the human colon. *ISME J* **13**, 1437-1456 (2019).

288. Bourassa, M.W., Alim, I., Bultman, S.J. & Ratan, R.R. Butyrate, neuroepigenetics and the gut microbiome: Can a high fiber diet improve brain health? *Neurosci Lett* **625**, 56-63 (2016).
289. Canani, R.B., *et al.* Potential beneficial effects of butyrate in intestinal and extraintestinal diseases. *World J Gastroenterol* **17**, 1519-1528 (2011).
290. Gu, M., *et al.* Roseburia Abundance Associates With Severity, Evolution and Outcome of Acute Ischemic Stroke. *Front Cell Infect Microbiol* **11**, 669322 (2021).
291. Nie, K., *et al.* Roseburia intestinalis: A Beneficial Gut Organism From the Discoveries in Genus and Species. *Front Cell Infect Microbiol* **11**, 757718 (2021).
292. Dudakov, J.A., Hanash, A.M. & van den Brink, M.R. Interleukin-22: immunobiology and pathology. *Annu Rev Immunol* **33**, 747-785 (2015).
293. Bernink, J.H., Spits, H. & de Jonge, W.J. A new edge to immune surveillance by the neural system. *Cell Res* **26**, 1178-1179 (2016).
294. Xu, F., *et al.* New pathway ameliorating ulcerative colitis: focus on Roseburia intestinalis and the gut-brain axis. *Therap Adv Gastroenterol* **14**, 17562848211004469 (2021).
295. Sekikawa, A., *et al.* Effect of S-equol and Soy Isoflavones on Heart and Brain. *Curr Cardiol Rev* **15**, 114-135 (2019).
296. Kim, J.H., Lim, C. & Cho, S. Ischemic-time associated reductions in equol monosulfate plasma levels in a mouse model of ischemic stroke: support the existence of a 'brain-gut axis'. *Neuroreport* **32**, 458-464 (2021).
297. Yu, W., *et al.* Equol is neuroprotective during focal cerebral ischemia and reperfusion that involves p-Src and gp91(phox). *Curr Neurovasc Res* **11**, 367-377 (2014).
298. Kumar, A., Singh, A. & Ekavali. A review on Alzheimer's disease pathophysiology and its management: an update. *Pharmacol Rep* **67**, 195-203 (2015).
299. Lane, C.A., Hardy, J. & Schott, J.M. Alzheimer's disease. *European journal of neurology* **25**, 59-70 (2018).
300. Sery, O., Povova, J., Misek, I., Pesak, L. & Janout, V. Molecular mechanisms of neuropathological changes in Alzheimer's disease: a review. *Folia neuropathologica* **51**, 1-9 (2013).
301. Modrego, P. & Lobo, A. A good marker does not mean a good target for clinical trials in Alzheimer's disease: the amyloid hypothesis questioned. *Neurodegenerative disease management* (2019).
302. Briggs, R., Kennelly, S.P. & O'Neill, D. Drug treatments in Alzheimer's disease. *Clinical medicine (London, England)* **16**, 247-253 (2016).
303. Cummings, J.L., Morstorf, T. & Zhong, K. Alzheimer's disease drug-development pipeline: few candidates, frequent failures. *Alzheimers Res Ther* **6**, 37 (2014).
304. Cummings, J., Lee, G., Ritter, A., Sabbagh, M. & Zhong, K. Alzheimer's disease drug development pipeline: 2019. *Alzheimers Dement (N Y)* **5**, 272-293 (2019).
305. Jack, C.R., Jr., *et al.* NIA-AA Research Framework: Toward a biological definition of Alzheimer's disease. *Alzheimers Dement* **14**, 535-562 (2018).
306. Jack, C.R., Jr., *et al.* A/T/N: An unbiased descriptive classification scheme for Alzheimer disease biomarkers. *Neurology* **87**, 539-547 (2016).

307. Josephs, K.A., *et al.* Tau aggregation influences cognition and hippocampal atrophy in the absence of beta-amyloid: a clinico-imaging-pathological study of primary age-related tauopathy (PART). *Acta Neuropathol* **133**, 705-715 (2017).
308. Jagust, W.J., *et al.* Relationships between biomarkers in aging and dementia. *Neurology* **73**, 1193-1199 (2009).
309. Zhang, Y. & Liu, S. Analysis of structural brain MRI and multi-parameter classification for Alzheimer's disease. *Biomed Tech (Berl)* **63**, 427-437 (2018).
310. Ward, A., *et al.* Prevalence of apolipoprotein E4 genotype and homozygotes (APOE ϵ 4/4) among patients diagnosed with Alzheimer's disease: a systematic review and meta-analysis. *Neuroepidemiology* **38**, 1-17 (2012).
311. McDonald, D., *et al.* An improved Greengenes taxonomy with explicit ranks for ecological and evolutionary analyses of bacteria and archaea. *ISME J* **6**, 610-618 (2012).
312. Crane, P.K., *et al.* Development and assessment of a composite score for memory in the Alzheimer's Disease Neuroimaging Initiative (ADNI). *Brain Imaging Behav* **6**, 502-516 (2012).
313. Gibbons, L.E., *et al.* A composite score for executive functioning, validated in Alzheimer's Disease Neuroimaging Initiative (ADNI) participants with baseline mild cognitive impairment. *Brain Imaging Behav* **6**, 517-527 (2012).
314. Jack, C.R., *et al.* Tracking pathophysiological processes in Alzheimer's disease: an updated hypothetical model of dynamic biomarkers. *The Lancet neurology*. **12**, 207-216 (2013).
315. Lu, D., *et al.* Multimodal and Multiscale Deep Neural Networks for the Early Diagnosis of Alzheimer's Disease using structural MR and FDG-PET images. *Sci Rep* **8**, 5697 (2018).
316. Ding, Y., *et al.* A Deep Learning Model to Predict a Diagnosis of Alzheimer Disease by Using (18)F-FDG PET of the Brain. *Radiology* **290**, 456-464 (2019).
317. Trzepakz, P.T., *et al.* Comparison of neuroimaging modalities for the prediction of conversion from mild cognitive impairment to Alzheimer's dementia. *Neurobiol Aging* **35**, 143-151 (2014).
318. Dong, A., *et al.* Heterogeneity of neuroanatomical patterns in prodromal Alzheimer's disease: links to cognition, progression and biomarkers. *Brain* **140**, 735-747 (2017).
319. Wang, Y., *et al.* Diagnosis and prognosis of Alzheimer's disease using brain morphometry and white matter connectomes. *Neuroimage Clin* **23**, 101859 (2019).
320. Vlassenko, A.G., Benzinger, T.L. & Morris, J.C. PET amyloid-beta imaging in preclinical Alzheimer's disease. *Biochim Biophys Acta* **1822**, 370-379 (2012).
321. Mathotaarachchi, S., *et al.* Identifying incipient dementia individuals using machine learning and amyloid imaging. *Neurobiol Aging* **59**, 80-90 (2017).
322. Landau, S.M., *et al.* Amyloid deposition, hypometabolism, and longitudinal cognitive decline. *Ann Neurol* **72**, 578-586 (2012).
323. Jackson, R.L., Bajada, C.J., Rice, G.E., Cloutman, L.L. & Lambon Ralph, M.A. An emergent functional parcellation of the temporal cortex. *NeuroImage*. **170**, 385-399 (2018).

324. Cavanna, A.E. & Trimble, M.R. The precuneus: a review of its functional anatomy and behavioural correlates. *Brain* **129**, 564-583 (2006).
325. Chayer, C. & Freedman, M. Frontal lobe functions. *Curr Neurol Neurosci Rep* **1**, 547-552 (2001).
326. Opitz, B. Memory function and the hippocampus. *Front Neurol Neurosci* **34**, 51-59 (2014).
327. Sperling, R.A., *et al.* The impact of amyloid-beta and tau on prospective cognitive decline in older individuals. *Ann Neurol* **85**, 181-193 (2019).
328. Bejanin, A., *et al.* Tau pathology and neurodegeneration contribute to cognitive impairment in Alzheimer's disease. *Brain* **140**, 3286-3300 (2017).
329. Huber, C.M., Yee, C., May, T., Dhanala, A. & Mitchell, C.S. Cognitive Decline in Preclinical Alzheimer's Disease: Amyloid-Beta versus Tauopathy. *J Alzheimers Dis* **61**, 265-281 (2018).
330. Mielke, M.M., *et al.* Association of Plasma Total Tau Level With Cognitive Decline and Risk of Mild Cognitive Impairment or Dementia in the Mayo Clinic Study on Aging. *JAMA Neurol* **74**, 1073-1080 (2017).
331. Risacher, S.L., *et al.* Alzheimer disease brain atrophy subtypes are associated with cognition and rate of decline. *Neurology* **89**, 2176-2186 (2017).
332. Jeong, H.S., Park, J.S., Song, I.U., Chung, Y.A. & Rhie, S.J. Changes in cognitive function and brain glucose metabolism in elderly women with subjective memory impairment: a 24-month prospective pilot study. *Acta neurologica Scandinavica* **135**, 108-114 (2017).
333. Seghier, M.L. The angular gyrus: multiple functions and multiple subdivisions. *Neuroscientist* **19**, 43-61 (2013).
334. Mergenthaler, P., Lindauer, U., Dienel, G.A. & Meisel, A. Sugar for the brain: the role of glucose in physiological and pathological brain function. *Trends Neurosci* **36**, 587-597 (2013).
335. Lin, A.L., Coman, D., Jiang, L., Rothman, D.L. & Hyder, F. Caloric restriction impedes age-related decline of mitochondrial function and neuronal activity. *J Cereb Blood Flow Metab* **34**, 1440-1443 (2014).
336. Neth, B.J. & Craft, S. Insulin Resistance and Alzheimer's Disease: Bioenergetic Linkages. *Front Aging Neurosci* **9**, 345 (2017).
337. Kakimoto, A., *et al.* Age-Related Sex-Specific Changes in Brain Metabolism and Morphology. *J Nucl Med* **57**, 221-225 (2016).
338. Kim, J., Chey, J., Kim, S.E. & Kim, H. The effect of education on regional brain metabolism and its functional connectivity in an aged population utilizing positron emission tomography. *Neurosci Res* **94**, 50-61 (2015).
339. Wu, L., Zhang, X. & Zhao, L. Human ApoE Isoforms Differentially Modulate Brain Glucose and Ketone Body Metabolism: Implications for Alzheimer's Disease Risk Reduction and Early Intervention. *J Neurosci* **38**, 6665-6681 (2018).
340. Riedel, B.C., Thompson, P.M. & Brinton, R.D. Age, APOE and sex: Triad of risk of Alzheimer's disease. *J Steroid Biochem Mol Biol* **160**, 134-147 (2016).
341. Arenaza-Urquijo, E.M., *et al.* The metabolic brain signature of cognitive resilience in the 80+: beyond Alzheimer pathologies. *Brain* **142**, 1134-1147 (2019).

342. Bentourkia, M., *et al.* Comparison of regional cerebral blood flow and glucose metabolism in the normal brain: effect of aging. *J Neurol Sci* **181**, 19-28 (2000).
343. Wallace, D.C. A mitochondrial paradigm of metabolic and degenerative diseases, aging, and cancer: a dawn for evolutionary medicine. *Annu Rev Genet* **39**, 359-407 (2005).
344. MahmoudianDehkordi, S., *et al.* Altered bile acid profile associates with cognitive impairment in Alzheimer's disease-An emerging role for gut microbiome. *Alzheimers Dement* **15**, 76-92 (2019).
345. Nho, K., *et al.* Altered bile acid profile in mild cognitive impairment and Alzheimer's disease: Relationship to neuroimaging and CSF biomarkers. *Alzheimers Dement* **15**, 232-244 (2019).
346. Thambisetty, M., Beason-Held, L., An, Y., Kraut, M.A. & Resnick, S.M. APOE epsilon4 genotype and longitudinal changes in cerebral blood flow in normal aging. *Arch Neurol* **67**, 93-98 (2010).
347. Reiman, E.M., *et al.* Correlations between apolipoprotein E epsilon4 gene dose and brain-imaging measurements of regional hypometabolism. *Proceedings of the National Academy of Sciences of the United States of America* **102**, 8299-8302 (2005).
348. Reiman, E.M., *et al.* Declining brain activity in cognitively normal apolipoprotein E epsilon 4 heterozygotes: A foundation for using positron emission tomography to efficiently test treatments to prevent Alzheimer's disease. *Proceedings of the National Academy of Sciences of the United States of America* **98**, 3334-3339 (2001).
349. Fleisher, A.S., *et al.* Apolipoprotein E epsilon4 and age effects on florbetapir positron emission tomography in healthy aging and Alzheimer disease. *Neurobiol Aging* **34**, 1-12 (2013).
350. Reiman, E.M., *et al.* Functional brain abnormalities in young adults at genetic risk for late-onset Alzheimer's dementia. *Proceedings of the National Academy of Sciences of the United States of America* **101**, 284-289 (2004).
351. Wakabayashi, T., *et al.* Differential effects of diet- and genetically-induced brain insulin resistance on amyloid pathology in a mouse model of Alzheimer's disease. *Mol Neurodegener* **14**, 15 (2019).
352. Craft, S., *et al.* Cerebrospinal fluid and plasma insulin levels in Alzheimer's disease: relationship to severity of dementia and apolipoprotein E genotype. *Neurology* **50**, 164-168 (1998).
353. Rorbach-Dolata, A. & Piwovar, A. Neurometabolic Evidence Supporting the Hypothesis of Increased Incidence of Type 3 Diabetes Mellitus in the 21st Century. *Biomed Res Int* **2019**, 1435276 (2019).
354. Craft, S., *et al.* Intranasal insulin therapy for Alzheimer disease and amnesic mild cognitive impairment: a pilot clinical trial. *Arch Neurol* **69**, 29-38 (2012).
355. de la Monte, S.M. Early intranasal insulin therapy halts progression of neurodegeneration: progress in Alzheimer's disease therapeutics. *Aging health* **8**, 61-64 (2012).
356. Chapman, C.D., Schioth, H.B., Grillo, C.A. & Benedict, C. Intranasal insulin in Alzheimer's disease: Food for thought. *Neuropharmacology* **136**, 196-201 (2018).

357. Wang, Y. & Brinton, R.D. Triad of Risk for Late Onset Alzheimer's: Mitochondrial Haplotype, APOE Genotype and Chromosomal Sex. *Front Aging Neurosci* **8**, 232 (2016).
358. Lin, A.L., Zhang, W., Gao, X. & Watts, L. Caloric restriction increases ketone bodies metabolism and preserves blood flow in aging brain. *Neurobiol Aging* **36**, 2296-2303 (2015).
359. Zhang, Y., *et al.* Ketosis proportionately spares glucose utilization in brain. *J Cereb Blood Flow Metab* **33**, 1307-1311 (2013).
360. Nagpal, R., Neth, B.J., Wang, S., Craft, S. & Yadav, H. Modified Mediterranean-ketogenic diet modulates gut microbiome and short-chain fatty acids in association with Alzheimer's disease markers in subjects with mild cognitive impairment. *EBioMedicine* (2019).
361. Ma, D., *et al.* Ketogenic diet enhances neurovascular function with altered gut microbiome in young healthy mice. *Sci Rep* **8**, 6670 (2018).
362. Hoffman, J.D., *et al.* Dietary inulin alters the gut microbiome, enhances systemic metabolism and reduces neuroinflammation in an APOE4 mouse model. *PLoS One* **14**, e0221828 (2019).
363. Xia, C., *et al.* Association of In Vivo [18F]AV-1451 Tau PET Imaging Results With Cortical Atrophy and Symptoms in Typical and Atypical Alzheimer Disease. *JAMA Neurol* **74**, 427-436 (2017).
364. Fox, P.T., Raichle, M.E., Mintun, M.A. & Dence, C. Nonoxidative glucose consumption during focal physiologic neural activity. *Science* **241**, 462-464 (1988).
365. Lin, A.L., Fox, P.T., Hardies, J., Duong, T.Q. & Gao, J.H. Nonlinear coupling between cerebral blood flow, oxygen consumption, and ATP production in human visual cortex. *Proc Natl Acad Sci U S A* **107**, 8446-8451 (2010).
366. Pike, C.J. Sex and the development of Alzheimer's disease. *J Neurosci Res* **95**, 671-680 (2017).
367. Jack, C.R., *et al.* Update on the magnetic resonance imaging core of the Alzheimer's disease neuroimaging initiative. *Alzheimer's & dementia : the journal of the Alzheimer's Association* **6**, 212-220 (2010).
368. Jagust, W.J., *et al.* The Alzheimer's Disease Neuroimaging Initiative positron emission tomography core. *Alzheimer's & dementia : the journal of the Alzheimer's Association* **6**, 221-229 (2010).
369. van der Walt, S., *et al.* scikit-image: image processing in Python. *PeerJ* **2**, e453 (2014).
370. Landau, S.M., *et al.* Associations between cognitive, functional, and FDG-PET measures of decline in AD and MCI. *Neurobiol Aging* **32**, 1207-1218 (2011).
371. 2016 Alzheimer's disease facts and figures. *Alzheimer's & dementia : the journal of the Alzheimer's Association* **12**, 459-509 (2016).
372. Yin, F., Sancheti, H., Patil, I. & Cadenas, E. Energy metabolism and inflammation in brain aging and Alzheimer's disease. *Free Radic Biol Med* **100**, 108-122 (2016).
373. Belloy, M.E., Napolioni, V. & Greicius, M.D. A Quarter Century of APOE and Alzheimer's Disease: Progress to Date and the Path Forward. *Neuron* **101**, 820-838 (2019).

374. Hammond, T.C., *et al.* beta-amyloid and tau drive early Alzheimer's disease decline while glucose hypometabolism drives late decline. *Commun Biol* **3**, 352 (2020).
375. Pini, L., *et al.* Brain atrophy in Alzheimer's Disease and aging. *Ageing Res Rev* **30**, 25-48 (2016).
376. Klosinski, L.P., *et al.* White Matter Lipids as a Ketogenic Fuel Supply in Aging Female Brain: Implications for Alzheimer's Disease. *EBioMedicine* **2**, 1888-1904 (2015).
377. Yu, Y., Herman, P., Rothman, D.L., Agarwal, D. & Hyder, F. Evaluating the gray and white matter energy budgets of human brain function. *Journal of cerebral blood flow and metabolism : official journal of the International Society of Cerebral Blood Flow and Metabolism* **38**, 1339-1353 (2018).
378. Morland, C., Henjum, S., Iversen, E.G., Skrede, K.K. & Hassel, B. Evidence for a higher glycolytic than oxidative metabolic activity in white matter of rat brain. *Neurochem Int* **50**, 703-709 (2007).
379. Varma, V.R., *et al.* Brain and blood metabolite signatures of pathology and progression in Alzheimer disease: A targeted metabolomics study. *PLoS Med* **15**, e1002482 (2018).
380. Baloni, P., *et al.* Metabolic Network Analysis Reveals Altered Bile Acid Synthesis and Metabolism in Alzheimer's Disease. *Cell Rep Med* **1**, 100138 (2020).
381. Wang, J., *et al.* Peripheral serum metabolomic profiles inform central cognitive impairment. *Scientific reports* **10**, 14059 (2020).
382. Schmitt, F.A., *et al.* "Preclinical" AD revisited: neuropathology of cognitively normal older adults. *Neurology* **55**, 370-376 (2000).
383. Bancher, C., Braak, H., Fischer, P. & Jellinger, K.A. Neuropathological staging of Alzheimer lesions and intellectual status in Alzheimer's and Parkinson's disease patients. *Neurosci Lett* **162**, 179-182 (1993).
384. Jaarsma, D., Veenma-van der Duin, L. & Korf, J. N-acetylaspartate and N-acetylaspartylglutamate levels in Alzheimer's disease post-mortem brain tissue. *J Neurol Sci* **127**, 230-233 (1994).
385. Zhao, Y., *et al.* Leucine supplementation via drinking water reduces atherosclerotic lesions in apoE null mice. *Acta Pharmacol Sin* **37**, 196-203 (2016).
386. Chun, J., *et al.* International Union of Pharmacology. XXXIV. Lysophospholipid Receptor Nomenclature. *Pharmacological Reviews* **54**, 265-269 (2002).
387. Fujii, A., Allen, T.J. & Nestel, P.J. A 1,3-diacylglycerol-rich oil induces less atherosclerosis and lowers plasma cholesterol in diabetic apoE-deficient mice. *Atherosclerosis* **193**, 55-61 (2007).
388. Kennedy, M.B. Synaptic Signaling in Learning and Memory. *Cold Spring Harb Perspect Biol* **8**, a016824 (2013).
389. van der Velpen, V., *et al.* Systemic and central nervous system metabolic alterations in Alzheimer's disease. *Alzheimers Res Ther* **11**, 93 (2019).
390. Chyan, Y.J., *et al.* Potent neuroprotective properties against the Alzheimer beta-amyloid by an endogenous melatonin-related indole structure, indole-3-propionic acid. *J Biol Chem* **274**, 21937-21942 (1999).

391. He, B., *et al.* Transmissible microbial and metabolomic remodeling by soluble dietary fiber improves metabolic homeostasis. *Sci Rep* **5**, 10604 (2015).
392. Wang, G., *et al.* Plasma metabolite profiles of Alzheimer's disease and mild cognitive impairment. *J Proteome Res* **13**, 2649-2658 (2014).
393. Hipkiss, A.R. Could carnosine or related structures suppress Alzheimer's disease? *Journal of Alzheimer's disease : JAD* **11**, 229-240 (2007).
394. Dere, E., *et al.* Neuronal histamine and the interplay of memory, reinforcement and emotions. *Behav Brain Res* **215**, 209-220 (2010).
395. Choudhary, A.K. & Lee, Y.Y. The debate over neurotransmitter interaction in aspartame usage. *J Clin Neurosci* **56**, 7-15 (2018).
396. Jenkins, T.A., Nguyen, J.C., Polglaze, K.E. & Bertrand, P.P. Influence of Tryptophan and Serotonin on Mood and Cognition with a Possible Role of the Gut-Brain Axis. *Nutrients* **8**(2016).
397. Yoshida, Y., *et al.* Hydroxyoctadecadienoic acid and oxidatively modified peroxiredoxins in the blood of Alzheimer's disease patients and their potential as biomarkers. *Neurobiol Aging* **30**, 174-185 (2009).
398. Lind, A., *et al.* Regional Myo-Inositol, Creatine, and Choline Levels Are Higher at Older Age and Scale Negatively with Visuospatial Working Memory: A Cross-Sectional Proton MR Spectroscopy Study at 7 Tesla on Normal Cognitive Ageing. *The Journal of neuroscience : the official journal of the Society for Neuroscience* **40**, 8149-8159 (2020).
399. Blusztajn, J.K., Lopez Gonzalez-Coviella, I., Logue, M., Growdon, J.H. & Wurtman, R.J. Levels of phospholipid catabolic intermediates, glycerophosphocholine and glycerophosphoethanolamine, are elevated in brains of Alzheimer's disease but not of Down's syndrome patients. *Brain Res* **536**, 240-244 (1990).
400. Velenosi, T.J., *et al.* Untargeted metabolomics reveals N, N, N-trimethyl-L-alanyl-L-proline betaine (TMAP) as a novel biomarker of kidney function. *Scientific reports* **9**, 6831 (2019).
401. Suri, S., *et al.* Effect of age and the APOE gene on metabolite concentrations in the posterior cingulate cortex. *Neuroimage* **152**, 509-516 (2017).
402. Eckhardt, M., Yaghootfam, A., Fewou, S.N., Zoller, I. & Gieselmann, V. A mammalian fatty acid hydroxylase responsible for the formation of alpha-hydroxylated galactosylceramide in myelin. *Biochem J* **388**, 245-254 (2005).
403. Nho, K., *et al.* Serum Metabolites Associated with Brain Amyloid Beta Deposition, Cognitive Dysfunction, and Alzheimer's Disease Progression. *bioRxiv*, 2020.2011.2025.394262 (2020).
404. Kling, M.A., *et al.* Circulating ethanolamine plasmalogen indices in Alzheimer's disease: Relation to diagnosis, cognition, and CSF tau. *Alzheimer's & dementia : the journal of the Alzheimer's Association* **16**, 1234-1247 (2020).
405. Huynh, K., *et al.* Concordant peripheral lipidome signatures in two large clinical studies of Alzheimer's disease. *Nat Commun* **11**, 5698 (2020).
406. Zhao, N., *et al.* Alzheimer's Risk Factors Age, APOE Genotype, and Sex Drive Distinct Molecular Pathways. *Neuron* **106**, 727-742 e726 (2020).
407. Cortes-Canteli, M. & Iadecola, C. Alzheimer's Disease and Vascular Aging: JACC Focus Seminar. *J Am Coll Cardiol* **75**, 942-951 (2020).

408. Tusso, P., Stoll, S.R. & Li, W.W. A plant-based diet, atherogenesis, and coronary artery disease prevention. *Perm J* **19**, 62-67 (2015).
409. Garabadu, D., Agrawal, N., Sharma, A. & Sharma, S. Mitochondrial metabolism: a common link between neuroinflammation and neurodegeneration. *Behav Pharmacol* **30**, 642-652 (2019).
410. Chen, Z. & Zhong, C. Oxidative stress in Alzheimer's disease. *Neurosci Bull* **30**, 271-281 (2014).
411. Del Bo, C., *et al.* Overview of Human Intervention Studies Evaluating the Impact of the Mediterranean Diet on Markers of DNA Damage. *Nutrients* **11**(2019).
412. Calvo-Flores Guzman, B., *et al.* The GABAergic system as a therapeutic target for Alzheimer's disease. *J Neurochem* **146**, 649-669 (2018).
413. Kao, Y.C., Ho, P.C., Tu, Y.K., Jou, I.M. & Tsai, K.J. Lipids and Alzheimer's Disease. *Int J Mol Sci* **21**(2020).
414. Ferreira-Vieira, T.H., Guimaraes, I.M., Silva, F.R. & Ribeiro, F.M. Alzheimer's disease: Targeting the Cholinergic System. *Curr Neuropharmacol* **14**, 101-115 (2016).
415. McAdams-DeMarco, M.A., *et al.* Dementia, Alzheimer's Disease, and Mortality after Hemodialysis Initiation. *Clin J Am Soc Nephrol* **13**, 1339-1347 (2018).
416. Mahley, R.W. Central Nervous System Lipoproteins: ApoE and Regulation of Cholesterol Metabolism. *Arterioscler Thromb Vasc Biol* **36**, 1305-1315 (2016).
417. Huang, Y. & Mahley, R.W. Apolipoprotein E: structure and function in lipid metabolism, neurobiology, and Alzheimer's diseases. *Neurobiology of disease* **72 Pt A**, 3-12 (2014).
418. Yanckello, L.M., *et al.* Apolipoprotein E genotype-dependent nutrigenetic effects to prebiotic inulin for modulating systemic metabolism and neuroprotection in mice via gut-brain axis. *Nutr Neurosci*, 1-11 (2021).
419. Lin, A.L., *et al.* APOE genotype-dependent pharmacogenetic responses to rapamycin for preventing Alzheimer's disease. *Neurobiol Dis* **139**, 104834 (2020).
420. Davis, S.M., Collier, L.A., Messmer, S.J. & Pennypacker, K.R. The Poststroke Peripheral Immune Response Is Differentially Regulated by Leukemia Inhibitory Factor in Aged Male and Female Rodents. *Oxid Med Cell Longev* **2020**, 8880244 (2020).
421. Longuet-Higgins, M.S. On the Shannon-Weaver index of diversity, in relation to the distribution of species in bird censuses. *Theor Popul Biol* **2**, 271-289 (1971).
422. Mallick, H., *et al.* Multivariable Association Discovery in Population-scale Metagenomics Studies. *bioRxiv*, 2021.2001.2020.427420 (2021).
423. Benakis, C., *et al.* The microbiome-gut-brain axis in acute and chronic brain diseases. *Curr Opin Neurobiol* **61**, 1-9 (2020).
424. Park, M.J., *et al.* Reproductive Senescence and Ischemic Stroke Remodel the Gut Microbiome and Modulate the Effects of Estrogen Treatment in Female Rats. *Transl Stroke Res* **11**, 812-830 (2020).
425. Ahmed, S. & Spence, J.D. Sex differences in the intestinal microbiome: interactions with risk factors for atherosclerosis and cardiovascular disease. *Biol Sex Differ* **12**, 35 (2021).
426. Shin, N.R., Whon, T.W. & Bae, J.W. Proteobacteria: microbial signature of dysbiosis in gut microbiota. *Trends Biotechnol* **33**, 496-503 (2015).

427. Rizzatti, G., Lopetuso, L.R., Gibiino, G., Binda, C. & Gasbarrini, A. Proteobacteria: A Common Factor in Human Diseases. *Biomed Res Int* **2017**, 9351507 (2017).
428. Rivera-Chavez, F., Lopez, C.A. & Baumler, A.J. Oxygen as a driver of gut dysbiosis. *Free Radic Biol Med* **105**, 93-101 (2017).
429. Vogt, N.M., *et al.* Gut microbiome alterations in Alzheimer's disease. *Sci Rep* **7**, 13537 (2017).
430. Magne, F., *et al.* The Firmicutes/Bacteroidetes Ratio: A Relevant Marker of Gut Dysbiosis in Obese Patients? *Nutrients* **12**(2020).
431. Binda, C., *et al.* Actinobacteria: A relevant minority for the maintenance of gut homeostasis. *Dig Liver Dis* **50**, 421-428 (2018).
432. Azman, A.S., Mawang, C.I., Khairat, J.E. & AbuBakar, S. Actinobacteria-a promising natural source of anti-biofilm agents. *Int Microbiol* **22**, 403-409 (2019).
433. Wexler, A.G. & Goodman, A.L. An insider's perspective: Bacteroides as a window into the microbiome. *Nat Microbiol* **2**, 17026 (2017).
434. Qi, X., *et al.* Gut microbiota-bile acid-interleukin-22 axis orchestrates polycystic ovary syndrome. *Nat Med* **25**, 1225-1233 (2019).
435. Yuan, Y., *et al.* Changes in the gut microbiota during and after commercial helium-oxygen saturation diving in China. *Occup Environ Med* **76**, 801-807 (2019).
436. Wang, K., *et al.* Parabacteroides distasonis Alleviates Obesity and Metabolic Dysfunctions via Production of Succinate and Secondary Bile Acids. *Cell Rep* **26**, 222-235 e225 (2019).
437. Derrien, M., Vaughan, E.E., Plugge, C.M. & de Vos, W.M. Akkermansia muciniphila gen. nov., sp. nov., a human intestinal mucin-degrading bacterium. *Int J Syst Evol Microbiol* **54**, 1469-1476 (2004).
438. Sonoyama, K., *et al.* Response of gut microbiota to fasting and hibernation in Syrian hamsters. *Appl Environ Microbiol* **75**, 6451-6456 (2009).
439. Zhang, T., Li, Q., Cheng, L., Buch, H. & Zhang, F. Akkermansia muciniphila is a promising probiotic. *Microb Biotechnol* **12**, 1109-1125 (2019).
440. Pan, F., *et al.* Predominant gut Lactobacillus murinus strain mediates anti-inflammatory effects in calorie-restricted mice. *Microbiome* **6**, 54 (2018).
441. Wilck, N., *et al.* Salt-responsive gut commensal modulates TH17 axis and disease. *Nature* **551**, 585-589 (2017).
442. Arya, A.K. & Hu, B. Brain-gut axis after stroke. *Brain Circ* **4**, 165-173 (2018).
443. Kubota, M., *et al.* Lactobacillus reuteri DSM 17938 and Magnesium Oxide in Children with Functional Chronic Constipation: A Double-Blind and Randomized Clinical Trial. *Nutrients* **12**(2020).
444. Yan, Y., *et al.* CCL19 and CCR7 Expression, Signaling Pathways, and Adjuvant Functions in Viral Infection and Prevention. *Front Cell Dev Biol* **7**, 212 (2019).
445. Iida, Y., *et al.* Local injection of CCL19-expressing mesenchymal stem cells augments the therapeutic efficacy of anti-PD-L1 antibody by promoting infiltration of immune cells. *J Immunother Cancer* **8**(2020).
446. Comerford, I., *et al.* A myriad of functions and complex regulation of the CCR7/CCL19/CCL21 chemokine axis in the adaptive immune system. *Cytokine Growth Factor Rev* **24**, 269-283 (2013).

447. Adachi, K., *et al.* IL-7 and CCL19 expression in CAR-T cells improves immune cell infiltration and CAR-T cell survival in the tumor. *Nat Biotechnol* **36**, 346-351 (2018).
448. Xu, Z., *et al.* CCL19 suppresses angiogenesis through promoting miR-206 and inhibiting Met/ERK/Elk-1/HIF-1alpha/VEGF-A pathway in colorectal cancer. *Cell Death Dis* **9**, 974 (2018).
449. Liu, Y., *et al.* Ischemic stroke damages the intestinal mucosa and induces alteration of the intestinal lymphocytes and CCL19 mRNA in rats. *Neurosci Lett* **658**, 165-170 (2017).
450. Noor, S. & Wilson, E.H. Role of C-C chemokine receptor type 7 and its ligands during neuroinflammation. *J Neuroinflammation* **9**, 77 (2012).
451. Mor, A., *et al.* Blockade of CCL24 with a monoclonal antibody ameliorates experimental dermal and pulmonary fibrosis. *Ann Rheum Dis* **78**, 1260-1268 (2019).
452. Segal-Salto, M., *et al.* A blocking monoclonal antibody to CCL24 alleviates liver fibrosis and inflammation in experimental models of liver damage. *JHEP Rep* **2**, 100064 (2020).
453. Zhang, J., *et al.* High-Content Genome-Wide RNAi Screen Reveals CCR3 as a Key Mediator of Neuronal Cell Death. *eNeuro* **3**(2016).
454. Chen, K. & Kolls, J.K. Interleukin-17A (IL17A). *Gene* **614**, 8-14 (2017).
455. El-Hakim, Y., *et al.* Sex differences in stroke outcome correspond to rapid and severe changes in gut permeability in adult Sprague-Dawley rats. *Biol Sex Differ* **12**, 14 (2021).
456. Luo, X.J., *et al.* The interleukin 3 gene (IL3) contributes to human brain volume variation by regulating proliferation and survival of neural progenitors. *PLoS One* **7**, e50375 (2012).
457. Jore, M.M., *et al.* Structural basis for therapeutic inhibition of complement C5. *Nat Struct Mol Biol* **23**, 378-386 (2016).
458. Costa, C., *et al.* Role of complement component C5 in cerebral ischemia/reperfusion injury. *Brain Res* **1100**, 142-151 (2006).
459. Messmer, S.J., *et al.* Extended Middle Cerebral Artery Occlusion (MCAO) Model to Mirror Stroke Patients Undergoing Thrombectomy. *Transl Stroke Res* (2021).
460. Ottesen, A., *et al.* Enrichment dynamics of *Listeria monocytogenes* and the associated microbiome from naturally contaminated ice cream linked to a listeriosis outbreak. *BMC Microbiol* **16**, 275 (2016).
461. Ponnusamy, D., *et al.* Cross-talk among flesh-eating *Aeromonas hydrophila* strains in mixed infection leading to necrotizing fasciitis. *Proc Natl Acad Sci U S A* **113**, 722-727 (2016).
462. Hasan, N.A., *et al.* Microbial community profiling of human saliva using shotgun metagenomic sequencing. *PLoS One* **9**, e97699 (2014).
463. Lax, S., *et al.* Longitudinal analysis of microbial interaction between humans and the indoor environment. *Science* **345**, 1048-1052 (2014).
464. Yushkevich, P.A., *et al.* User-guided 3D active contour segmentation of anatomical structures: significantly improved efficiency and reliability. *Neuroimage* **31**, 1116-1128 (2006).

465. Mehra, M., *et al.* Preclinical acute ischemic stroke modeling. *J Neurointerv Surg* **4**, 307-313 (2012).
466. Martha, S.R., *et al.* Expression of Cytokines and Chemokines as Predictors of Stroke Outcomes in Acute Ischemic Stroke. *Front Neurol* **10**, 1391 (2019).
467. Liaw, A. & Wiener, M. Classification and Regression by RandomForest. *Forest* **23**(2001).

VITA

Tyler Christian Hammond

Education

2010-2016 Brigham Young University, Provo, Utah
Bachelor of Science in Neuroscience

Professional Positions Held

2013-2016 Lab Assistant, Brigham Young University
Mentor: Jeffrey Edwards, Department of Physiology and
Developmental Biology

2013-2016 Bulgarian Teacher, Missionary Training Center, Provo, Utah

Scholastic and Professional Honors

2010-2016 Heritage Full Tuition Scholarship, Brigham Young University,
Provo, Utah

2015 Student Mentoring Grant, Office of Research and Creative
Activities, Brigham Young University, Provo, Utah

2015 3rd Place Winner of Best Papers, Chiasm: BYU Undergraduate
Journal of Neuroscience

2016 Valedictorian, Brigham Young University, Provo, Utah

2016-2024 MD/PhD Scholarship, University of Kentucky, Lexington,
Kentucky

2018 Travel Award, American College of Nutrition, Seattle, Washington

2018 Travel Award, Graduate Student Congress, University of
Kentucky, Lexington, Kentucky

- 2018 Travel Award, International Conference on Precision Nutrition, Chania, Greece
- 2019 Travel Award, International Society for Magnetic Resonance Imaging, Montreal, Canada
- 2020 Saha Cardiovascular Research Award, University of Kentucky, Lexington, Kentucky
- 2020 McCuller's Scholar, Sanders-Brown Center on Aging, Lexington, Kentucky
- 2020 Poster Presentation Award, Markesbery Symposium, Lexington, Kentucky
- 2022 Travel Award, Graduate Student Congress, University of Kentucky, Lexington, Kentucky
- 2022 Travel Award, International Society for Cerebral Blood Flow and Metabolism, Glasgow, Scotland

Publications

- 2018 Miller, R., Marriott, D., Trotter, J., **Hammond, T.**, Lyman, D., Call, T., Walker, B., Christensen, N., Haynie, D., Badura, Z., Homan, M., Edwards, J. (2018). Running exercise mitigates the negative consequences of chronic stress on dorsal hippocampal long-term potentiation in male mice. *Neurobiology of Learning and Memory.*, 149, 28-38
- 2019 Hoffman, J., Yanckello, L., Chlipala, G., **Hammond, T.**, McCulloch, S., Parikh, I., Sun, S., Morganti, J., Green, G., Lin, A. (2019). Dietary inulin alters the gut microbiome, enhances systemic metabolism and reduces neuroinflammation in an APOE4 mouse model. *PLoS One.*, 14(8):e0221828
- 2020 **Hammond, T.***, Xing, X.*, Ma, D., Nho, K., Crane, P., Elahi, F., Ziegler, D., Liang, T., Cheng, Q., Jacobs, N., Lin, A., (2020) β -amyloid and tau drive early Alzheimer's disease decline while glucose hypometabolism drives late decline. *Communications Biology*, 3(1), 352. doi:10.1038/s42003-020-1079-x
- 2021 Yanckello LM, Hoffman JD, Chang YH, Lin P, Nehra G, Chlipala G, McCulloch SD, **Hammond TC**, Yackzan AT, Lane AN, Green SJ, Hartz AMS, Lin AL. Apolipoprotein E genotype-dependent nutrigenetic effects to prebiotic inulin for modulating systemic

metabolism and neuroprotection in mice via gut-brain axis. *Nutr Neurosci.* 2021 Mar 5:1-11. doi: 10.1080/1028415X.2021.1889452. Epub ahead of print. PMID: 33666538.

2021

Messmer SJ, Salmeron KE, Frank JA, McLouth CJ, Lukins DE, **Hammond TC**, Lin AL, Fraser JF, Pennypacker KR. Extended Middle Cerebral Artery Occlusion (MCAO) Model to Mirror Stroke Patients Undergoing Thrombectomy. *Transl Stroke Res.* 2021 Aug 16. doi: 10.1007/s12975-021-00936-y. Epub ahead of print. PMID: 34398389.